

UNIVERSITY OF READING

**Stress signalling to cardiac gene expression and cell death**

Sam J Leonard

Submitted for the degree of Doctor of Philosophy

School of Biological Sciences

March 2017

## **Abstract**

**Background:** Cardiovascular diseases such as heart failure and myocardial infarction are associated with increased oxidative stress, the release of pro-inflammatory cytokines such as tumour necrosis factor- $\alpha$  (TNF $\alpha$ ) and interleukin 1 $\beta$  (IL1 $\beta$ ) and increased death of the contractile cardiomyocytes. Oxidative stress (exemplified by H<sub>2</sub>O<sub>2</sub>) is a pivotal modulator of the balance between the life and death of cardiomyocytes. H<sub>2</sub>O<sub>2</sub> promotes cardiomyocyte apoptosis, induces substantial changes in gene expression and activates the three principal mitogen-activated protein kinase (MAPK) pathways (ERK1/2, JNKs and p38-MAPKs), which regulate gene expression in other cell types. However, the roles of the MAPK pathways in regulation of cardiomyocyte gene expression in response to H<sub>2</sub>O<sub>2</sub> are yet to be reported. A further pathway that may play important roles cardiac survival vs death is regulated by the protein kinase, RIPK1. In non-cardiac cell types, TNF $\alpha$  signals via RIPK1 to cytoprotection or cell death, depending on the cellular environment. Polyubiquitinated RIPK1 promotes cytoprotection through activation of NF $\kappa$ B, JNKs and p38-MAPKs while phosphorylation and activation of RIPK1 kinase activity is associated with induction of necroptosis, a novel regulated cell death modality.

**Hypotheses:** The first hypothesis is that ERK1/2, JNKs and p38-MAPKs play substantial roles in regulation of cardiomyocyte RNA expression during cardiomyocyte apoptosis induced by H<sub>2</sub>O<sub>2</sub>. The second hypothesis is that RIPK1, which can signal to cytoprotection through NF $\kappa$ B and MAPKs, or to cell death by apoptosis or necroptosis, makes important contributions to mediating the balance between life and death of cardiomyocytes.

**Results:** To dissect the roles of the MAPK pathways in the cardiomyocyte RNA expression response to H<sub>2</sub>O<sub>2</sub>, neonatal rat cardiomyocytes were untreated or exposed to H<sub>2</sub>O<sub>2</sub> (0.2 mM, 2 h) with or without pre-treatment (15 min) with PD184352 (2  $\mu$ M, inhibits ERK1/2 signalling), JNK-IN-8 (1  $\mu$ M, inhibits JNKs) or SB203580 (0.7  $\mu$ M, inhibits p38-MAPK $\alpha/\beta$ ) or to the inhibitors alone (2 h 15 min). RNA expression profiles were determined using Affymetrix microarrays and GeneSpring software. PD184352 alone downregulated 92 and upregulated 32 RNAs, indicating that ERK1/2 influence basal gene expression. JNK-IN-8 and SB203580 affected expression of 14 and 6 RNAs, respectively. H<sub>2</sub>O<sub>2</sub> upregulated 295, and downregulated 195 RNAs, of which 43% and 44%, respectively, were unaffected by any inhibitor. MAPK inhibitors affected the upregulation of 37% (PD184352), 25% (JNK-IN-8) or 28% (SB203580) RNAs, and affected the downregulation of 33% (PD184352), 28% (JNK-IN-8) or 35% (SB203580) RNAs. Microarray data for selected genes were validated using qPCR. To examine the roles of cardiac RIPK1, neonatal rat cardiomyocytes were exposed to various

pathophysiological stimuli and extracts immunoblotted with antibodies to RIPK1. Pro-inflammatory cytokines (TNF $\alpha$  or IL1 $\beta$ ) induced the appearance of reduced mobility RIPK1 bands within 5 – 15 min, consistent with phosphorylation but not ubiquitinylation. Further evidence of RIPK1 phosphorylation in response to IL1 $\beta$  was obtained using anion-exchange chromatography. Additionally, the p38-MAPK $\alpha/\beta$  inhibitor SB203580 attenuated the appearance of reduced mobility RIPK1 bands in response to IL1 $\beta$ , suggestive of a potential novel regulatory mechanism of RIPK1. Concentrations of H<sub>2</sub>O<sub>2</sub> that promote apoptosis or necrosis (>0.2 mM) resulted in reduced mobility bands of RIPK1, maximal at 60 min. Reduced mobility bands of RIPK1 were also detected in adult male rat hearts perfused with H<sub>2</sub>O<sub>2</sub> (0.2 mM, 60 min) or subjected to ischaemia-reperfusion. To explore the regulation of RIPK1 by phosphorylation and ubiquitinylation in cardiomyocytes, adenoviruses expressing exogenous FLAG-tagged wild type and mutant RIPK1 were produced. However, the exogenously expressed RIPK1 constructs appeared to undergo cleavage when expressed in cardiomyocytes.

**Conclusions:** The three main MAPK pathways play substantial yet differential roles in the regulation of RNA expression in response to H<sub>2</sub>O<sub>2</sub>, with the greatest contribution by ERK1/2 and smaller roles for JNKs and p38-MAPK $\alpha/\beta$ . Furthermore, RIPK1 in neonatal cardiomyocytes or whole adult hearts exhibits reduced mobility in response to oxidative stress or pro-inflammatory cytokines, likely reflective of phosphorylation and potentially activation. Accordingly, RIPK1 may play important roles in modulating the balance of life vs death of cardiomyocytes. This response may, in part, be mediated by p38-MAPK signalling.

## **Acknowledgements**

The research detailed in this thesis would not have been possible without the advice, support, patience and guidance of my supervisor Professor Angela Clerk, to whom I am extremely grateful. I also thank my co-supervisor Professor Peter Sugden for useful and invariably humorous discussions.

I am indebted to Dr. Steve Fuller for his support in the laboratory, and for his invaluable practical advice and assistance with the production of adenoviruses. Thanks also to all of my colleagues in the research group, past and present, particularly Dr. Michelle Hardyman and Dr. Kerry Rostron who have made the process of conducting this research a pleasure.

## **Declaration**

I confirm that this is my own work and the use of all material from other sources has been properly and fully acknowledged.

The immunoblots in Chapter Three, Figs. 3.1 and 3.3 were performed by Dr. Kerry Rostron. Dr. Michelle Hardyman provided assistance with the qPCR expression analysis in Chapter Three.

Unless otherwise indicated, all other experimental work and analyses were conducted by myself.

Sam J Leonard

## **Publications and abstracts**

### **Publications**

Fuller, S. J., Osborne, S. A., **Leonard, S. J.**, Hardyman, M. A., Vaniotis, G., Allen, B. G., Sugden, P. H. & Clerk, A. (2015). Cardiac protein kinases: the cardiomyocyte kinome and differential kinase expression in human failing hearts. *Cardiovasc Res*, 108, 87-98.

### **Abstracts**

**Leonard, S. J.**, Sugden, P. H. & Clerk, A. Dissecting the roles of mitogen-activated protein kinases (MAPK) cascades in the mRNA expression response to H<sub>2</sub>O<sub>2</sub> in cardiomyocytes. British Society for Cardiovascular Research Autumn Meeting, 2014, Reading: "Cardiovascular Signalling in Health and Disease".

**Leonard, S.J.**, Young, B.J., Fuller, S. J., Sugden, P. H. & Clerk, A. Expression of receptor-interacting protein kinases 1, 2 and 3 (RIPKs 1, 2 and 3) in the heart and their regulation by ischaemia/reperfusion vs oxidative stress. British Cardiovascular Society Annual Conference, 2014, Manchester

**Leonard, S. J.**, Sugden, P. H. & Clerk, A. Mitogen-activated protein kinase (MAPK) pathways play a significant role in regulation of cardiomyocyte mRNA expression in response to H<sub>2</sub>O<sub>2</sub>. 33rd Annual Meeting of the International Society for Heart Research European Section, 2015, Bordeaux

## Contents

<b>Abstract</b>	<b>2</b>
<b>Acknowledgements</b>	<b>4</b>
<b>Declaration</b>	<b>5</b>
<b>Publications and abstracts</b>	<b>6</b>
<b>Abbreviations</b>	<b>19</b>
<b>Chapter One - Introduction</b>	<b>22</b>
1.1 The heart and heart failure .....	23
1.2 Redox signalling and oxidative stress in the heart .....	26
1.2.1 The role of redox reactions in intracellular signalling	26
1.2.2 Modulation of cardiomyocyte life and death by oxidative stress	31
1.2.3 Regulation of cardiomyocyte gene expression by oxidative stress	37
1.3 Mitogen-activated protein kinase (MAPK) signalling.....	39
1.3.1 Activation and roles of the MAPK cascades	39
1.3.1.1 Extracellular signal-regulated kinases 1 and 2 (ERK1/2)	41
1.3.1.2 c-Jun N-terminal kinases (JNKs)	43
1.3.1.3 p38-mitogen activated protein kinases (p38-MAPKs)	45
1.3.2 Regulation of cardiomyocyte gene expression by ERK1/2, JNKs and p38-MAPKs	48
1.4 Pro-inflammatory cytokines and their roles in the heart .....	51
1.4.1 Interleukin 1 $\beta$ (IL1 $\beta$ ) and its role in the heart	52
1.4.2 Tumour necrosis factor-alpha (TNF $\alpha$ ) and its role in the heart	55
1.5 Receptor interacting protein kinases (RIPKs) and necroptosis .....	61

1.5.1	Regulated necrosis - necroptosis	61
1.5.2	Regulation of RIPK1 signalling by post-translational modifications	66
1.5.2.1	Regulation of RIPK1 signalling by ubiquitinylation	66
1.5.2.2	Regulation of RIPK1 signalling by phosphorylation	67
1.5.3	RIPKs and necroptosis in the heart	72
1.6	Hypothesis and aims.....	74
<b>Chapter Two – General Methods</b>		<b>75</b>
2.1	Materials and reagents.....	76
2.2	Agonists and inhibitors .....	77
2.3	Cell cultures .....	78
2.3.1	Preparation of neonatal rat ventricular myocytes	78
2.3.2	Human Embryonic Kidney 293 (HEK 293) cultures	79
2.4	Heart perfusions.....	79
2.5	SDS-polyacrylamide gel electrophoresis (SDS-PAGE) and immunoblotting.	80
2.5.1	Preparation of total protein extracts	80
2.5.2	Preparation of cytosolic and nuclear protein enriched (NPE) extracts	81
2.5.3	Bio-Rad protein assay	81
2.5.4	SDS-PAGE and immunoblotting	82
2.6	Immunoprecipitations .....	83
2.7	Total RNA extraction .....	84
2.8	Quantitative real time polymerase chain reaction (qPCR) .....	85
2.9	Agarose gel electrophoresis of DNA.....	88

2.10	General methods for the generation of adenoviruses expressing RIPK1 .....	88
2.10.1	Amplification of plasmids	88
2.10.2	Colony screen PCR	88
2.10.3	Spin column purification of DNA	91
2.10.4	Plasmid isolation using the alkaline lysis miniprep method	91
2.10.5	Plasmid isolation using the alkaline lysis maxiprep method	92
2.10.6	Sequencing of plasmid DNA	94
2.10.7	Generation of adenoviral plasmids	94
2.10.7.1	Homologous recombination of shuttle vectors with the pAdeasy-1 plasmid	94
2.10.7.2	Colony screen PCR for homologous recombination and purification of adenoviral plasmids	95
2.10.8	Production and propagation of adenoviral particles in HEK 293 cells	96
2.11	Fast protein liquid chromatography .....	98
2.12	Statistical analysis.....	98

**Chapter Three - Regulation of cardiomyocyte gene expression by mitogen-activated protein kinases in response to H<sub>2</sub>O<sub>2</sub> 99**

3.1	Introduction .....	100
3.2	Methods .....	102
3.2.1	Preparation of cytosolic and nuclear protein enriched (NPE) extracts	102
3.2.2	Microarray sample preparation	103
3.2.3	Microarray data analysis	103
3.2.4	Validation of microarray data using qPCR	105

3.3	Results.....	105
3.3.1	Nuclear localisation of activated MAPKs in cardiomyocytes exposed to H <sub>2</sub> O <sub>2</sub>	105
3.3.2	Selective pharmacological inhibition of ERK1/2, JNK and p38-MAPK signalling	112
3.3.3	Regulation of basal cardiomyocyte RNA expression by MAPKs	118
3.3.4	Regulation of cardiomyocyte RNA expression by MAPKs in response to H <sub>2</sub> O <sub>2</sub>	120
3.3.4.1	Effects of MAPK inhibitors on cardiomyocyte RNA expression induced by H <sub>2</sub> O <sub>2</sub>	122
3.3.5	Validation of microarray data using qPCR	128
3.4	Discussion.....	136
3.4.1	Confirmation of MAPK inhibitor specificity	136
3.4.2	Contributions of ERK1/2, JNK and p38-MAPK signalling to cardiomyocyte gene expression in response to H <sub>2</sub> O <sub>2</sub>	137
3.4.3	Nuclear localisation of activated MAPKs in response to H <sub>2</sub> O <sub>2</sub>	143
3.4.4	Conclusions and further work	145
<b>Chapter Four – Effects of pathophysiological stimuli on receptor-interacting protein kinases (RIPKs) in the heart</b>		<b>147</b>
4.1	Introduction .....	148
4.2	Methods .....	150
4.2.1	Neonatal rat ventricular cardiomyocytes and immunoblotting	150
4.2.2	Anion-exchange fast protein liquid chromatography (FPLC)	150
4.3	Results.....	151

4.3.1	Effects of oxidative stress on RIPKs in neonatal rat cardiomyocytes and adult rat hearts	151
4.3.2	Effects of pro-inflammatory cytokines (TNF $\alpha$ and IL1 $\beta$ ) on RIPK1 in neonatal rat cardiomyocytes	156
4.3.2.1	Effects of TNF $\alpha$ on RIPK1 in cardiomyocytes	156
4.3.2.2	Effects of IL1 $\beta$ on RIPK1 in cardiomyocytes	158
4.3.3	Effect of SB203580 on the RIPK1 response to IL1 $\beta$ in neonatal rat cardiomyocytes	162
4.4	Discussion.....	164
4.4.1	Differential signalling to RIPK1 by pro-inflammatory cytokines vs oxidative stress	164
4.4.2	Phosphorylation vs ubiquitinylation of RIPK1	165
4.4.3	Significance of observations for cardiomyocyte death	168
Chapter Five - Generation of adenoviruses for expression of RIPK1 in cardiomyocytes		<b>172</b>
5.1	Introduction .....	173
5.2	Methods .....	174
5.2.1	Identification of candidate RIPK1 activation loop phosphorylation and ubiquitinylation sites	174
5.2.2	Generation of shuttle vectors expressing FLAG-tagged RIPK1 constructs	174
5.2.2.1	Generation of shuttle vectors expressing FLAG-tagged wild-type RIPK1 (FLAG-RIPK1-Shut)	174

5.2.2.2	Generation of shuttle vectors expressing FLAG-tagged S161A mutant RIPK1 (FLAG-S161A-Shut)	181
5.2.2.3	Generation of shuttle vectors expressing FLAG-tagged S166A mutant RIPK1 (FLAG-S166A-Shut)	182
5.2.2.4	Generation of shuttle vectors expressing FLAG-tagged T183A mutant RIPK1 (FLAG-T183A-Shut)	183
5.2.2.5	Generation of shuttle vectors expressing FLAG-tagged K376R mutant RIPK1 (FLAG-K376R-Shut)	184
5.2.3	Generation of adenoviruses expressing FLAG-tagged RIPK1 constructs	188
5.2.4	Transfection of HEK 293 cell cultures	189
5.2.5	Infection of cardiomyocytes with adenoviruses	189
5.2.6	Immunoprecipitations	190
5.3	Results.....	190
5.3.1	Identification of candidate RIPK1 activation loop phosphorylation sites and ubiquitinylation sites	190
5.3.2	Generation of shuttle vectors expressing FLAG-tagged wild-type and mutant RIPK1	193
5.3.3	Expression of shuttle vectors expressing FLAG-tagged wild-type and mutant RIPK1 in HEK 293 cells	198
5.3.4	Generation of adenoviruses expressing wild-type and mutant RIPK1	201
5.3.5	Adenoviral expression of FLAG-tagged RIPK1 proteins in cardiomyocytes	203
5.4	Discussion.....	207

5.4.1	Expression of FLAG-tagged RIPK1 constructs	207
5.4.2	Investigating the causes of reduced RIPK1 electrophoretic mobility	209
5.4.3	Identification of the RIPK1 activation loop phosphorylation site (ALPS)	211
5.4.4	RIPK1 signalling to NFκB and MAPKs in cardiomyocytes	213
<b>Chapter Six – Summary, discussion and future work</b>		<b>214</b>
6.1	Overview and summary of results .....	215
6.1.1	Regulation of cardiomyocyte RNA expression by MAPKs in response to oxidative stress	215
6.1.2	Effects of pathophysiological stimuli on cardiac RIPKs	215
6.2	Discussion.....	217
6.2.1	Stress signalling in cardiomyocytes and the heart	217
6.2.2	Study limitations	222
6.2.2.1	Use of pharmacological inhibitors	222
6.2.2.2	Use of neonatal rat cardiomyocytes	223
6.3	Future work.....	225
6.3.1	Regulation of cardiomyocyte gene expression by MAPKs in response to H <sub>2</sub> O <sub>2</sub>	225
6.3.2	Regulation and roles of RIPK1 in the heart	226
<b>APPENDIX I: SDS-PAGE GEL RECIPES</b>		<b>228</b>
<b>APPENDIX II: MICROARRAY DATA TABLES</b>		<b>253</b>
<b>APPENDIX III: Mouse RIPK1 DNA sequence and mutations</b>		<b>323</b>
<b>APPENDIX IV: Mouse RIPK1 protein sequence and mutations</b>		<b>324</b>



## **List of figures and tables**

### **Chapter One - Introduction**

Figure 1.1. Generation of reactive oxygen species (ROS)	<b>28</b>
Figure 1.2. Activation of the mitochondrial apoptosis pathway	<b>34</b>
Figure 1.3. Mitogen-activated protein kinase cascades	<b>40</b>
Figure 1.4. IL1 $\beta$ receptor signalling	<b>53</b>
Figure 1.5. TNF $\alpha$ signalling to inflammation/cytoprotection and apoptosis	<b>58</b>
Figure 1.6. Formation of the necrosome	<b>64</b>
Figure 1.7. RIPK1 domain structure and post-translational modifications	<b>71</b>

### **Chapter Two – General Methods**

Table 2.1. Agonists and inhibitors	<b>77</b>
Table 2.2. Antibodies used for immunoblotting	<b>83</b>
Table 2.3. Primers used in qPCR validation of microarray data	<b>87</b>
Figure 2.1. PCR conditions for colony screens	<b>90</b>
Figure 2.2. Schematic of the generation of adenoviral plasmids expressing FLAG-tagged wild-type and mutant RIPK1 constructs	<b>94</b>

### **Chapter Three – Regulation of cardiomyocyte gene expression by mitogen-activated protein kinases in response to H<sub>2</sub>O<sub>2</sub>**

Figure 3.1. Nuclear signalling of ERK1/2 in response to H <sub>2</sub> O <sub>2</sub> in cardiomyocytes	<b>107</b>
Figure 3.2. Nuclear signalling of JNKs in response to H <sub>2</sub> O <sub>2</sub> in cardiomyocytes	<b>109</b>
Figure 3.3. Nuclear signalling of p38-MAPKs in response to H <sub>2</sub> O <sub>2</sub> in cardiomyocytes	<b>111</b>
Figure 3.4. Inhibition of ERK1/2 signalling by PD184352	<b>113</b>
Figure 3.5. Inhibition of JNK signalling by JNK-IN-8	<b>115</b>
Figure 3.6. Inhibition of p38-MAPK signalling by SB203580	<b>117</b>
Figure 3.7. Regulation of baseline cardiomyocyte RNA expression by PD184352, JNK-IN-8 or SB203580	<b>119</b>
Figure 3.8. Changes in cardiomyocyte RNA expression induced by H <sub>2</sub> O <sub>2</sub>	<b>121</b>
Table 3.1. Numbers of RNAs upregulated by H <sub>2</sub> O <sub>2</sub> and affected by MAPK inhibitors	<b>122</b>
Table 3.2. Numbers of RNAs downregulated by H <sub>2</sub> O <sub>2</sub> and affected by MAPK inhibitors	<b>123</b>
Figure 3.9. Effects of MAPK inhibitors on cardiomyocyte RNA expression induced by H <sub>2</sub> O <sub>2</sub>	<b>124</b>
Figure 3.10. Gene Ontology analysis of genes upregulated by H <sub>2</sub> O <sub>2</sub> and changed further by MAPK inhibitors – classification by Biological Process	<b>126</b>
Figure 3.11. Gene Ontology analysis of genes upregulated by H <sub>2</sub> O <sub>2</sub> and changed further by MAPK inhibitors – classification by Protein Class	<b>127</b>
Figure 3.12. Validation of microarray data by qPCR: RNAs inhibited by MAPK inhibitors alone	<b>129</b>

Figure 3.13. Validation of microarray data by qPCR: mRNAs encoding transcription factors	<b>131</b>
Figure 3.14. Validation of microarray data by qPCR: effects of MAPK inhibitors on expression of antioxidant mRNAs induced by H <sub>2</sub> O <sub>2</sub>	<b>133</b>
Figure 3.15. Validation of microarray data by qPCR: effects of MAPK inhibitors on expression of dual-specificity phosphatase (Dusp) mRNAs induced by H <sub>2</sub> O <sub>2</sub>	<b>135</b>

#### **Chapter Four – Effects of pathophysiological stimuli on receptor-interacting protein kinases (RIPKs) in the heart**

Figure 4.1. Effects of oxidative stress on RIPK1 in cardiomyocytes	<b>153</b>
Figure 4.2. Effects of ischaemia/reperfusion and H <sub>2</sub> O <sub>2</sub> on RIPKs in adult rat hearts	<b>155</b>
Figure 4.3. Effects of TNF $\alpha$ on RIPK1 in cardiomyocytes	<b>157</b>
Figure 4.4. Effects of IL1 $\beta$ on RIPK1 in cardiomyocytes	<b>159</b>
Figure 4.5. Anion-exchange FPLC of RIPK1 in IL1 $\beta$ treated cardiomyocyte extracts	<b>161</b>
Figure 4.6. Effects of SB203580 on the RIPK1 response to IL1 $\beta$ in cardiomyocytes	<b>163</b>

#### **Chapter Five – Generation of adenoviruses for expression of RIPK1 in cardiomyocytes**

Figure 5.1. Construction of the oligonucleotide cassette encoding the FLAG-tag	<b>175</b>
Figure 5.2. Plasmid map of the FLAG-RIPK1-Shut vector	<b>176</b>
Figure 5.3. General strategy for introducing mutations using PCR	<b>180</b>

Table 5.1. Primers used in generation of wild-type and mutant FLAG-tagged RIPK1 constructs	<b>186</b>
Figure 5.4. PCR conditions for generation of wild-type and mutant RIPK1 constructs	<b>187</b>
Figure 5.5. Identification of conserved RIPK1 phosphorylation and ubiquitinylation sites	<b>192</b>
Figure 5.6. Generation of the wild-type and mutant RIPK1 DNA constructs	<b>194</b>
Figure 5.7. Colony screening for shuttle vectors expressing FLAG-tagged wild-type and mutant RIPK1 constructs	<b>195</b>
Figure 5.8. FLAG-tagged wild-type and mutant RIPK1 shuttle vector sequence chromatograms	<b>197</b>
Figure 5.9. Expression of FLAG-tagged wild-type and mutant RIPK1 shuttle vectors in HEK 293 cells	<b>200</b>
Figure 5.10. Colony screening for adenoviral plasmids expressing FLAG-tagged wild-type and mutant RIPK1	<b>202</b>
Figure 5.11. Expression of FLAG-tagged RIPK1 in cardiomyocytes	<b>205</b>
Figure 5.12. Effects of IL1 $\beta$ on FLAG-tagged RIPK1 constructs in cardiomyocytes	<b>206</b>

## Abbreviations

ALPS	Activation loop phosphorylation site
ANOVA	Analysis of variance
AP-1	Activator protein-1
Apaf1	Apoptotic protease-activating-factor-1
ASK1	Apoptosis signal-regulating kinase 1
ATF	Activating transcription factor
BSA	Bovine serum albumen
CA	Constitutively active
CARD	Caspase recruitment domain
cIAP	Cellular inhibitor of apoptosis protein
CMV	Cytomegalovirus
DD	Death domain
DMEM	Dulbecco's modified Eagle's medium
DMSO	Dimethyl sulphoxide
DN	Dominant negative
DTT	Dithiothreitol
Dusp	Dual-specificity phosphatase
E64	Trans-epoxysuccinyl-L-leucylamido-(4-guanidino)butane
EDTA	Ethylenediamine tetra-acetic acid
EGF	Epidermal growth factor
EGTA	Ethylene glycol tetra-acetic acid
ERK	Extracellular signal-regulated kinase
ET-1	Endothelin-1
FADD	Fas-associated protein with death domain
FGF	Fibroblast growth factor
FPLC	Fast protein liquid chromatography
GPCR	G protein-coupled receptor
HF	Heart failure
IKK	Inhibitor of $\kappa$ B-kinase
IL	Interleukin
IL1R1	Interleukin-1 receptor 1
IL1Ra	Interleukin-1 receptor antagonist
IL1RAcPs	Interleukin-1 receptor accessory proteins
InsP <sub>3</sub>	inositol 1,4,5-trisphosphate
IPC	Ischaemic preconditioning

IR	Ischaemia reperfusion
IRAK	Interleukin-1 receptor associated kinase
JNK	c-Jun N-terminal kinase
Klf	Krüppel-like factor
KO	Knockout
LUBAC	linear ubiquitin assembly complex
MAP3K	Mitogen-activated protein kinase kinase kinase
MAPK	Mitogen-activated protein kinase
MAPKAPK	Mitogen-activated protein kinase activated protein kinase
MI	Myocardial infarction
MKK	Mitogen-activated protein kinase kinase
MPTP	Mitochondrial permeability transition pore
MSK	Mitogen- and stress-activated kinase
MyD88	myeloid differentiation primary response protein 88
NADH	Nicotinamide adenine dinucleotide
NFκB	Nuclear factor κB
NOS	Nitric oxide synthase
NOX	NAD(P)H oxidase
NPE	Nuclear protein-enriched
PAGE	Polyacrylamide electrophoresis
PARP	Poly(ADP-ribose) polymerase
PBS	Phosphate-buffered saline
PCR	Polymerase chain reaction
PDGF	Platelet-derived growth factor
PI	Propidium iodide
PKA	Protein kinase A
PKC	Protein kinase C
PMSF	Phenylmethylsulfonyl fluoride
PtdInsP <sub>2</sub>	Phosphatidylinositol-4,5,bisphosphate
qPCR	Quantitative real-time polymerase chain reaction
RIPK	Receptor-interacting protein kinase
ROS	Reactive oxygen species
RPTK	Receptor protein tyrosine kinase
RSK	p90 ribosomal S6 kinase
SEM	Standard error of the mean
siRNA	Small interfering RNA

SMAC	Second mitochondria-derived activator of caspases
SNK	Student-Newman-Keuls (post-test)
SOD	Superoxide dismutase
SWOP	Second window of protection
TAB	Transforming growth factor- $\beta$ -activated kinase binding protein
TAK1	Transforming growth factor- $\beta$ -activated kinase
TBST	Tris-buffered saline containing 0.1% Tween 20
TNF	Tumour necrosis factor
TNFR	Tumour necrosis factor receptor
TRADD	Tumour necrosis factor receptor 1 related death domain protein
TRAF	Tumour necrosis factor receptor associated factor
TRAIL	Tumour necrosis factor-related apoptosis inducing ligand
TUNEL	Terminal deoxynucleotidyl dUTP nick-end labelling
$\Delta\psi_m$	Mitochondrial membrane potential

## **Chapter One - Introduction**

## 1.1 The heart and heart failure

Cardiovascular diseases and heart failure (HF) are leading causes of morbidity and mortality worldwide, representing an increasing economic and societal burden, particularly in industrialised nations (Laflamme and Murry, 2011; Azad and Lemay, 2014). The heart executes a vital function, pumping blood around the body to deliver oxygen and nutrients to, and remove waste products from, perfused tissues. The beating of the heart is achieved by the synchronised, rhythmic contraction of the cardiomyocytes, the contractile muscle cells of the heart. Although representing only ~30% of the total cell number in the heart, cardiomyocytes account for approximately 75% of the volume of the mature myocardium. The remainder is predominantly composed of a heterogeneous population of other cell types including, (in varying proportions) fibroblasts, vascular smooth muscle cells and endothelial cells (Buja and Vela, 2008; Souders et al., 2009; Pinto et al., 2016).

In contrast with lower vertebrates such as the newt and the zebrafish, which can effectively regenerate tracts of damaged myocardium through cardiomyocyte proliferation (Oberpriller and Oberpriller, 1974; Poss et al., 2002), the consensus is that mammalian cardiomyocytes cease to proliferate during the perinatal period, withdrawing from the cell cycle and undergoing terminal differentiation (Ahuja et al., 2007). As a result, cardiomyocytes do not readily divide in order to replace dead, damaged or dying cells as can occur routinely in other tissues with different cell types. Thus, although a healthy heart and its constituent cardiomyocytes are robust, and demonstrate resistance to perturbations in the cellular environment, terminal differentiation of cardiomyocytes renders the heart vulnerable to chronic stresses such as hypertension as well as severe, acute, pathophysiological stressors such as myocardial infarction (MI) and ischaemia reperfusion (IR) (Nadruz, 2015; Hausenloy and Yellon, 2013). In response to such insults, cardiomyocytes may undergo autophagy, necrosis or a regulated form of cell death such as apoptosis or necroptosis (Chiong et al., 2011; Clerk et al., 2003; Koshinuma et al., 2014). The resulting cardiomyocyte fallout may impair cardiac pump function, rendering the heart's ability to deliver blood insufficient to meet the body's

requirements. Although there is evidence supporting the existence of a subpopulation of multipotent progenitor cells capable of giving rise to the various cardiac cell types, including cardiomyocytes (Beltrami et al., 2003), considerable controversy remains as to the nature of these cells and their significance *in vivo*. Regardless, any endogenous repair mechanisms are evidently insufficient to fully ameliorate the cardiac damage caused by pathophysiological stresses, necessitating the development of effective therapeutic interventions.

In order to maintain sufficient cardiac output following cardiomyocyte death, surviving cardiomyocytes may undergo hypertrophy, an increase in cell size in the absence of cytokinesis and concomitant increase in cell number. This is characterised by a recapitulation of the immediate early and “foetal” gene expression programmes with induction of c-Fos and c-Jun (classic AP-1 transcription factor constituents) and  $\beta$ -myosin heavy chain, amongst others (Clerk et al., 2007a; Dorn et al., 2003; Pandya and Smithies, 2011). These changes in gene expression, together with augmented protein synthesis, result in morphological changes that increase cardiomyocyte function (increases in size and myofibrillogenesis) (Sugden and Clerk, 1998). While hypertrophy is initially an adaptive and compensatory response to myocardial injury and reduced cardiomyocyte number, continued chronic stress and increased workload may lead to continued cardiomyocyte death, accompanied by a significant inflammatory response, resulting in a decompensated state and ultimately HF (Van Berlo et al., 2013; Petersen and Felker, 2006). The hypertrophic response to myocardial insult is also commonly coincident with an increased rate of deposition of extracellular matrix by cardiac fibroblasts. This cardiac fibrosis further contributes to myocardial “stiffness” and impaired contractility, and to the progression to HF (Krenning et al., 2010; Ho et al., 2010).

As discussed above, the heart and the cardiomyocytes exhibit a wide range of changes in response to the varied pathophysiological stresses encountered, including changes in gene expression and protein synthesis as well cell morphology and tissue structure. To understand if, and how, these changes contribute to the development of cardiac hypertrophy and heart failure, it is essential to establish whether these changes merely correlate with cardiac

pathologies, or if there is a causal link. Some changes might also be beneficial and promote adaptation to the encountered stress. Understanding the consequences of these changes may facilitate development of effective treatments for heart disease. To ascertain whether these changes are adaptive, deleterious or only correlative, chemical or genetic approaches may be adopted to either inhibit or potentiate the processes thought to lead to the observed changes, followed by assessment of the effects of such intervention on functional readouts such as cell death. For example, if inhibiting a process can be demonstrated (through multiple consistent lines of evidence) to have a protective effect, this process can reasonably be inferred to have a detrimental effect. Similarly, if inhibiting processes leading to a putatively beneficial change has a detrimental result, the change can be regarded as adaptive. Accordingly, therapeutics strategies may seek to either inhibit deleterious changes, or to augment those that are adaptive.

The cellular processes occurring in cardiomyocytes, including survival, gene expression, hypertrophy and death in response to pathophysiological stresses are regulated and modulated by complex signalling pathways (Matsui et al., 2003; Clerk et al., 2007a; Clerk et al., 2003), and there is evidence of significant cross talk between these pathways. Developing a detailed mechanistic understanding of these signalling pathways and the functions they regulate represents a significant conceptual and technical challenge. However, doing so holds great potential from both a basic science and clinical viewpoint, and may facilitate advances in the development of sophisticated and rational therapeutic approaches in treating MI and HF. Accordingly, intensive research efforts in recent decades have sought to identify the stimuli and signalling pathways responsible for regulating cardiomyocyte hypertrophy and gene expression, and the balance between cardiomyocyte life and death.

## 1.2 Redox signalling and oxidative stress in the heart

### 1.2.1 The role of redox reactions in intracellular signalling

In recent decades, it has become increasingly recognised that oxidation and reduction (redox) reactions are associated with important physiological and pathological roles and processes. Production of reactive oxygen species (ROS) incidental to aerobic respiration has been acknowledged for several decades, as has the production of oxidants by phagocytes in the defence against invading microorganisms (Harman, 1956; Babior, 1984).

Major forms of ROS include superoxide anion ( $\text{O}_2^{\cdot-}$ ),  $\text{H}_2\text{O}_2$ , hydroxyl radical ( $\text{OH}^{\cdot}$ ) and hydroxyl anion ( $\text{OH}^-$ ). These are produced by sequential incomplete single electron reduction of molecular  $\text{O}_2$  (Bartz and Piantadosi, 2010) (Fig. 1.1A). Sources of ROS are numerous and varied, although the major contributor to ROS production *in vivo* is oxidative phosphorylation in the mitochondria (Balaban et al., 2005). During oxidative phosphorylation, controlled oxidation of electron donors such as nicotinamide adenine dinucleotide (NADH) results in a potential across the mitochondrial inner membrane ( $\Delta\psi_m$ ) and this potential is subsequently used to drive phosphorylation of ADP to produce ATP. At various points in this process, electrons from NADH or other donors may “leak” to react with  $\text{O}_2$ , thus forming ROS (Fig. 1.1A) (Balaban et al., 2005). In addition to the mitochondria, intracellular ROS are also produced by a number of dedicated enzymes, including the various non-phagocyte NAD(P)H oxidase (NOX) and xanthine oxidase family members. ROS are also produced by uncoupled nitric oxide synthases (NOS) (Fig. 1.1B) (Schieber and Chandel, 2014; Lambeth, 2004; Montezano and Touyz, 2012).

Other enzymes and factors function intracellularly in professional antioxidant defence and conversion of ROS to less damaging species, including superoxide dismutases (SODs), glutathione peroxidases, peroxiredoxins, glutaredoxin and thioredoxin, catalase and glutathione. Importantly, ROS serve as precursors to other reactive species. For example, the various SOD enzymes dismutate  $\text{O}_2^{\cdot-}$  generated by mitochondria and NOX to produce  $\text{H}_2\text{O}_2$  (Fig.

1.1B), which is thence processed by catalase, glutathione peroxidases and peroxiredoxins to prevent excess  $H_2O_2$  accumulation. In the presence of ferrous ions,  $H_2O_2$  can also be converted through the Fenton reaction to produce the highly reactive  $\cdot OH$  (Fig. 1.1B) (Schieber and Chandel, 2014; Lambeth, 2004).

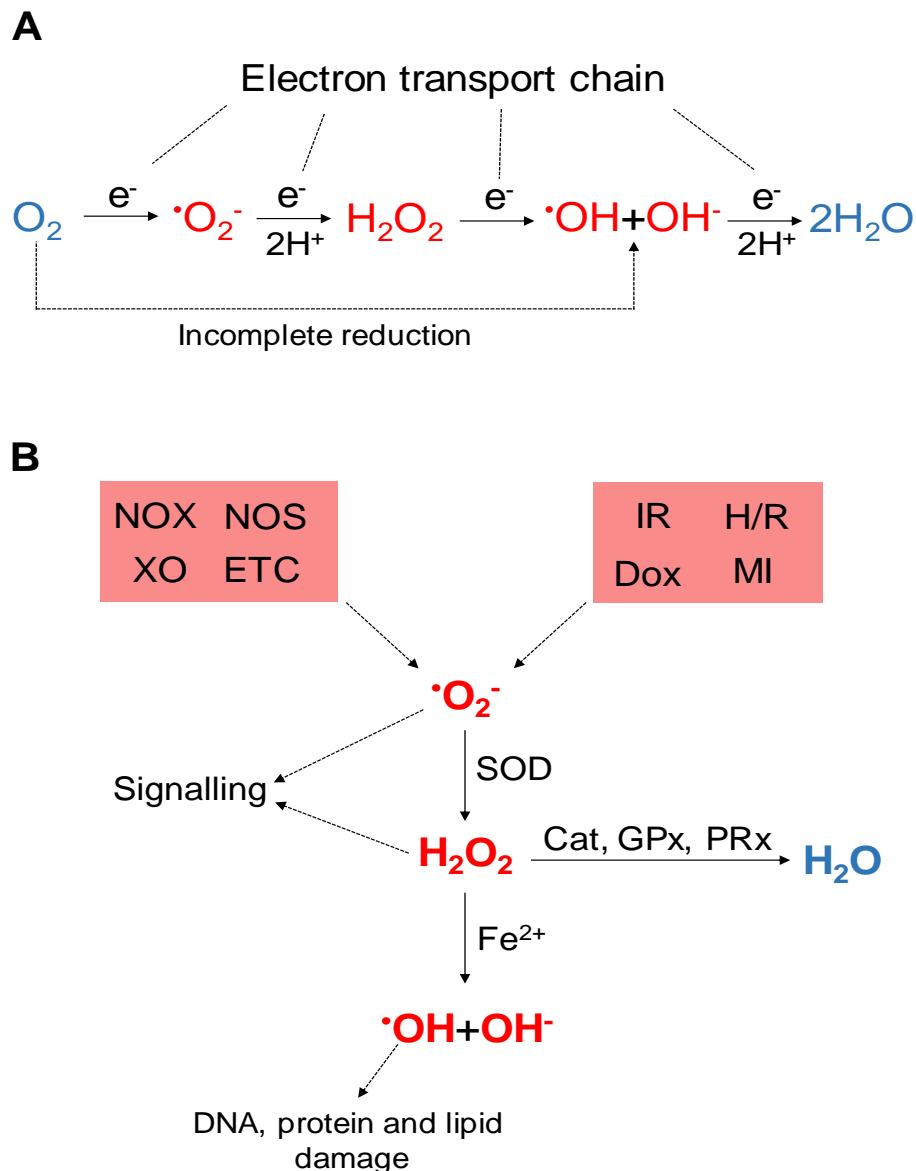


**Figure 1.1 Generation of reactive oxygen species (ROS)**

(A) Production of ROS through incomplete reduction of O<sub>2</sub>. Electrons “leaking” from the mitochondrial electron transport chain (ETC) during aerobic respiration cause sequential single electron (e<sup>-</sup>) reduction of O<sub>2</sub> to superoxide anion (·O<sub>2</sub><sup>-</sup>), H<sub>2</sub>O<sub>2</sub>, hydroxyl radical (·OH) and hydroxyl anion (OH<sup>-</sup>). (B) Intracellular sources of ROS. ROS are produced by NADPH oxidases (NOX), uncoupled nitric oxide synthases (NOS), xanthine oxidases (XO) and secondary to aerobic respiration in the mitochondrial ETC. ROS are also produced during pathophysiological processes including ischaemia and reperfusion (IR), hypoxia and reoxygenation (H/R), myocardial infarction (MI) and following exposure to drugs such as doxorubicin (Dox). Superoxide dismutases (SOD) increase the rate of ·O<sub>2</sub><sup>-</sup> conversion to H<sub>2</sub>O<sub>2</sub>, which can be reduced by catalase (Cat), glutathione peroxidases (GPx) or peroxiredoxins (PRx) to produce H<sub>2</sub>O. H<sub>2</sub>O<sub>2</sub> may also be converted to ·OH and OH<sup>-</sup> through Fenton chemistry in the presence of Fe<sup>2+</sup>. ·O<sub>2</sub><sup>-</sup> and H<sub>2</sub>O<sub>2</sub> can modulate signalling pathways and cellular processes, while ·OH is typically damaging to biomolecules.

The various forms of ROS are small, diffusible molecules and as such fulfil many criteria required of second messengers in signalling. ROS function in signal transduction by inducing specific oxidative modifications in target signalling molecules, particularly of thiol-containing methionine and cysteine residues (Kaya et al., 2015; Garcia-Santamarina et al., 2014). Perhaps the most extensively characterised modification induced by ROS is the oxidation of protein cysteine thiols by  $H_2O_2$ , and this is arguably the most salient oxidative modification with respect to intracellular signalling. Despite the relatively low abundance of cysteine residues generally, they are frequently found in functional regions of proteins (Garcia-Santamarina et al., 2014). Oxidation-sensitive cysteine thiols typically have a low  $pK_a$  and at physiological pH tend to exist as the deprotonated thiolate anion (Cys-S<sup>-</sup>). Thiolate anions are readily oxidised by  $H_2O_2$  to form the highly reactive sulfenic species (Cys-SOH) which may result in effects such as changes in enzyme activity or formation of intra- or inter-protein disulfide bonds with vicinal thiols, resulting in protein conformational changes (Burgoyne et al., 2012; Schieber and Chandel, 2014). Thus, fluctuations in ROS production can result in activation or modulation of signalling pathways. A transient increase in intracellular  $H_2O_2$  secondary to ligand binding was established as a key mediator of platelet-derived growth factor (PDGF) signalling in vascular smooth muscle cells by Sundaresan and colleagues (Sundaresan et al., 1995) and a similar scenario was subsequently demonstrated as a requisite for epidermal growth factor (EGF) signalling, using A431 human carcinoma cells (Bae et al., 1997; Finkel, 2011).

Increases in intracellular ROS levels can also elicit responses by targeting proteins which repress the activation of specific signalling pathways. For example, apoptosis signal-regulating kinase 1 (ASK1) is maintained in an inactive complex by binding to the redox-sensitive protein thioredoxin. Exposure to ROS leads to thioredoxin oxidation, resulting in dissociation from ASK1 and promoting activation of ASK1 and downstream effects in regulation of apoptosis (Saitoh et al., 1998). A further well-established redox-sensitive target is the catalytic site cysteine of protein tyrosine phosphatase superfamily members. Protein tyrosine phosphatases including PTP1B and Shp2 execute key roles in regulation of tyrosine phosphorylation status,

with important implications for signal transduction downstream of tyrosine phosphorylation events. Protein tyrosine phosphatase catalytic site cysteines exhibit a particularly low  $pK_a$  relative to other cysteines and are thus readily oxidised by  $H_2O_2$ , resulting in inhibition of phosphatase activity and activation of key signalling pathways such as mitogen-activated protein kinases (MAPKs, see section 1.3) (Bae et al., 1997; Lee et al., 1998; Lee and Esselman, 2002; Meng et al., 2002).

A key characteristic of signalling modifications is reversibility, as regulation of magnitude and duration of signalling is required to ensure an appropriate response. Accordingly, oxidation of thiolate anions to the Cys-SOH form is reversible by reducing agents, but in the presence of substantially elevated  $H_2O_2$  concentrations, thiolate anions may undergo higher-order oxidation to the sulfinic (Cys-SO<sub>2</sub>H) or sulfonic (Cys-SO<sub>3</sub>H) forms, which may be irreversible and hence deleterious due to permanent effects on protein structure and function (Schieber and Chandel, 2014; Garcia-Santamarina et al., 2014). The necessity for redox modifications in signalling to be rapid and reversible has also led to evolution of mechanisms for spatiotemporal control of ROS production and removal. For example, mitochondria may undergo translocation to the perinuclear region in response to hypoxia, leading to directed accumulation of nuclear ROS and resulting in modulation of transcriptional activity (Al-Mehdi et al., 2012). Similarly, localisation of antioxidant enzymes and other proteins such as glutathione and thioredoxin is directed to specific compartments to counteract high levels of ROS production, thus ensuring tight regulation of intracellular ROS concentrations and resulting redox modifications (Kaludercic et al., 2014).

Despite the important homeostatic and physiological signalling roles of redox reactions, dysregulation of redox signalling and excess production of ROS is deleterious and results in increased oxidative stress. Oxidative stress can be defined as an imbalance in production of ROS relative to the antioxidant defence mechanisms of a biological system, thus resulting in cellular damage. Increased oxidative stress is associated with aging, the pathogenesis of cancers and neurodegenerative disorders and cardiovascular diseases including

atherosclerosis, HF and IR injury (Pashkow, 2011; Tsutsui et al., 2011). While the majority of ROS are produced by mitochondria as a by-product of aerobic respiration, production of ROS is also potentiated by pathological processes including IR and hypoxia/reoxygenation (Fig. 1.1B) (Hausenloy and Yellon, 2013). ROS are also elaborated following administration (whether experimentally or in a clinical setting) of cardiotoxic agents such as chelerythrine, and the anti-cancer drugs doxorubicin and fluorouracil (Sawyer et al., 2002; Clerk et al., 2007a; Pai and Nahata, 2000). Pathologically elevated levels of intracellular ROS (i.e. oxidative stress) can result in cell damage, as ROS directly induce deleterious modifications of biomolecules including DNA, lipids, and proteins (Finkel, 2011).

### **1.2.2 Modulation of cardiomyocyte life and death by oxidative stress**

In the heart, redox modifications of methionine and cysteine residues in myocardial proteins can effect changes in activity and structure of diverse targets including ion transporters, receptors, kinases, and phosphatases, leading to activation of signalling pathways and potentially to oxidative stress and perturbations of homeostasis (Burgoyne et al., 2012). Amongst the most severe insults encountered by the heart is IR, such as that encountered during acute MI and following thrombolytic therapy. While IR has a wide range of effects on cardiomyocytes, it is associated with extensive cardiomyocyte death and a significant increase in ROS and oxidative stress (Hausenloy and Yellon, 2013). The cessation of blood flow, and therefore provision of oxygen, to the myocardium during ischaemia results in suppression of aerobic respiration and ATP production, increased ATP hydrolysis and concomitant acidosis, and overload of  $\text{Ca}^{2+}$  and  $\text{Na}^+$  due to disturbance of ATP-dependent ion transporter activity (Hausenloy and Yellon, 2013). Counterintuitively, despite the cessation of oxygen supply, ROS levels actually increase during ischaemia due to incomplete reduction of residual myocardial  $\text{O}_2$  (Zweier et al., 1987; Becker et al., 1999). Reintroduction of  $\text{O}_2$  upon reperfusion, however, causes a profound increase in ROS production, frequently characterised as a “ROS burst”, as

a result of resumption of aerobic phosphorylation (Hearse et al., 1973; Raedschelders et al., 2012).

Oxidative stress is a pivotal regulator of the balance between cardiomyocyte survival and death, and the level of stress encountered is a key determinant of the response. High levels of ROS causing severe oxidative stress are cardiotoxic and result in cardiomyocyte necrosis, while moderate levels are permissive for regulated death and thus promote apoptosis (Von Harsdorf et al., 1999; Cook et al., 1999b; Kwon et al., 2003). Conversely, low levels of ROS may be cardioprotective. Brief periods of non-lethal ischaemia, resulting in increased ROS, can confer enhanced myocardial resistance to subsequent ischaemic insult, a phenomenon referred to as ischaemic preconditioning (IPC) (Murry et al., 1986). IPC has a biphasic response consisting of a transient early period of protection that develops rapidly upon ischaemia and disappears after 2 – 4 h, and a delayed onset “second window of protection” (SWOP) that manifests 12 – 24 h after ischaemia and persists for several days. Although the exact mechanisms underlying the response are not fully understood, ROS are clearly implicated, and some investigations indicate that the SWOP is induced by *de novo* protein synthesis and transcription of cardioprotective genes as a result of signalling pathways activated downstream of ROS (Rizvi et al., 1999). Indeed, inhibition of ROS production during ischaemia abrogates the protective effect of IPC and results in the absence of the SWOP (Sun et al., 1996). Exposure of neonatal and/or adult rat cardiomyocytes to low levels of directly applied ROS in the form of H<sub>2</sub>O<sub>2</sub> may also confer protection, and some investigators report induction of hypertrophy (Aikawa et al., 1997; Kwon et al., 2003; Chen et al., 2000).

Severe myocardial insult resulting from IR, associated with high levels of ROS production and oxidative stress, results in necrotic cardiomyocyte death (or a combination of both necrosis and apoptosis) and thus contributes to development of conditions such as HF (McCully et al., 2004; Gandhi et al., 2011). Direct exposure of adult rat cardiomyocytes or cardiac-derived H9c2 cells to H<sub>2</sub>O<sub>2</sub> also results in necrosis at higher concentrations (0.3 – 1 mM, depending on the cell type) as determined using propidium iodide (PI) incorporation (Kwon et al., 2003;

Wang et al., 2013; Wang et al., 2015). Moderate H<sub>2</sub>O<sub>2</sub> concentrations, however, can result in regulated apoptotic death through the “intrinsic” (or mitochondrial) pathway. Apoptosis is characterised by the ordered, ATP-dependent dismantling and removal of cellular components, and is generally considered to proceed largely in the absence of an inflammatory response (Mcilwain et al., 2013). Apoptosis is executed by a family of endopeptidases, the cysteine-dependent aspartate-directed proteases (caspases) which, as implied by their name, mediate the cysteine-dependent cleavage of peptide bonds, directed by specific Asp residues in their substrates (Mcilwain et al., 2013).

Activation of caspases through the intrinsic pathway is precipitated by the release of cytochrome *c* into the cytoplasm from the inner mitochondrial membrane (Fig. 1.2), resulting in formation of the large, caspase activating complex known as the apoptosome (Zou et al., 1997; Acehan et al., 2002). Once released, cytochrome *c* binds to the WD-40 domain of the apoptotic protease-activating-factor-1 (Apaf1) adapter protein (Fig. 1.2), leading to Apaf1 heptamerisation and exposure of the Apaf1 caspase recruitment domain (CARD) (Fig. 1.2) (Acehan et al., 2002). The Apaf1 CARD provides a docking site for the binding of “initiator” caspase-9, which is activated following hetero-oligomerisation directed by Apaf1. Thence, caspase-9 mediates cleavage and activation of the “effector” caspase-3 resulting in proteolytic dismantling of cellular constituents and apoptosis (Fig. 1.2) (Mcilwain et al., 2013; Shiozaki et al., 2002). The release of cytochrome *c* from the inner mitochondrial membrane is regulated by factors including opening of the mitochondrial permeability transition pore (MPTP), associated with loss of  $\Delta\psi_m$  and impairment of ATP production through oxidative phosphorylation (Halestrap et al., 2004). Cytochrome *c* release is also influenced by the activity of the Bcl-2 family proteins, which variously function in both anti- and pro-apoptotic roles (Czabotar et al., 2014).

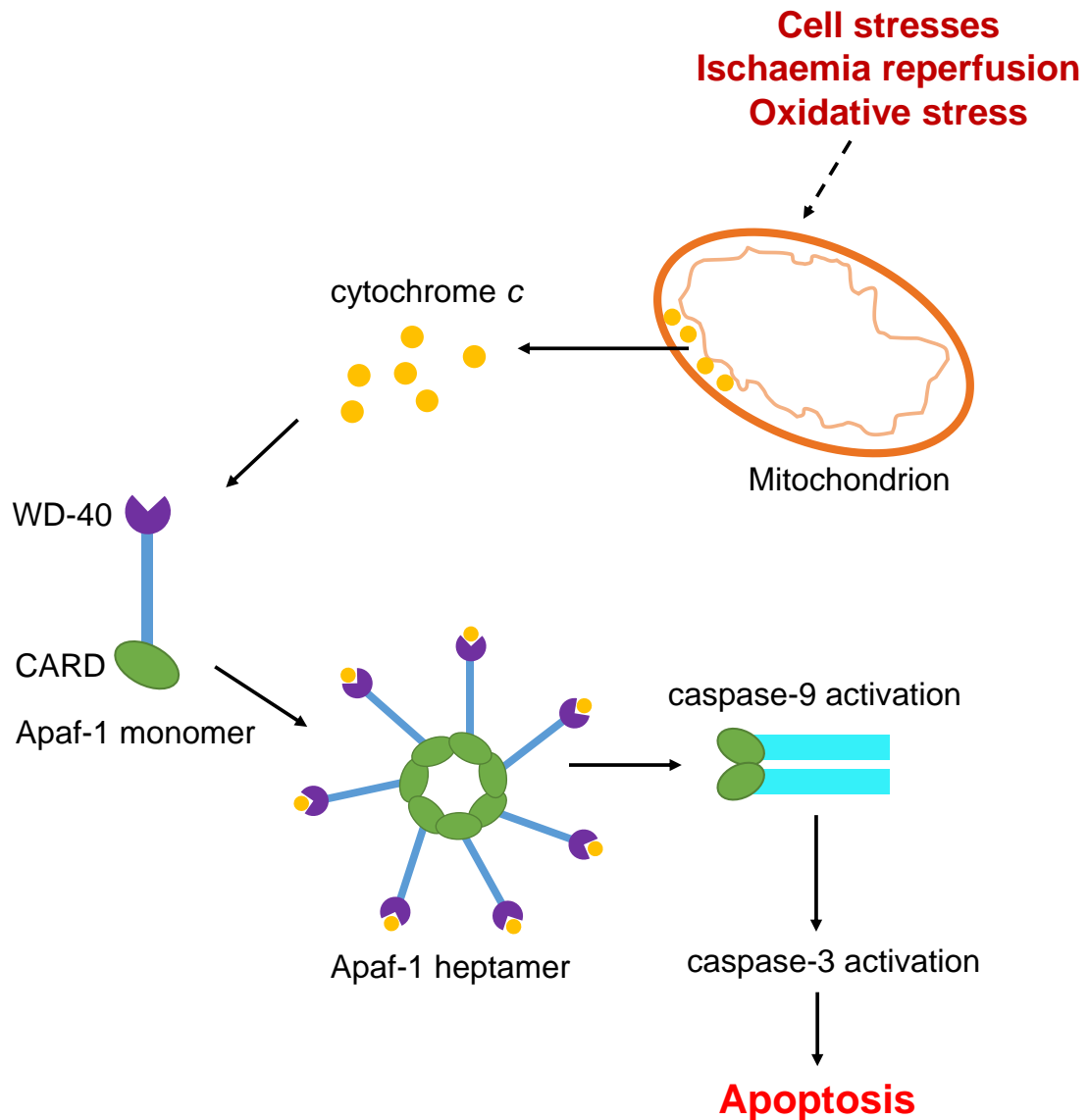


**Figure 1.2 Activation of the mitochondrial apoptosis pathway**

Exposure to cellular stresses including ischaemia reperfusion or oxidative stress (exemplified by  $H_2O_2$ ) results in the release of cytochrome *c* from the inner mitochondrial membrane. Cytochrome *c* binds to the WD-40 domains of Apaf-1 resulting in assembly of the Apaf-1 heptamer and exposure of the Apaf-1 caspase recruitment domain (CARD). Interaction between the Apaf-1 and pro-caspase-9 CARDS leads to activation of initiator caspase-9. Caspase-9 then cleaves and activates effector caspase-3, resulting in cell death through apoptosis.

Numerous investigations indicate that cultured neonatal and/or adult rat cardiomyocytes, or H9c2 cardiac-derived cells, exposed to moderate H<sub>2</sub>O<sub>2</sub> concentrations (0.1 – 0.5 mM; depending on the specific cell type) die by apoptosis (Cook et al., 1999b; Von Harsdorf et al., 1999; Chen et al., 2000; Kwon et al., 2003; Hong et al., 2001; Clerk et al., 2007b). Using neonatal cardiomyocytes, von Harsdorf *et al.* (Von Harsdorf et al., 1999) demonstrated that exposure to H<sub>2</sub>O<sub>2</sub> reduced cardiomyocyte viability and increased terminal deoxynucleotidyl dUTP nick-end labelling (TUNEL)-positive nuclei, reflective of DNA fragmentation and apoptotic death. Cardiomyocyte apoptosis initiated by administration of xanthine oxidase in the presence of xanthine could be rescued with the addition of exogenous SOD, catalase, or a combination thereof, indicating that both <sup>•</sup>O<sub>2</sub><sup>-</sup> and H<sub>2</sub>O<sub>2</sub> induce apoptosis (Von Harsdorf et al., 1999). Cook and colleagues (Cook et al., 1999b) also reported induction of neonatal cardiomyocyte apoptosis following exposure to H<sub>2</sub>O<sub>2</sub> using several different readouts. Exposure to H<sub>2</sub>O<sub>2</sub> resulted in activation of caspase-3 and cleavage of poly(ADP-ribose) polymerase, an established caspase-3 substrate, and a progressive increase in TUNEL-positive cardiomyocyte nuclei (Cook et al., 1999b).

Exposure of cardiomyocytes to H<sub>2</sub>O<sub>2</sub> is associated with a progressive increase of cytochrome c in the cytoplasm, indicating release from the mitochondria in response to oxidative stress (Cook et al., 1999b; Von Harsdorf et al., 1999), and this is temporally associated with a reduction in  $\Delta\psi_m$ , a phenomenon potentially reflective of opening of the MPTP or other pores in the mitochondrial membrane. However,  $\Delta\psi_m$  is partially restored following 45 – 60 min exposure to H<sub>2</sub>O<sub>2</sub> (Cook et al., 1999b). Since cytochrome c and  $\Delta\psi_m$  are required for oxidative phosphorylation in the mitochondria (Huttemann et al., 2011), the partial restoration of  $\Delta\psi_m$  and residual levels of mitochondrial cytochrome c may be reflective of continued capacity for respiration and ATP production, potentially influencing whether cardiomyocyte death proceeds through ATP-dependent apoptosis or otherwise by necrosis.

Induction of cardiomyocyte apoptosis by H<sub>2</sub>O<sub>2</sub> is also associated with differential regulation of Bcl-2 family members. Antiapoptotic members including the prototypic Bcl-2 and the related

Bcl-xL are expressed in neonatal rat hearts and this is sustained throughout maturation to adulthood. Conversely, expression of the pro-apoptotic Bcl-2 family members, Bad and Bax, are subject to developmental downregulation (Cook et al., 1999b). In unstimulated cardiomyocytes, Bcl-2 localises predominantly to the mitochondria while Bad is detected primarily in the cytoplasm. H<sub>2</sub>O<sub>2</sub> exposure induces loss of Bcl-2, and accumulation of Bad, at the mitochondria. Conversely, Bad rapidly shuttles to the mitochondria following H<sub>2</sub>O<sub>2</sub> exposure, preceding cytochrome c release, potentially indicative of a role for Bad in initiation of the intrinsic pathway of cardiomyocyte apoptosis in response to H<sub>2</sub>O<sub>2</sub> (Cook et al., 1999b).

In addition to directly applied oxidative stress in the form of H<sub>2</sub>O<sub>2</sub>, ROS are also pivotal in mediating cardiomyocyte apoptosis in response to other pathophysiological insults. Clinical use of the antineoplastic anthracycline doxorubicin is limited by its well-established cardiotoxic effects, which are associated with increased cardiomyocyte apoptosis (Arola et al., 2000; Childs et al., 2002). Administration of doxorubicin causes accumulation of H<sub>2</sub>O<sub>2</sub> and mitochondrial <sup>•</sup>O<sub>2</sub><sup>-</sup> in the intact heart (Doroshov, 1983), and activates the mitochondrial pathway to apoptosis in cardiomyocytes; an effect which is inhibited by exposure to antioxidants (Kotamraju et al., 2000). The protein kinase C (PKC) inhibitor chelerythrine also induces apoptosis in cardiomyocytes and adult rat hearts, albeit in a PKC-independent manner (Yamamoto et al., 2001). Like doxorubicin, chelerythrine induces apoptosis through the mitochondrial pathway and this can be inhibited by administration of antioxidants, indicating a central role of ROS in induction of cardiomyocyte apoptosis in this context (Yamamoto et al., 2001). As with IR in whole organs, deprivation of oxygen during hypoxia followed by reoxygenation results in increased ROS production in cultured cells (Kang et al., 2000) and can lead to an increase in cell death. Adult rat cardiomyocytes subjected to hypoxia exhibit increased apoptotic death relative to normoxic controls, and induction of apoptosis is increased further in response to reintroduction of oxygen following hypoxia (Kang et al., 2000).

### 1.2.3 Regulation of cardiomyocyte gene expression by oxidative stress

As discussed in section 1.2.2, oxidative stress is a key regulator of the balance between survival and death of cardiomyocytes, and increased oxidative stress is associated with the pathogenesis of conditions such as HF. The response of the cardiomyocyte depends on the extent of the oxidative stress encountered, and ranges from cytoprotection and survival in response to low levels to death by apoptosis or necrosis in response to moderate or high levels, respectively.

H<sub>2</sub>O<sub>2</sub>, a physiologically relevant form of oxidative stress, is generated in the myocardium following ischaemia with or without reperfusion (Slezak et al., 1995). Since H<sub>2</sub>O<sub>2</sub> is relatively stable (compared to the much more reactive <sup>•</sup>O<sub>2</sub><sup>-</sup>, <sup>•</sup>OH and OH<sup>-</sup> species) and easily manipulable under experimental conditions, it has become an important means of inducing, and investigating the effects of, oxidative stress in cardiac model systems. As discussed, H<sub>2</sub>O<sub>2</sub> promotes apoptotic cell death, and this response is coincident with substantial changes in cardiomyocyte gene expression (Kemp et al., 2003; Clerk et al., 2007b). The changes in gene expression induced by H<sub>2</sub>O<sub>2</sub> are both time and concentration dependent, and these changes probably contribute at least in part to the ultimate response of the cell.

Microarray expression profiling investigations indicate that exposure of neonatal rat cardiomyocytes to H<sub>2</sub>O<sub>2</sub> results in both upregulation and downregulation of genes. Exposure to a non-toxic H<sub>2</sub>O<sub>2</sub> concentration (0.04 mM) results in changes in relatively few genes (Kemp et al., 2003; Clerk et al., 2007b). However, a pro-apoptotic H<sub>2</sub>O<sub>2</sub> concentration of 0.2 mM induces far more substantial changes in RNA expression following a 2 – 24 h exposure time, representing 649 established genes (Clerk et al., 2007b). Many of the upregulated genes code for proteins associated with cytoprotection and/or antioxidation, including Gclc (glutamate-cysteine ligase catalytic subunit), Gclm (glutamate-cysteine ligase regulatory subunit, Nqo1 (NAD(P)H quinone dehydrogenase 1), Txnrd1 (thioredoxin reductase 1), Fdx1 (ferredoxin 1) and Glx1 (glutaredoxin 1). Notably, the cyclin-dependent kinase inhibitor p21<sup>Cip1/Waf1</sup> is upregulated in response to H<sub>2</sub>O<sub>2</sub> (Kemp et al., 2003; Clerk et al., 2007b), and, while its role in

the heart has not been well-established, p21<sup>Cip1/Waf1</sup> induces cell cycle arrest and cytoprotection in other systems (Barnouin et al., 2002). Furthermore, a detailed investigation examining expression of the rat orthologue of Mdm2 confirmed that pro-apoptotic H<sub>2</sub>O<sub>2</sub> concentrations lead to upregulation of Mdm2 mRNA and protein (Pikkarainen et al., 2009). Knockdown of Mdm2 protein in neonatal rat cardiomyocytes also resulted in potentiation of apoptosis induced by H<sub>2</sub>O<sub>2</sub>, suggestive of a protective effect of Mdm2 upregulation in response to H<sub>2</sub>O<sub>2</sub> (Pikkarainen et al., 2009).

In addition to genes with putatively cytoprotective functions, numerous genes associated with regulation of transcription and intracellular signalling are also upregulated. These include the dual-specificity phosphatases (Dusps), several Krüppel-like factor (Klf) family members and early growth response (Egr) 1 – 4 transcription factors (Clerk et al., 2007b), suggesting that at least some of the changes in gene expression during H<sub>2</sub>O<sub>2</sub>-induced apoptosis are associated with expression of factors involved in regulation of the ongoing response to the encountered oxidative stress. Cardiomyocytes exposed to 0.1 – 0.5 mM H<sub>2</sub>O<sub>2</sub> are ~25 – 75% TUNEL-positive following 16 – 24 h exposure, indicative of DNA fragmentation and an advanced stage of apoptosis (Cook et al., 1999b). Although changes in expression of the largest number of genes occur in response to H<sub>2</sub>O<sub>2</sub> at times of 2 – 4 h, early in apoptosis, changes in a small number of genes are also detectable up to 24 h (Clerk et al., 2007b), suggesting a sustained active response to the increase in oxidative stress by some cardiomyocytes.

These investigations indicate that pro-apoptotic H<sub>2</sub>O<sub>2</sub> concentrations induce changes in the expression of a large number of genes in cardiomyocytes, while non-toxic H<sub>2</sub>O<sub>2</sub> levels have a substantially lesser impact. The identities and functions of those genes upregulated during H<sub>2</sub>O<sub>2</sub>-induced apoptosis (including those associated with cytoprotection and antioxidation as well as regulators of transcription and intracellular signalling) strongly suggest that these changes influence the ultimate response of the cardiomyocyte and contribute to the process of apoptosis. However, the intracellular signalling pathways and regulatory mechanisms associated with the induction of these changes in gene expression are yet to be elucidated.

### **1.3 Mitogen-activated protein kinase (MAPK) signalling**

The MAPKs are highly conserved and ubiquitously expressed proline-directed Ser/Thr protein kinases. They represent some of the most important, and most extensively characterised, transcytoplasmic signalling pathways delivering signals from extracellular stimuli to the nucleus (Widmann et al., 1999; Zhang and Liu, 2002). While other MAPKs such as extracellular signal-regulated kinase (ERK) 5 have been identified (Lee et al., 1996), the three best-characterised MAPK pathways are ERK1/2, the c-Jun N-terminal kinases (JNKs) and the p38-MAPKs. Generally, signalling through these MAPKs is associated with diverse cellular functions including growth and proliferation, differentiation and death (Zhang and Liu, 2002; Roux and Blenis, 2004).

#### **1.3.1 Activation and roles of the MAPK cascades**

All MAPK pathways consist of hierarchical cascades that lead to the phosphorylation and concomitant activation of terminal effector kinases (Fig. 1.3). Canonically, MAPK kinase kinases (MAP3Ks) phosphorylate and activate MAPK kinases (MKKs). Thence, MKKs dually phosphorylate MAPKs on threonine and tyrosine residues within a conserved Thr-Xaa-Tyr kinase regulatory motif, resulting in the full activation and downstream effects of the MAPKs (Rose et al., 2010). The various MAPK subfamilies are differentially activated in response to diverse stimuli and are coupled to a variety of cell surface receptor types.

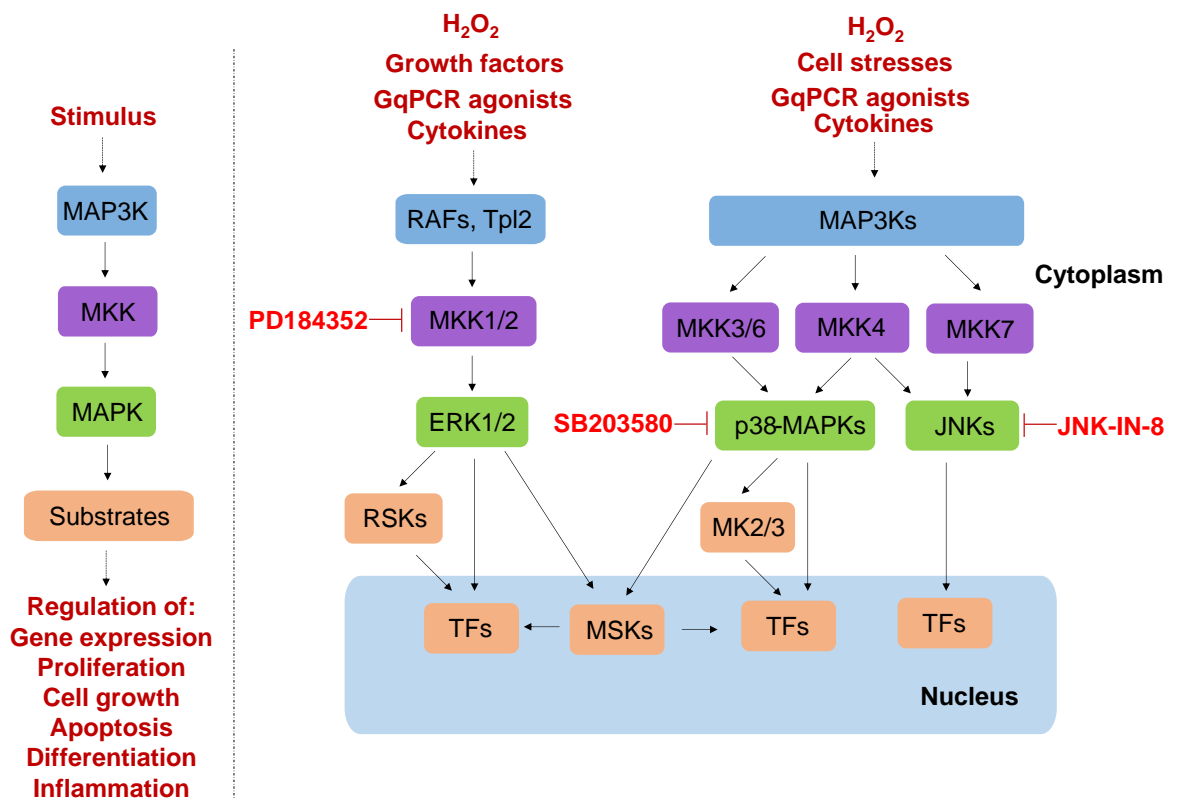


**Figure 1.3 Mitogen-activated protein kinase (MAPK) cascades**

The best characterised MAPKs, ERK1/2, JNKs and p38-MAPKs are the terminal members of three-tiered phosphorylation cascades.  $H_2O_2$  (as an example of oxidative stress), growth factors (e.g. EGF, PDGF, FGF), agonists of receptors coupled to Gq alpha subunits (GqPCR agonists; e.g. ET-1, phenylephrine, A61603) and cytokines lead to activation of Raf family or Tpl2 MAP3Ks, resulting in phosphorylation and activation of MKK1/2 and thence ERK1/2. ERK1/2 phosphorylate substrates including p90 ribosomal S6 kinases (RSKs), mitogen- and stress-activated kinases (MSKs) and a number of transcription factors (e.g. Elk-1, GATA4, c-Fos, c-Jun) leading to modulation of transcription and other cellular processes. Inhibition of MKK1/2 with PD184352 blocks ERK1/2 activation. JNKs and p38-MAPKs are most potently activated by oxidative and cellular stresses, cytokines and to a lesser extent by GqPCR agonists. MKK3/6 preferentially activate p38-MAPKs while MKK7 activates JNKs. MKK4 can activate both p38-MAPKs and JNKs. MAPK3Ks upstream of JNKs and p38-MAPKs are not well defined but may include ASK1 and MEKKs. Substrates of p38-MAPKs include MAPKAPK2/3 (MK2/3), MSKs and various transcription factors (e.g. MEF2C, ATF2). Targets of JNKs are primarily transcription factors (e.g. c-Jun, ATF2). Activity of p38-MAPK $\alpha/\beta$  is inhibited by SB203580 while JNKs are inhibited by JNK-IN-8.

### 1.3.1.1 Extracellular signal-regulated kinases 1 and 2 (ERK1/2)

The prototypic MAPK family members are ERK1/2 are encoded by the *MAPK3* and *MAPK1* genes, producing the ERK1 and ERK2 products, respectively. ERK1/2 are also commonly referred to as p44- and p42-MAPKs, reflecting their respective molecular weights (ERK1, ~44 kDa; ERK2, ~42 kDa). ERK1/2 are activated by phosphorylation within a Thr-Glu-Tyr activation loop (Thr202 and Tyr204 in human ERK1) by their MKKs, MKK1/2 (Fig. 1.3), while the most extensively characterised upstream kinases for the ERK1/2 cascade are kinases of the Raf family, c-Raf, A-Raf and B-Raf) (Fig. 1.3). (Payne et al., 1991; Wortzel and Seger, 2011). MKK1/2 (and thence ERK1/2) are also activated by a further MAP3K, Tpl2, in some conditions, for example in response to lipopolysaccharide (Dumitru et al., 2000; Martel et al., 2013). Once activated, ERK1/2 modulate the activities of their various substrates by preferentially phosphorylating Ser/Thr residues within Pro-Xaa-Ser/Thr-Pro sequence motifs (Davis, 1993).

Target substrates are located in both the cytoplasmic and nuclear compartments and include transcription factors as well as other kinases, referred to as MAPK-activated protein kinases (MAPKAPKs) (Fig. 1.3). Nuclear substrates of activated ERK1/2 include numerous DNA binding transcription factors (e.g. Elk1, GATA4, c-Fos, c-Jun), whose transactivating activities or affinities for binding other transcription factors and proteins are modulated by phosphorylation, allowing ERK1/2 to directly influence regulation of transcription (Roskoski, 2012; Plotnikov et al., 2011). Amongst the best characterised kinase substrates of ERK1/2 are the p90 ribosomal S6 kinases (RSKs) and the mitogen- and stress-activated kinases (MSKs) (Fig. 1.3). The MSKs and their substrates are predominantly localised in the nucleus and are associated with regulation of transcription and inflammation (Reyskens and Arthur, 2016). In common with ERK1/2, RSKs are generally localised to the cytoplasm under basal conditions but can phosphorylate and regulate substrates in both the cytoplasm and the nucleus upon stimulation, influencing processes including cell cycle progression and transcription. However, the consensus sequences for phosphorylation by RSKs, Arg/Lys-Xaa-Arg-Xaa-Xaa-Ser/Thr (Pearce et al., 2010), are different to those for ERK1/2 and accordingly their substrates are

distinct. This affords divergent signalling from ERK1/2 and RSKs, influencing different processes depending on the specific substrates targeted (Roux and Blenis, 2004).

Activation of the ERK1/2 cascade in cardiomyocytes is typically associated with ligand stimulation of membrane-bound receptors, particularly receptor protein tyrosine kinases (RPTKs) and G protein-coupled receptors (GPCRs) (Clerk et al., 2007a). RPTK agonists associated with activation of ERK1/2 in cardiomyocytes include several peptide growth factors (Clerk et al., 2006). While the exact mechanisms by which the receptors respond is dependent on the specific stimulus, binding of RPTKs by their cognate ligand generally induces receptor oligomerisation or conformational change followed by activation of intrinsic tyrosine kinase activity, leading to autophosphorylation of specific tyrosine residues in the receptor intracellular domain. This forms the basis for the assembly of an active signalling complex, recruiting scaffold proteins (e.g. Grb2) and nucleotide exchange factors (e.g. Sos) through association of phospho-tyrosine residues on the receptor with Src homology 2 or phospho-tyrosine binding domains located on the scaffold proteins. Localisation of the guanine nucleotide exchange factor Sos in the vicinity of the small G-protein Ras promotes exchange of GDP for GTP to produce the active GTP-bound Ras form. Activated Ras then promotes recruitment and activation of Raf family MAP3Ks to initiate the ERK1/2 cascade (Schlessinger, 2000; Clerk et al., 2006). Stimulation of RPTKs may also be coupled (dependent on the specific scaffolding and adapter molecules) to activation of the ERK1/2 cascade through activation of phospholipase C (PLC)  $\gamma$  and PKC isoforms (Clerk et al., 2006; Clerk et al., 2007a). EGF, PDGF and fibroblast growth factor (FGF) all activate the ERK1/2 cascade in cardiomyocytes, and are associated with induction of the hypertrophic phenotype (Bogoyevitch et al., 1994; Clerk et al., 2006).

Stimulation of members of the large, highly conserved GPCR superfamily is also associated with activation of ERK1/2, and signalling through G $\alpha_q$  subunits is arguably most salient with respect to cardiomyocytes. Stimulation of GqPCRs results in exchange of GDP for GTP on the G $\alpha_q$  subunit, promoting activation of PLC $\beta$ , which hydrolyses the membrane phospholipid

phosphatidylinositol-4,5-bisphosphate (PtdInsP<sub>2</sub>) to diacylglycerol (DAG) and inositol 1,4,5-trisphosphate (InsP<sub>3</sub>). This results in the activation of DAG-sensitive PKC isoforms and thence ERK1/2 (Sugden and Clerk, 1997; Clerk and Sugden, 1999). Important GqPCR agonists leading to ERK1/2 activation in cardiomyocytes include endothelin-1 (ET-1) and the  $\alpha$ -adrenergic agonists phenylephrine and A61603. These are associated with induction of hypertrophy and modulation of gene expression (Kennedy et al., 2006; Cullingford et al., 2008b; Marshall et al., 2010; Amirak et al., 2013).

Importantly, and in common with the JNKs and p38-MAPKs (discussed below), oxidative stress (exemplified by H<sub>2</sub>O<sub>2</sub>) induces ERK1/2 activation in cardiomyocytes. In cardiomyocytes, ERK1/2 are activated in response to pro-apoptotic H<sub>2</sub>O<sub>2</sub> concentrations although the degree and duration of activation is time and concentration dependent and varies depending on the experimental system used (i.e. in isolated neonatal rat cardiomyocytes vs perfused adult rat hearts) (Clerk et al., 1998a; Clerk et al., 1998b; Aikawa et al., 1997). In the context of exposure to H<sub>2</sub>O<sub>2</sub> it is possible that activation of ERK1/2 signalling is associated with promotion of cardiomyocyte survival, as pharmacological inhibition of the pathway increases cardiomyocyte apoptosis induced by H<sub>2</sub>O<sub>2</sub> (Aikawa et al., 1997).

### **1.3.1.2 c-Jun N-terminal kinases (JNKs)**

JNKs are expressed as ~46 and ~54 kDa proteins (p46-JNKs and p54-JNKs, respectively) with at least ten distinct isoforms derived from alternatively spliced variants of the three JNK genes, of which *JNK1* and *JNK2* are expressed universally (Davis, 2000). JNKs are activated by phosphorylation of Thr and Tyr residues in a Thr-Pro-Tyr activation motif by their upstream dual-specificity kinases MKK4 and MKK7 (Fig. 1.3) (Sanchez et al., 1994; Foltz et al., 1998; Lawler et al., 1998). There are numerous upstream activators of MKK4/7 depending on the input, including ASK1, MEKK1-4, TAK1 and DLK (Cargnello and Roux, 2011).

JNK activity was originally characterised in the context of Ser/Thr phosphorylation of microtubule-associated protein 2 in response to cycloheximide (Kyriakis and Avruch, 1990). However, JNKs are now known to be induced by a range of stimuli including pro-inflammatory cytokines such as tumour necrosis factor (TNF)  $\alpha$  and interleukin (IL) 1 $\beta$ , and particularly by cellular stresses including ultraviolet radiation, hyperosmotic shock and oxidative stress (Clerk and Sugden, 1999; Davis, 2000; Rose et al., 2010). In non-cardiac cells, JNKs regulate activity of the transcription factor c-Jun by phosphorylation of two serine residues (Ser63 and Ser73) in the N-terminal transactivation region (Hibi et al., 1993). JNKs also regulate activity of other transcription factors (ATF2, Elk1, Sap1a, p53 etc.) either by directly modulating transcriptional transactivation activity or regulating protein stability and abundance (Cavigelli et al., 1995; Whitmarsh et al., 1997; Fuchs et al., 1998; Clerk et al., 2002). In non-cardiac systems, JNK activity is associated with diverse functions including proliferation and regulation of both the extrinsic and intrinsic apoptotic pathways (Cargnello and Roux, 2011).

In cardiomyocytes, JNKs are potently activated by cellular stresses including hyperosmotic shock, anisomycin and oxidative stress in the form of pro-apoptotic H<sub>2</sub>O<sub>2</sub> concentrations and secondary to hypoxia/reoxygenation (Clerk and Sugden, 1997b; Clerk et al., 1998b; Laderoute and Webster, 1997). JNKs are also activated in isolated cardiomyocytes in response to TNF $\alpha$  and IL1 $\beta$  (Clerk et al., 1999) as well as, to a lesser degree, by GPCR agonists including ET-1 (Clerk et al., 2007a). In intact hearts, JNKs are powerfully stimulated by H<sub>2</sub>O<sub>2</sub>, and during reperfusion following ischaemia (but not during ischaemia) and are also activated in response to GPCR agonists such as phenylephrine and angiotensin II (Bogoyevitch et al., 1996; Lazou et al., 1998; Yano et al., 1998). Since JNKs are activated in cardiac tissues by both cytotoxic stresses and agonists associated with induction of hypertrophy, there are conflicting data as to whether activation of cardiac JNKs is associated with cytoprotection, hypertrophy or death. In one investigation, adenovirally-mediated overexpression of constitutively active (CA) MKK7 (resulting in selective activation of JNKs) in cardiomyocytes led to development of a hypertrophic phenotype (Wang et al., 1998b). Conversely, *in vivo* expression of a CA MKK7

mutant in mice resulted in cardiomyopathy and death (Petrich et al., 2002; Petrich et al., 2003). Some studies also indicate that JNK (and p38-MAPK) activities are elevated relative to donor hearts in failing human hearts (Cook et al., 1999a; Haq et al., 2001), although it is unclear whether activation of JNKs in this context is a protective or maladaptive response. Similarly, additional evidence from transgenic mice expressing dominant negative (DN) forms of JNK1/2 indicates that these mice develop cardiac hypertrophy in response to pressure overload, suggestive of a role for JNK signalling in suppression of hypertrophy (Liang et al., 2003). Furthermore, adenovirally-mediated expression of a DN JNK mutant attenuates H<sub>2</sub>O<sub>2</sub>-induced death of adult rat cardiomyocytes, suggestive that JNKs are pro-apoptotic in this context (Kwon et al., 2003).

The controversy regarding the specific roles of JNKs in mediating cardiac hypertrophy and survival vs death may result, at least in part, from differences in observations made in different model systems, whether experiments are conducted *in vivo* or *in vitro* and whether signalling is manipulated using pharmacological or genetic approaches. One potential reason for the discrepant observations regarding the roles of JNKs in signalling to hypertrophy vs death is the differential localisation and compartmentalisation of signalling components between cultured neonatal cardiomyocytes and whole hearts *in vivo* (Liang and Molkentin, 2003). Differential localisation of signalling molecules, such as JNKs, between neonatal and adult cardiomyocytes might be expected to result in disparate responses upon stimulation, for example due to factors such as availability of substrates. It is probable therefore, that the specific roles of JNKs vary, dependent on factors such as the stimulus encountered, duration of signalling and cell context and status.

#### **1.3.1.3 p38-mitogen activated protein kinases (p38-MAPKs)**

Six isoforms of p38-MAPK are derived from alternatively spliced transcripts of four genes. *MAPK14* codes for two isoforms of p38-MAPK $\alpha$ , *MAPK11* codes for two isoforms of p38-

MAPK $\beta$  while *MAPK12* and *MAPK13* code for p38-MAPK $\gamma$  and p38-MAPK $\delta$ , respectively. p38-MAPK $\alpha$  is the predominant isoform in the heart, with lower expression of p38-MAPK $\beta$  and p38-MAPK $\gamma$  (Cargnello and Roux, 2011; Marber et al., 2011). Upstream MKKs for the p38-MAPKs include MKK3 and 6 (Fig. 1.3), although despite conserved activation loop motifs amongst the various p38-MAPK isoforms, there is differential regulation by the MKKs 3 and 6. MKK6 effectively activates p38-MAPK $\alpha/\beta/\gamma$  while MKK3 is unable to efficiently activate p38-MAPK $\beta$  (Enslin et al., 1998). MKK4 (most closely associated with activation of JNKs), also activates p38-MAPKs in some contexts (Winston et al., 1997). Upstream MAP3Ks for the p38-MAPKs include ASK1, DLK1, MEK3/4 and ZAK (Cuadrado and Nebreda, 2010).

Substrates of the p38-MAPKs are numerous and varied, and the diversity of p38-MAPK targets is reflective of the pleiotropic effects of the pathway. In common with ERK1/2, p38-MAPK substrates include both transcription factors and MAPKAPKs (Fig. 1.3). The principal kinases activated by p38-MAPKs are MAPKAPK 2 and 3, which, in turn, phosphorylate the small heat shock protein 25/27 (HSP25/27) on multiple serine residues (Rouse et al., 1994); (Stokoe et al., 1992). Other targets include MSK 1 and 2 (Roux and Blenis, 2004). Additionally, and in common with JNKs and ERK1/2, p38-MAPKs regulate transcription by direct phosphorylation of transcription factors including CREB, ATF1/2/6, MEF2C, ternary complex factors and p53 (Hazzalin et al., 1996; Whitmarsh et al., 1997; Zarubin and Han, 2005). p38-MAPKs also indirectly modulate the stability of pro-inflammatory transcripts through phosphorylation of the mRNA-binding protein tristetraprolin (Brooks and Blakeshear, 2013).

Like the JNKs, activation of p38-MAPKs in cardiac tissues is most closely associated with cellular stresses. In cardiomyocytes, p38-MAPKs are potently activated by pro-apoptotic concentrations of H<sub>2</sub>O<sub>2</sub>, resulting in activation of MAPKAPK2 and phosphorylation of Hsp25/27 (Clerk et al., 1998b), and are also stimulated by TNF $\alpha$  and IL1 $\beta$  (Clerk et al., 1999). In whole hearts, p38-MAPKs (and their substrate MAPKAPK2) are activated by H<sub>2</sub>O<sub>2</sub> and high aortic pressure. In contrast with JNKs, p38-MAPKs in whole hearts are ROS-dependently activated

during global ischaemia, and this is sustained or increased upon reperfusion (Bogoyevitch et al., 1996; Clerk et al., 1998a).

In common with investigations into the roles of JNKs in the heart (discusses in Section 1.3.1.2), studies have produced inconsistent and even dichotomous results regarding the roles of p38-MAPKs in signalling to cardiac apoptosis vs cytoprotection. However, the reported disparity may be due, at least in part, to differing functions of the various isoforms. Interpretation of the literature is further complicated by the widespread use of p38-MAPK inhibitors such as SB203580, that inhibit both the p38-MAPK $\alpha/\beta$  (but not other) isoforms (Kumar et al., 1997). Adenoviral overexpression of CA MKK3/6 mutants in cardiomyocytes resulted in a characteristic hypertrophic phenotype, with enhanced atrial natriuretic factor expression and increased cell surface area and sarcomeric organisation (Wang et al., 1998a). These effects were enhanced by co-expression of wild-type p38-MAPK $\beta$  and suppressed by a DN p38-MAPK $\alpha$ . Overexpression of CA MKK3 (which preferentially activates p38-MAPK $\alpha$  rather than p38-MAPK $\beta$ ) also enhanced cardiomyocyte apoptosis, a response potentiated by co-expression of wild-type p38-MAPK $\alpha$  and attenuated by a DN p38-MAPK $\alpha$  mutant, indicating a pro-hypertrophic and cytoprotective function for the  $\beta$ -isoform and a death-promoting role for the  $\alpha$ -isoform (Wang et al., 1998a). Furthermore, transgenic mice expressing cardiomyocyte-specific CA MKK3 and CA MKK6 develop an early lethal cardiomyopathy (Liao et al., 2001). However, mice expressing only CA MKK3 exhibited significant myocyte atrophy, ventricular wall thinning and compromised diastolic function, which were absent in mice expressing CA MKK6 (Liao et al., 2001). These observations were supported by Saurin *et al.* (2000), who showed that p38-MAPK $\alpha$  is potently activated by experimentally induced ischaemia of cultured neonatal rat ventricular myocytes while the  $\beta$ -isoform is significantly inhibited. The same study also demonstrated that cardiomyocytes expressing a DN p38-MAPK $\alpha$  mutant are resistant to ischaemia. Moreover, p38-MAPK $\beta$  activation is selectively increased in porcine hearts that have undergone ischaemic preconditioning (Schulz et al., 2003), suggestive of a protective effect of the  $\beta$ -isoform. Thus, use of SB203580 to interrogate the roles of p38-MAPKs may

potentially confound interpretation of results, because, while the deleterious effects of p38-MAPK $\alpha$  would be inhibited, so would the putative protective effect of selective p38-MAPK $\beta$  activation during preconditioning. This notion is supported by the lack of any protective effect of SB203580 against ischaemia in cardiomyocytes expressing an SB203580-resistant variant p38-MAPK $\alpha$  containing a mutation of the key gatekeeper Thr106 residue, required for the interaction between p38-MAPK $\alpha/\beta$  and SB203580 (Tong et al., 1997; Martin et al., 2001).

Considered together, these observations suggest divergent roles of the p38-MAPK $\alpha$  and p38-MAPK $\beta$  isoforms, with perhaps a pro-hypertrophic and cardioprotective role for the  $\beta$ -isoform and a death-promoting function for p38-MAPK $\alpha$ . As noted for the JNKs, it is possible that the specific responses induced by activation of p38-MAPKs is dependent on a number of factors including location, duration and intensity of the signal and cardiomyocyte context.

### **1.3.2 Regulation of cardiomyocyte gene expression by ERK1/2, JNKs and p38-MAPKs**

In other systems, the ERK1/2, JNK and p38-MAPK pathways play major roles in global regulation of gene expression (Turjanski et al., 2007). As discussed above, the different MAPK pathways target a wide range of substrates and, accordingly, influence regulation of gene expression at multiple levels. Both the ERK1/2 and p38-MAPK pathways phosphorylate and activate different kinases which in turn modulate activity of various downstream substrates to influence gene expression. ERK1/2 primarily target RSKs while p38-MAPKs activate MAPKAPK2/3 thus conferring additional specificity to the cellular response to activating stimuli. However, both pathways target MSK1/2, representing a point of convergence of the two signals (Roux and Blenis, 2004; Cargnello and Roux, 2011). All three principal MAPK pathways (and their respective MAPKAPKs) translocate to the nucleus and upon stimulation phosphorylate transcription factors. This directly alters binding affinities for specific gene promoters and may affect transcription factor stability or association with other factors.

In addition to regulation of transcription *per se*, MAPKs also influence global gene expression through regulation of transcript stability and by influencing the rate of protein translation. A key role of the p38-MAPK pathway is in regulation of the stability of pro-inflammatory transcripts including those for prostaglandin-endoperoxide synthase 2 (COX2) and TNF $\alpha$  (Dean et al., 1999). One well-established mechanism is through p38-MAPK/MAPKAPK2-mediated phosphorylation of RNA-binding proteins such as tristetraprolin. Tristetraprolin binds AU-rich elements in the 3'-UTR of mRNAs such as TNF $\alpha$ , leading to their destabilisation and degradation. Phosphorylation of tristetraprolin is associated with inhibition of this function and this promotes accumulation of pro-inflammatory transcripts (Hitti et al., 2006). Signalling through the ERK1/2 cascade influences translation and protein synthesis through phosphorylation of the eukaryotic initiation factor 4E, which promotes recruitment of mRNAs to the ribosome (Ellederova et al., 2008; Shveygert et al., 2010).

Investigations examining the role of ERK1/2 in cardiomyocytes indicate that the pathway makes major contributions to gene expression in response to GqPCR agonists, namely ET-1, phenylephrine and A61603, with at least some of the response being mediated by activation of RSKs secondary to ERK1/2 stimulation. Furthermore, these changes in gene expression are associated with induction of hypertrophy (Kennedy et al., 2006; Cullingford et al., 2008b; Cullingford et al., 2008a; Marshall et al., 2010; Amirak et al., 2013). ERK1/2 are also implicated in upregulation of mRNA for c-Jun, an important immediate early gene (Clerk et al., 2002). The roles of JNKs and p38-MAPKs in regulation of cardiomyocyte gene expression, however, are less clear. Potent activation of JNKs in response to anisomycin and hyperosmotic shock in neonatal rat cardiomyocytes results in phosphorylation of c-Jun and ATF2 transcription factors, thus presumably influencing transcriptional regulation by these factors (Clerk and Sugden, 1997b). Inhibition of JNK signalling by overexpression of JNK-interacting protein 1 also suppresses upregulation of  $\beta$ -myosin heavy chain, atrial natriuretic factor, skeletal muscle alpha-actin and ventricular myosin light chain-2 in response to ET-1 and PE, further supporting a role for JNKs in modulation of cardiomyocyte gene expression (Finn et al., 2001).

As discussed, ERK1/2, JNKs and p38-MAPKs in cardiomyocytes and hearts are activated in response to pro-apoptotic H<sub>2</sub>O<sub>2</sub> concentrations (Clerk et al., 1998a; Clerk et al., 1998b; Kwon et al., 2003) and exposure of cardiomyocytes to H<sub>2</sub>O<sub>2</sub> is associated with induction of substantial changes in gene expression (Kemp et al., 2003; Clerk et al., 2007b). The substrate profiles of ERK1/2, JNKs and p38-MAPKs, including MAPKAPKs, nuclear-localised transcription factors and RNA-binding proteins is strongly suggestive of key roles in regulation of the cardiomyocyte gene expression response to H<sub>2</sub>O<sub>2</sub>, and these pathways potentially influence the balance between life and death of cardiomyocytes in this context.

One potential experimental strategy to dissect the roles of these pathways in regulation of gene expression is to use an inhibitor approach to microarray expression profiling. Potent and selective pharmacological inhibitors of MKK1/2 (the upstream activators of ERK1/2) such as U0126 (Favata et al., 1998) and PD184352 (Sebolt-Leopold et al., 1999) have been used in previous microarray expression profiling experiments to infer the roles of ERK1/2 in regulation of cardiomyocyte gene expression in response to ET-1, phenylephrine and A61603 (Kennedy et al., 2006; Marshall et al., 2010; Amirak et al., 2013). PD184352 is an allosteric, non-ATP-competitive inhibitor and, when used at concentrations of 1 – 2 µM, potently inhibits MKK1/2 activity and therefore activation of ERK1/2 (Bain et al., 2007). PD184352's mechanism of action confers a high level of selectivity towards MKK1/2 (Ohren et al., 2004) and although PD184352 can also inhibit MKK5 (the upstream activator of ERK5), this only occurs at higher concentrations (10 µM) (Mody et al., 2001).

SB203580 (Cuenda et al., 1995), is an established inhibitor of p38-MAPK $\alpha$  (the predominant isoform expressed in the myocardium) and p38-MAPK $\beta$  (expressed in heart at lower levels) (Marber et al., 2011). SB203580 displays an ATP-competitive mechanism of action and binds to both the activated form of p38-MAPK $\alpha/\beta$  to inhibit ATP binding and phosphotransferase activity, as well as the inactive form of p38-MAPK, thus reducing its rate of activation (Young et al., 1997; Frantz et al., 1998). Although widely used with the intention to inhibit p38-MAPK $\alpha/\beta$ , SB203580 is known to have off-target effects on several other kinases including c-

Raf, GSK3 $\beta$ , CK1, GAK. SB203580 is also a particularly potent inhibitor of RIPK2 (Bain et al., 2007; Hall-Jackson et al., 1999; Godl et al., 2003). When used at higher concentrations (10  $\mu$ M), the compound also inhibits JNKs in cardiomyocytes and adult hearts (Clerk and Sugden, 1998). While SB203580 remains useful in exploring roles of p38-MAPK $\alpha/\beta$ , off target effects cannot be ruled out and ideally, results should be corroborated using structurally unrelated p38-MAPK inhibitors with a distinct mechanism of action, such as BIRB 796 (Bain et al., 2007).

While compounds such as SP600125 (Bennett et al., 2001) and AS601245 (Gaillard et al., 2005) have been described as inhibitors of JNKs, their poor selectivity and potency has limited the potential to investigate the role of JNK pathway signalling. However, a potent and selective inhibitor, JNK-IN-8 (Zhang et al., 2012), has recently become available. JNK-IN-8 targets, and covalently binds to, a conserved cysteine residue preceding the JNK DFG-motif, resulting in a conformational change that blocks substrate binding (Zhang et al., 2012). Compared to conventional ATP-competitive kinase inhibitors, JNK-IN-8 exhibits higher selectivity towards its intended target, having no significant inhibitory activity against any other kinase in the "Kinativ™" chemical proteomics screening approach (Zhang et al., 2012; Liu et al., 2013). Accordingly, availability of JNK-IN-8 permits an inhibitor approach to investigate the contribution of JNKs in regulating cardiomyocyte gene expression.

#### **1.4 Pro-inflammatory cytokines and their roles in the heart**

Cytokines are low molecular weight proteins that play central roles in the regulation of immune and inflammatory responses, thus mediating a wide range of cellular processes including proliferation, differentiation, survival, and death. Cytokines are implicated in the development and progression of diverse pathologies, and are associated with both adaptive and maladaptive responses in the heart (Oppenheim, 2001; Hedayat et al., 2010). Major cytokines include the interferons, TNF superfamily members and IL family members. While some cytokines are constitutively expressed in some cell systems, production and release of

cytokines is typically induced in response to injurious stimulation. Circulating cytokines then bind their cognate receptors expressed on the surface of target cells to induce specific responses (Medzhitov and Horng, 2009).

#### **1.4.1 Interleukin 1 $\beta$ (IL1 $\beta$ ) and its role in the heart**

The IL1 family currently contains eleven members, of which IL1 $\alpha$  and IL1 $\beta$  are amongst the best characterised (Luheshi et al., 2009). Both IL1 $\alpha$  and IL1 $\beta$  bind and signal through the same receptor, the IL1 receptor 1 (IL1R1). The structures and biological effects of IL1 $\alpha$  and IL1 $\beta$  are similar but not identical (Brikos et al., 2007), although most studies focus on IL1 $\beta$ . IL1R1 is also targeted by the antagonist of IL1 signalling, IL1Ra, which blocks receptor stimulation by IL1 $\alpha/\beta$  (Arend et al., 1998). IL1R1 interacts with co-receptors, IL1R accessory proteins (IL1RAcPs), and ligand binding results in recruitment of additional proteins to form a stable signalling complex at the membrane, containing IL1R1, IL1RAcPs, IL1R-associated kinase (IRAK) 4 and myeloid differentiation primary response protein 88 (MyD88) (Fig. 1.4) (Lingel et al., 2009; Brikos et al., 2007). Upon stable association with the receptor, IRAK4 autophosphorylates and subsequently phosphorylates IRAKs 1 and 2, resulting in recruitment of TRAF6 (Cao et al., 1996; Brikos et al., 2007). Complexes containing IRAKs 1 and 2 and TRAF6 dissociate from the receptor complex and thence mediate activation of transforming growth factor- $\beta$ -activated kinase (TAK1). Once active, TAK1 phosphorylates the inhibitor of  $\kappa$ B-kinases (IKKs) and thus promotes activation of nuclear factor  $\kappa$ B (NF $\kappa$ B) and NF $\kappa$ B-dependent gene expression (Fig. 1.4). TAK1 also signals to activation of MAPKs (see section 1.3 for a discussion of the MAPK pathways) (Brikos et al., 2007; Takaesu et al., 2000; Weber et al., 2010) (Fig. 1.4). Generally, IL1 is a major initiator and mediator of immune and inflammatory responses and is implicated in the pathogenesis of infectious, autoinflammatory, autoimmune and degenerative diseases (Garlanda et al., 2013).

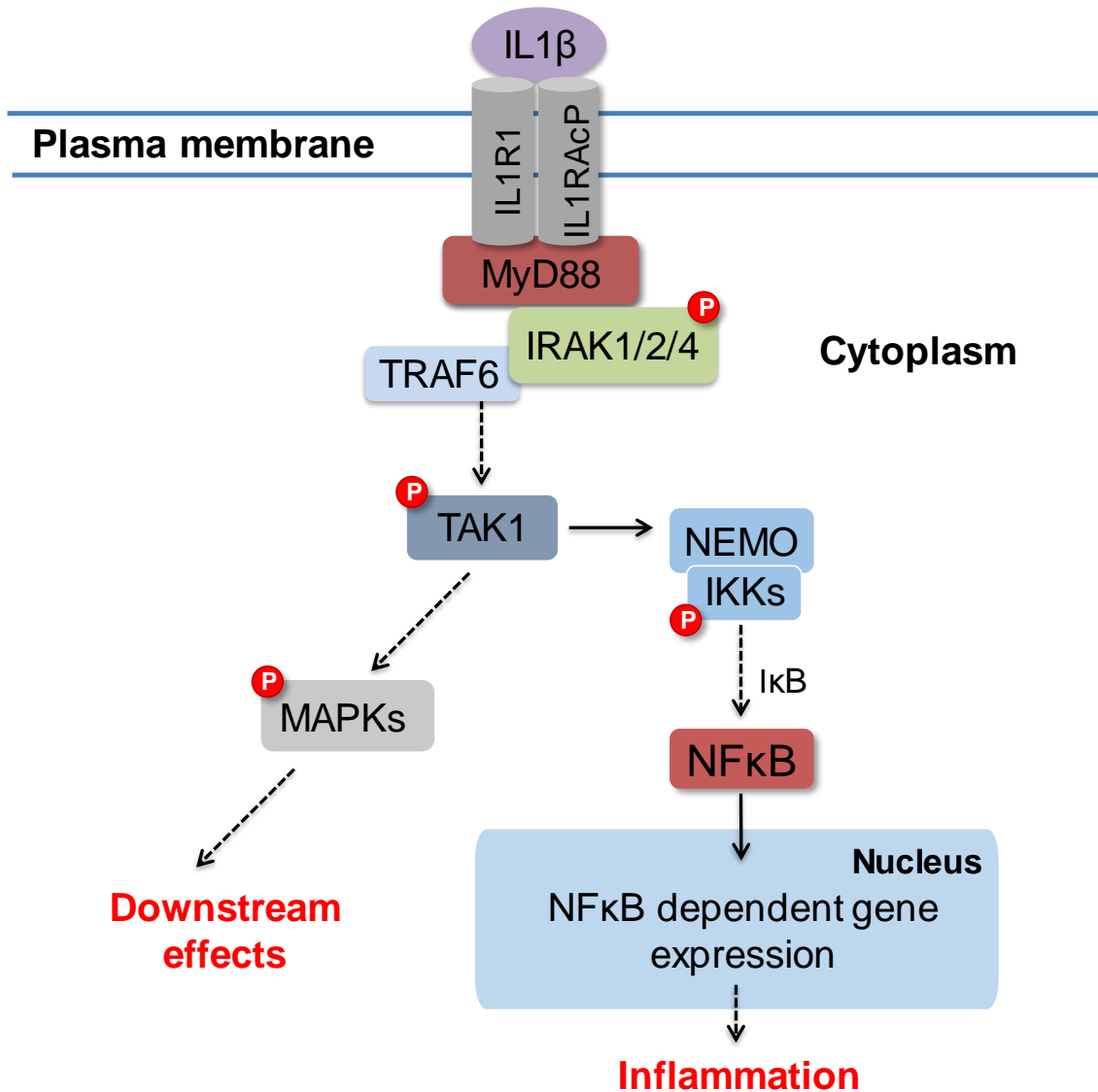


**Figure 1.4 IL1 $\beta$  receptor signalling**

IL1 $\beta$  stimulation leads to assembly of a complex containing IL1R1, ILRAcPs, MyD88 and IRAK4. IRAK4 becomes activated by autophosphorylation and phosphorylates and activates IRAKs 1 and 2, resulting in recruitment of TRAF6. Complexes containing TRAF6 and IRAKs 1 and 2 mediate activation of TAK1. TAK1 phosphorylates and activates the IKKs which thence phosphorylate I $\kappa$ B, leading to its proteasomal degradation. NF $\kappa$ B then translocates to the nucleus to regulate pro-inflammatory gene expression. TAK1 also mediates activation of MAPK pathways.

Acute MI results in a significant inflammatory response, and IL1 $\beta$  is significantly upregulated in post-infarction rat and mouse hearts (Herskowitz et al., 1995; Yue et al., 1998; Dewald et al., 2004). To investigate the roles of IL1 signalling in the post-infarcted heart, Bujak *et al.* (2008) employed an IL1R1 knockout (KO) mouse model. IL1R1 KO mouse hearts exhibited significantly reduced neutrophil infiltration following IR and markedly delayed infiltration of macrophages. Expression of chemokines and cytokines (including TNF $\alpha$  and IL1 $\beta$ ) was also reduced post-IR in IL1R1 KO heart (Bujak et al., 2008). Taken together, these observations indicate a role for IL1 signalling through the IL1R1 in mediation of the inflammatory response to IR. IL1R1 KO hearts also exhibited delayed infiltration of myofibroblasts into the post-infarct myocardium and decreased collagen deposition in the peri-infarct region, demonstrating a role for IL1 signalling in mediating fibrosis in response to MI (Bujak et al., 2008). In a further study, direct administration of IL1 $\beta$  to mice through intraperitoneal injection resulted in reduced left ventricular fractional shortening, suggestive of a role for IL1 $\beta$  in mediating development of cardiac contractile dysfunction (Van Tassel et al., 2013). Antagonism of IL1 signalling by overexpression of IL1Ra resulted in reduced infarct size in rat hearts subjected to IR (Suzuki et al., 2001) and, in common with the study by Bujak *et al.*, (2008) this was associated with a reduction in neutrophil infiltration into the myocardium, reflective of a dampened inflammatory response. Overexpression of IL1Ra also led to significantly reduced incidence of TUNEL-positive cardiomyocytes and DNA fragmentation in the post-ischaemic area, indicative of attenuation of apoptotic death (Suzuki et al., 2001).

In cultured neonatal rat cardiomyocytes, IL1 $\beta$  activates the three principal MAPK pathways (discussed in section 1.3) and leads to phosphorylation of c-Jun and ATF2 transcription factors, thus presumably influencing their transactivating activities and thereby modulating transcriptional activity (Clerk et al., 1999). IL1 $\beta$  also induces upregulation of c-Jun protein, potentially reflecting enhanced stability (and therefore reduced degradation) in response to phosphorylation (Clerk et al., 1999). A later investigation confirmed that IL1 $\beta$  induces substantial changes in cardiomyocyte gene expression (Barrett et al., 2013). Focussing on

early transcriptomic changes in response to IL1 $\beta$ , expression profiling using Affymetrix microarrays indicated upregulation of 338 and downregulation of 237 RNAs. Classification of genes changed by IL1 $\beta$  demonstrated that most were associated with inflammation and signalling, with those relating to inflammation, apoptosis signalling, interleukin signalling and Toll receptor signalling being particularly highly represented (Barrett et al., 2013).

Therefore, IL1 $\beta$  mediates post-infarction inflammation and cell death in the heart and activates intracellular signalling pathways in cardiomyocytes, associated with substantial changes in gene expression.

#### **1.4.2 Tumour necrosis factor-alpha (TNF $\alpha$ ) and its role in the heart**

The prototypic TNF family member, TNF $\alpha$ , binds to the TNF receptor (TNFR) 1, the best characterised and most highly expressed member of the TNFR superfamily, and TNFR2. Other important TNFR superfamily members include the Fas receptor, which mediates apoptosis in response to binding by Fas ligand, and TNF-related apoptosis inducing ligand (TRAIL) receptors, DR 4 and 5 (Clerk et al., 2003; Locksley et al., 2001). TNF $\alpha$  has pleiotropic effects, and stimulation of TNFR1 activates signalling pathways which lead to a number of different responses including cell survival and inflammation or caspase activation and apoptosis, depending on cell context and signalling events downstream of receptor binding (Clerk et al., 2003). TNF $\alpha$  can also signal to a novel form of regulated cell death, necroptosis (Zhou and Yuan, 2014), discussed in section 1.5.

Binding of TNF $\alpha$  to TNFR1 results in the rapid (within minutes) assembly of a multiprotein complex at the membrane, referred to as complex I, which activates pro-survival and pro-inflammatory signalling through NF $\kappa$ B (Micheau and Tschopp, 2003) (Fig. 1.5). TNF $\alpha$  stimulation causes receptor trimerisation, recruitment of the adapter molecule TNFR1-associated death domain (DD) protein (TRADD) and receptor-interacting protein kinase (RIPK) 1 (Fig. 1.5). RIPK1 plays a central role in mediating signalling through TNFR1 and although

RIPK1 is a Ser/Thr protein kinase, its role in complex I is as a scaffold protein and is independent of its kinase activity. TRADD also recruits TNF receptor associated factor (TRAF) 2, followed by the cellular inhibitor of apoptosis proteins (cIAP) 1 and 2. cIAP1/2 and the linear ubiquitin assembly complex (LUBAC) are E3 ubiquitin ligases and mediate extensive polyubiquitylation of RIPK1 through K63-linkages (cIAPs) and M1-linkages (LUBAC) (Fig. 1.5). This facilitates efficient recruitment, retention and activation of a complex containing TAK1 binding protein (TAB) 1 and 2 and TAK1 (Fig. 1.5). Linear polyubiquitylation stabilises RIPK1 in complex I and also allows recruitment of the NF $\kappa$ B essential modulation (NEMO) adapter protein, which regulates formation of the IKK complex. TAK1 activates IKKs, which phosphorylate I $\kappa$ B, resulting in its K48-linked ubiquitylation and proteasomal degradation (Kanayama et al., 2004; Ea et al., 2006; Varfolomeev et al., 2008; Haas et al., 2009; Gerlach et al., 2011). I $\kappa$ B retains NF $\kappa$ B in the cytoplasm and thus its degradation relieves repression of NF $\kappa$ B, which translocates to the nucleus to mediate expression of NF $\kappa$ B-dependent genes (Fig. 1.5). Target genes include pro-inflammatory genes and the pro-survival protein cFLIP, which binds to and inhibits caspase-8 and thus blocks apoptosis (Micheau et al., 2001). TAK1 also transmits the signal from TNF $\alpha$  to activation of MAPKs (Fig. 1.5) (see section 1.3 for a discussion of the MAPK pathways) (Liu et al., 1996; Devin et al., 2003; Lee et al., 2004).

In addition to the pro-inflammatory and pro-survival function of signalling through complex I, TNF $\alpha$  can activate the death receptor, or “extrinsic”, pathway to caspase activation and apoptosis. Like the intrinsic/mitochondrial pathway detailed in section 1.2.2, the death receptor pathway induces activation of initiator, and thence executioner, caspases, resulting in ATP-dependent dismantling and removal of the cell. Deubiquitylation of RIPK1 by enzymes including CYLD and A20 results in dissociation of complex I, representing an important switch in TNF $\alpha$  signalling from inflammation and survival to death (Fig. 1.5) (Wertz et al., 2004; Ofengeim and Yuan, 2013). A secondary complex (referred to as complex IIa) forms in the cytosol and contains TRADD, RIPK1, Fas-associated protein with DD (FADD) and caspase-8 (Fig. 1.5). Complex IIa mediates dimerisation and proteolytic activation of initiator caspase-8,

which then activates executioner caspases (e.g. caspase-3/7) to induce apoptosis (Fig. 1.5) (Micheau and Tschopp, 2003). Caspase-8 also negatively regulates RIPK1 activity in complex IIa through cleavage of RIPK1 in the kinase domain (Lin et al., 1999).

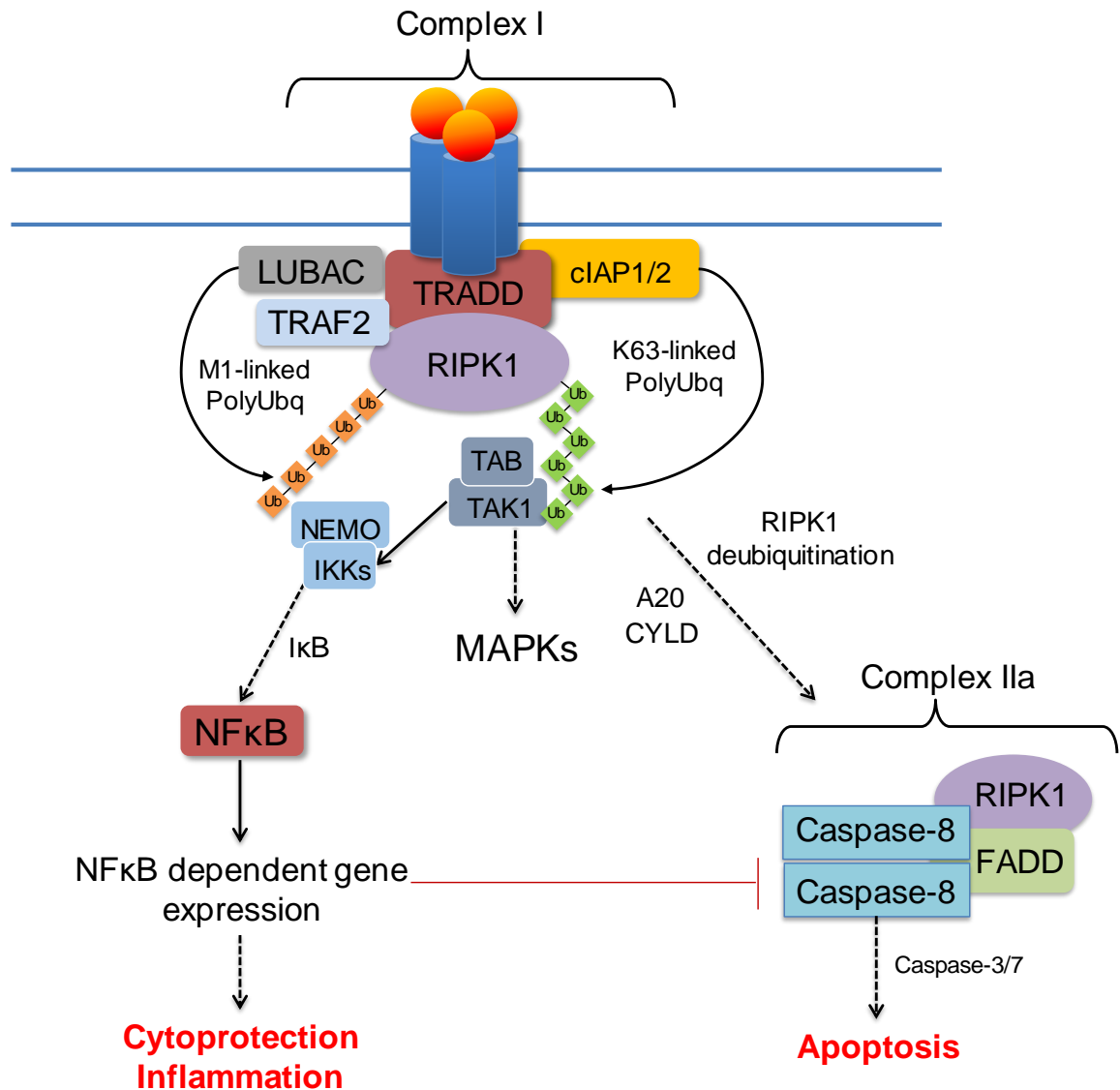


**Figure 1.5 TNF $\alpha$  signalling to inflammation/cytoprotection and apoptosis**

TNF $\alpha$  promotes TNFR1 trimerisation and assembly of complex I. TRADD associates with TNFR1 and recruits RIPK1, which undergoes M1-linked polyubiquitinylation (PolyUbq) by LUBAC and K63-linked PolyUbq by cIAP1/2. M1-linked PolyUbq recruits NEMO and the IKKs and K63-linked PolyUbq recruits the TAB/TAK1 complex. Active TAK1 mediates activation of MAPKs. TAK1 phosphorylates IKKs which then phosphorylate I $\kappa$ B, resulting in its degradation. NF $\kappa$ B thence translocates to the nucleus to regulate pro-inflammatory and pro-survival gene expression, resulting in inhibition of caspase-8 and cytoprotection. Deubiquitinylation of RIPK1 (e.g. by CYLD and A20) leads to formation of complex IIa. FADD recruits caspase-8, which dimerises and becomes active. Caspase-8 then mediates activation of executioner caspases (e.g. caspase-3 and -7) leading to apoptosis.

Due to the anti-apoptotic effects of TNF $\alpha$  signalling through complex I, engagement of TNFR1 by TNF $\alpha$  is not necessarily sufficient to induce apoptosis in most cell types. Accordingly, many investigations induce apoptosis using cotreatment with TNF $\alpha$  and transcription inhibitors such as actinomycin D, protein translation inhibitors such as cycloheximide, or proteasome inhibitors such as MG132. Inhibition of the proteasome prevents degradation of I $\kappa$ B and thus NF $\kappa$ B is retained in its inactive form in the cytoplasm, whereas disruption of transcription and/or translation blocks NF $\kappa$ B-dependent upregulation of pro-survival molecules such as cFLIP, thus permitting activation of caspase-8 and apoptosis (Lin et al., 1999; Micheau et al., 2001; Kreuz et al., 2001; Kim and Song, 2002). A further caspase-8 activating complex, complex IIb may also form under conditions of cIAP depletion. As detailed above, cIAPs polyubiquitinylate RIPK1 to induce NF $\kappa$ B and suppress apoptosis. cIAP depletion, for example using second mitochondria-derived activator of caspases (Smac) or Smac mimetics, results in formation of complex IIb, leading to RIPK1 kinase-dependent activation of caspase-8 and apoptosis (Vince et al., 2007; Varfolomeev et al., 2007; Wang et al., 2008; Tenev et al., 2011).

Increased levels of TNF $\alpha$  and inflammation are likely to play an important role in development and progression of HF and other cardiovascular diseases, although pleiotropically acting TNF $\alpha$  may have deleterious effects or alternatively confer cardioprotection (Higuchi et al., 2004; Monden et al., 2007; Hamid et al., 2009). The exact effects of TNF $\alpha$  on the myocardium are likely to be highly specific to the concentration encountered, the physiological and cellular context (i.e. whether the heart is healthy or compromised and the relative expression of pro-death and pro-survival factors), and experimental systems employed. Circulating TNF $\alpha$  levels are significantly elevated in human patients with severe HF (Levine et al., 1990; McMurray et al., 1991) and TNF $\alpha$  mRNA and protein expression is increased, relative to donor hearts, in hearts from patients with dilated cardiomyopathy and ischaemic heart disease (Torre-Amione et al., 1996). TNF $\alpha$  levels are also elevated following MI in human patients (Valgimigli et al., 2004) and in animal models of MI (Jacobs et al., 1999), suggestive of a role for TNF $\alpha$  in post-infarction inflammation and remodelling. Numerous studies implicate TNF $\alpha$  in development of

cardiac dysfunction, associated with induction of cardiomyocyte apoptosis, left ventricular remodelling and progression to HF (Kubota et al., 1997b; Kubota et al., 1997a; Bryant et al., 1998; Li et al., 2000). (Sivasubramanian et al., 2001; Haudek et al., 2007). Although these investigations are indicative of an association between TNF $\alpha$  exposure and cardiac death and dysfunction, all utilised transgenic mouse models overexpressing TNF $\alpha$ . The observations made, while undoubtedly valuable in illustrating the impact of TNF $\alpha$  on cardiac cells and the heart, were made in the context of chronic exposure to high TNF $\alpha$  concentrations, which may not reflect physiological conditions or those encountered in patients. Two parallel studies by Kubota *et al.* (1997a, b) highlight the importance of the extent of TNF $\alpha$  exposure in the ultimate response. Both studies used  $\alpha$ -MHC promoter-driven constructs with an aim to achieve cardiac specific overexpression of TNF $\alpha$  in live mice. However, the first study used a variant of the transgene with a deletion of the TNF $\alpha$  3' AU-rich destabilising sequence. This resulted in profound TNF $\alpha$  overexpression, a very severe HF phenotype characterised by myocarditis and cardiomegaly, and 100% mortality by the 11<sup>th</sup> day (Kubota et al., 1997a). In the second study, the destabilising sequence was left intact resulting in more moderate TNF $\alpha$  expression and a less severe phenotype (Kubota et al., 1997b). Accordingly, the TNF $\alpha$  expression levels and duration of exposure are clearly of central importance in the impact of TNF $\alpha$  on the heart and directly influence observations made in model systems.

Investigations examining the effects of TNF $\alpha$  on cardiac cells in culture also indicate heterogeneity in responses depending on the model systems and conditions used. Exposure to TNF $\alpha$  alone has been reported to induce DNA fragmentation and an increase in TUNEL-positive cells in isolated adult rat cardiomyocytes, indicative of induction of apoptosis (Krown et al., 1996). However, neonatal rat cardiomyocytes may demonstrate resistance to apoptosis in response to TNF $\alpha$  alone (Krown et al., 1996; Bergmann et al., 2001), and some studies have shown that additional intervention such as inhibiting the protective NF $\kappa$ B response is required to induce apoptosis in response to TNF $\alpha$  in these cells. Using neonatal rat cardiomyocytes, and cardiac derived H9c2 cells, Bergmann *et al.* (2001) reported nuclear translocation of NF $\kappa$ B,

but not apoptosis, following TNF $\alpha$  exposure. However, inhibition of NF $\kappa$ B signalling using a proteasome inhibitor, MG132 (thus preventing I $\kappa$ B degradation), or adenoviral overexpression of a degradation-resistant I $\kappa$ B mutant, sensitised these cells to TNF $\alpha$ -induced apoptosis (Bergmann et al., 2001). TNF $\alpha$  also activates the three main MAPK pathways in neonatal rat cardiomyocytes, associated with increased phosphorylation of the c-Jun and ATF2 transcription factors (Clerk et al., 1999). Thus, these signalling pathways presumably make important contributions to the overall response of cardiomyocyte.

## **1.5 Receptor interacting protein kinases (RIPKs) and necroptosis**

### **1.5.1 Regulated necrosis - necroptosis**

As discussed in section 1.2.2, apoptosis is characterised by a well-ordered, ATP-dependent dismantling and removal of cellular components with minimal inflammatory response. In contrast, necrosis has generally been regarded as the accidental, uncontrolled death of a cell in response to overwhelming stress. Necrosis involves swelling of the organelles, permeabilisation and rupture of the plasma membranes, and concomitant release of “damage associated molecular patterns” such as HMGB1 into the extracellular space, triggering immune cell recruitment and a significant inflammatory response (Scaffidi et al., 2002; Pittman and Kubes, 2013). However, recent research has reinforced the notion that the conceptualisation of cell death as occurring either by regulated apoptosis or unregulated necrosis is a false dichotomy. In 2005, Degterev and colleagues described a novel, non-apoptotic cell death modality, which they termed necroptosis. Necroptotic death is associated with morphological and biochemical features of necrosis yet is sensitive to pharmacological inhibition, thus indicative of a regulated process (Degterev et al., 2005). Since necroptosis is a regulated process, it may be possible to target the pathway pharmacologically. As a result, interest in this novel cell death pathway has led to intensive research efforts and rapidly expanding

knowledge of necroptosis, which is centrally regulated by the receptor-interacting protein kinases (RIPKs) 1 and 3.

Necroptotic death can be elicited by a range of stress stimuli including death receptor ligands (e.g. TNF $\alpha$ , TRAIL, FasL), interferons, Toll-like receptor agonists (e.g. polyinosinic:polycytidylic acid, lipopolysaccharide) and viral infection (e.g. HSV-1, vaccinia virus) (Jouan-Lanhouet et al., 2012; Holler et al., 2000; He et al., 2011; Robinson et al., 2012; Wang et al., 2014c). Insights into the molecular regulation of necroptosis have predominantly arisen through investigations of TNF $\alpha$  signalling through TNFR1 in non-cardiac systems, particularly in immune and inflammatory cells. As detailed in section 1.4.2 and Fig. 1.5, TNF $\alpha$  stimulation results in assembly of pro-survival/pro-inflammatory complex I at the membrane, which can be disassociated under certain conditions leading to pro-apoptotic complex IIa/b in the cytosol (Fig. 1.5). In complex IIa, caspase-8 inhibits RIPK1 activity by cleaving RIPK1 (Cho et al., 2009). However, under conditions refractory to caspase activation, for example in the presence of pan-caspase inhibitor zVAD-fmk or viral caspase inhibitor proteins such as B13R, RIPK1 can become activated and incorporate a further, necroptosis-inducing complex known as the necrosome (Fig. 1.6) (Li and Beg, 2000; Cho et al., 2009; Duprez et al., 2012).

Activation of RIPK1 kinase activity is a crucial trigger in induction of necroptosis. Catalytically active RIPK1 associates with RIPK3 through RIP-homotypic interaction motifs (RHIMs), 66- and 88- amino acid sequences in the C-terminal portions of RIPK1 and RIPK3, respectively (Sun et al., 2002). Interaction between RIPK1 and RIPK3 results in RIPK1-dependent phosphorylation and activation of RIPK3. Oligomerisation of RIPK1:RIPK3 heterodimeric units produces a functional, amyloid-like, necrosome (Fig. 1.6) (He et al., 2009; Cho et al., 2009; Li et al., 2012). The formation of the necrosome, and induction of necroptosis in most conditions, can be suppressed with the specific inhibitor of RIPK1 kinase activity, necrostatin-1 (Nec-1) or its derivatives (Fig. 1.6) (Degterev et al., 2008; Degterev et al., 2005). Downstream of necrosome formation, RIPK3 phosphorylates a pseudokinase, mixed lineage kinase domain-like protein (MLKL) (Fig. 1.6) (Sun et al., 2012; Wang et al., 2014a). MLKL phosphorylation

results in a conformational change and release of an N-terminal “four helix bundle domain” (4HBD), facilitating MLKL oligomerisation (Dondelinger et al., 2014; Hildebrand et al., 2014). The associated MLKL complexes translocate to the plasma membrane, where they mediate membrane permeabilisation, ion influx, and cellular swelling, all early hallmarks of necroptosis (Fig. 1.6) (Cai et al., 2014; Wang et al., 2014a). Some investigations indicate that MLKL induces necroptosis by binding of basic residues in the 4HBD to membrane phosphatidylinositol phosphates, although the exact mechanisms through which MLKL mediates cell death continue to be debated (Sun et al., 2012; Wu et al., 2013; Cai et al., 2014; Dondelinger et al., 2014; Hildebrand et al., 2014).

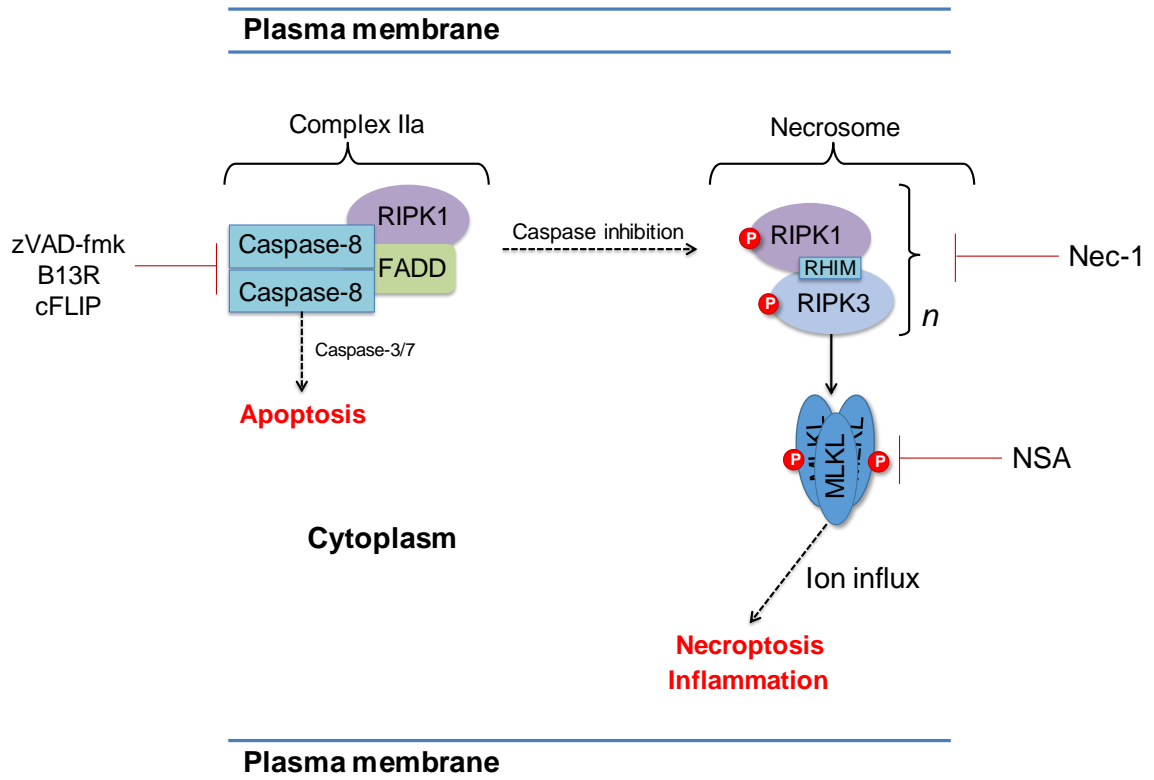


**Figure 1.6 Formation of the necrosome**

Inhibition of caspases (for example by zVAD-fmk, cFLIP or the viral protein B13R) suppresses TNF $\alpha$ -induced apoptosis and results in phosphorylation and activation of RIPK1. RIPK1 and RIPK3 associate through their RIP-homotypic interaction motifs (RHIM) leading to phosphorylation and activation of RIPK3. RIPK1:RIPK3 heterodimeric units oligomerise to form the amyloid-like necrosome signalling complex, which can be inhibited with necrostatins, specific inhibitors of RIPK1 kinase activity (e.g. Nec-1). RIPK3 becomes phosphorylated and in turn phosphorylates MLKL. MLKL oligomerises and translocates to the membrane, leading to membrane permeabilisation, ion influx, necroptotic death and inflammation. Necrosulfonamide (NSA) specifically suppresses MLKL-induced necroptosis.

Increased cell death is a key contributor to numerous disease states, and thus developing an understanding of the mechanisms governing cell death is crucial in identifying novel therapeutic strategies. The discovery of necroptosis as a regulated form of necrotic death may hold great potential for treating pathologies associated with increased cell death.

Accumulating evidence indicates that necroptotic death makes an important contribution to development and progression of diseases in multiple systems. In their early investigation characterising necroptosis, Degterev *et al.* (2007) demonstrated that Nec-1 confers neuroprotection during transient focal cerebral ischaemia in mice, resulting in reduced infarct size. Necroptosis is also implicated in other neurodegenerative disorders and contributes to motor neuron death in humanised models of familial and sporadic amyotrophic lateral sclerosis (Re *et al.*, 2014). The pathway is also activated in multiple sclerosis in human patients. Ofengeim *et al.* (2015) reported elevated expression of RIPKs 1 and 3 in tissue samples from human multiple sclerosis patients relative to healthy controls, associated with increased phosphorylation of RIPKs 1 and 3. Interaction between RIPK1 and RIPK3 (i.e. the necrosome) was detected in multiple sclerosis, but not control samples, and caspase-8 activation was found to be defective in multiple sclerosis, a requisite for induction of necroptosis (Fig. 1.6). Notably, Ofengeim and colleagues also reported significantly elevated expression of the caspase-8 inhibitory protein cFLIP<sub>L</sub> in multiple sclerosis tissue samples, potentially reflecting a physiologically relevant mechanism for defective caspase activation (Ofengeim *et al.*, 2015). In a mouse model of kidney IR injury, administration of Nec-1 (either prior to IR or 15 min after reperfusion) resulted in significantly reduced renal damage and increased survival, centrally implicating RIPK1 kinase mediated necroptosis in kidney IR injury (Linkermann *et al.*, 2012). Genetic deletion of RIPK3 or MLKL or inhibition of RIPK1 with Nec-1 also ameliorates renal proximal tubule death and inflammation in response to the anti-cancer drug cisplatin (Tristao *et al.*, 2012; Xu *et al.*, 2015). Emerging evidence also strongly implicates RIPKs and necroptosis in cardiac pathologies, as discussed in detail in section 1.5.3.

## **1.5.2 Regulation of RIPK1 signalling by post-translational modifications**

As discussed in sections 1.4.2 and 1.5.1, RIPK1 is a pleiotropic protein that plays central roles in signalling to cytoprotection, or otherwise to cell death through apoptosis or necroptosis. Whether RIPK1 induces cytoprotective signalling or promotes cell death is critically regulated by post-translational modifications, particularly ubiquitinylation and phosphorylation. Established phosphorylation and ubiquitinylation sites are indicated in Fig. 1.7.

### **1.5.2.1 Regulation of RIPK1 signalling by ubiquitinylation**

Ubiquitin is a small (76 a.a.; ~8.5 kDa) protein that can be conjugated to other ubiquitin molecules through homotypic linkages at seven different lysine residues; and can also be linked through the initiator methionine residue to produce linear chains. Linkage at different residues is associated with induction of different cellular responses (Peng et al., 2003; Chyan et al., 2004). Accordingly, RIPK1 ubiquitinylation status is a key determinant of whether RIPK1 signals to survival or death.

As detailed in section 1.4.2 and Fig. 1.5, RIPK1 is a central component of the pro-survival TNF $\alpha$ -induced complex I. In complex I, RIPK1 functions as a scaffold protein and undergoes extensive polyubiquitinylation by several E3 ligases. Polyubiquitinylation stabilises the association of RIPK1 in the receptor complex and provides docking sites for other signalling components, resulting in the activation of the pro-survival NF $\kappa$ B and MAPK pathways. Addition of K63-linked polyubiquitin chains to RIPK1 at K377 (see. Fig. 1.7), probably by cIAP1/2, provides a docking site for the TAB:TAK1 complex and results in TAK1 induction and a signal through to activation of MAPKs. Linear ubiquitination by LUBAC results in recruitment and stabilisation of NEMO and IKKs, which are activated by TAK1 to promote NF $\kappa$ B induction (Lee et al., 2004; Ea et al., 2006; Haas et al., 2009; Vince et al., 2007; O'donnell et al., 2007; Gerlach et al., 2011). Thus, linear and K63-linked RIPK1 polyubiquitinylation co-ordinately promote activation of pro-survival signalling downstream of TNFR1. Indeed, impaired polyubiquitinylation of RIPK1 in complex I, whether by depletion of cIAPs, disruption of LUBAC,

or as a result of deubiquitylating activities, results in inhibition of RIPK1 pro-survival signalling through NF $\kappa$ B and leads to apoptotic or necroptotic death following formation of complex II or the necrosome (Kovalenko et al., 2003; Wertz et al., 2004; Bertrand et al., 2008; Berger et al., 2014).

Deubiquitylation of RIPK1 is associated with cessation of cytoprotective signalling and induction of apoptotic or necroptotic signalling, and accordingly it was previously assumed that RIPK1 was not modified by ubiquitylation in the necrosome. However, recent investigations report ubiquitylation of RIPK1 within the necrosome, suggestive for a role for ubiquitylation in regulation of necroptotic death. de Almagro *et al.* (2015) reported that RIPK1 modified with K63-linked and linear polyubiquitin linkages is present in the necrosome in numerous human and mouse cell lines following treatment with TNF $\alpha$ , Smac mimetic and caspase inhibition (i.e. under necroptotic conditions) but not in response to TNF $\alpha$  and Smac mimetic alone (i.e. apoptotic conditions). A further study from the same research group indicated that polyubiquitylation of RIPK1 at K115 (see. Fig. 1.7) is required for necroptosis in HT29 cells in response to TNF $\alpha$ , Smac mimetic and caspase inhibition, as a modified HT29 line carrying a RIPK1 K115R mutation was resistant to necroptosis under these conditions. Suppression of RIPK1 kinase activity using different necrostatin compounds indicated that RIPK1 polyubiquitylation in the necrosome was dependent on RIPK1 catalytic activity. Furthermore, phosphorylation of RIPK1, RIPK3 and MLKL in the necrosome was demonstrated to be dependent on polyubiquitylation of RIPK1. This study also demonstrated the *in vivo* relevance of RIPK1 ubiquitylation in the necrosome in response to kidney IR injury (De Almagro et al., 2017).

#### **1.5.2.2 Regulation of RIPK1 signalling by phosphorylation**

As discussed, RIPK1 catalytic activity is key in promoting necroptosis and, as might be expected of a Ser/Thr kinase, RIPK1 signalling is also regulated by phosphorylation of RIPK1

itself. Abundant evidence indicates that assembly of the necrosome is driven by phosphorylation of RIPK1 and RIPK3, and requires RIPK1 kinase activity, although phosphorylation of RIPK1 in response to TNF $\alpha$ , cycloheximide and zVAD-fmk is abolished in RIPK3<sup>-/-</sup> mouse embryonic fibroblasts (Cho et al., 2009). Thus, RIPK3 directly or indirectly mediates phosphorylation of RIPK1 to trigger formation of the necrosome and induction of necroptosis. However, the phosphorylation sites required for RIPK1 activation and promotion of necroptosis, and the kinase(s) responsible, are yet to be clearly characterised.

To date, numerous RIPK1 phosphorylation sites have been identified through site-specific experimental means and/or mass spectrometry, including Ser6, Ser14/Ser15, Ser20, Ser25, Ser89, Ser161, Ser166, Ser303, Ser320 and Ser330/331 (Degterev et al., 2008; McQuade et al., 2013; Ofengeim et al., 2015; Newton et al., 2016b). Protein kinases typically require phosphorylation of a key residue in their activation loop (the activation loop phosphorylation site, ALPS) for efficient catalytic activity. Accordingly, structural modelling comparing the kinase domains of B-Raf and RIPK1 led Degterev *et al.* to propose that Ser161 (see. Fig. 1.7) is the RIPK1 ALPS due to sequence similarity with the regulatory Thr598 autophosphorylation site of B-Raf (Degterev et al., 2008; Zhang and Guan, 2000). Mutation of Ser161 to non-phosphorylatable alanine resulted in a ~40% reduction in cellular necroptosis in the study by Degterev *et al.* (2008). However, McQuade and colleagues reported that S161A mutation of RIPK1 resulted in only a modest (~21%) reduction of RIPK1 kinase activity, suggesting that Ser161 is unlikely to be the ALPS, and that other sites are required for RIPK1 activation. McQuade *et al.* (2013) also mutated Ser166 (see. Fig. 1.7) to alanine, resulting in a ~71% attenuation of RIPK1 catalytic activity, and suggesting that Ser166 may be the RIPK1 ALPS. However, the authors did not acknowledge the observation or report any follow-up investigation, and therefore the RIPK1 ALPS is yet to be formally identified and characterised. In common with Ser14/15, Ser20, and Ser161, Ser166 has been identified as an autophosphorylation site and as a result has been described as a marker of RIPK1 activation

by some investigators (Degterev et al., 2008; Berger et al., 2014; Ofengeim et al., 2015; Newton et al., 2016b).

While questions regarding the phosphorylation sites required for activation of RIPK1 and promotion of necroptosis remain, some phosphorylation sites implicated in negative regulation of RIPK1 catalytic activity and suppression of RIPK1-dependent apoptosis and necroptosis have been characterised. McQuade *et al.* (2013) reported that mutation of Ser89 (see Fig. 1.7) to alanine unexpectedly resulted in RIPK1 hyperactivation, indicating that phosphorylation of Ser89 inhibits RIPK1 kinase activation. This observation was corroborated by the suppression of RIPK1 catalytic activity in response to mutation of Ser89 to a phosphomimetic aspartic acid residue. However, even though the residue is highly evolutionarily conserved (Mcquade et al., 2013), RIPK1 phosphorylation at Ser89 has not yet been demonstrated to occur *in vivo*. Accordingly, determining the functional relevance in (patho)physiological conditions requires further investigation.

Although RIPK1 phosphorylation is necessary for induction of necroptosis, RIPK1 phosphorylation in TNFR1 complex I is also implicated in suppressing RIPK1-mediated cell death. Dondelinger *et al.* (2015) demonstrated that, in addition to their function in cytoprotection through activation of NF $\kappa$ B (see section 1.4.2 and Fig. 1.5), the IKKs also protect against RIPK1 kinase-dependent apoptosis and necroptosis in an NF $\kappa$ B-independent manner by direct phosphorylation of RIPK1 in complex I. IKK $\alpha$  and IKK $\beta$  were found to differentially phosphorylate RIPK1, and this was associated with suppressed integration of the RIPK1-kinase dependent complex IIb or the necrosome. Importantly, the protective role of IKK-mediated RIPK1 phosphorylation was also confirmed *in vivo*. Wild-type mice, and transgenic mice expressing a kinase-deficient RIPK1 (K45A) mutant were injected with TNF $\alpha$  and the IKK $\alpha/\beta$  inhibitor TPCA-1. Although TPCA-1 alone had no deleterious effects, TPCA-1 in combination with TNF $\alpha$  led to 100% mortality of wild-type mice but not RIPK1<sup>K45A/K45A</sup> mice, indicating suppression of RIPK1 kinase-dependent apoptosis and necroptosis by IKKs. The results obtained using genetic manipulation of RIPK1 kinase activity were corroborated using

pharmacological means, as wild-type mice injected with TNF $\alpha$  and TPCA-1 in the presence of the Nec-1 analogue Nec-1s were protected against death. Mass spectrometric analysis identified a number of sites phosphorylated by IKK $\alpha/\beta$  including Ser25, Ser166, Ser296, Ser331 and Ser416 (Dondelinger et al., 2015) although, notably, the putative inhibitory Ser89 site reported by McQuade *et al.* (2013) was not identified.

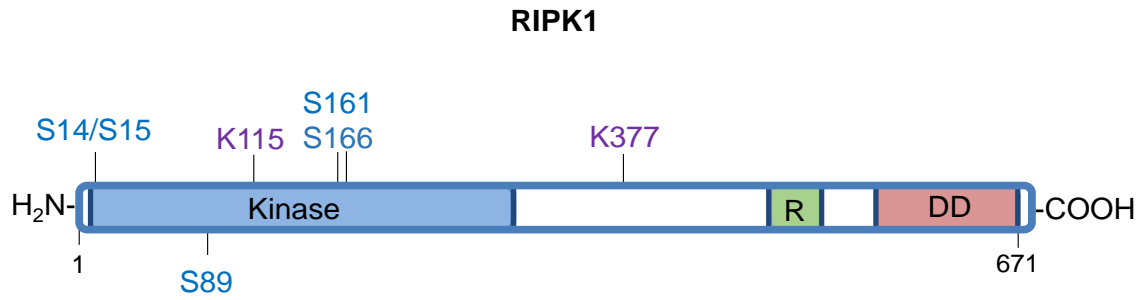


**Figure 1.7 RIPK1 domain structure and post-translational modifications**

Established RIPK1 phosphorylation sites (in blue) and ubiquitinylation sites (in purple) are indicated. Only those sites determined by site-specific experimental means (i.e. using mutational analysis, site specific antibodies) are shown. Residue positions refer to human RIPK1. R denotes the receptor-interacting protein homotypic interaction motif (RHIM). DD denotes the death domain.

### 1.5.3 RIPKs and necroptosis in the heart

To date, there have been relatively few published studies relating to RIPKs and necroptosis in the heart. However, the available data indicate an important role for RIPKs 1 and 3 in mediating necroptotic death of cardiac cells, and accordingly suggest a potentially important role for necroptosis in cardiac pathologies including MI and HF.

A number of studies demonstrate that the selective inhibitor of RIPK1, Nec-1 (Degterev et al., 2008), affords cardioprotection in response to varied stresses, suggesting that RIPK1 kinase activity has deleterious effects in the heart. Experiments using Nec-1 *in vitro* demonstrate reduced necrotic death of cardiac-derived H9c2 cells in response to directly applied oxidative stress in the form of tert-butyl hydroperoxide or H<sub>2</sub>O<sub>2</sub> (Smith et al., 2007; Wang et al., 2015). Nec-1 also has similar protective effects in the whole heart. Nec-1 administration during myocardial IR in mice *in vivo* results in reduced infarct size with a reduction in necrotic cell death (Smith et al., 2007; Lim et al., 2007; Oerlemans et al., 2012; Qin et al., 2016). Importantly, Nec-1 also improves functional outcomes following reperfusion, preserving ejection fraction and attenuating adverse remodelling post-infarction, with significantly reduced left ventricular wall thinning and fibrosis (Oerlemans et al., 2012). A further study reported a protective effect of a combination of Nec-1 and zVAD-fmk administered prior to reperfusion in guinea pig hearts subjected to global ischaemia *ex vivo*, although this investigation did not seek to assess the effects on IR of either agent in isolation and therefore cannot distinguish between RIPK1- or caspase-dependent effects (Koshinuma et al., 2014). The cardioprotective effects of Nec-1 have also been replicated in larger mammals, with Nec-1 administration resulting in improved cardiac performance and reduced immune cell infiltration in a pig model of IR injury (Koudstaal et al., 2015).

As discussed in Section 1.5.1, induction of necroptosis is associated with phosphorylation of RIPK1 and RIPK3, and the formation of RIPK1:RIPK3 complexes (Cho et al., 2009). Notably, IR in mouse hearts induces a significant increase in serine phosphorylation of, and association between, RIPKs 1 and 3, and this is reduced by Nec-1, suggestive of disruption of necrosome

formation and suppression of necroptosis (Oerlemans et al., 2012). Adenovirally-mediated overexpression of RIPK3 in cardiomyocytes is also sufficient to induce formation of RIPK1:RIPK3 complexes, resulting in promotion of necroptotic death (Luedde et al., 2014). Furthermore, cardiac expression of RIPK1, RIPK3 and MLKL protein is increased following 24 h reperfusion (Oerlemans et al., 2012; Qin et al., 2016). RIPK3 protein expression is also enhanced in the peri-infarct region of mouse hearts subjected to ischaemia (24 h) (Luedde et al., 2014), although it has not been established whether this occurs in cardiomyocytes or other non-myocyte cardiac cells. Inhibition of RIPK1 using Nec-1 (Oerlemans et al., 2012) or genetic RIPK3 deficiency (Luedde et al., 2014) is associated with reduced production of ROS as a result of IR in hearts, and RIPK3 deficiency also results in reduced infarct volume following ischaemic insult (Luedde et al., 2014; Newton et al., 2016a; Zhang et al., 2016), and enhances cardiac allograft acceptance (Pavlosky et al., 2014).

Suppression of certain cytoprotective mechanisms sensitises cardiomyocytes to necroptosis. Overexpression of an inactive DN form of the MAP3K TAK1, crucial for activation of IKKs and thence NF $\kappa$ B (see Fig. 1.5), predisposes cardiomyocytes to necroptotic death in response to TNF $\alpha$  stimulation (Li et al., 2014). This is rescued by Nec-1, implicating a central role for RIPK1 kinase activity, but is insensitive to zVAD-fmk and is thus distinct from apoptosis (Li et al., 2014). Moreover, TAK1 deficient mice exhibit a severe phenotype characterised by cardiac dysfunction, concomitant with increased cardiac fibrosis and release of HMGB1. This is associated with impaired cytoprotective signalling through TNF $\alpha$ -induced complex I and enhanced assembly of pro-apoptotic complex IIa (comprising FADD, RIPK1 and caspase-8, see Fig. 1.5) and the necroptotic RIPK1:RIPK3 complex (see Fig 1.6). These effects are ameliorated by Nec-1 administration, reinforcing the relevance of RIPK1 and its catalytic activity in cardiac necroptosis in certain cellular contexts (Li et al., 2014).

As discussed, there are relatively few published studies relating to the roles of RIPKs and necroptosis in the heart, although several studies implicate necroptosis in cardiac cell death in certain circumstances. However, further investigation is required to characterise the

contribution of necroptosis to cardiac pathologies and to elucidate the molecular regulation of RIPKs 1 and 3 in the heart.

## **1.6 Hypothesis and aims**

As discussed throughout this chapter, the heart is subjected to numerous and varied stresses, resulting in activation of intracellular signalling pathways, changes in gene expression and modulation of the balance between cardiomyocyte survival and death.

There are two distinct, yet thematically related, aspects to this project. The first hypothesis is that the three main MAPK pathways, ERK1/2, JNKs and p38-MAPKs, play important roles in regulation of cardiomyocyte gene expression in response to oxidative stress. This project aims to employ a pharmacological inhibitor approach to microarray expression profiling to determine the relative contribution of each MAPK pathway to cardiomyocyte mRNA expression in response to a pro-apoptotic concentration of H<sub>2</sub>O<sub>2</sub>, a physiologically relevant form of oxidative stress.

The second hypothesis is that other, novel, signalling pathways make important contributions to the regulation of cardiomyocyte survival vs death in response to stresses. This study seeks to examine the potential role of RIPK1 in the heart by exploring the regulation of cardiac RIPK1 in response to various pathophysiological stimuli.

## **Chapter Two – General Methods**

## 2.1 Materials and reagents

Unless otherwise stated, solutions and buffers were prepared using Milli-Q H<sub>2</sub>O. General laboratory chemicals were purchased from VWR or Sigma-Aldrich. Details of other reagents and materials are listed below.

**Molecular biology reagents:** Kanamycin sulphate, lysogeny broth (LB), LB agar, lysozyme, phenol and chloroform were obtained from Sigma-Aldrich. Spin Column Gel Extraction Kits were from NBS Biologicals Ltd. PacI, PmeI, KpnI, HindIII, calf intestinal alkaline phosphatase and CutSmart Buffer were from New England Biolabs. Promega *Pfu* polymerase, 10× *Pfu* buffer, Promega FuGene<sup>®</sup> HD, Taq DNA polymerase, 10× Taq DNA polymerase buffer, deoxynucleotide triphosphates, 1 Kb Plus DNA Ladder, UltraPure<sup>™</sup> agarose, T4 DNA ligase and SYBR<sup>®</sup> Safe DNA gel stain were from Thermo Fisher Scientific. Polyplus-transfection jetPRIME<sup>®</sup> was from Source BioScience. TrypLE Express dissociation reagent was from Thermo Fisher Scientific.

**Cell culture:** Cell culture dishes (60, 100 and 150 mm dishes and 35 and 60 mm Primaria dishes) were from VWR. Change to Dulbecco's modified Eagle's medium (DMEM, containing 4.5 g/L D-glucose, L-glutamine and 25 mM HEPES) and Medium 199, 10× Dulbecco's phosphate buffered saline (PBS), L-glutamine, penicillin/streptomycin and foetal calf serum (FCS) were from Gibco. Gelatin and laminin were from Sigma-Aldrich.

**Protein extraction and immunoprecipitations:** Benzamidine, dithiothreitol (DTT), 2-mercaptoethanol, phenylmethylsulphonyl fluoride (PMSF) and EZview<sup>™</sup> red anti-FLAG M2 affinity gel beads were from Sigma-Aldrich. Triton X-100 was from VWR. Leupeptin hemisulphate was from Tocris Bioscience. Microcystin-LR was from Enzo Life Sciences

**qPCR and RNA extraction:** RNA Bee was from AMS Biotechnology Ltd. 96-well plates and iTaq Universal SYBR Green Supermix were from Bio-Rad. High Capacity cDNA Reverse Transcription Kits and MicroAmp Optical Adhesive Film were from Thermo Fisher Scientific.

**SDS-PAGE and immunoblotting:** Antibodies for immunoblotting were obtained from Cell Signalling Technology, Sigma-Aldrich or Dako, as detailed in Table 2.2. Amersham ECL Prime Western Blotting Detection Reagents were from GE Healthcare. Mini-PROTEAN TGX 10% precast gels, Precision Plus Protein™ Kaleidoscope™, nitrocellulose membrane (0.45 µm) and Bio-Rad Protein Assay reagent were from Bio-Rad. TEMED, ammonium persulphate and bromophenol blue were from Sigma-Aldrich. Bovine serum albumin was from Santa Cruz Biotechnology. Whatman no. 1 filter paper, Whatman 3MM paper, acrylamide 40% (w/v), bis-acrylamide 2% (w/v) and Tween 20 were from VWR.

## 2.2 Agonists and inhibitors

Stocks of agonists and inhibitors were prepared as indicated in Table 2.1 and were added directly to tissue culture medium or perfusate to produce the final concentrations, as indicated.

**Table 2.1 Agonists and Inhibitors**

Agonist/Inhibitor	Solvent/Diluent	Source	Stock Concentration
Calyculin A	DMSO	Enzo Life Sciences	200 µM (2000x)
H <sub>2</sub> O <sub>2</sub>	Milli-Q H <sub>2</sub> O	Sigma-Aldrich	0.01 – 10 M (1000x)
JNK-IN-8	DMSO	Millipore	1 mM (1000x)
PD184352	DMSO	Alexis Biochemicals	2 mM (1000x)
Recombinant rat IL1β	PBS+0.1% BSA	R&D Systems	50 µg/ml (2000x)
Recombinant rat TNFα	Milli-Q H <sub>2</sub> O	R&D Systems	20 µg/ml (1000x)
SB203580	DMSO	Enzo Life Sciences	0.7 mM (1000x)

## 2.3 Cell cultures

### 2.3.1 Preparation of neonatal rat ventricular myocytes

Primary cultures of neonatal ventricular cardiomyocytes were routinely prepared by Prof. Angela Clerk. Cardiomyocyte preparations were also performed by Dr. Stephen J. Fuller, Dr. Kerry A. Rostron or Dr. Lorna R. Fiedler. Neonatal (2 – 4 d) Sprague-Dawley rats, purchased from Harlan Laboratories or Charles River Laboratories UK, were sacrificed by cervical dislocation and decapitated. The hearts were removed under sterile conditions and the ventricles separated from the atria. The ventricles were minced using forceps, washed in ice-cold digestion buffer [116 mM NaCl, 20 mM HEPES, 0.8 mM Na<sub>2</sub>HPO<sub>4</sub>, 5.6 mM glucose, 5.4 mM KCl and 0.8 mM MgSO<sub>4</sub>, (pH 7.35)] and transferred to a sterile 100 ml Schott bottle. The ventricles were dissociated by serial digestion with 0.4 mg/ml collagenase and 0.6 mg/ml pancreatin in sterile digestion buffer. All digestions were performed at 37°C with shaking in a water bath. The supernatant from the first digestion (5 min, 160 cycles/min shaking) was removed and discarded. Suspensions from subsequent digestions (20 min, 2 × 25 min, 20 min, 10 min, 136 cycles/min shaking) were transferred to a sterile 50 ml Falcon tube followed by the addition of 2 ml FCS. Cells were recovered by centrifugation (5 min, 60×g) and resuspended in 4 ml FCS, followed by storage in an incubator (37°C, 5% CO<sub>2</sub>) for the duration of the subsequent digestions. Following all digestions, the pooled cells were recovered by centrifugation (5 min, 60×g) and the resulting cell pellet resuspended in plating medium [(DMEM)/Medium 199 4:1 (v/v), 15% (v/v) FCS, 100 units/ml penicillin and streptomycin].

Cardiomyocyte content was enriched by pre-plating on uncoated plastic tissue culture dishes (30 min), to remove adherent non-cardiomyocytes. Cardiomyocytes were plated at a density of 4×10<sup>6</sup> cells/dish on 60 mm Primaria dishes pre-coated with sterile 1% (w/v) gelatin (Sigma-Aldrich UK) and maintained in an incubator (37°C, 5% CO<sub>2</sub>). After 18 h myocytes were confluent and beating spontaneously. Twenty-four hours prior to exposure to stimuli, serum-containing medium was withdrawn from cardiomyocytes followed by replacement with serum-free maintenance medium [DMEM/medium 199 4:1 (v/v), 100 units/ml penicillin and

streptomycin].

### **2.3.2 Human Embryonic Kidney 293 (HEK 293) cultures**

Human Embryonic Kidney 293 (HEK 293) cell cultures were established by thawing frozen cell aliquots at 37°C followed by resuspension in growth medium [DMEM containing 10% FCS (v/v), 1% (v/v) glutamine and 50 units/ml penicillin and streptomycin]. The cells were recovered by centrifugation (500×g, 5 min) and resuspended in growth medium. Cells were plated onto 100 mm tissue culture dishes and grown to confluence in an incubator (37°C, 5% CO<sub>2</sub>). In order to expand cultures or prepare cells for experimentation, cells were harvested using TrypLE Express dissociation reagent. Growth medium was removed and cultures washed twice in 1× PBS. Cells were dissociated by addition of 1 ml TrypLE Express, followed by incubation at 37°C until cells were detached. Cells were then resuspended in growth medium and plated onto 60, 100 or 150 mm tissue culture dishes, as required, and maintained in an incubator (37°C, 5% CO<sub>2</sub>).

### **2.4 Heart perfusions**

Hearts were perfused by Dr. Stephen J. Fuller. Adult Sprague-Dawley rat hearts were perfused retrogradely for the indicated times at a pressure of 10 kilopascals (70 mm Hg) with Krebs-Henseleit bicarbonate-buffered saline [25 mM NaHCO<sub>3</sub>, 119 mM NaCl, 4.7 mM KCl, 2.5 mM CaCl<sub>2</sub>, 1.2 mM KH<sub>2</sub>PO<sub>4</sub> (pH 7.6)] at 37°C, supplemented with 10 mM glucose and equilibrated with 95% O<sub>2</sub>/5% CO<sub>2</sub>. Perfusate and heart temperature were maintained at 37°C using a water-jacketed apparatus. For hearts subjected to ischaemia reperfusion, the aortic perfusion line was clamped for the specified times to cease the flow of perfusate. This was followed by removal of the clamp to allow reperfusion for the indicated times. Stocks of treatments, as indicated, were prepared at 1000× the desired final concentration and were added directly to

the perfusate. Following perfusions, hearts were frozen by clamping between aluminium tongs cooled in liquid N<sub>2</sub> (freeze-clamped) and the tissue pulverised under liquid N<sub>2</sub>. The powders were stored at -80°C.

## **2.5 SDS-polyacrylamide gel electrophoresis (SDS-PAGE) and immunoblotting**

### **2.5.1 Preparation of total protein extracts**

Unless stated otherwise, for cardiomyocyte extracts, stocks of agonists and inhibitors were prepared as described in Table 2.1 and were added directly to the tissue culture medium to give the final concentrations as stated, for the indicated times. Following treatments, primary cardiomyocyte cultures (4×10<sup>6</sup> cells) were washed twice with ice-cold 1× PBS and scraped into 150 µl ice-cold extraction buffer (20 mM glycerophosphate, 50 mM NaF, 2 mM ethylenediamine tetra-acetic acid (EDTA), 10 mM benzamidine, 0.2 mM Na<sub>3</sub>VO<sub>4</sub>, 5 mM DTT and 1% (w/v) Triton X100) containing protease inhibitors [200 µM leupeptin, 10 µM E64 and 300 µM PMSF] and the PP2A inhibitor microcystin (4 µM). Samples were centrifuged in an Eppendorff microcentrifuge (5 min, 10,000×g, 4°C) and the supernatants boiled with 0.33 volume 4× SDS-PAGE sample buffer [330 mM Tris-HCl (pH 6.8), 10% (w/v) sodium dodecyl sulphate (SDS), 133 mM DTT, 13% (v/v) glycerol and 0.2 mg/ml bromophenol blue]. Protein content was quantified using the Bio-Rad Protein Assay (see Section 2.5.3 for details) and samples were stored at -20°C.

Total protein extracts from perfused hearts were prepared by homogenising 50 mg of frozen heart powders (prepared as described in section 2.4) in six volumes of extraction buffer (as described above) and extracted on ice (10 min). Lysates were centrifuged (10000×g, 5 min, 4°C) and supernatant protein extracts boiled with 0.33 volumes of 4× sample buffer. Protein content was quantified using the Bio-Rad Protein Assay (as described in section 2.5.3) and samples stored at -20°C.

### **2.5.2 Preparation of cytosolic and nuclear protein-enriched (NPE) extracts**

Cytosolic and nuclear protein-enriched (NPE) extracts were prepared using an adaptation of the method described by vor *et al.* (1983). Cardiomyocytes ( $4 \times 10^6$  in 60 mm tissue culture dishes) were washed twice with ice-cold PBS and scraped into 150  $\mu$ l buffer A [10 mM HEPES, pH 7.9, 10 mM KCl, 1.5 mM  $MgCl_2$ , 0.3 mM  $Na_3VO_4$ , 200  $\mu$ M leupeptin, 10  $\mu$ M E64, 5 mM DTT, 300  $\mu$ M PMSF, 4  $\mu$ M microcystin]. Following extraction on ice (10 min), the samples were centrifuged (10000 $\times$ g, 5 min, 4°C) and the supernatants (i.e. the cytosolic fractions) were removed to a clean tube and boiled with 0.33 volume of 4 $\times$  sample buffer.

For the preparation of NPE extracts, the pellets resulting from the previous centrifugation step were resuspended in 50  $\mu$ l of buffer C [20 mM HEPES, (pH 7.9), 420 mM NaCl, 1.5 mM  $MgCl_2$ , 0.2 mM EDTA, 25%, (v/v) glycerol, 0.3 mM  $Na_3VO_4$ , 200  $\mu$ M leupeptin, 10  $\mu$ M E64, 5 mM DTT, 300  $\mu$ M PMSF, 4  $\mu$ M microcystin] and extracted on ice for 60 min, with periodic vortex-mixing at 10 – 15 min intervals. Samples were then centrifuged (10000 $\times$ g, 5 min, 4°C) and the supernatant NPE extracts transferred to a clean tube and boiled with 0.5 volume of 4 $\times$  sample buffer.

Protein content in the cytosolic and NPE extracts was determined using the Bio-Rad protein assay, as described in section 2.5.3.

### **2.5.3 Bio-Rad protein assay**

Protein content in extracts was quantified using an adaptation of the Bio-Rad Protein Assay, which is itself based on the Bradford method (Bradford, 1976). The colorimetric assay is based on the colour change exhibited by binding of Coomassie brilliant blue G-250 dye to basic and aromatic amino acid side chains. The extent of the colour change is determined by the concentration of the protein present and therefore can be used as an indication of protein content in a sample.

Protein content in samples was quantified by comparison to a BSA standard curve. Standard curves (ranging from 0 – 10 µg protein in 2 µg increments) were produced by diluting BSA (0.2 mg/ml) in Milli-Q H<sub>2</sub>O, to a total volume of 100 µl. Protein samples (1 – 5 µl) were also diluted in Milli-Q H<sub>2</sub>O to a total volume of 100 µl. Bio-Rad Protein Assay solution was diluted 1:5 and filtered through Whatman No. 1 filter paper. The diluted, filtered, solution (1 ml) was added to the samples and standard curve with vortex-mixing and the absorbance of the solutions at 595 nm was read using a spectrophotometer. Protein content in samples was calculated by interpolation.

#### **2.5.4 SDS-PAGE and immunoblotting**

Protein extracts (quantities as indicated) were separated using 10% polyacrylamide resolving gels with 6% polyacrylamide stacking gels (see Appendix I for gel recipes) or using Bio-Rad Mini-PROTEAN TGX 10% precast gels. Electrophoresis was conducted for one hour at 160 V using the Bio-Rad Mini-PROTEAN III system with SDS-PAGE running buffer [25 mM Tris base, 192 mM glycine, 0.1% (w/v) SDS]. Molecular weight markers used were Precision Plus Protein Kaleidoscope (5 µl). Following electrophoresis, proteins were transferred electrophoretically to nitrocellulose membranes using Whatman 3MM paper and a Bio-Rad Trans-Blot semi-dry transfer cell (10 V, 1 h) with Towbin transfer buffer [25 mM Tris base, 192 mM glycine, 20% (w/v) methanol]. Membranes were incubated in 5% (w/v) non-fat milk powder in Tris-buffered saline [50 mM Tris-HCl (pH 7.6), 150 mM NaCl containing 0.1% (v/v) Tween 20 (TBST)] to block non-specific binding sites (60 min, 20°C). Membranes were then washed in TBST and incubated with primary antibodies as indicated (see Table 2.2 for details) diluted in 5% (w/v) bovine serum albumin (BSA) in TBST (16 h, 4°C). The membranes were washed in TBST (3 × 5 min, 20°C) and incubated with horseradish peroxidase-coupled secondary antibodies in TBST (1:5000 dilution) containing 1% (w/v) non-fat milk powder (1 h, 20°C). The membranes were then washed again in TBST (3 × 5 min, 20°C).

Immunoreactive bands were visualised using enhanced chemiluminescence (Amersham ECL Prime Western Blotting Detection Reagents) and detected using an ImageQuant LAS 4000 Mini system (GE Healthcare). Densitometric analysis of immunoblots was performed using ImageQuantTL Software (GE Healthcare).

**Table 2.2 Antibodies used for immunoblotting.**

CST, Cell Signalling Technology, Inc.

<b>Protein</b>	<b>Species</b>	<b>Supplier (cat. no.)</b>	<b>Dilution</b>
ERK1/2	Rabbit mAb	CST (4695)	1:1000
Phospho-ERK1/2 (T202/Y204)	Rabbit mAb	CST (4370)	1:1000
JNKs	Rabbit pAb	CST (9252)	1:1000
Phospho-JNKs (T183/Y185)	Rabbit mAb	CST (4668)	1:1000
c-Jun	Rabbit mAb	CST (9165)	1:1000
Phospho-c-Jun (S63)	Rabbit mAb	CST (2361)	1:1000
p38-MAPK	Rabbit pAb	CST (9212)	1:1000
Phospho-p38-MAPK (T180/T182)	Rabbit mAb	CST (4511)	1:1000
MAPKAPK2	Rabbit mAb	CST (12155)	1:1000
Phospho-MAPKAPK2 (T222)	Rabbit mAb	CST (3316)	1:1000
Phospho-MAPKAPK2 (T334)	Rabbit mAb	CST (3007)	1:1000
RIPK1	Rabbit mAb	CST (3493)	1:1000
RIPK3	Rabbit pAb	CST (14401)	1:1000
FLAG-tag	Rabbit pAb	Sigma (F7452)	1:1000
Anti-rabbit Ig/HRP	Goat pAb	Dako (P0448)	1:5000

## 2.6 Immunoprecipitations

Cardiomyocytes ( $4 \times 10^6$  in 60 mm dishes) or HEK 293 cells were treated as indicated and washed twice with ice-cold 1x PBS. Cells were extracted by scraping into 150  $\mu$ l ice-cold immunoprecipitation buffer [20 mM Tris/HCl (pH 7.5), 300 mM KCl, 5 mM MgCl<sub>2</sub>, 5 mM NaF, 1 mM EDTA, 0.2 mM Na<sub>3</sub>VO<sub>4</sub>, 2  $\mu$ M microcystin LR, 10% (v/v) glycerol, 1% (v/v) Triton X-100 and 0.05% 2-mercaptoethanol; containing protease inhibitors [200  $\mu$ M leupeptin, 10  $\mu$ M E64 and 300  $\mu$ M PMSF]. Lysates were vortex mixed and extracted on ice (10 min) followed by centrifugation (5 min, 10000xg, 4°C). A portion (30  $\mu$ l) of the lysates was boiled with 2x SDS-

PAGE sample buffer (5 min) for immunoblotting to assess protein input. A sample of supernatant (5 µl) was also retained for protein quantification as described in section 2.5.3.

For immunoprecipitations, 100 µl total cell lysate was removed to a clean pre-chilled tube containing EZview™ red anti-FLAG M2 affinity gel beads (20 µl of a 1:1 slurry in immunoprecipitation buffer) and immunoprecipitations performed on a rotating mixer (18 h, 4°C). Following immunoprecipitation, the samples were centrifuged (5 min, 10000×g, 4°C) and the supernatants retained and boiled with 2× SDS-PAGE sample buffer (5 min). The pelleted anti-FLAG beads were washed with immunoprecipitation buffer (3×, 0.7 ml per wash) and the final pellets boiled with 2× SDS-PAGE sample buffer (5 min). Samples were stored at -20°C.

## **2.7 Total RNA extraction**

Total RNA was extracted from neonatal cardiomyocytes using RNA Bee, following the manufacturer's instructions. For neonatal rat ventricular cardiomyocytes, addition of agonists and inhibitors was staggered and cells were harvested simultaneously. RNA Bee (1 ml per  $4 \times 10^6$  cells) was added to cells, which were scraped and repeatedly pipetted to ensure cell lysis. Chloroform (0.2 ml) was added and the samples shaken (30 s), and then incubated on ice (5 min). The resulting homogenate was centrifuged (12000×g, 15 min, 4°C) to separate the phases. The upper aqueous phase (containing RNA) was removed to a clean pre-chilled tube, taking care to avoid the interphase layer. RNA was precipitated by addition of 0.5 ml isopropanol and the samples were incubated at room temperature for 5-10 min. RNA was then pelleted by centrifugation (12000×g, 15 min, 4°C). The supernatant was discarded and the pelleted RNA washed twice by centrifugation with 1 ml 75% (v/v) ethanol (12000×g, 10 min, 4°C), discarding the supernatant ethanol after each wash. RNA was air dried briefly and then dissolved in 20 – 40 µl nuclease-free water. RNA purity and concentration were assessed using a nanophotometer and  $A_{260}/A_{280}$  values of 1.9-2.1 were considered acceptable. Extracted RNA was stored at -80°C.

## 2.8 Quantitative real time polymerase chain reaction (qPCR)

cDNAs were reverse transcribed from extracted RNA using High Capacity cDNA Reverse Transcription Kits. Total RNA extracted from neonatal cardiomyocytes was diluted to 0.2 µg/µl with nuclease-free H<sub>2</sub>O. A 2× reverse transcription mastermix was produced containing (per 20 µl reaction): 10× RT Buffer (2 µl), 25× dNTP mix 100 mM (0.8 µl), 10× Random Primers (2 µl), MultiScribe™ reverse transcriptase (1 µl) and nuclease free H<sub>2</sub>O (9.2 µl). The diluted RNA (5 µl, 1 µg) was added to 15 µl mastermix, gently pipetted to mix and centrifuged briefly (10000×g, 15 s, 4°C). Reactions were then incubated at 25°C (10 min) followed by 37°C (120 min) and finally 85°C (5 min). Following reverse transcription, cDNAs were diluted 1:15 with the addition of nuclease-free water (280 µl) and were stored at -80°C.

qPCR was conducted using an ABI Real-Time PCR 7500 system (Applied Biosystems). qPCR reactions (25 µl) were analysed in Optical 96-well reaction plates. A qPCR mastermix was produced for each gene analysed, containing (per reaction) 12.5 µl iTaq Universal SYBR Green Supermix and primers (5 µl). The mastermix (17.5 µl) was pipetted into each well, followed by the cDNA template (7.5 µl). Details of primers used are found in Table 2.3. The plates were sealed with MicroAmp Optical Adhesive Film and the plates were centrifuged (600×g, 5 min, 4°C) to ensure the reactions were collected at the bottom of each well. qPCR was performed using absolute quantification with standard curve protocol. Five-point standard curves were produced, with each point assigned a quantity value of 1000, 500, 250, 125 or 62.5 (arbitrary units). The standard curves were produced by pooling equal volumes of each cDNA sample. An aliquot of this pooled cDNA was retained and was assigned the quantity value of 1000. The remainder was diluted twofold in series for a total of four dilutions to produce the 500, 250, 125 and 62.5 points of the standard curve. qPCR cycling conditions were 50°C (2 min), 95°C (10 min) and then forty cycles of 95°C (15 sec) and 60°C (1 min). Dissociation-curve analysis was routinely performed for each primer pair to ensure the absence of aberrant amplification products and primer dimers. “No template control” reactions, in which nuclease-

free water (7.5  $\mu$ l) is substituted for the cDNA template, were carried out to verify the absence of contaminants in the qPCR mastermix.

**Table 2.3 Primers used in qPCR validation of microarray data**

Oligonucleotide primers were either designed and synthesised by PrimerDesign (PD) or designed using Primer Express software and synthesised by Eurofins.

Gene Symbol	Accession No.	Product length (bp)	Position	Sense Primer	Antisense Primer	Source
Atf3	NM_012912	132	993-1124	AGCAGGATCGCACTAATGGG	ACAAC TTC AATGATGATGAATGTTCTCAC	PD
Ctgf	NM_022266	131	796-926	CTATGATGCGAGCCA ACTGC	GAGACGACTCTGCTTCTCCAG	PD
Dusp2	NM_00101208	110	1235-1344	ACTTGC GAAATTAATTGAACTCTAAA	ACATGGTTTCTGCTTGTCCACAG	PD
Dusp4	NM_022199	108	519-626	TCCCAGCACAAATGAGTCCTT	GCACTGCCGAGGTAGAGG	PD
Dusp5	NM_133578	97	1970-2066	CCTTGGACTTTGGCATGGTTT	GGGTCTGACAACTTTCTGAATGA	PD
Dusp8	NM_00110851	96	964-1059	TGTCTTCTGACGACGCATACA	TCCTCTCATACTCCAGCAACTG	PD
Egr1	NM_012551	116	1049-1164	TCAGTCGTAGTGACCACCTTAC	GGTATGCCTCTTGCGTTCATC	PD
Egr3	NM_017086	125	134-258	ATTACACTCAGATGGCTACAGAGA	CAAGTAGGTCACGGTCTTGTTG	PD
Gapdh	NM_002046.3	93	552-664	CCAAGGTCATCCATGACA ACTT	AGGGGCCATCCACAGTCTT	Eurofins
Gclc	NM_012815.2	78	880-957	TGCCCAATTGTTATGGCTTTG	TCCCCAGCGACAATCAATG	Eurofins
Hmox1	NM_012580.2	82	779-860	GACAGAGGAACACAAAGACCAGAGT	GGTAGTATCTGAACCAGGCTAGCA	Eurofins
Jun	NM_021835	81	2241-2321	CTTCTGTAGTGCTCCGTAAGAAC	CGCAATCTAGCCTGGTACTCA	PD
Nqo1	NM_017000.3	83	163-245	GACATCACAGGGGAGCCG	CTCAGGCGCCTTCCTTATAC	Eurofins
Txnrd1	NM_031614.2	90	318-407	AGCTAAGGAGGCAGCCAAATT	CCCCCGAGACCCCATCT	Eurofins

## **2.9 Agarose gel electrophoresis of DNA**

DNA samples were mixed with 0.2 vol SDS gel-loading buffer [0.2 mM EDTA (pH 8.0), 50% (v/v) glycerol, 0.2% (v/v) bromophenol blue] and subjected to electrophoresis through 1 or 2% agarose gels containing a 1:10000 dilution of SYBR<sup>®</sup> Safe DNA Gel Stain. 1 Kb Plus DNA Ladder was used to ensure products were of the correct size. Electrophoresis was conducted using TBE buffer [45 mM Tris (pH 8.0), 4 mM boric acid, 1 mM EDTA] for 30 – 45 min at 65 – 70 V. The products were visualised using UV transillumination.

## **2.10 General methods for the generation of adenoviruses expressing RIPK1**

### **2.10.1 Amplification of plasmids**

Plasmids were amplified by heat shock transformation into ultracompetent XL10-Gold *Escherichia coli* cells. Plasmid DNA (4 µl for ligation reactions, 0.1 µg for purified plasmids) was added to a 100 µl aliquot of XL10-Gold cells and swirled gently to mix. The cells were incubated on ice (30 min) followed by heat-shock (42°C, 50 s). After incubating on ice for a further 2 min, 1 ml LB was added and the cells were incubated in a rotary shaker (37°C, 60 min, 250 rpm). The cells were then spread using a sterile inoculation loop onto warm LB agar plates containing kanamycin (50 µg/ml) and incubated upside down overnight at 37°C.

### **2.10.2 Colony screen PCR**

For screening of bacterial colonies to confirm the presence of plasmids, a PCR mastermix (400 µl) was assembled containing Taq polymerase (10 units, 2 µl), 10× Taq polymerase buffer (40 µl), dNTP mixture (2 mM of each nucleotide, 40 µl), nuclease-free H<sub>2</sub>O (312 µl) and forward and reverse primers (1 µM, 2 µl each primer). Details of primers used are found in Table 2.3. Single colonies were picked with a sterile cocktail stick and transferred directly to 25 µl aliquots of the PCR screen mastermix. The high temperature (94°C) during the denaturation stage of

the PCR ruptures the bacterial cells, thus releasing DNA to be used as template for the screen. Cycling conditions are detailed in Fig. 2.1.

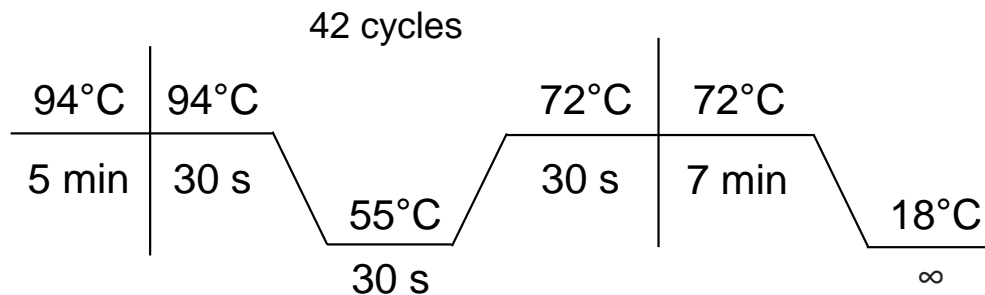
Products from PCR screens were electrophoresed on 1 or 2% agarose gels as described in section 2.9 and visualised using UV transillumination. The sticks used to pick the colonies were transferred to clean tubes containing 300  $\mu$ l LB containing kanamycin (50  $\mu$ g/ml) and shaken at 37°C to allow colony growth during PCR screens. Positive colonies (i.e. those producing PCR products of the correct size) were inoculated into 5 ml LB containing kanamycin (50  $\mu$ g/ml) and incubated in a rotary shaker overnight (37°C, 250 rpm) followed by plasmid isolation using the alkaline lysis minipreparation method, described in section 2.10.4

**Table 2.3 Primers used in colony PCR screens**

Primer pair 1 was used for screens for the FLAG-RIPK1-Shut plasmid. Pair 2 was used in screens for the FLAG-S161A-Shut, FLAG-S166A-Shut and FLAG-T183A-Shut plasmids. Pair 3 was used in screens for the FLAG-K376R-Shut plasmids. Pairs 4 and 5 were used in screens for homologous recombination for all adenoviral plasmids.

Primer Pair	Name	Sequence (5' – 3')	Tm (°C)
1	RIPK1_Fwd	GACAAGGGTACCATGCAACCAGACATGTCCTTGGAC	67.9
	KpnI_Rev	CATGTAGTAAAGGGTCCACCATTGTTCTTC	60.4
2	ShutF	GGTCTATATAAGCAGAGCTG	55.3
	S166A_Rev	CTTAGTCAGTTTGGCCCATGTCTTAAA	56.7
3	K376R_Fwd	TGTGCAGGCTAGGCTGCAAGAGG	58.9
	ShutR	GTGGTATGGCTGATTATGATCAG	60.6
4	AdV_184F	CAACGTTGTTGCCATTGCTG	51.8
	AdV_184R	TGTAAGCCCACTGCAAGCTA	51.8
5	Adv_300F	CAGAAACCCGCAGACATGTT	51.8
	Adv_300R	CCCCATGCTTTTTGATGCGT	51.8

**A**



**B**

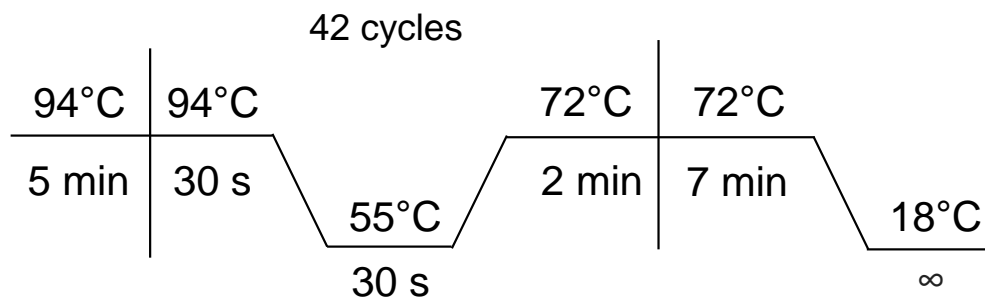


**Figure 2.1 PCR conditions for colony screens**

(A) PCR conditions for screening colonies expressing wild-type RIPK1, S161A, S166A, and T183A constructs. (B) PCR conditions for screening colonies expressing K376R constructs.

### **2.10.3 Spin column purification of DNA**

Plasmids and PCR products were purified using Spin Column Gel Extraction Kits, according to the manufacturer's instructions. For purification of PCR products subjected to agarose gel electrophoresis, the DNA bands were excised from the gel and the bands weighed. Excised bands were dissolved in Binding Buffer (400  $\mu$ l/100 mg gel) by heating to 55°C with gentle shaking. For purification of plasmids or PCR products in solution, the solutions were mixed with 3 $\times$  vol. Binding Buffer. The resulting solutions were loaded onto spin columns and incubated to allow adsorption of DNA to the silica membrane (20°C, 2 min). The samples were centrifuged (1 min, 10000 $\times$ g, 20°C) and the flow-through discarded. The bound DNA was washed twice with ethanol-containing Wash Buffer (700  $\mu$ l) using centrifugation (1 min, 10000 $\times$ g, 20°C), discarding the flow-through between washes. A further centrifugation step (1 min, 10000 $\times$ g, 20°C) was used to remove residual wash buffer. Purified DNA was then eluted from the columns using elution buffer (35  $\mu$ l, 2 mM Tris-HCl pH 8.0~8.5) by centrifugation (1 min, 10000 $\times$ g, 20°C).

### **2.10.4 Plasmid isolation using the alkaline lysis minipreparation method**

Colonies of XL10-Gold or BJ5183-AD-1 *E. coli* carrying plasmids were inoculated into 5 ml LB broth and grown overnight in a rotary shaker (37°C, 250 rpm). The bacteria were recovered under centrifugation (1 min, 12,000 $\times$  g, 4°C) and the plasmids purified using the alkaline lysis minipreparation method. Bacterial pellets were resuspended in 100  $\mu$ l ice-cold Solution I [50 mM glucose, 25 mM Tris (pH 8.0), 10 mM EDTA (pH 8.0)]. Bacteria were lysed by adding 200  $\mu$ l freshly prepared Solution II [0.2 M NaOH, 1% (w/v) SDS] and tubes were rapidly inverted five times. Following incubation (5 min, 20°C), 150  $\mu$ l Solution III [3 M potassium acetate in 11.5% (v/v) acetic acid] was added and tubes were gently inverted to mix. Samples were incubated on ice (5 min) and centrifuged (5 min, 12000 $\times$ g, 4°C). The supernatants were transferred to clean tubes and nucleic acids precipitated with 2 $\times$  vol. absolute ethanol, with

gentle mixing. Precipitations were carried out at 20°C for 2 min, followed by recovery of nucleic acids by centrifugation (5 min, 12000×g, 4°C). The pelleted nucleic acids were washed with 1 ml 70% ethanol, residual ethanol aspirated and air-dried (10 min, 20°C). The pellets were then dissolved in 50 µl TE buffer [10 mM Tris (pH 8.0), 1 mM EDTA] containing pancreatic RNase (20 µg/ml) to digest residual RNA (30 min, 20°C). Plasmid DNA was then spin column purified as detailed in section 2.10.3 and eluted in 35 µl elution buffer. Stocks of plasmids were stored at -20°C.

### **2.10.5 Plasmid isolation using the alkaline lysis maxipreparation method**

Colonies of XL10-Gold *E. coli* carrying plasmids were inoculated into 500 ml LB containing kanamycin (50 µg/ml) and grown overnight in a rotary shaker (37°C, 250 rpm). Following overnight growth, bacteria were recovered by centrifugation in 500 ml centrifuge buckets (15 min, 3600×g, 16°C) and the resulting pellets rinsed with STE solution [100 mM NaCl, 10 mM Tris-HCl (pH 8.0), 1 mM EDTA]. The supernatants were drained and pellets were resuspended in 18 ml ice-cold Solution I [50 mM glucose, 25 mM Tris (pH 8.0), 10 mM EDTA, (pH 8.0)] with gentle shaking. Bacterial walls were disrupted by the addition of 2 ml lysozyme [(10 mg/ml in 10 mM Tris (pH 8.0)], with gentle shaking and incubation at room temperature (5 min, 20°C). 40 ml Solution II was added [0.2 M NaOH, 1% (w/v) SDS] and the solution was shaken, followed by incubation at room temperature for 5 min. Following the addition of 20 ml Solution III [3 M potassium acetate in 11.5% (v/v) acetic acid] the solutions were shaken and incubated on ice for 5 min followed by centrifugation (15 min, 3600×g, 16°C). To remove the flocculent white precipitate, the supernatants were then filtered through two layers of cloth into 45 ml isopropanol in 250 ml centrifuge buckets, shaken, and centrifuged to pellet nucleic acids (15 min, 3600×g, 16°C). The resulting pellets were gently rinsed with ethanol [70% (v/v)]. The centrifuge buckets were inverted to drain, and residual ethanol gently wiped away with paper towel. The pellets were then dissolved in 3 ml TE buffer [10 mM Tris (pH 8.0), 1 mM EDTA]

and the resulting solution was poured into 15 ml tubes containing 5 M LiCl (3 ml). The tubes were inverted gently to mix and centrifuged (15 min, 3600×g, 16°C).

The supernatants were poured into 50 ml tubes containing 7 ml isopropanol and the pellets discarded. The tubes were centrifuged to pellet nucleic acids (15 min, 3600×g, 16°C) and the supernatants discarded. Pelleted nucleic acids were rinsed gently with ethanol [70% (v/v)] and inverted to drain. Residual ethanol was gently wiped away using paper towel. RNA was then digested by resuspension of pellets in 0.5 ml TE buffer containing pancreatic RNase (20 µg/ml) with shaking in a rotary shaker (30 min, 25°C, 250 rpm). Following digestion of RNA, the solution was transferred to a 1.5 ml tube and 600 µl 1.6 M NaCl/13% polyethylene glycol was added to precipitate plasmids DNA. The plasmid DNA was then pelleted in a microfuge (1 min, 12000×g, 4°C). After discarding the supernatants, the pelleted DNA was resuspended in 500 µl TE buffer and purified by extraction by shaking in phenol (500 µl) by followed by centrifugation (5 min, 12000×g, 4°C). The uppermost phase (~450 µl) was removed to a clean 1.5 ml tube and the process was repeated for extraction in phenol:chloroform (250 µl of each) followed by chloroform alone (500 µl). Plasmid DNA was precipitated by mixing with 10 M ammonium acetate (100 µl) followed by addition of 1 ml absolute ethanol. Precipitation was carried out at 20°C for 10 min followed by recovery of plasmid DNA by centrifugation (5 min, 12000×g, 4°C). The pellets were then washed with 1 ml ethanol [70% (v/v)], aspirated to remove residual ethanol and air-dried (10 min, 20°C). The purified plasmid DNA was then dissolved in 500 µl TE buffer and the concentrations determined using a nanophotometer. Stocks of the plasmids were stored at -20°C.

### 2.10.6 Sequencing of plasmid DNA

Shuttle vector and adenoviral plasmids (5 µl per reaction at 100 ng/µl) were supplied to Source BioScience for sequencing using specific primers (5 µl per reaction at 3.2 pmol/µl). Details of primers use for sequencing are found in Table 2.4.

**Table 2.4 Primers used for sequencing of shuttle vector and adenoviral plasmids**

Primer	Sequence (5' – 3')	Length	Tm (°C)
ShutF	GGTCTATATAAGCAGAGCTG	20	55.3
ShutR	GTGGTATGGCTGATTATGATCAG	23	58.9
RIPK1_Fwd	GACAAGGGTACCATGCAACCAGACATGTCCTTGGAC	36	67.9
KpnI_Fwd	GAAGAACAATGGTGGAAACCCTTTACTACATG	31	60.4
T183A_Fwd	GTGAGCAGCACCGCTAA GAAGAACAAT	27	59.7
K376R_Fwd	TGTGCAGGCTAGGCTGC AAGAGG	23	60.6

### 2.10.7 Generation of adenoviral plasmids

#### 2.10.7.1 Homologous recombination of shuttle vectors with the pAdeasy-1 plasmid

To produce adenoviral plasmids, shuttle vector plasmids were linearised and transformed into BJ5183-AD-1 *E. coli* to undergo homologous recombination with the pAdeasy-1 plasmid (which is pre-transformed into BJ5183-AD-1 cells) (see Fig. 2.2). Shuttle vector plasmids (2 µg) were linearised by digestion with PmeI (10 units, 1 µl) in 50 µl reactions containing 10x CutSmart® Buffer (5 µl) and nuclease-free H<sub>2</sub>O. The plasmids were digested at 37°C for 3 h. After 2 h, 1 µl calf intestinal alkaline phosphatase was added to the reactions followed by incubation at 37°C for a further hour. The linearised shuttle vector plasmids (2 µl) were heat-shock transformed into BJ5183-AD-1 cells as described for XL10-Gold cells in section 2.10.1. The cells were plated onto LB agar plates containing kanamycin (50 µg/ml) and incubated upside down overnight at 37°C. The pAdeasy-1 adenoviral plasmid carries the ampicillin resistance gene, and this is exchanged for the kanamycin resistance gene carried by the shuttle vector plasmids when homologous recombination occurs. Accordingly, colony growth on kanamycin plates serves as an indication that homologous recombination has taken place.

Similarly, the presence of small bacterial colonies is indicative of recombination as the recombinant adenoviral plasmid is a large construct and results in slowly growing colonies.

#### **2.10.7.2 Colony screen PCR for homologous recombination and purification of adenoviral plasmids**

Small, well isolated single colonies were picked using a sterile cocktail stick and screened for the presence of the recombinant adenoviral plasmid, as described in section 2.10.2 using the AdV\_184F/AdV\_184R and AdV\_300F/AdV\_300R (details of primers are found in Table 2.3 and PCR conditions in Fig. 2.1). PCR using these primer pairs produces in a single 184 bp band if recombination has been successful and the adenoviral plasmid is present. Two bands (of 184 bp and 300 bp) indicates that homologous recombination has not occurred and that the shuttle vector is present. Positive colonies were transferred to 5 ml LB containing kanamycin (50 µg/ml) and were incubated overnight in a rotary shaker (37°C, 250 rpm) before purification of adenoviral plasmids using the alkaline lysis minipreparation method, as described in section 2.10.4. The concentration of purified plasmids was determined using a nanophotometer and the plasmids were stored at -20°C.

The adenoviral plasmids were amplified by heat shock transformation of 0.1 µg plasmid into XL10-Gold *E. coli* as described in section 2.10.1. The transformed cells were spread onto warm LB agar plates containing kanamycin (50 µg/ml) and incubated upside down overnight at 37°C. Single colonies were picked using a sterile cocktail stick and screened for the presence of the recombinant adenoviral plasmid as described in section 2.10.2. Positive colonies were inoculated into 500 ml LB containing kanamycin (50 µg/ml) and grown overnight in a rotary shaker (37°C, 250 rpm) and the plasmids isolated using the alkaline lysis maxipreparation method as described in section 2.10.5. The isolated plasmids were resuspended in 500 µl TE buffer, the concentrations determined, and then stored at -20°C.

### **2.10.8 Production and propagation of adenoviral particles in HEK 293 cells**

To produce adenoviral particles, the recombinant adenoviral plasmids were linearised and transfected into HEK 293 cells (see Fig. 2.2). Recombinant adenoviral plasmids (50 µg) were digested with PacI (3 h, 37°C) in 100 µl reactions containing 10× CutSmart Buffer (10 µl), PacI (20 units, 2 µl) and nuclease-free H<sub>2</sub>O. Following digestion, the cut plasmid DNA was precipitated from the reaction mixture. Nuclease free H<sub>2</sub>O (80 µl) was added to a total volume of 180 µl followed by addition of 3 M sodium acetate (20 µl). The reactions were gently mixed and DNA precipitated by addition of absolute ethanol (600 µl) with incubation on ice (5 min) and at room temperature (20°C, 5 min). The precipitated DNA was pelleted by centrifugation (2 min, 10000×g, 4°C) and the supernatant was discarded. The pellets were washed with 70% ethanol (1 ml), briefly air dried and dissolved in 35 µl elution buffer.

The digested plasmid DNA (5 µg) was then transfected into HEK 293 cells using either jetPRIME<sup>®</sup> or FuGene<sup>®</sup> HD transfection reagents. For transfection using jetPRIME<sup>®</sup>, HEK 293 cells were cultured in 60 mm dishes and grown to ~70% confluence. The PacI-digested adenoviral plasmid DNA (5 µg) was gently mixed into 200 µl jetPRIME<sup>®</sup> buffer followed by addition of jetPRIME<sup>®</sup> reagent (10 µl). The mixture was vortex mixed (10 s) followed by incubation at room temperature (20°C, 10 min). The mixture was then added dropwise to the HEK 293 cultures with gentle rocking. For transfection using FuGene<sup>®</sup> HD, plasmid DNA (5 µg) was gently mixed with 200 µl sterile DMEM (37°C) and FuGene<sup>®</sup> reagent (10 µl) added with gentle mixing. The mixtures were incubated at room temperature (20°C, 10 min) and added dropwise to HEK 293 cultures at ~70% confluence in 60 mm dishes. Transfected cultures were incubated (37°C, 5% CO<sub>2</sub>) for 7 – 10 days until detachment and rounding of cells was observed (indicative of adenoviral infection). Infected cells were collected in culture medium and freeze-thawed for four cycles in a methanol and dry ice bath, with brief vortexing between each cycle. Cell debris was pelleted with centrifugation (5 min, 4000×g, 4°C) and the supernatant primary adenoviral stocks used to infect further HEK 293 cultures for amplification of adenoviruses.

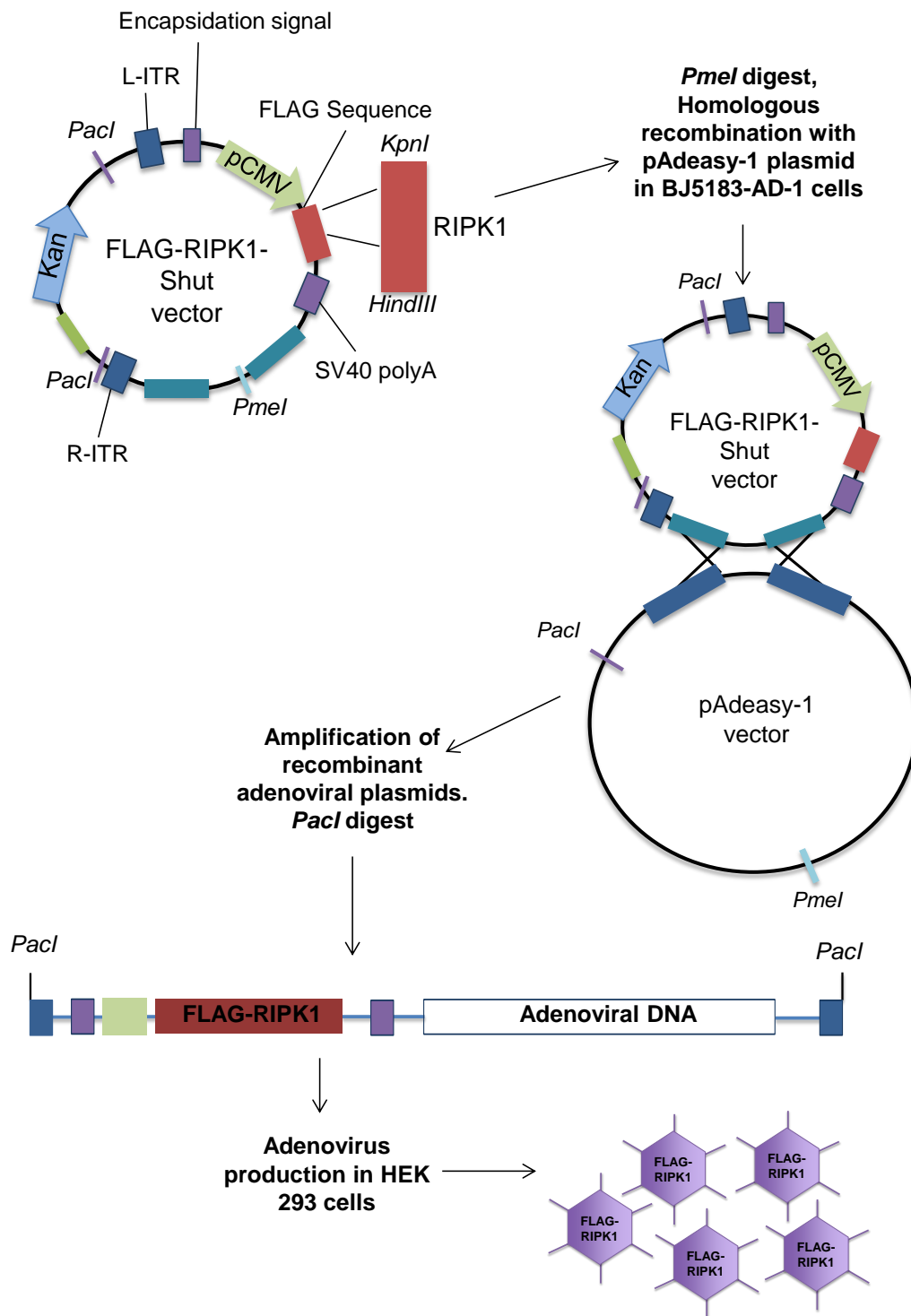


**Figure 2.2 Schematic of the generation of adenoviral plasmids expressing FLAG-tagged wild-type and mutant RIPK1 constructs**

Sequence verified shuttle vector plasmids expressing FLAG-tagged wild-type and mutant RIPK1 constructs were linearised with PmeI and transformed into BJ5183-AD-1 *E. coli* to undergo homologous recombination with the pAdeasy-1 adenoviral plasmid. Resulting colonies were screened and recombinant RIPK1 adenoviral plasmids isolated from positive colonies. Adenoviral plasmids were linearised with PacI and transfected into HEK 293 cells for production of adenoviral particles.

### **2.11 Fast protein liquid chromatography**

Anion-exchange FPLC was performed in collaboration with Prof. Angela Clerk using a Mono Q HR 5/5 FPLC column and an Äkta FPLC system (both GE Healthcare). Following exposure to agonists as described, five 60 mm dishes of neonatal rat ventricular myocytes were washed twice with ice-cold PBS and harvested into a total of 300 µl extraction buffer [20 mM β-glycerophosphate (pH 7.5), 50 mM NaF, 2 mM EDTA, 1% (v/v) Triton X-100, 5 mM DTT, 10 mM benzamidine, 200 µM leupeptin, 10 µM E64, 300 µM PMSF]. The lysates were extracted on ice (10 min), centrifuged to remove cell debris (10,000×g, 5 min, 4°C), and the resulting supernatants removed to a clean tube. The extracts were further clarified with a second centrifugation (10,000×g, 5 min, 4°C) and the supernatant extracts removed to a clean tube.

The extracts were loaded into a Mono Q HR 5/5 FPLC column pre-equilibrated with Mono Q Buffer A [50 mM Tris/HCl (pH 7.3), 2 mM EDTA, 2 mM ethylene glycol tetra-acetic acid (EGTA), 0.1% (v/v) 2-mercaptoethanol, 5% (v/v) glycerol, 0.03% (v/v) Brij-35, 0.3 mM Na<sub>3</sub>VO<sub>4</sub>, 1 mM benzamidine and 4 µg/ml leupeptin]. Following a 4 ml isocratic wash, bound proteins were eluted from the column with a linear NaCl gradient (20 ml, 0 – 0.4 M) at a flow rate of 1 ml/min. The NaCl gradient was formed by mixing Mono Q Buffer A with Mono Q Buffer B (Mono Q Buffer A containing 1 M NaCl). Fractions (0.5 ml) were collected with an automated fraction collector. Samples of each fraction were retained and boiled with 0.33 vol. 4× SDS-PAGE sample buffer (5 min).

### **2.12 Statistical analysis**

Results are expressed as means ± standard error of the mean (SEM) with n referring to the number of independent observations made. Unless otherwise stated, statistical significance of the differences between means was analysed using a one-way analysis of variance (ANOVA), applying a Student-Newman-Keuls (SNK) post-test. Statistical analyses were performed using GraphPad Prism 4. p<0.05 was considered statistically significant.

**Chapter Three - Regulation of cardiomyocyte gene expression by  
mitogen-activated protein kinases in response to H<sub>2</sub>O<sub>2</sub>**

### 3.1 Introduction

Oxidative stress is a key modulator of the balance between life and death of cardiomyocytes and the response is dictated by the level of stress. Moderate concentrations of H<sub>2</sub>O<sub>2</sub> (a physiologically relevant form of oxidative stress) permit regulated cardiomyocyte death through apoptosis, while at higher levels (>1 mM), death occurs by necrosis (Aikawa et al., 1997; Cook et al., 1999b; Kang et al., 2000; Kwon et al., 2003). Conversely, low levels of H<sub>2</sub>O<sub>2</sub> may have a hormetic effect and promote cytoprotection, while some investigators report induction of hypertrophy (Ytrehus et al., 1995; Valen et al., 1998; Kwon et al., 2003). H<sub>2</sub>O<sub>2</sub> induces substantial changes in cardiomyocyte gene expression, effects which are both time and concentration dependent. Previous investigations have used Affymetrix microarrays to determine the changes in cardiomyocyte gene expression induced by H<sub>2</sub>O<sub>2</sub> (Kemp et al., 2003; Clerk et al., 2007b). Exposure of cardiomyocytes to a non-toxic H<sub>2</sub>O<sub>2</sub> concentration (0.04 mM) results in changes in relatively few genes. Exposure to a pro-apoptotic H<sub>2</sub>O<sub>2</sub> concentration (0.2 mM) however, results in changes in a far greater number of genes at (649 mRNAs changed at 2 – 4 h) (Kemp et al., 2003; Clerk et al., 2007b). Amongst these, genes putatively associated with cytoprotection/modulation of apoptosis and antioxidation (e.g. Hsp70, Sod1, Hox1, p21<sup>cip1/waf1</sup>) are highly represented, as well as those associated with transcriptional regulation and intracellular signalling. The upregulation of these genes presumably reflects their importance in the cardiomyocyte response to H<sub>2</sub>O<sub>2</sub> as apoptosis proceeds (Kemp et al., 2003; Clerk et al., 2007b).

In addition to promoting changes in gene expression, pro-apoptotic H<sub>2</sub>O<sub>2</sub> concentrations also induce activation of intracellular signalling pathways including the three principal MAPK cascades, ERK1/2, JNKs and p38-MAPKs, in neonatal cardiomyocytes and adult perfused hearts (Clerk et al., 1998b; Clerk et al., 1998a). Investigations in cardiomyocytes indicate a major role for ERK1/2 in regulation of gene expression in response to the GqPCR agonists including ET-1, phenylephrine and A61603 (Kennedy et al., 2006; Cullingford et al., 2008a; Cullingford et al., 2008b; Marshall et al., 2010; Amirak et al., 2013). In cardiomyocytes, JNKs

phosphorylate c-Jun and ATF2 in response to cellular stresses (i.e. sorbitol; anisomycin) thus presumably regulating their transactivating activities and/or stability and influencing gene expression (Clerk and Sugden, 1997b). However, the role of JNKs and p38-MAPKs in regulating cardiomyocyte gene expression have yet to be elucidated. Moreover, the roles of any of the MAPKs in regulating changes in global gene expression profiles in cardiomyocytes exposed to H<sub>2</sub>O<sub>2</sub> have never been reported.

One strategy to investigate the roles of MAPKs in regulation of gene expression is an inhibitor approach coupled with microarray analysis. Selective and potent pharmacological inhibitors of MKK1/2 (the upstream activators of ERK1/2) such as U0126 (Favata et al., 1998) and PD184352 (Sebolt-Leopold et al., 1999) have long been available. These inhibitors have been used successfully in previous microarray expression profiling experiments to characterise the roles of ERK1/2 in regulation of cardiomyocyte gene expression (Kennedy et al., 2006; Amirak et al., 2013). In this investigation, PD184352 was used at 2 µM, a concentration that potently inhibits MKK1/2 activity, and therefore activation of ERK1/2 (Bain et al., 2007). PD184352's allosteric, non-ATP-competitive mechanism of action confers a high level of selectivity towards MKK1/2 (Ohren et al., 2004) and, although it can also inhibit MKK5 (the upstream activator of ERK5), this only occurs at higher concentrations (10 µM) (Mody et al., 2001). SB203580 (Cuenda et al., 1995), is an established inhibitor of p38-MAPK $\alpha$  (the predominant isoform expressed in heart) and p38-MAPK $\beta$  (expressed in heart at lower levels) (Marber et al., 2011). However, although widely used as a p38-MAPK $\alpha/\beta$  inhibitor, SB203580 also inhibits GSK3 $\beta$  and c-Raf (less potently than p38-MAPKs), CK1 and GAK (with similar potency) and RIPK2 (with greater potency) (Bain et al., 2007; Hall-Jackson et al., 1999; Godl et al., 2003). The compound also inhibits JNKs in cardiomyocytes and adult hearts at higher concentrations (Clerk and Sugden, 1998). While the reported effects of SB203580 on JNKs and c-Raf are of minimal concern here due to the low (0.7 µM) concentration to be used, non-p38-MAPK $\alpha/\beta$  dependent effects cannot be entirely ruled out in interpretation of any changes in RNA expression induced by SB203580. The poor selectivity of reported JNK inhibitors such as

SP600125 (Bennett et al., 2001) and AS601245 (Gaillard et al., 2005) has limited the potential to investigate the role of JNK pathway signalling. However, a potent and selective inhibitor, JNK-IN-8 (Zhang et al., 2012), has recently become available. JNK-IN-8 targets, and covalently binds to, a conserved cysteine residue preceding the JNK DFG-motif and thus exhibits higher selectivity compared to conventional kinase inhibitors, having no significant inhibitory activity against any other kinase in the “Kinativ™” chemical proteomics screening approach (Zhang et al., 2012; Liu et al., 2013). Accordingly, availability of JNK-IN-8 permits an inhibitor approach to investigate the contribution of JNKs in regulating cardiomyocyte gene expression.

The primary aim in this chapter is to establish the roles of ERK1/2, JNK and p38-MAPK signalling in the regulation cardiomyocyte gene expression in response to a pro-apoptotic concentration of H<sub>2</sub>O<sub>2</sub> (0.2 mM), using inhibitors of each pathway. ERK1/2 signalling was inhibited using PD184352. JNK signalling was inhibited using JNK-IN-8, while SB203580 was used to inhibit p38-MAPK $\alpha/\beta$  signalling.

## **3.2 Methods**

### **3.2.1 Preparation of cytosolic and nuclear protein enriched (NPE) extracts**

Cytosolic and nuclear protein enriched (NPE) extracts were prepared using the method described by Dignam *et al.* (1983) as described in Chapter Two, Section 2.5.2. Cardiomyocytes were treated as indicated, washed twice with ice-cold PBS and scraped into 150  $\mu$ l cytosolic extraction buffer. Following extraction on ice (10 min), the samples were centrifuged (10000 $\times$ g, 5 min, 4°C) and the supernatants (i.e. the cytosolic fractions) removed to a clean tube and boiled with 0.33 volume of 4 $\times$  sample buffer. For the preparation of NPE extracts, the resulting pellets from the previous centrifugation step were resuspended in 50  $\mu$ l of nuclear extraction buffer and extracted on ice for 60 min, with periodic vortex-mixing at 10 – 15 min intervals. Samples were then centrifuged (10000 $\times$ g, 5 min, 4°C) and the supernatant NPE extracts

transferred to a clean tube and boiled with 0.5 volume of 4x sample buffer. Protein content for both the cytosolic and NPE fractions was quantified using the Bio-Rad Protein Assay as described in Chapter Two, Section 2.5.4.

### **3.2.2 Microarray sample preparation**

Cardiomyocytes were either untreated, or exposed to 0.2 mM H<sub>2</sub>O<sub>2</sub> (2 h) with or without pre-treatment (15 min) with 2 µM PD184352, 1 µM JNK-IN-8 or 0.7 µM SB203580, or to each inhibitor alone (2 h 15 min). Additions of agonist/inhibitors was staggered and the cardiomyocytes were harvested simultaneously. Total RNA was extracted as described in Chapter Two, Section 2.7. Extracted RNA was stored at -80°C.

To minimise variation between cardiomyocyte preparations, equal amounts of RNA from two separate cardiomyocyte preparations were pooled to produce a single sample for microarray hybridisation. For expression profiling of cardiomyocytes exposed to the inhibitors in isolation, three such samples were hybridised to separate microarrays (i.e. n=3 independent samples analysed per condition). For cardiomyocytes exposed to H<sub>2</sub>O<sub>2</sub> in the presence or absence of the inhibitors and for unexposed control cardiomyocytes, four such samples for each condition were hybridised to separate arrays (i.e. n=4 independent samples analysed per condition). Total RNA was supplied to Source BioScience for confirmatory quality control using a nanophotometer and by obtaining an RNA integrity number (Agilent Technologies Ltd.), followed by preparation and hybridisation to Affymetrix GeneChip Rat Gene 2.0 ST arrays according to their protocols.

### **3.2.3 Microarray data analysis**

The analysis was performed by Prof. Angela Clerk. Microarray data (.CEL files) were imported into GeneSpring 14.5 (Agilent Technologies) and normalised using the PLIER16 algorithm, with normalisation per gene to the median of the controls. Probe sets were filtered by

expression, removing those below the lowest 20th percentile and then removing any with expression values below 50 in the raw data in all samples for any condition. The initial analysis was for MAPK inhibitors alone relative to unstimulated controls. Probe sets were selected on the basis of 1.5-fold change relative to controls. Statistical analysis used one-way ANOVA with SNK post-test and a Benjamini-Hochberg false discovery rate (FDR) correction. Probe sets were selected with a corrected value of  $p < 0.05$ .

To study the effects of MAPK inhibitors on the changes induced by  $H_2O_2$ , significant changes induced by  $H_2O_2$  were first identified. Probe sets were selected on the basis of 1.5-fold increase or decrease with  $H_2O_2$  relative to unstimulated controls and statistical analysis used a moderated t-test with a Benjamini-Hochberg FDR correction. Probe sets were selected with a corrected value of  $p < 0.05$ . With respect to the effects of the three MAPK inhibitors on the changes induced by  $H_2O_2$ , probe sets were selected on the basis of a  $> 1.25$ -fold difference in expression between  $H_2O_2$  alone and  $H_2O_2$  in the presence of inhibitors. Probe sets changed by inhibitors fall into two groups: Group I contains those of high confidence with statistically significant changes in the presence of inhibitor (one-way ANOVA with SNK post-test and a Benjamini-Hochberg FDR correction, corrected value  $p < 0.05$ ) while Group II contains those of lower confidence which were changed  $> 1.25$ -fold but were not statistically significant.

### **3.2.3.1 Gene Ontology analysis of microarray expression data**

Data for genes identified by the microarray analysis as being upregulated in response to  $H_2O_2$  and further changed by the MAPK inhibitors were subjected to Gene Ontology analysis using the PANTHER GO-slim tool (Mi *et al.*, 2013). For each MAPK inhibitor, a list of genes of established identity (identified by gene symbol) was uploaded to the PANTHER Workspace and analysed using the PANTHER GO-slim tool, classifying genes by Biological Process or Protein Class, as indicated in the figure legends.

### **3.2.4 Validation of microarray data using qPCR**

Cardiomyocytes were untreated, or exposed to 0.2 mM H<sub>2</sub>O<sub>2</sub> (2 h) with or without pre-treatment (15 min) with 2 μM PD184352, 1 μM JNK-IN-8 or 0.7 μM SB203580, or to each inhibitor alone (2 h 15 min). Additions of agonist/inhibitors were staggered and the cardiomyocytes were harvested simultaneously. Total RNA was extracted as described in Chapter Two, Section 2.7 and qPCR was performed as described in Chapter Two, Section 2.8, using specific primers. Genes identified by microarray analysis were selected for validation based on their responses to the various treatments. Expression values were normalised to values for Gapdh and then to the mean of the controls. RNAs extracted for qPCR analysis (n=3/4 independent cardiomyocyte preparations) were not those used for microarray analyses.

## **3.3 Results**

### **3.3.1 Nuclear localisation of activated MAPKs in cardiomyocytes exposed to H<sub>2</sub>O<sub>2</sub>**

In non-cardiac cells, ERK1/2, JNKs and p38-MAPKs each modulate transcriptional activity by phosphorylating nuclear-localised substrates. It is thus necessary to determine if active forms of these kinases are present in the nucleus. To examine the nuclear localisation of activated MAPKs, cardiomyocytes were exposed to 0.2 mM H<sub>2</sub>O<sub>2</sub> for 0 – 60 min and cytosolic and NPE (nuclear protein-enriched) fractions immunoblotted with antibodies to phosphorylated (i.e. activated) or total ERK1/2, JNKs or p38-MAPKs. H<sub>2</sub>O<sub>2</sub> promoted maximal activation of both ERK1 and ERK2 at 20 – 30 min with similar profiles of activation in both the cytosolic and NPE fractions. (Fig. 3.1, A and B) In the NPE fraction, there was a significant increase in phospho-ERK1 relative to control following 10 min H<sub>2</sub>O<sub>2</sub> stimulation (3.26±0.17-fold, p<0.0001). There was also a significant increase in phospho-ERK2 in the NPE fraction following 20 min H<sub>2</sub>O<sub>2</sub> stimulation (2.37±0.09-fold relative to control, p<0.01). (Fig. 3.1, A and B). In unstimulated cardiomyocytes, the relative proportions of nuclear-localised total ERK1 and ERK2 differed: 21±3% of total ERK1 and 43±8% of total ERK2 were nuclear localised (Fig. 3.1C). However,

there was no significant change in localisation of either total ERK1 or ERK2 protein in response to H<sub>2</sub>O<sub>2</sub> (Fig. 3.1C).

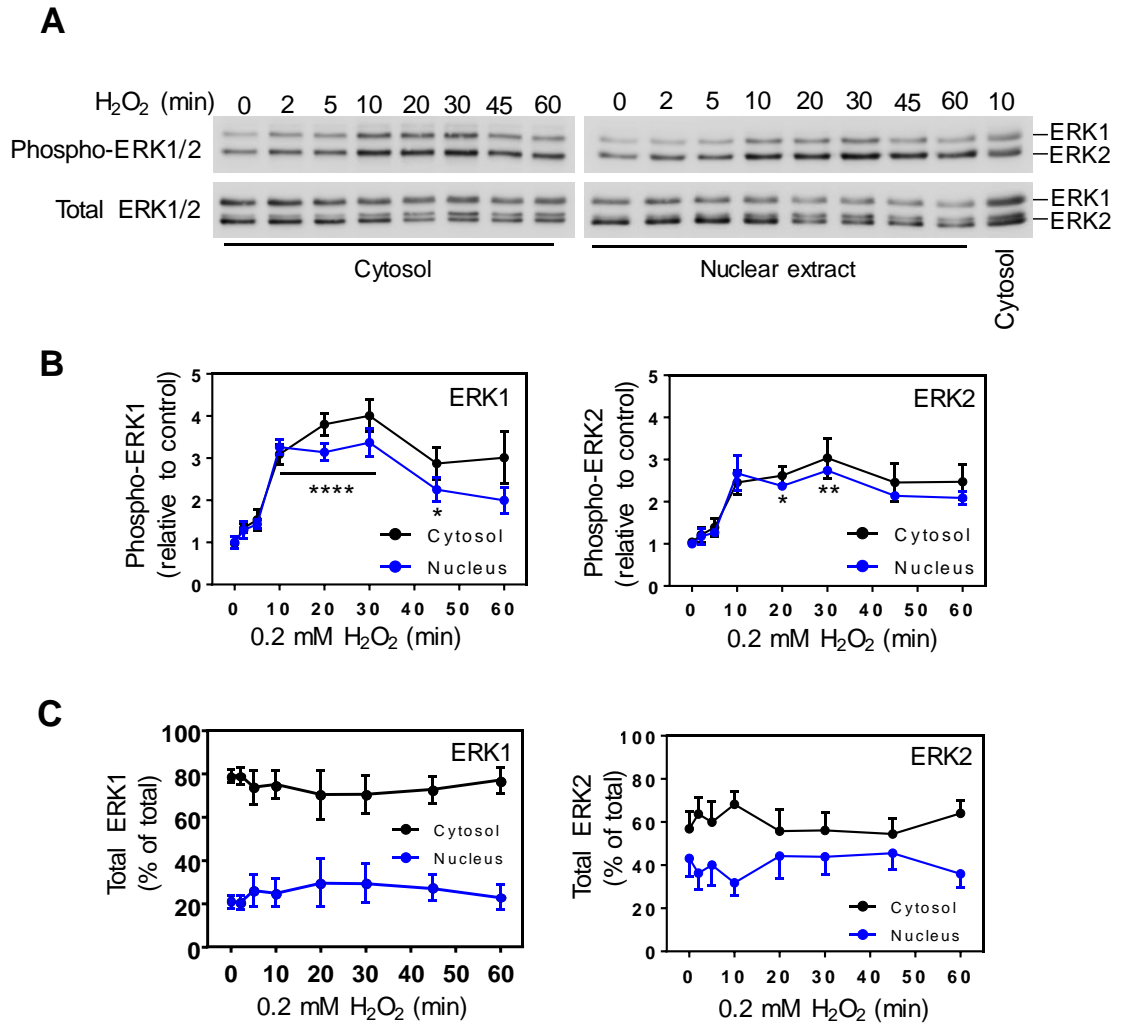


**Figure 3.1 Nuclear signalling of ERK1/2 in response to H<sub>2</sub>O<sub>2</sub> in cardiomyocytes.**

(A) Cardiomyocytes were either unstimulated or exposed to 0.2 mM H<sub>2</sub>O<sub>2</sub> (2 – 60 min). Cytosolic and NPE extracts were immunoblotted with antibodies to phosphorylated or total ERK1/2. (B) and (C) Densitometric analysis of the immunoblots in (A). Results are means ± SEM (n=4 independent cardiomyocyte preparations) and are normalised to the mean of control values. \*, p<0.05; \*\*, p<0.01; \*\*\*\*, p<0.0001 relative to nuclear extract control (one-way ANOVA with Tukey post-test).

Maximal, significant, activation of p46- and p54-JNKs was detected in the cytosolic fraction following 10 min H<sub>2</sub>O<sub>2</sub> exposure (Fig. 3.2, A and B). Activation of p46-JNKs in the cytosolic fraction was 5.7±0.75-fold relative to control (p<0.001) with a 4.33±0.36-fold increase in p54-JNK activation (p<0.01) (Fig. 3.2, A and B). In the NPE fraction, activation of p46-JNKs was 2.57±0.53-fold relative to control at 10 min, although this was not statistically significant. There was also an increase in activated p54-JNKs in the NPE fraction at 10 min (to 1.74±0.48-fold) although, as with the p46-JNKs, this was not statistically significant (Fig. 3.2, A and B).

Total JNKs were predominantly localised to the cytoplasm in unstimulated cardiomyocytes (Fig. 3.2C). While 19±5% of total p46-JNKs and 11±3% of total p54-JNKs were nuclear localised (Fig. 3.2C), there was no significant change in localisation of total JNK protein in response to H<sub>2</sub>O<sub>2</sub> (Fig. 3.2C).

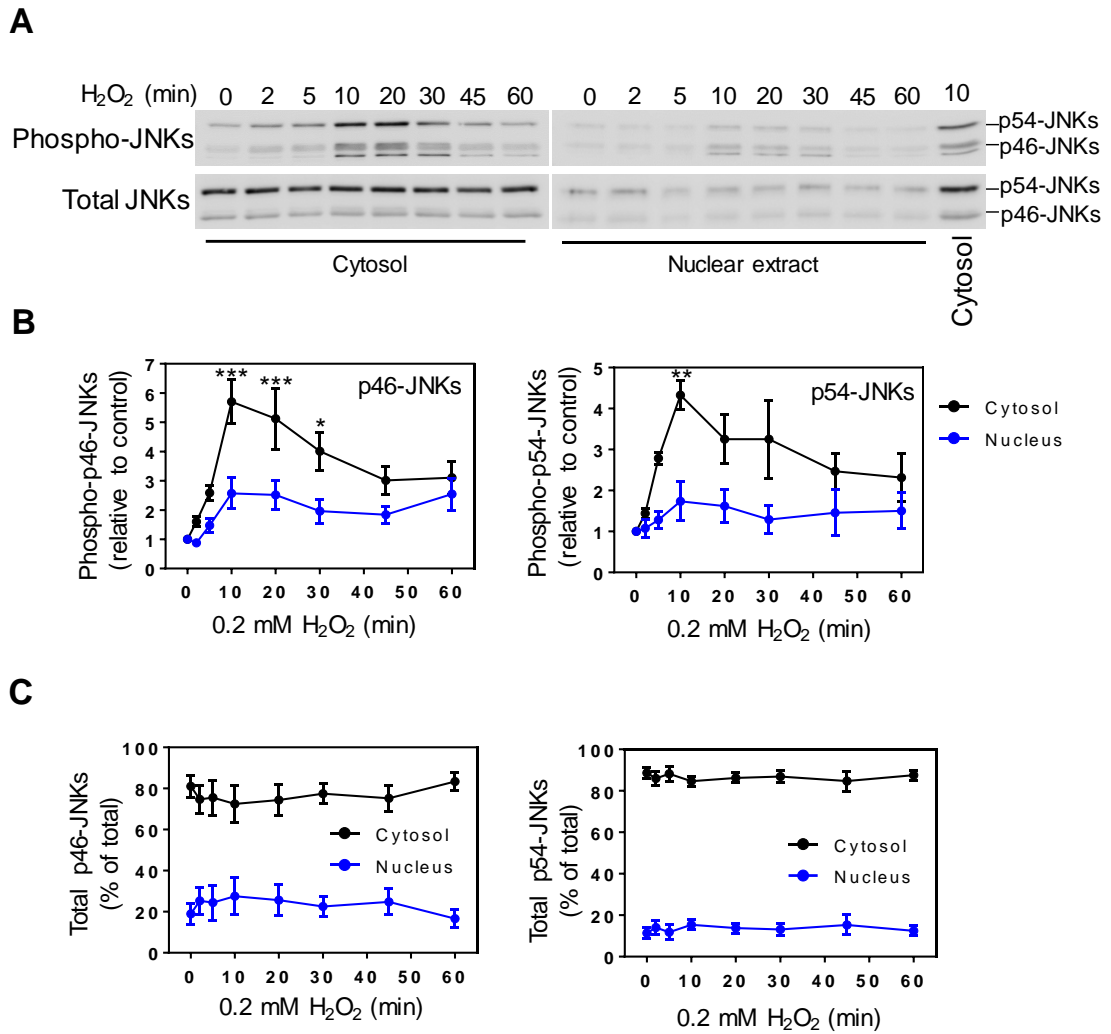


**Figure 3.2 Nuclear signalling of JNKs in response to H<sub>2</sub>O<sub>2</sub> in cardiomyocytes.**

(A) Cardiomyocytes were unstimulated or exposed to 0.2 mM H<sub>2</sub>O<sub>2</sub> (2 – 60 min). Cytosolic and NPE extracts were immunoblotted with antibodies to phosphorylated or total JNKs. (B) and (C) Densitometric analysis of the immunoblots in (A). Results are means ± SEM (n=4 independent cardiomyocyte preparations) and are normalised to the mean of control values. \*, p<0.05; \*\*, 0.01; \*\*\*, p<0.001 relative to cytosolic extract control (one-way ANOVA with Tukey post-test).

H<sub>2</sub>O<sub>2</sub> exposure induced a significant increase in activated p38-MAPKs in the cytoplasmic fraction after 2 min (5.80±1.8-fold relative to control, p<0.05) with a maximal response at 5 min (7.8±1.37-fold relative to control, p<0.001) (Fig. 3.3, A and B). H<sub>2</sub>O<sub>2</sub> induced a 1.8±0.23-fold, increase in phospho-p38-MAPKs in the NPE fraction at 2 min, although this was not statistically significant (Fig. 3.3, A and B).

Total p38-MAPKs were predominantly localised to the cytoplasm of unstimulated cardiomyocytes. Although 10±0.5% of total p38-MAPKs were localised to the nucleus under basal conditions, (Fig. 3.3C), H<sub>2</sub>O<sub>2</sub> did not induce a significant change in localisation of total p38-MAPK protein (Fig. 3.3C).

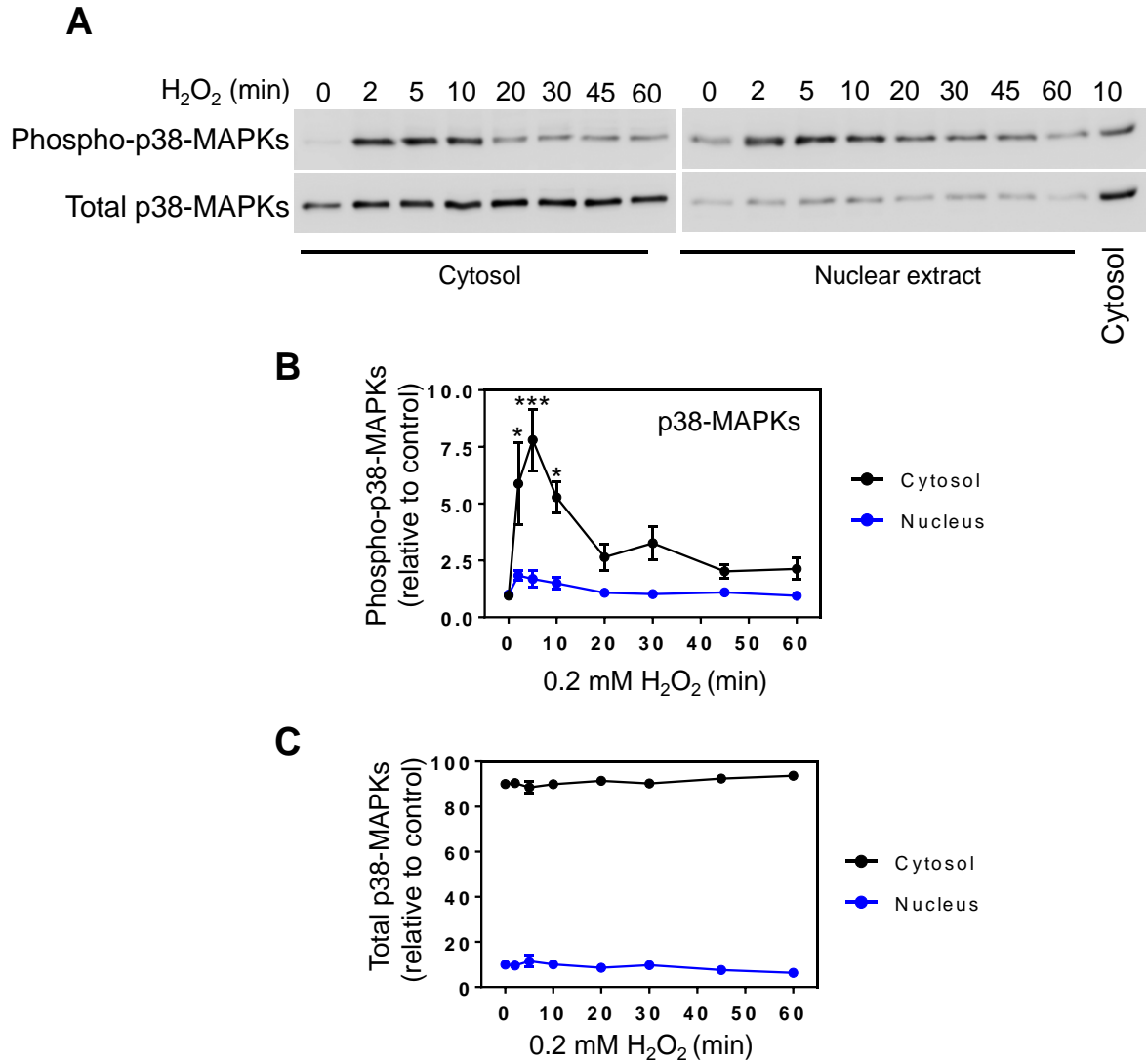


**Figure 3.3 Nuclear signalling of p38-MAPKs in response to H<sub>2</sub>O<sub>2</sub> in cardiomyocytes.**

(A) Cardiomyocytes were unstimulated or exposed to 0.2 mM H<sub>2</sub>O<sub>2</sub> (2 – 60 min). Cytosolic and NPE extracts were immunoblotted with antibodies to phosphorylated or total p38-MAPKs. (B) and (C) Densitometric analysis of the immunoblots in (A). Results are means ± SEM (n=4 independent cardiomyocyte preparations) and are normalised to the mean of control values. \*, p<0.05; \*\*\*, p<0.001 relative to cytosolic extract control (one-way ANOVA with Tukey post-test).

### 3.3.2 Selective pharmacological inhibition of ERK1/2, JNK and p38-MAPK signalling.

PD184352 was used to inhibit ERK1/2 signalling (Sebolt-Leopold et al., 1999), JNK-IN-8 was used to inhibit JNK signalling (Zhang et al., 2012) and SB203580 was used to inhibit p38-MAPK $\alpha/\beta$  signalling (Cuenda et al., 1995). To assess the potency and selectivity of the pharmacological inhibitors to be used, cardiomyocytes were untreated or exposed to H<sub>2</sub>O<sub>2</sub> (0.2 mM, 10 min) with or without 15 min pre-treatment with 2  $\mu$ M PD184352, 1  $\mu$ M JNK-IN-8 or 0.7  $\mu$ M SB203580; or to each inhibitor in isolation (25 min). PD184352 inhibits MKK1/2, which activate ERK1/2 (Sebolt-Leopold et al., 1999). Immunoblotting of cytosolic fractions for total and phosphorylated (i.e. activated) ERK1/2 demonstrated that exposure to PD184352 alone significantly reduced baseline ERK1/2 phosphorylation relative to control (Fig 3.4, A and B). Phospho-ERK1 was reduced to 0.04 $\pm$ 0.01-fold while phospho-ERK2 was decreased to 0.03 $\pm$ 0.01-fold relative to control values. There was no significant effect of JNK-IN-8 or SB203580 on baseline ERK1/2 phosphorylation (Fig 3.4, A and B). H<sub>2</sub>O<sub>2</sub> induced a significant increase in phosphorylated ERK1 relative to control (3.92 $\pm$ 0.44-fold) and this was significantly reduced by PD184352 to below baseline levels (0.08 $\pm$ 0.02-fold) (Fig 3.4, A and B). H<sub>2</sub>O<sub>2</sub> induced a 3.3 $\pm$ 0.53-fold increase in phospho-ERK2. This was not statistically significant, although the response of ERK2 to H<sub>2</sub>O<sub>2</sub> was significantly reduced by PD184352 to below baseline levels (0.09 $\pm$ 0.02-fold) (Fig 3.4, A and B). H<sub>2</sub>O<sub>2</sub> exposure also resulted in detection of reduced mobility ERK2 bands (Fig 3.4, A and B). The appearance of these bands was abolished by exposure to PD184352 (Fig. 3.4A, lower blot). Neither JNK-IN-8 nor SB203580 had a significant effect on baseline ERK1/2 phosphorylation or response of ERK1/2 to H<sub>2</sub>O<sub>2</sub> (Fig 3.4, A and B).

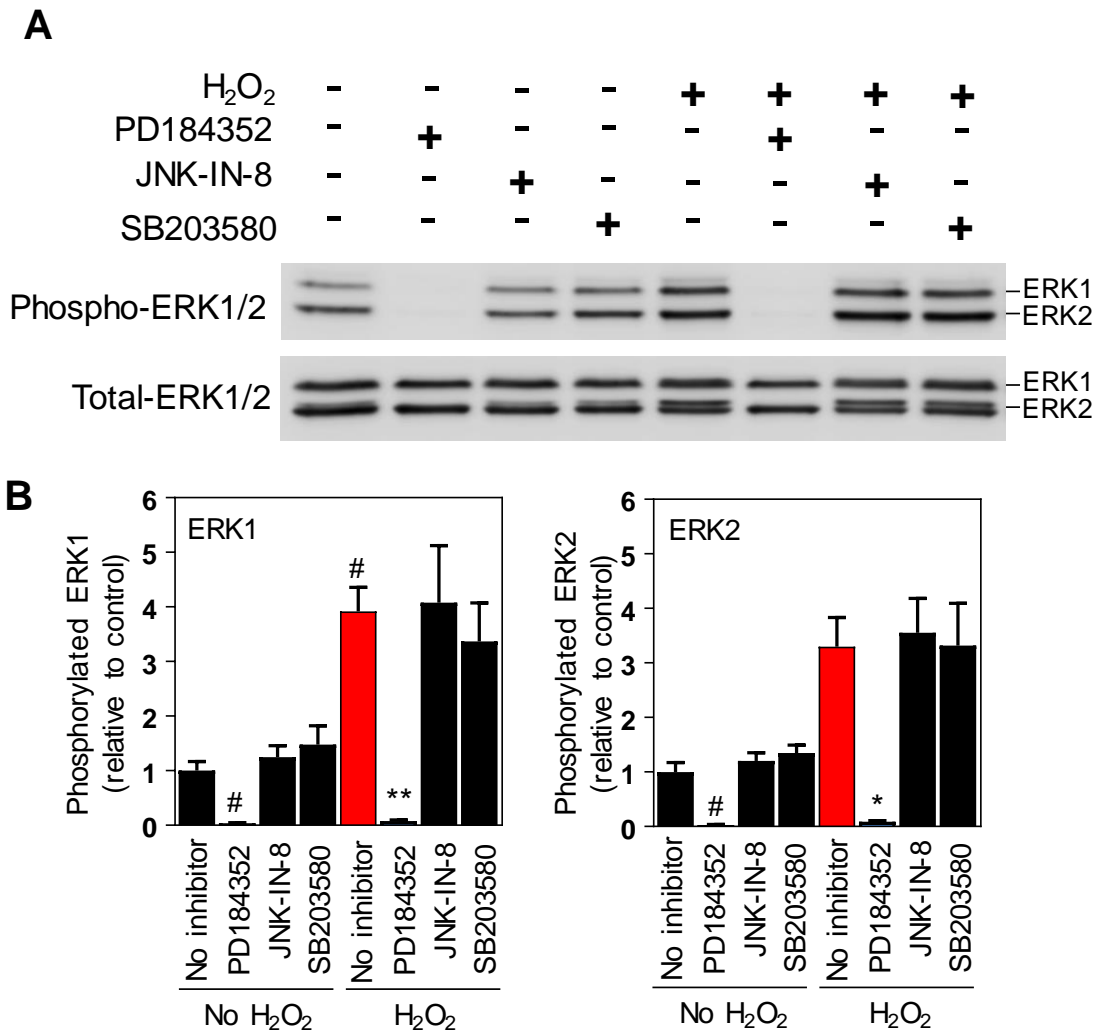


**Figure 3.4 Inhibition of ERK1/2 signalling by PD184352.**

(A) Cardiomyocytes were unstimulated or exposed to 0.2 mM H<sub>2</sub>O<sub>2</sub> (10 min), with or without pre-treatment (15 min) with 2 μM PD184352, 1 μM JNK-IN-8 or 0.7 μM SB203580, or exposed to the inhibitors in isolation (25 min). Cytosolic protein extracts (10 μg) were immunoblotted with antibodies to phosphorylated or total ERK1/2. (B) Densitometric analysis of the immunoblots in (A). Values for phospho-ERK1/2 were normalised to total ERK1/2. Results are means ± SEM (n=5 independent cardiomyocyte preparations) relative to the mean of the control values. #, p<0.05 relative to control. \*, p<0.05; \*\*, p<0.01 relative to H<sub>2</sub>O<sub>2</sub> alone (one-way ANOVA with Tukey post-test).

As JNK-IN-8 inhibits activity of JNKs rather than JNK activation *per se* (Zhang et al., 2012), the effects of the inhibitors on phosphorylation of c-Jun (a direct substrate of JNKs) were assessed using antibodies to c-Jun phosphorylated on a transactivating domain phosphorylation site, Ser63 (May et al., 1998). JNK-IN-8 (but not PD184352 or SB203580) had a significant effect on phosphorylation of c-Jun at Ser63, reducing phospho-c-Jun to  $0.43 \pm 0.1$ -fold relative to control (Fig. 3.5, A and B). Exposure to  $H_2O_2$  led to a significant increase in phospho-c-Jun to  $1.98 \pm 0.11$ -fold compared to control and JNK-IN-8 significantly reduced the response to  $H_2O_2$  to below control values (Fig. 3.5, A and B). However, there was no significant effect of either PD184352 or SB203580 on the phosphorylation of c-Jun in response to  $H_2O_2$  (Fig. 3.5, A and B).

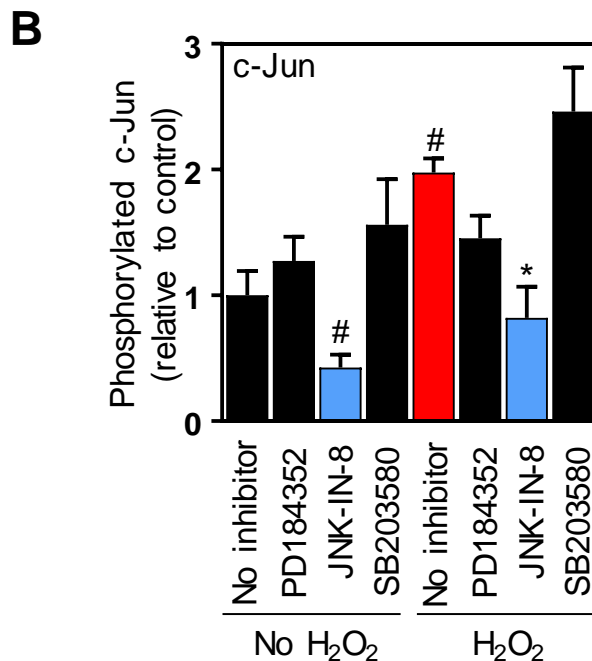
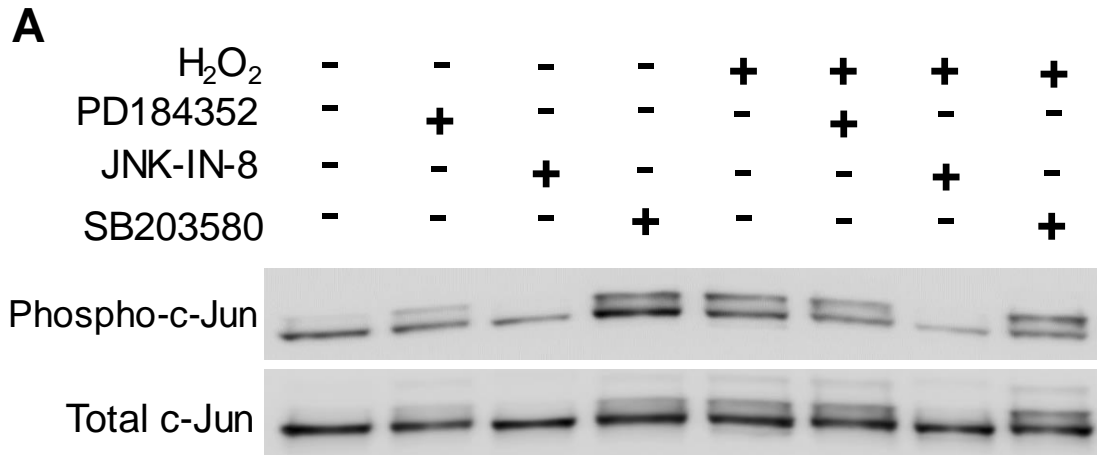


**Figure 3.5 Inhibition of JNK signalling by JNK-IN-8.**

(A) Cardiomyocytes were unstimulated (controls) or exposed to 0.2 mM H<sub>2</sub>O<sub>2</sub> (10 min), with or without pre-treatment (15 min) with 2 μM PD184352, 1 μM JNK-IN-8 or 0.7 μM SB203580, or exposed to the inhibitors in isolation (25 min). Nuclear protein enriched extracts (15 μg) were immunoblotted with antibodies to phospho-c-Jun (pSer63) or total-c-Jun (lower panels). (B) Densitometric analysis of the immunoblots in (A). Values for phospho-proteins were normalised to total protein values. Results are means ± SEM (n=5 independent cardiomyocyte preparations) relative to mean of the control values. #, p<0.05 relative to control. \*, p<0.05 relative to H<sub>2</sub>O<sub>2</sub> alone (one-way ANOVA with Tukey post-test).

SB203580 is an established inhibitor of p38-MAPK $\alpha/\beta$  isoforms in cardiomyocytes (Clerk et al., 1998b). To confirm efficacy and selectivity of SB203580 in inhibiting p38-MAPK $\alpha/\beta$  in response to H<sub>2</sub>O<sub>2</sub>, cytosolic fractions were immunoblotted with antibodies to phosphorylated and total MAPKAPK2, a well-characterised substrate of p38-MAPKs. MAPKAPK2 was detected as two bands; of ~42 kDa and ~49 kDa, presumably reflecting detection of the isoform variants AAO34665.1 (predicted molecular weight ~44 kDa) and XP\_017454181.1 (predicted molecular weight ~50 kDa). None of the inhibitors alone had a significant effect on phosphorylation of either MAPKAPK2 species (Fig. 3.6, A and B). H<sub>2</sub>O<sub>2</sub> led to a significant increase in phosphorylation of the 50 kDa MAPKAPK2 form compared to control (to 15.6±1.38-fold) (Fig. 3.6, A and B) and SB203580 significantly inhibited this response to 2.0±0.28-fold relative to control (Fig. 3.6, A and B). Similarly, exposure to H<sub>2</sub>O<sub>2</sub> resulted in a 7.96±0.82-fold increase in phosphorylation of the 44 kDa MAPKAPK2 form relative to control (Fig. 3.6, A and B) and SB203580 significantly inhibited this to 1.88±0.39-fold compared to control (Fig. 3.6, A and B). Neither PD184352 nor JNK-IN-8 had a significant effect on the response of MAPKAPK2 to H<sub>2</sub>O<sub>2</sub> (Fig. 3.6, A and B).

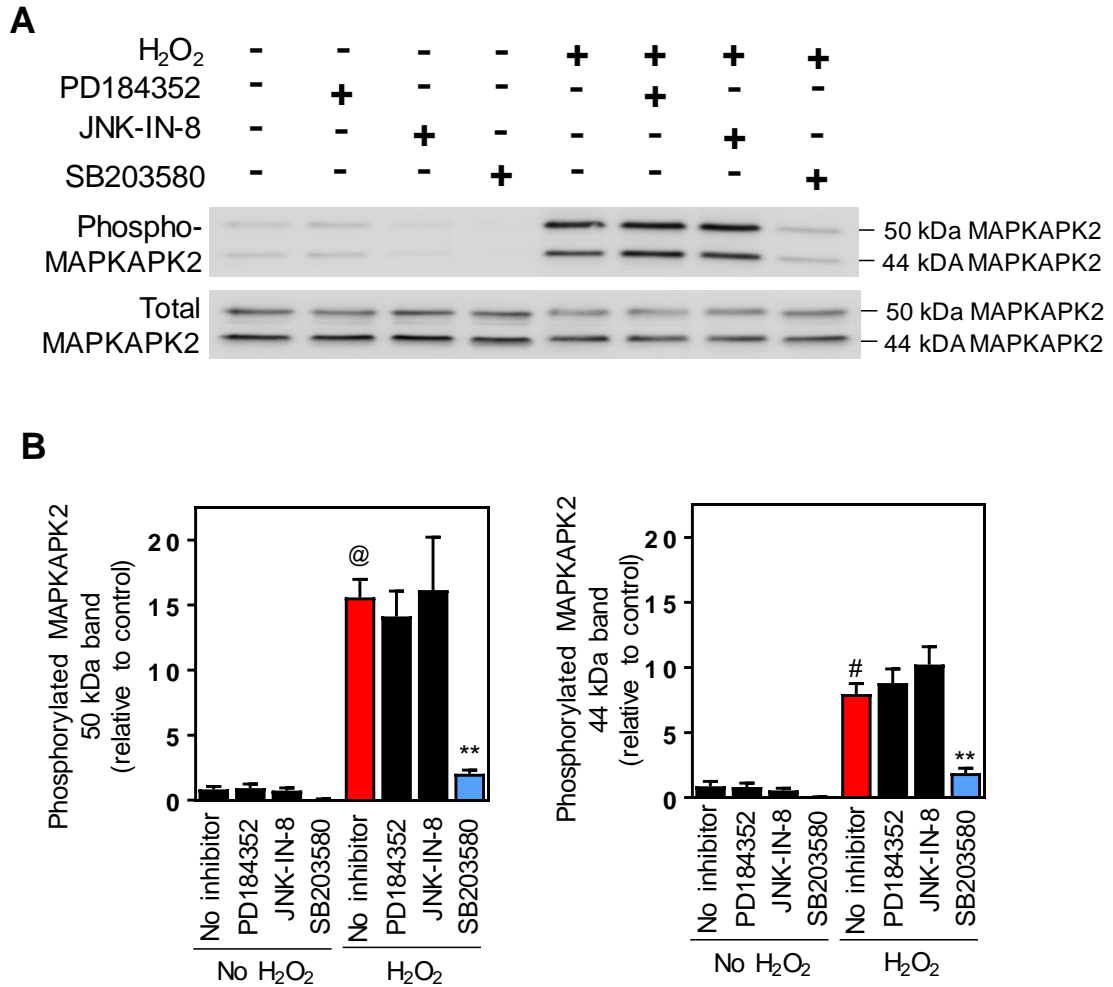


**Figure 3.6 Inhibition of p38-MAPK signalling by SB203580.**

(A) Cardiomyocytes were unstimulated (controls) or exposed to 0.2 mM H<sub>2</sub>O<sub>2</sub> (10 min), with or without pre-treatment (15 min) with 2 μM PD184352, 1 μM JNK-IN-8 or 0.7 μM SB203580; or exposed to the inhibitors in isolation (25 min). Cytosolic protein extracts (10 μg) were immunoblotted for phospho-MAPKAPK2 (pThr222/pThr334) or total-MAPKAPK2 (lower panels). (B) Densitometric analysis of the immunoblots in (A). Values for phospho-MAPKAPK2 were normalised to values for total MAPKAPK2. Results are means ± SEM (n=5 independent cardiomyocyte preparations) relative to mean of the control values. #, p<0.05, @, p<0.01 relative to control. \*\*, p<0.01 relative to H<sub>2</sub>O<sub>2</sub> alone (one-way ANOVA with Tukey post-test).

### **3.3.3 Regulation of basal cardiomyocyte RNA expression by MAPKs**

Having confirmed the selectivity and efficacy of the selected MAPK inhibitors, the contributions of ERK1/2, JNK and p38-MAPK signalling to cardiomyocyte RNA expression were investigated using microarrays. Cardiomyocytes were exposed to each inhibitor in isolation (2 h 15 min). Expression profiling was performed using Affymetrix Rat Gene ST 2.0 microarrays and data analysed using GeneSpring Software.

Of the three MAPK inhibitors, PD184352 had the greatest effect on basal cardiomyocyte RNA expression, causing downregulation of 92, and upregulation of 32 RNAs (Fig. 3.7A and Appendix II, Table A1). JNK-IN-8 and SB203580, however, induced more minor changes in baseline RNA expression: JNK-IN-8 downregulated 12, and upregulated 2, RNAs (Fig. 3.7B and Appendix II, Table A2) while SB203580 downregulated only 1, and upregulated 5, RNAs (Fig. 3.7C and Appendix II, Table A3).

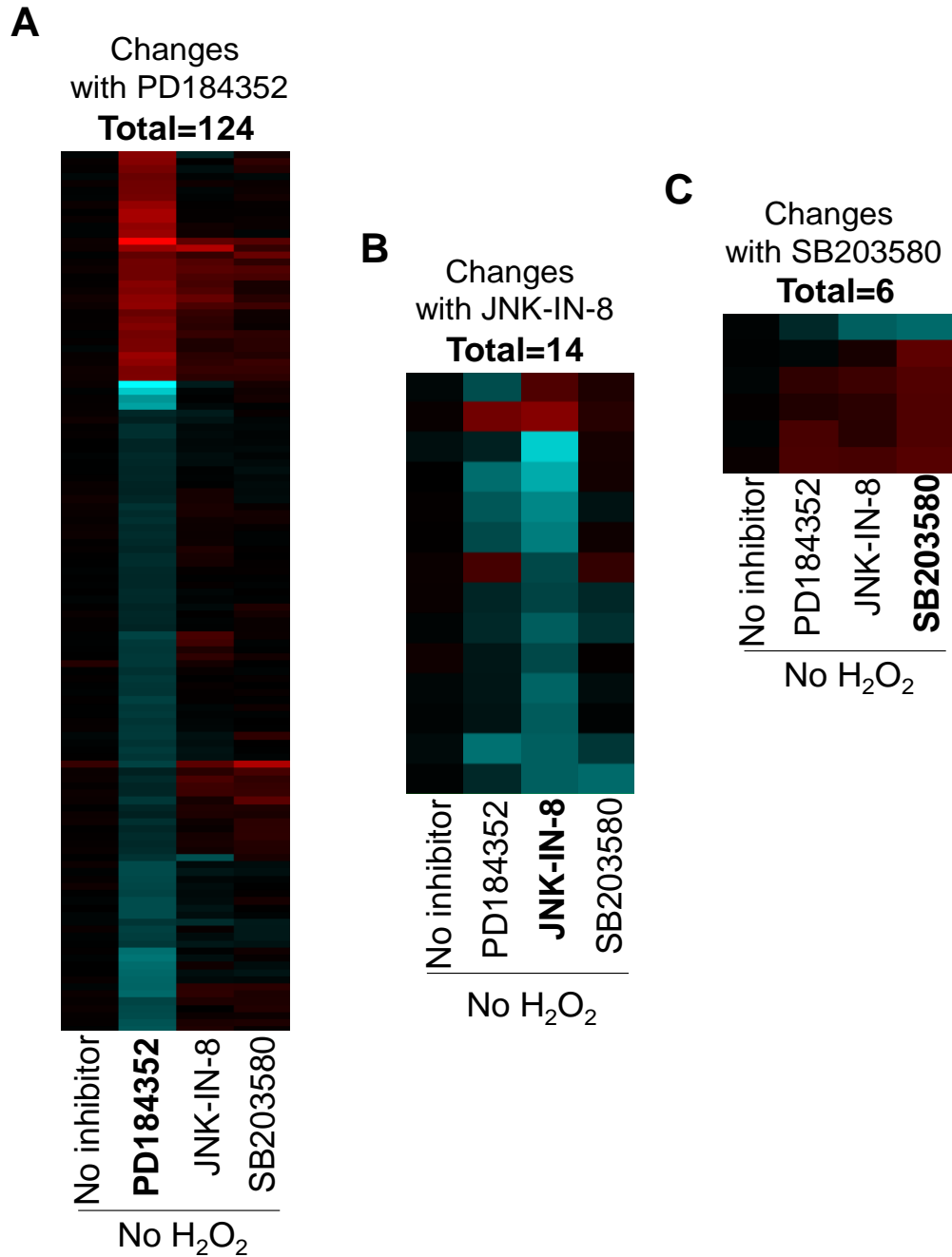


**Figure 3.7 Regulation of baseline cardiomyocyte RNA expression by PD184352, JNK-IN-8 or SB203580.**

Cardiomyocytes were unstimulated or exposed to PD184352 (2  $\mu$ M), JNK-IN-8 (1  $\mu$ M) or SB203580 (0.7  $\mu$ M) for 2 h 15 min. Changes in RNA expression were determined using Affymetrix Rat Gene 2.0 ST microarrays, using GeneSpring analysis to identify RNAs with significant changes in expression (>1.5-fold relative to control) and a significant effect of the inhibitors (one-way ANOVA with SNK post-test and Benjamini-Hochberg FDR correction,  $p < 0.05$ ). **(A)** Upregulation or downregulation by PD184352. **(B)** Upregulation or downregulation by JNK-IN-8. **(C)** Upregulation or downregulation by SB203580. Heatmaps range from -2.0 (cyan) through 0 (black) to 2.0 (red); Log<sub>2</sub> scale.

#### 3.3.4 Regulation of cardiomyocyte RNA expression by MAPKs in response to H<sub>2</sub>O<sub>2</sub>

Previous expression profiling studies indicate substantial changes in cardiomyocyte mRNA expression following a 2 h exposure to 0.2 mM H<sub>2</sub>O<sub>2</sub> (Kemp et al., 2003; Clerk et al., 2007b). Accordingly, cardiomyocytes were untreated or exposed to H<sub>2</sub>O<sub>2</sub> (0.2 mM, 2 h) with or without pre-treatment (15 min) with PD184352 (2 μM, inhibits ERK1/2 signalling), JNK-IN-8 (1 μM, inhibits JNK signalling) or SB203580 (0.7 μM, inhibits p38-MAPKα/β signalling).

The expression of a total of 490 transcripts was significantly changed in response to H<sub>2</sub>O<sub>2</sub> (Fig. 3.8 and Appendix II, Tables A4 – 5). Of these, 295 were upregulated in response to H<sub>2</sub>O<sub>2</sub> (Appendix II, Table A4) while the remaining 195 were downregulated (Appendix II, Table A5).

A manual analysis was conducted to compare the expression profile obtained in the present study to that generated previously (Clerk et al., 2007b), by comparing the respective lists of genes that were identified significantly upregulated (>1.5 fold, p<0.05) in response to H<sub>2</sub>O<sub>2</sub> from each study. Overall, a larger number of genes were identified by the previous study as being upregulated in response to H<sub>2</sub>O<sub>2</sub> (391 genes in Clerk *et al.*, 2007b vs 295 in the present study). A comparison of the two gene lists indicated that ~42% of the genes identified as upregulated in the present study were also identified as such by Clerk *et al.*

Changes with H<sub>2</sub>O<sub>2</sub>  
**Total=490**

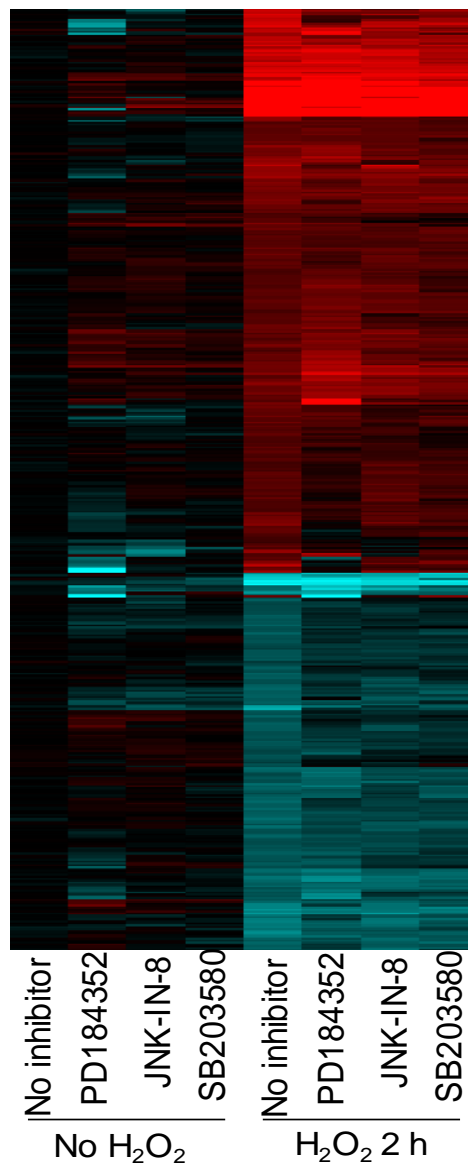


**Figure 3.8 Changes in cardiomyocyte RNA expression induced by H<sub>2</sub>O<sub>2</sub>**

Cardiomyocytes were unstimulated or exposed to H<sub>2</sub>O<sub>2</sub> (0.2 mM, 2 h) with or without pre-treatment (15 min) with PD184352 (2 μM), JNK-IN-8 (1 μM) or SB203580 (0.7 μM), or were exposed to the inhibitors alone (2 h 15 min). Changes in RNA expression were determined using Affymetrix Rat Gene 2.0 ST microarrays, using GeneSpring analysis to identify RNAs with significant increase or decrease in expression in response to H<sub>2</sub>O<sub>2</sub> (>1.5-fold change relative to control; moderated t-test with Benjamini-Hochberg FDR correction, p<0.05). Heatmaps range from -2.0 (cyan) through 0 (black) to 2.0 (red); Log<sub>2</sub> scale.

### 3.3.4.1 Effects of MAPK inhibitors on cardiomyocyte RNA expression induced by H<sub>2</sub>O<sub>2</sub>

Of the 295 transcripts upregulated in response to H<sub>2</sub>O<sub>2</sub>, the expression of 128 (~43%) was unchanged by any inhibitor (Appendix II, Table A6), while of the 195 transcripts downregulated in response to H<sub>2</sub>O<sub>2</sub>, the expression of 86 (~44%) was unaffected by any inhibitor (Appendix II, Table A7).

With respect to those RNAs upregulated in response to H<sub>2</sub>O<sub>2</sub>, PD184352 had the greatest effect of the inhibitors, with somewhat lesser effects of JNK-IN-8 or SB203580. PD184352 caused further changes in expression of ~37% of the transcripts induced by H<sub>2</sub>O<sub>2</sub> (Fig. 3.9A and Table 3.1). JNK-IN-8 further changed the expression of ~25% of the transcripts upregulated by H<sub>2</sub>O<sub>2</sub> (Fig. 3.9B and Table 3.1) while SB203580 further changed the expression of ~28% of transcripts induced by H<sub>2</sub>O<sub>2</sub> (Fig. 3.9C and Table 3.1).

**Table 3.1 Numbers of RNAs upregulated by H<sub>2</sub>O<sub>2</sub> and affected by MAPK inhibitors**

Results are the numbers of RNAs upregulated by H<sub>2</sub>O<sub>2</sub> and changed further in the presence of the inhibitors, as indicated. Group I refers to RNAs changed >1.25-fold relative to H<sub>2</sub>O<sub>2</sub> with a significant effect of the inhibitor (one-way ANOVA with SNK post-test and Benjamini-Hochberg FDR correction, p<0.05). Group II refers to RNAs changed >1.25-fold relative to H<sub>2</sub>O<sub>2</sub> alone but without a significant effect of the inhibitor. Details of specific RNAs regulated can be found in Appendix II.

	Upregulated by H <sub>2</sub> O <sub>2</sub>		Total
	Group I	Group II	
<b>PD184325</b>	66	42	108
<b>JNK-IN-8</b>	28	47	75
<b>SB203580</b>	24	60	84
<b>PD184352 and JNK-IN-8</b>	10	35	45
<b>PD184352 and SB203580</b>	8	29	37
<b>JNK-IN-8 and SB203580</b>	2	34	36
<b>All inhibitors</b>	7	11	18

Exposure to PD184352 resulted in changes in ~33% of the RNAs downregulated by H<sub>2</sub>O<sub>2</sub> (Fig. 3.9A and Table 3.2) while JNK-IN-8 resulted in further changes to ~28% of these transcripts (Fig. 3.9B and Table 3.2). However, SB2023580 had the greatest effect of the inhibitors on RNAs downregulated in response to H<sub>2</sub>O<sub>2</sub>, causing further changes in the expression of ~35% of these transcripts (Fig. 3.9C and Table 3.2).

**Table 3.2 Numbers of RNAs downregulated by H<sub>2</sub>O<sub>2</sub> and affected by MAPK inhibitors**

Results are the numbers of RNAs downregulated by H<sub>2</sub>O<sub>2</sub> and changed further in the presence of the inhibitors, as indicated. Group I refers to RNAs changed >1.25-fold relative to H<sub>2</sub>O<sub>2</sub> with a significant effect of the inhibitor (one-way ANOVA with SNK post-test and Benjamini-Hochberg FDR correction, p<0.05). Group II refers to RNAs changed >1.25-fold relative to H<sub>2</sub>O<sub>2</sub> alone but without a significant effect of the inhibitor. . Details of specific RNAs regulated can be found in Appendix II.

	Downregulated by H <sub>2</sub> O <sub>2</sub>		Total
	Group I	Group II	
<b>PD184325</b>	12	53	65
<b>JNK-IN-8</b>	4	50	54
<b>SB203580</b>	6	63	69
<b>PD184352 and JNK-IN-8</b>	2	33	35
<b>PD184352 and SB203580</b>	1	7	8
<b>JNK-IN-8 and SB203580</b>	2	23	25
<b>All inhibitors</b>	1	24	25

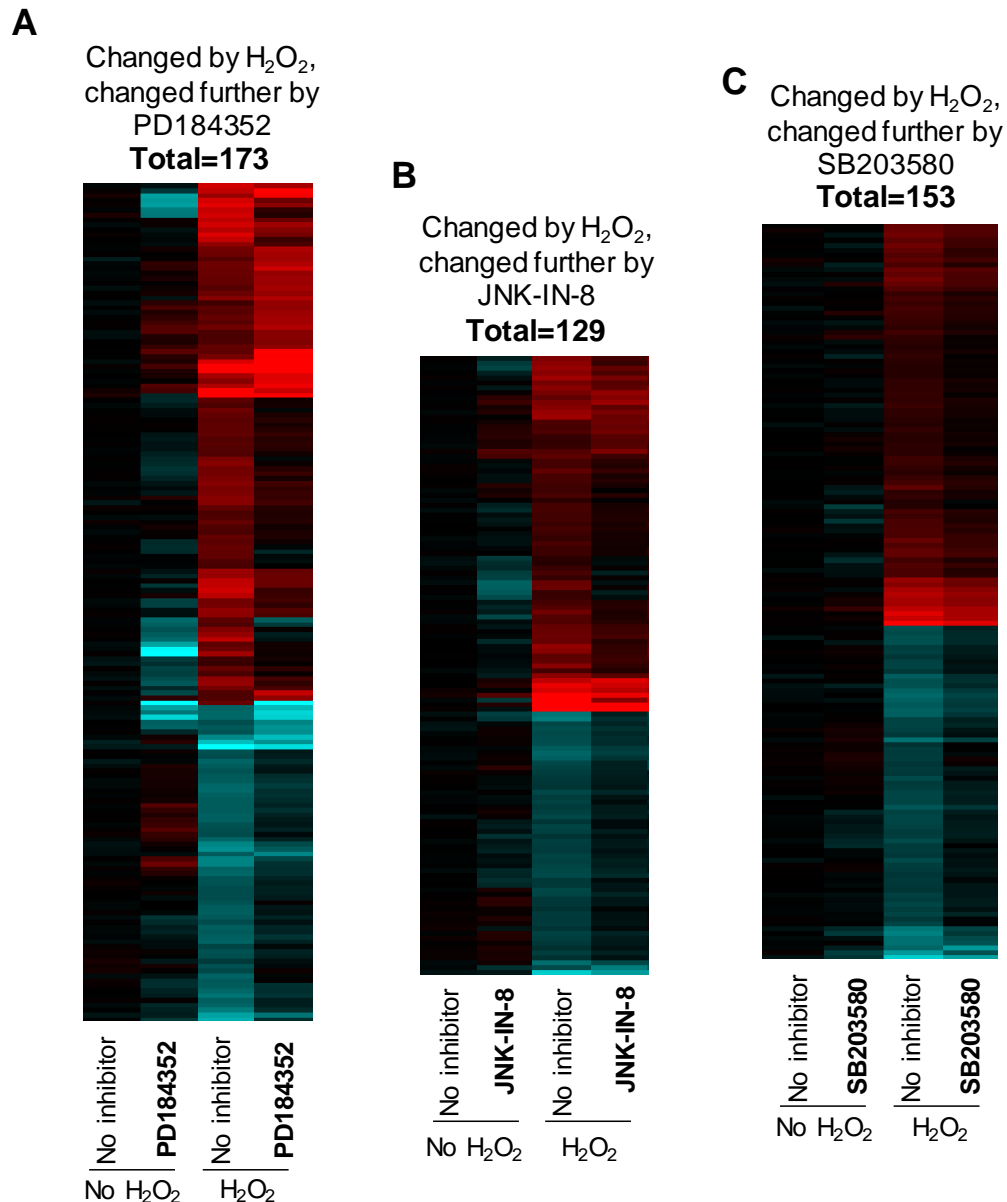


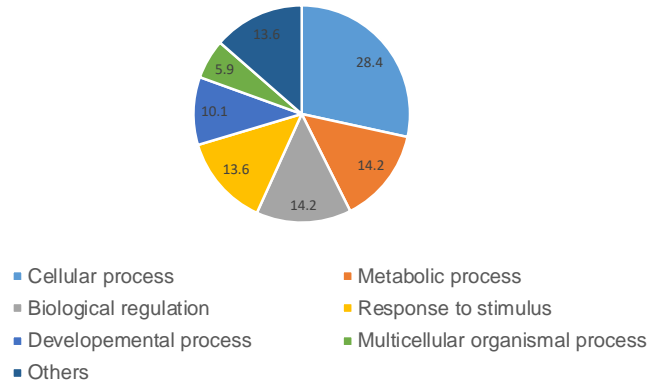
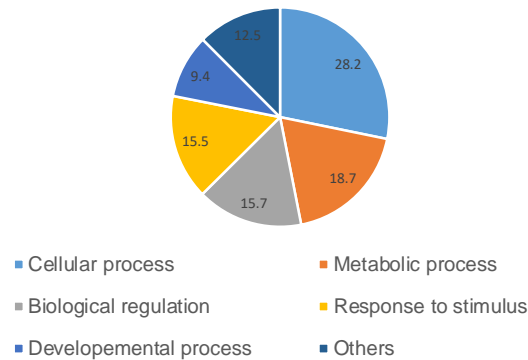
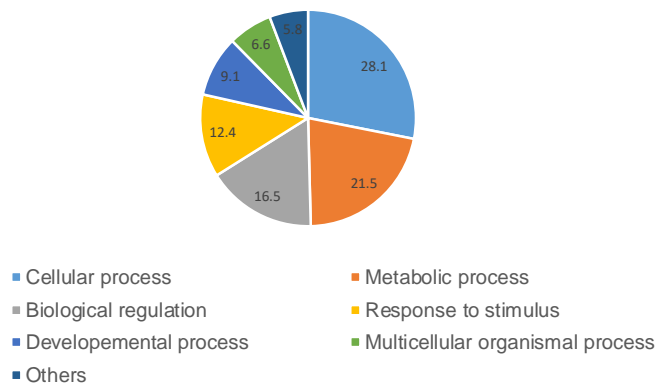
**Figure 3.9 Effects of MAPK inhibitors on cardiomyocyte RNA expression induced by H<sub>2</sub>O<sub>2</sub>.**

Cardiomyocytes were unstimulated or exposed to H<sub>2</sub>O<sub>2</sub> (0.2 mM, 2 h) with or without pre-treatment (15 min) with 2 μM PD184352, 1 μM JNK-IN-8 or 0.7 μM SB203580, or exposed to the inhibitors alone (2 h 15 min). Changes in RNA expression were determined using Affymetrix Rat Gene 2.0 ST microarrays, using GeneSpring analysis to identify RNAs with significant increase or decrease in expression in response to H<sub>2</sub>O<sub>2</sub> (>1.5-fold change relative to control; moderated t-test with Benjamini-Hochberg FDR correction,  $p < 0.05$ ). To identify RNAs changed in response to the inhibitors, RNAs were selected on the basis of a >1.25-fold change in the presence of PD184352, JNK-IN-8 or SB203580, with or without a significant effect of the inhibitor (one-way ANOVA with SNK post-test and Benjamini-Hochberg FDR correction,  $p < 0.05$ ). **(A)** RNAs changed by H<sub>2</sub>O<sub>2</sub> and changed further by PD184352. **(B)** RNAs changed by H<sub>2</sub>O<sub>2</sub> and further changed by JNK-IN-8. **(C)** RNAs changed by H<sub>2</sub>O<sub>2</sub> and changed further by SB203580. Heatmaps range from -2.0 (cyan) through 0 (black) to 2.0 (red); Log<sub>2</sub> scale.

In order to further examine the potential roles of the MAPK pathways in regulation of cardiomyocyte gene expression response to H<sub>2</sub>O<sub>2</sub>, the microarray data were subjected to Gene Ontology analysis. Data for genes upregulated in response to H<sub>2</sub>O<sub>2</sub> and whose expression was further changed by PD1845352, JNK-IN-8 or SB203580 was analysed using the PANTHER GO-slim tool, first classifying genes by Biological Process (Fig. 3.10) and then by Protein Class (Fig. 3.11).

The highest proportion of genes differentially regulated by each of the MAPK inhibitors were classified as being associated with Cellular process (GO:0009987), Metabolic process (GO:0008152), Biological regulation (GO:0065007) and Response to stimulus GO:0050896) (Fig. 3.10).

With regard to classification by Protein Class, the Gene Ontology analysis indicated that the highest proportion of genes differentially regulated by the three MAPK inhibitors encode Signalling molecules (PC00207) (Fig. 3.11). Genes encoding proteins associated with Nucleic acid binding (PC00171) and Transcription factors (PC00218) were also highly represented in the data for all three MAPK inhibitors (Fig. 3.11). Although genes associated with Enzyme modulator proteins were relatively highly represented in the data for PD184352 (Fig. 3.11A) and JNK-IN-8 (Fig 3.11B), the proportion was relatively lower for SB203580 (<5%). Notably, the proportion of Oxidoreductase genes (PC00176) was substantially higher amongst those differentially regulated by SB203580 (7.3% of all genes, Fig. 3.11C) when compared to PD184352 (1.8% of all genes, Fig. 3.11A) and particularly JNK-IN-8, with 0 differentially regulated genes classified in the Oxidoreductase category.

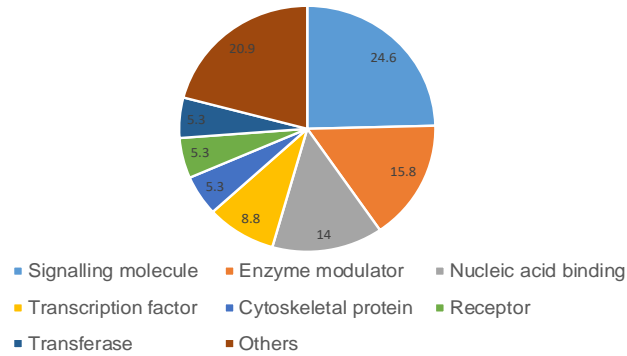
**A**Genes upregulated by H<sub>2</sub>O<sub>2</sub> and changed further by PD184352**B**Genes upregulated by H<sub>2</sub>O<sub>2</sub> and changed further by JNK-IN-8**C**Genes upregulated by H<sub>2</sub>O<sub>2</sub> and changed further by SB203580

**Figure 3.10 Gene Ontology analysis of genes upregulated by H<sub>2</sub>O<sub>2</sub> and changed further by MAPK inhibitors – classification by Biological Process**

Microarray expression data for genes upregulated by H<sub>2</sub>O<sub>2</sub> and changed further by MAPK inhibitors were analysed using the PANTHER GO-slim tool, classifying gene function by Biological Process. The data are shown in pie charts as the percentage of genes classified by PANTHER GO-slim as being associated with the processes listed in the chart keys. **(A)** Genes upregulated by H<sub>2</sub>O<sub>2</sub> and changed further by PD184352. **(B)** Genes upregulated by H<sub>2</sub>O<sub>2</sub> and changed further by JNK-IN-8. **(C)** Genes upregulated by H<sub>2</sub>O<sub>2</sub> and changed further by SB203580.

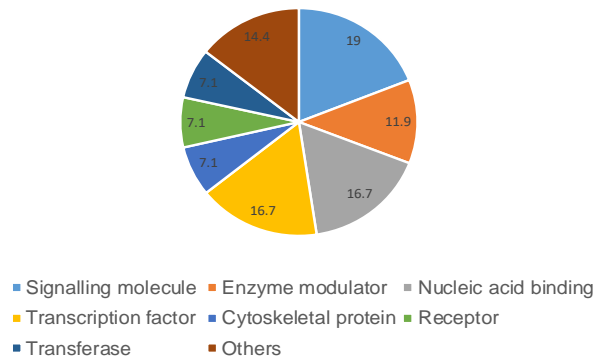
**A**

Genes upregulated by H<sub>2</sub>O<sub>2</sub> and changed further by PD184352



**B**

Genes upregulated by H<sub>2</sub>O<sub>2</sub> and changed further by JNK-IN-8



**C**

Genes upregulated by H<sub>2</sub>O<sub>2</sub> and changed further by SB203580

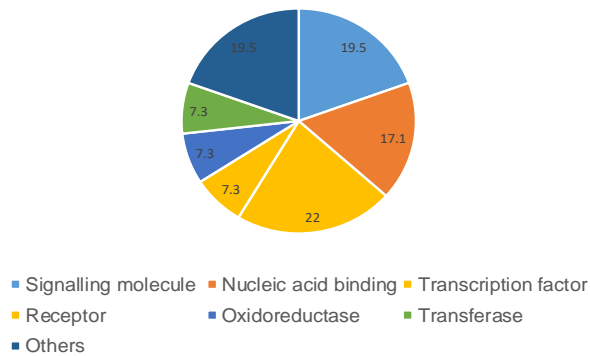


**Figure 3.11 Gene Ontology analysis of genes upregulated by H<sub>2</sub>O<sub>2</sub> and changed further by MAPK inhibitors – classification by Protein Class**

Microarray expression data for genes upregulated by H<sub>2</sub>O<sub>2</sub> and changed further by MAPK inhibitors were analysed using the PANTHER GO-slim tool, classifying gene function by Protein Class. The data are shown in pie charts as the percentage of genes classified by PANTHER GO-slim as being associated with the Protein Classes listed in the chart keys. **(A)** Genes upregulated by H<sub>2</sub>O<sub>2</sub> and changed further by PD184352. **(B)** Genes upregulated by H<sub>2</sub>O<sub>2</sub> and changed further by JNK-IN-8. **(C)** Genes upregulated by H<sub>2</sub>O<sub>2</sub> and changed further by SB203580.

### 3.3.5 Validation of microarray data using qPCR

While microarrays provide an overview of global changes in RNA expression in response to the different treatments, it is necessary to validate the data using a second, independent, method. Accordingly, the microarray data were validated by qPCR, using specific primers.

Three RNAs were selected for validation based on the effects of one or more of the inhibitors in isolation. Microarrays indicated that baseline mRNA expression of dual-specificity phosphatase (Dusp) 8 was downregulated in response to JNK-IN-8 and this was confirmed using qPCR (Fig. 3.10A). Downregulation of Jun mRNA in response to 2 h 15 min JNK-IN-8 exposure was not statistically significant when analysed by qPCR (Fig. 3.10B), although the expression profiles were similar to those for the microarray data. Microarray data indicate that baseline expression of connective tissue growth factor (Ctgf) was inhibited by PD184352 and JNK-IN-8. Although qPCR analysis demonstrated that JNK-IN-8 inhibited Ctgf expression to only  $0.42 \pm 0.04$ -fold relative to control, this was not statistically significant (Fig. 3.10C). Similarly, PD184352 had no significant effect on Ctgf expression, in the qPCR analysis (Fig. 3.10C). Generally, the microarray data were validated as the expression profiles were similar to those for the qPCR data, although the response of Ctgf in the qPCR analysis was lesser than that in the microarray data.

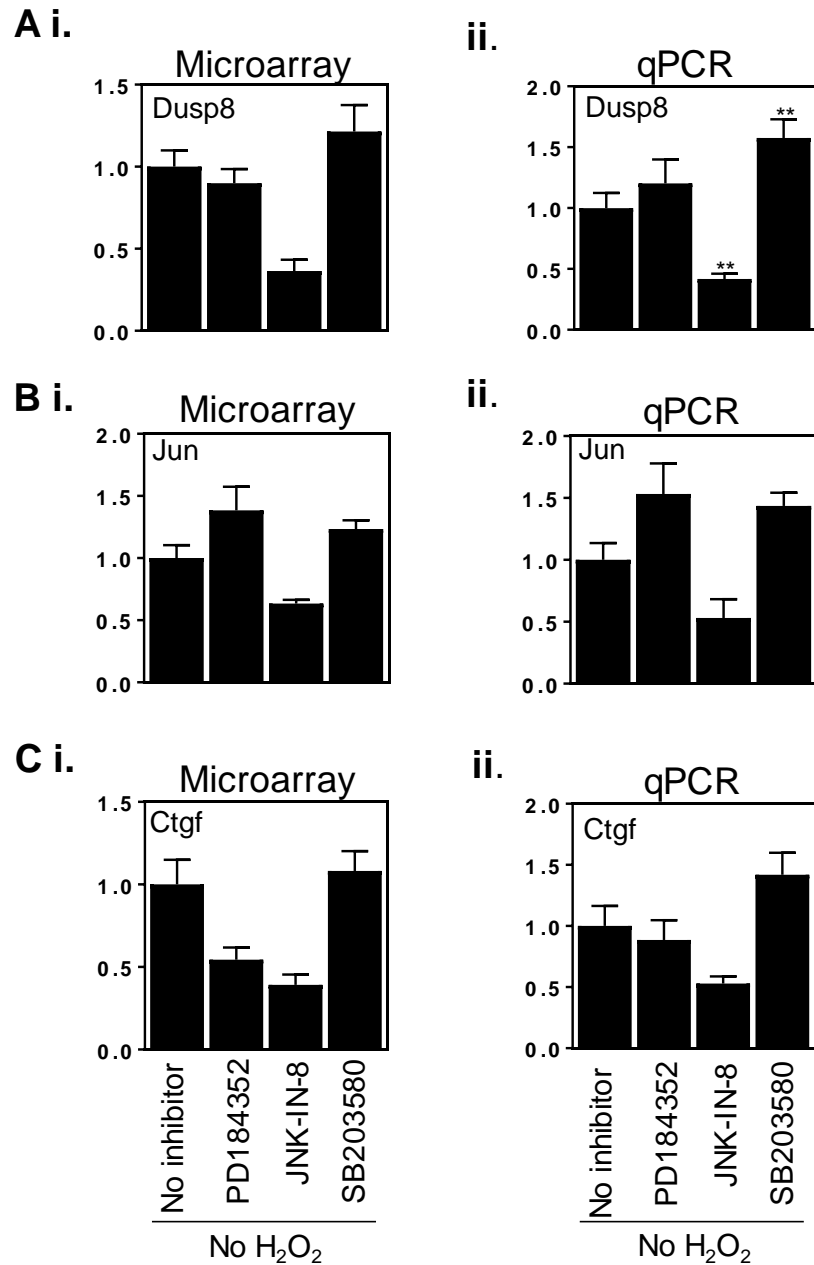


**Figure 3.12 Validation of microarray data by qPCR: RNAs inhibited by MAPK inhibitors alone**

Cardiomyocytes were unstimulated or exposed to PD184352 (2  $\mu$ M), JNK-IN-8 (1  $\mu$ M) or SB203580 (0.7  $\mu$ M) (2 h 15 min). Expression of mRNAs sensitive to one or more inhibitor was analysed using qPCR (**A**, Dusp8; **B**, Jun; **C**, Ctgf). Microarray results alone are shown in panels (i) and qPCR data in panels (ii). Results are means  $\pm$  SEM (n=4 independent cardiomyocyte preparations) and are normalised to the means of the controls. \*\*, p<0.01 relative to control (one-way ANOVA with SNK post-test).

With respect to mRNAs upregulated by H<sub>2</sub>O<sub>2</sub>, three groups were selected for validation using qPCR: mRNAs encoding transcription factors (Egr1, Egr3 and Atf3, Fig. 3.11), mRNAs encoding proteins associated with antioxidation (Hmox1, Gclc, Nqo1, and Txnrd1, Fig. 3.12) and mRNAs encoding dual-specificity phosphatases (Dusp2, Dusp4 and Dusp5, Fig. 3.13).

Upregulation of early growth response (Egr) 1 and Egr3 transcription factor mRNAs in response to H<sub>2</sub>O<sub>2</sub>, and the inhibition of the response by PD184352, was confirmed by qPCR (Fig. 3.11, A and B). The microarray data also indicated that the response of both Egr1 and Egr3 to H<sub>2</sub>O<sub>2</sub> was inhibited by JNK-IN-8, and this was reflected by qPCR analysis (Fig. 3.11, A and B). Upregulation of Atf3 in response to H<sub>2</sub>O<sub>2</sub> was confirmed by qPCR, as was the inhibition of the response by JNK-IN-8 (Fig. 3.11, C). The qPCR expression profiles for each of these mRNAs were generally similar to those from the microarray analysis, thus validating the microarray data.

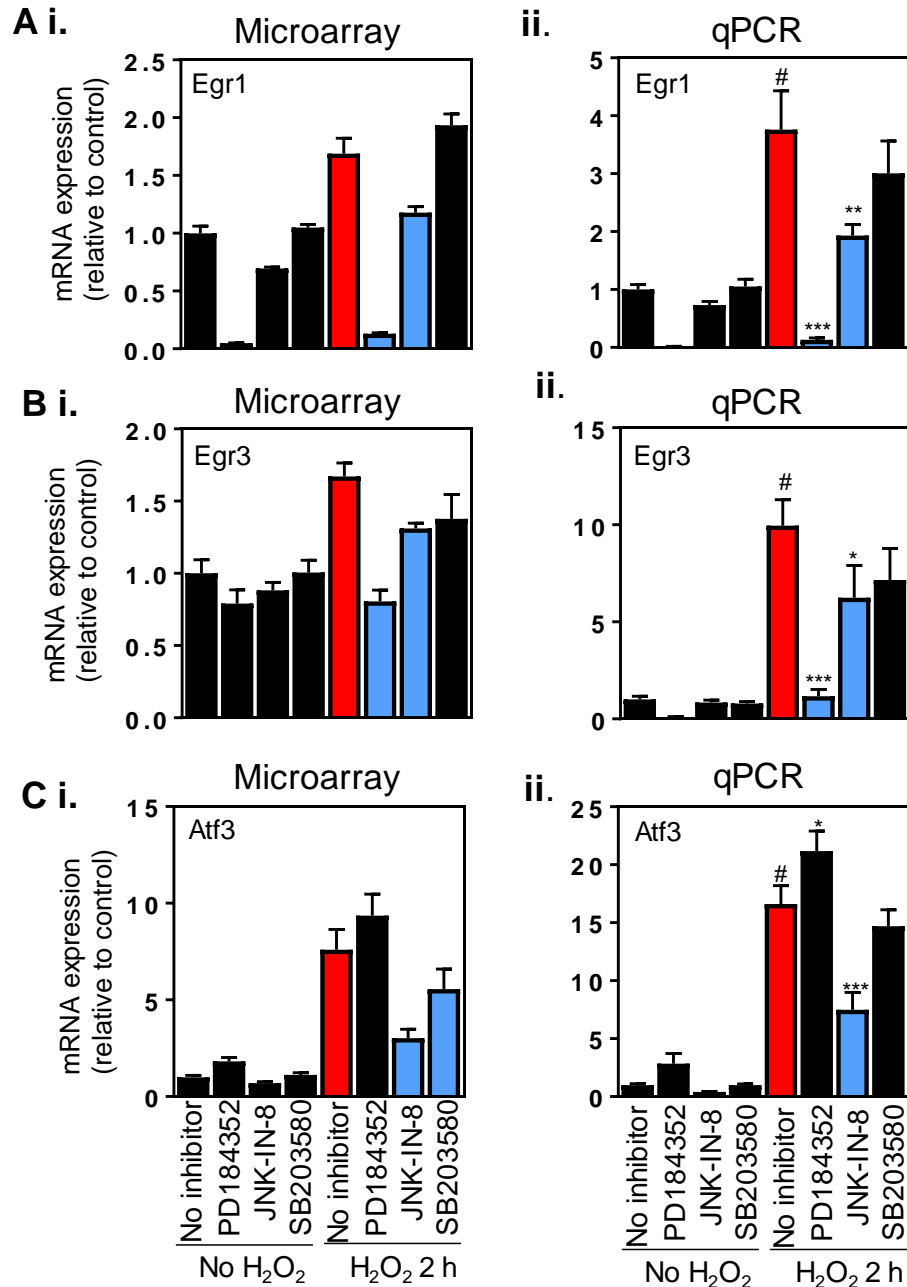


**Figure 3.13 Validation of microarray data by qPCR: mRNAs encoding transcription factors**

Cardiomyocytes were unstimulated or exposed to 0.2 mM H<sub>2</sub>O<sub>2</sub> (2 h) with or without 15 min pre-treatment with either PD184352 (2 μM), JNK-IN-8 (1 μM) or SB203580 (0.7 μM) or to each inhibitor in isolation (2 h 15 min). Expression of H<sub>2</sub>O<sub>2</sub>-responsive mRNAs encoding transcription factors were analysed using qPCR (A, Egr1; B, Egr3; C, Atf3). Microarray results alone are shown in panels (i) and qPCR data in panels (ii). Results are means ± SEM (n=4 independent cardiomyocyte preparations) and are normalised to the means of the controls. #, p<0.001 relative to control. \*, p<0.05; \*\*, p<0.01; \*\*\*p<0.001 relative to H<sub>2</sub>O<sub>2</sub> alone (one-way ANOVA with SNK post-test).

The microarray data indicate that several mRNAs associated with antioxidation were upregulated in response to H<sub>2</sub>O<sub>2</sub>. The data for four of these, heme oxygenase 1 (Hmox1), glutamate-cysteine ligase catalytic subunit (Gclc), NAD(P)H quinone dehydrogenase 1 (Nqo1) and thioredoxin reductase 1 (Txnrd1) were validated using qPCR. As with the microarrays, all were significantly upregulated in response to H<sub>2</sub>O<sub>2</sub> (0.2 mM, 2 h) (Fig. 3.12, A-D). Consistent with the microarray data, upregulation of Hmox1 was significantly attenuated by SB203580 (Fig. 3.12A) while upregulation of Gclc was significantly inhibited by PD184352 or SB203580 (Fig. 3.12B). In concordance with the microarray data, none of the inhibitors had any significant effect on the upregulation of either Nqo1 or Txnrd1 (Fig. 3.12, C and D, respectively).

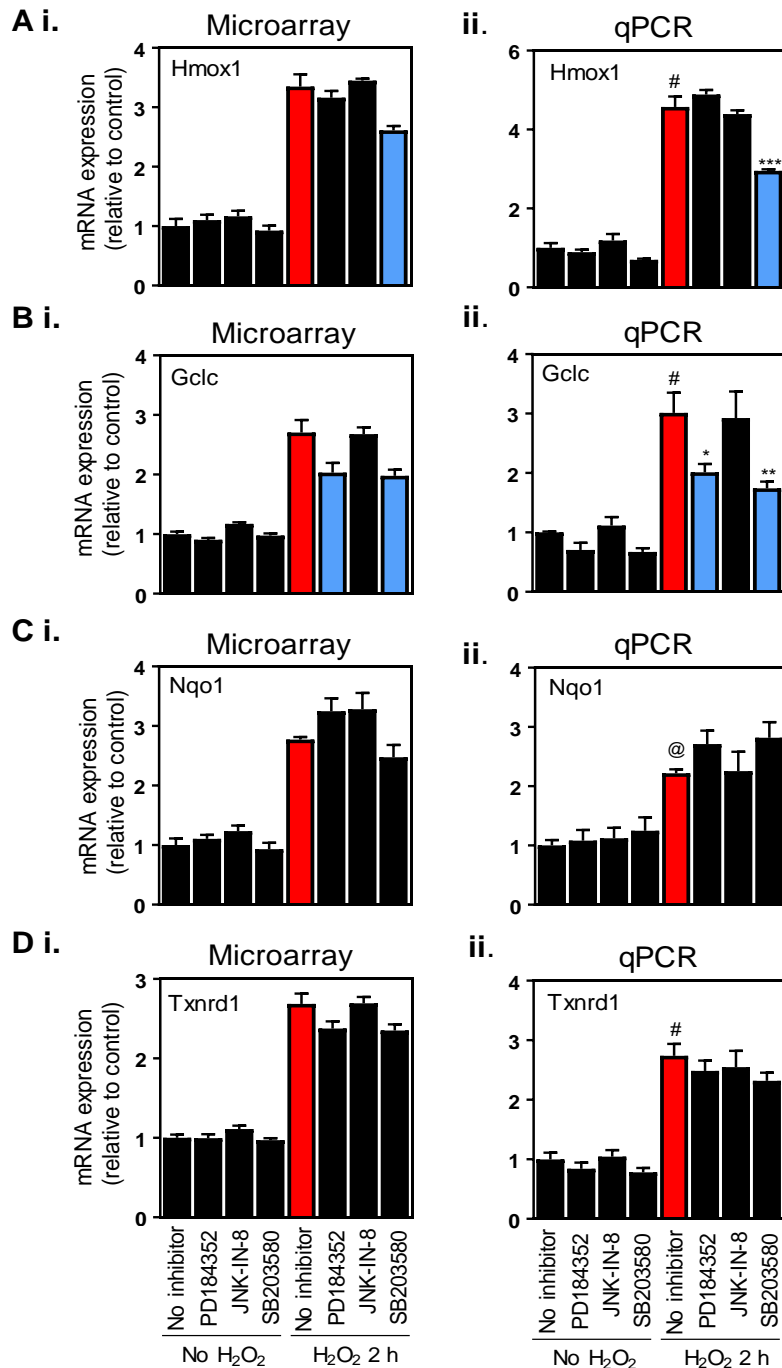


**Figure 3.14 Validation of microarray data by qPCR: effects of MAPK inhibitors on expression of antioxidant mRNAs induced by H<sub>2</sub>O<sub>2</sub>**

Cardiomyocytes were unstimulated or exposed to 0.2 mM H<sub>2</sub>O<sub>2</sub> (2 h) with or without 15 min pre-treatment with either PD184352 (2 μM), JNK-IN-8 (1 μM) or SB203580 (0.7 μM) or to each inhibitor in isolation (2 h 15 min). Expression of H<sub>2</sub>O<sub>2</sub>-responsive antioxidant mRNAs was analysed using qPCR (**A**, Hmox1; **B**, Gclc; **C**, Nqo1; **D**, Txnrd1). Microarray results alone are shown in panels (i) and qPCR data in panels (ii). Results are means ± SEM (n=3 independent cardiomyocyte preparations) and are normalised to the means of the controls. @, p<0.01, #, p<0.001 relative to control. \*, p<0.05; \*\*, p<0.01; \*\*\*, p<0.001 relative to H<sub>2</sub>O<sub>2</sub> alone (one-way ANOVA with SNK post-test).

Members of the Dusp family were also selected for validation using qPCR. Dusp2, Dusp4 and Dusp5 were identified as significantly upregulated in response to H<sub>2</sub>O<sub>2</sub> by the microarray analysis. In agreement with the microarray data, expression of Dusp2, Dusp4 and Dusp5 was significantly upregulated in response to 2 h H<sub>2</sub>O<sub>2</sub> exposure (Fig. 3.13, A-C). As with the microarrays, upregulation of Dusp2 was inhibited by PD1843523, JNK-IN-8 or SB203580 (Fig. 3.13A). Microarray analysis indicated that upregulation of both Dusp4 and Dusp5 was inhibited by PD184352 or SB203580 (Fig. 3.13, Bi and Ci). This was reflected by the qPCR analysis, which also revealed that JNK-IN-8 had a significant inhibitory effect of the response of Dusp4 and Dusp5 to 2 h H<sub>2</sub>O<sub>2</sub> exposure (Fig. 3.13, Bii and Cii).

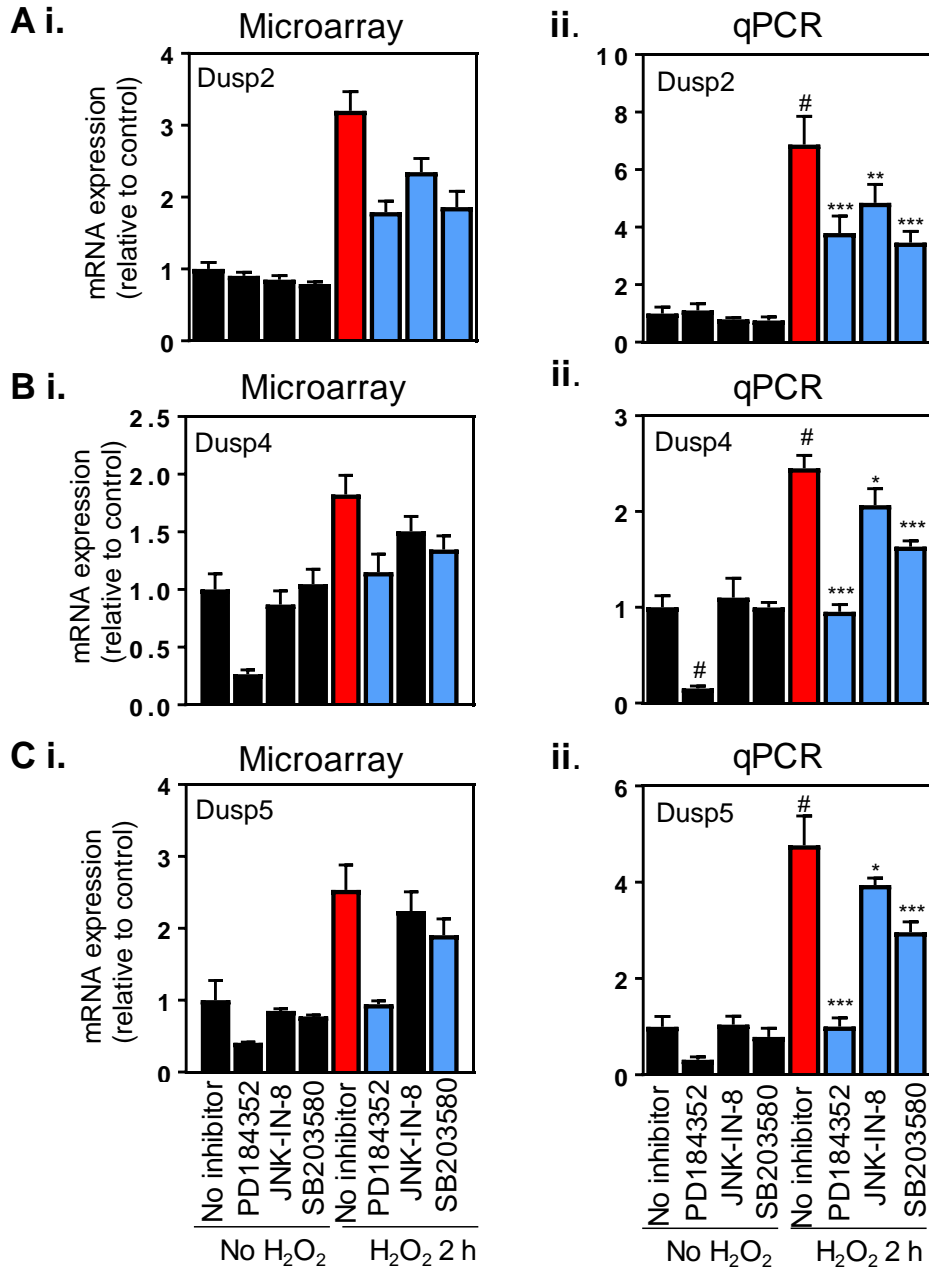


**Figure 3.15 Validation of microarray data by qPCR: effects of MAPK inhibitors on expression of dual-specificity phosphatase (Dusp) mRNAs induced by H<sub>2</sub>O<sub>2</sub>**

Cardiomyocytes were unstimulated or exposed to 0.2 mM H<sub>2</sub>O<sub>2</sub> (2 h) with or without 15 min pre-treatment with either PD184352 (2 μM), JNK-IN-8 (1 μM) or SB203580 (0.7 μM) or to each inhibitor in isolation (2 h 15 min). Expression of Dusp mRNAs was analysed using qPCR (**A**, Dusp2; **B**, Dusp4; **C**, Dusp5). Microarray results alone are shown in panels (i) and qPCR data in panels (ii). Results are means ± SEM (n=4 independent cardiomyocyte preparations) and are normalised to the means of the controls. #, p<0.001 relative to control. \*, p<0.05; \*\*, p<0.01; \*\*\*, p<0.001 relative to H<sub>2</sub>O<sub>2</sub> alone (one-way ANOVA with SNK post-test).

### **3.4 Discussion**

Death of cardiomyocytes, including by apoptosis, is closely associated with the pathogenesis of cardiovascular diseases including heart failure (Konstantinidis et al., 2012). Oxidative stress, exemplified by H<sub>2</sub>O<sub>2</sub>, is one of the principal insults encountered by the heart. Exposure to H<sub>2</sub>O<sub>2</sub> promotes apoptotic death of cardiomyocytes, induces substantial changes in gene expression and activates key intracellular signalling pathways including the three main MAPK pathways, ERK1/2, JNKs and p38-MAPKs (Cook et al., 1999b; Clerk et al., 1998a; Clerk et al., 1998b; Clerk et al., 2007b; Kwon et al., 2003; Kemp et al., 2003). It is assumed that the changes in gene (and protein) expression associated with H<sub>2</sub>O<sub>2</sub>-induced apoptosis are implicated in mediating the death response of cardiomyocytes, and that these changes are regulated, at least in part, by the MAPK pathways. In this chapter, the aim was to use a pharmacological inhibitor approach coupled with microarray analysis to dissect the roles of ERK1/2, JNKs and p38-MAPKs in regulation of cardiomyocyte RNA expression in response to a pro-apoptotic H<sub>2</sub>O<sub>2</sub> concentration.

#### **3.4.1 Confirmation of MAPK inhibitor specificity**

The experiments in this chapter relied heavily on the use of pharmacological inhibitors of the ERK1/2, JNK and p38-MAPK pathways to implicate these cascades in the cardiomyocyte gene expression response to H<sub>2</sub>O<sub>2</sub>. The potency and selectivity of the inhibitors employed here were confirmed (section 3.3.2). PD184352 (2 µM) potently inhibited the increase in activation of ERK1/2 in response to 0.2 mM H<sub>2</sub>O<sub>2</sub> (Fig. 3.4, A and B), with no significant inhibitory effects on JNKs or p38-MAPKs, as indicated by the lack of any change in phosphorylation of c-Jun or MAPKAPK2, respectively (Figs. 3.5 and 3.6). It should be noted, however, that while 10 min exposure to 0.2 mM H<sub>2</sub>O<sub>2</sub> induced a 3.3±0.53-fold increase in ERK2 activation, this was not statistically significant; although it is probable that the result would be significant with an increased sample size. The novel inhibitor of JNKs, JNK-IN-8 (Zhang et al., 2012), significantly

inhibited H<sub>2</sub>O<sub>2</sub>-induced phosphorylation of the established JNK substrate c-Jun (Fig. 3.5), with no significant effects on ERK1/2 or the p38-MAPK pathway (Fig. 3.4 and 3.6). In addition, JNK-IN-8 abolished the detection of reduced mobility c-Jun bands in response to H<sub>2</sub>O<sub>2</sub> (Fig. 3.5A), representing additional supporting evidence of inhibition of phosphorylation. SB203580 is widely used to inhibit activity of the p38-MAPK $\alpha/\beta$  isoforms (Cuenda et al., 1995). Here, SB203580 used at 0.7  $\mu$ M potently suppressed phosphorylation of the p38-MAPK substrate MAPKAPK2 in response to H<sub>2</sub>O<sub>2</sub> in cardiomyocytes (Fig. 3.6), with no significant inhibitory effect on either ERK1/2 or JNK signalling (Figs. 3.4 and 3.5).

### **3.4.2 Contributions of ERK1/2, JNK and p38-MAPK signalling to cardiomyocyte gene expression in response to H<sub>2</sub>O<sub>2</sub>**

Consistent with previous studies (Kemp et al., 2003; Clerk et al., 2007b), a pro-apoptotic H<sub>2</sub>O<sub>2</sub> concentration (0.2 mM) induced substantial changes in cardiomyocyte RNA expression after 2 h exposure, with changes in 490 RNAs (Fig. 3.8 and Appendix II, Tables A4 and A5). A preponderance of RNAs was upregulated (295 RNAs, ~60% of total) (Appendix II, Table A4) reinforcing the notion that at this early time during apoptosis, cardiomyocytes actively respond to the encountered insult, resulting in changes in gene expression that presumably regulate and contribute to the final response. Notably, and in agreement with earlier studies (Clerk et al., 2007b), numerous upregulated mRNAs encode DNA-binding transcription factors/regulators of transcription (including Egr1, Egr3, Atf3, Fos, Fosb, Fosl1, Jun, Klf4, Klf5 and Klf10) (Appendix II, Table A4), suggesting that part of the response to H<sub>2</sub>O<sub>2</sub> comprises expression of factors required for further downstream regulation of gene expression. Similarly, many mRNAs encoding receptor ligands were upregulated, including Inhba (inhibin beta-A), Ngf (nerve growth factor), Ereg (epiregulin), Areg (amphiregulin), Hbegf (heparin-binding EGF-like factor) and Lif (leukaemia inhibitory factor) (Appendix II, Table A4). Accordingly, if these are ultimately translated to protein and secreted, they may serve to propagate the cardiomyocyte response to H<sub>2</sub>O<sub>2</sub> in an autocrine or paracrine fashion.

Although substantial changes in RNA expression were detected in response to H<sub>2</sub>O<sub>2</sub>, fewer genes were identified as upregulated than in the previous study (295 vs the 391 identified in Clerk *et al.*, 2007b). Approximately 42% of genes upregulated by H<sub>2</sub>O<sub>2</sub> were identified as such by Clerk *et al.* Accordingly, while the data are reasonably reproducible, there are differences between the two data sets. The reasons for this are not immediately apparent, although it may be due at least in part to differences in analysis of the microarray data, and the fact that different microarrays were used in the two studies (Affymetrix GeneChip Rat Gene 2.0 ST microarrays in the present study vs Affymetrix GeneChip Rat Genome 230 2.0 microarrays in Clerk *et al.*, 2007b).

The principal aim in this chapter was to characterise the relative contributions of ERK1/2, JNKs and p38-MAPKs to the cardiomyocyte RNA expression response to H<sub>2</sub>O<sub>2</sub>. Microarray analysis indicated that PD184352 in isolation modulated expression of 134 RNAs (Fig. 3.7A and Appendix II, Table A1), suggesting that these RNAs are regulated under basal conditions by ERK1/2 in cardiomyocytes. Since 92 (~68%) of these were downregulated, ERK1/2 appear to have a primarily positive regulatory role in this context, with a smaller repressive function in baseline RNA expression (Fig. 3.7A and Appendix II, Table A1). Conversely, JNK-IN-8 and SB203580 promoted baseline changes in only 14 and 6 RNAs, respectively (Fig. 3.7, B and C and Appendix II, Tables A2 and A3), indicating a much smaller role for JNKs and p38-MAPK $\alpha/\beta$  in regulation of basal cardiomyocyte RNA expression. This observation is arguably expected due to their association with activation under stress conditions.

Microarray expression profiling indicated that ERK1/2, JNKs and p38-MAPK $\alpha/\beta$  contribute substantially, yet differentially, to cardiomyocyte RNA expression in response to H<sub>2</sub>O<sub>2</sub>. Of 295 RNAs upregulated in response to H<sub>2</sub>O<sub>2</sub>, the expression of 167 (~56%) was affected by one or more of PD184352, JNK-IN-8 or SB203580 (Fig. 3.9, Table 3.1 and Appendix II, Tables A9, A10, A15, A16 and A22). A similar proportion of the 195 RNAs downregulated by H<sub>2</sub>O<sub>2</sub> were affected by one, or more, MAPK inhibitor (Fig. 3.9, Table 3.2 and Appendix II, Tables A12, A13, A18 and A22). Of 295 RNAs upregulated by H<sub>2</sub>O<sub>2</sub>, PD184352 further changed expression

of 108, indicating that ERK1/2 regulate expression of ~37% of RNAs induced by H<sub>2</sub>O<sub>2</sub> (Fig. 3.9A, Table 3.1 and Appendix II, Tables A9 and A10). As observed with respect to baseline expression, a majority of these RNAs (74, ~69%) were positively regulated by ERK1/2. The effects of PD184352 on RNAs downregulated in response to H<sub>2</sub>O<sub>2</sub> also indicate that ERK1/2 effected changes in 33% of these genes (Fig. 3.9A, Table 3.2 and Appendix II, Tables A12 and A13). In this context, PD184352 served to relieve the downregulatory effect of H<sub>2</sub>O<sub>2</sub> on 57 RNAs (i.e. ERK1/2 promote their downregulation) (Appendix II, Table A13) but potentiated the downregulation of a further 8 RNAs (Appendix II, Table A12).

JNK-IN-8 exposure resulted in changes in 75 of the 295 RNAs induced by H<sub>2</sub>O<sub>2</sub>, implicating JNK signalling in regulation of ~25% of RNAs upregulated in response to 0.2 mM H<sub>2</sub>O<sub>2</sub> at 2 h (Fig. 3.9B, Table 3.1 and Appendix II, Tables A15 and A16). In common with ERK1/2, JNKs appear to have primarily a positive regulatory role: of 75 RNAs induced by H<sub>2</sub>O<sub>2</sub> and changed by JNK-IN-8, 63 (84%) were inhibited (Fig. 3.9B, Table 3.1 and Appendix II, Table A16). The data indicate that JNKs also play a negative regulatory role in response to H<sub>2</sub>O<sub>2</sub> as the extent of the downregulation of 53 RNAs was reduced in the presence of JNK-IN-8 (Fig. 3.9B, Table 3.2 and Appendix II, Table A18).

SB203580 resulted in changes in expression of 84 RNAs upregulated in response to H<sub>2</sub>O<sub>2</sub>, implicating p38-MAPK $\alpha/\beta$  in regulation of ~28% of induced RNAs (Fig. 3.9C, Table 3.1 and Appendix II, Table A20). As observed for ERK1/2 and JNKs, p38-MAPK $\alpha/\beta$  appear to play a principally positive role in this context, as SB203580 caused inhibition of 83 of the affected RNAs (Fig. 3.9C and Appendix II, Table A20), with a repressive effect of p38-MAPK $\alpha/\beta$  in regulation of only one transcript (Fig. 3.9C and Table Appendix II, Table A20). With respect to RNAs downregulated by H<sub>2</sub>O<sub>2</sub>, SB203580 returned the expression of 68 to similar levels to control values (implicating p38-MAPK $\alpha/\beta$  in their downregulation) and enhanced downregulation of only one RNA (Fig. 3.9C, Table 3.2 and Appendix II, Table A22).

To verify the changes in RNA expression determined using microarrays, microarray data for selected genes were validated using qPCR and using RNA extracted from cardiomyocyte preparations independent from those used in the microarray analysis. Although the absolute numerical values for changes in expression determined by the two independent techniques differed, generally, the microarray and qPCR data were in accord, with similar expression profiles (Figs. 3.10 – 3.13). Considered together, the microarray and qPCR expression profiling data demonstrate that ERK1/2, JNKs and p38-MAPK $\alpha/\beta$  all contribute to the cardiomyocyte RNA expression response to H<sub>2</sub>O<sub>2</sub> with, in terms of numbers of RNAs affected, a greater contribution by ERK1/2 and a relatively smaller contribution by JNKs and p38-MAPK $\alpha/\beta$ .

The expression profiling data presented here suggest a substantial role for ERK1/2 in regulation of cardiomyocyte RNA expression in response to H<sub>2</sub>O<sub>2</sub>. This observation agrees with previous studies in cardiomyocytes implicating ERK1/2 in regulation of RNA expression in response to other stimuli (Kennedy et al., 2006; Cullingford et al., 2008a; Marshall et al., 2010; Amirak et al., 2013). Indeed, several RNAs identified as targets of ERK1/2 in response to H<sub>2</sub>O<sub>2</sub> have been reported previously under different conditions. For example, induction of *Xirp1*, *Rgs2*, and *Klf5* by ET-1 is at least partially sensitive to inhibition of ERK1/2 activation using U0126 or PD184352 (Kennedy et al., 2006; Cullingford et al., 2008a; Marshall et al., 2010). A further study in the cardiac-related H9c2 cell line used the MKK1/2 inhibitor PD98059 to implicate ERK1/2 in induction of *Egr1* in response to 0.2 mM H<sub>2</sub>O<sub>2</sub>, as observed here (Fig. 3.11A). The same study also suggested a role for JNKs, but not p38-MAPK $\alpha/\beta$ , in upregulation of *Egr1* in accord with the data presented here (Fig. 3.11A), although the poorly-selective JNK inhibitors SP600125 and AS601245 were used (Aggeli et al., 2010).

Despite the relatively lesser roles of JNKs and p38-MAPK $\alpha/\beta$  in regulation of RNA expression under these conditions, these pathways may still play crucial roles in the cardiomyocyte response to H<sub>2</sub>O<sub>2</sub> through regulation of key genes. Interestingly, *Zfp36* was identified as a target of p38-MAPK $\alpha/\beta$  signalling (Appendix II, Table A20). *Zfp36* encodes tristetraprolin, a zinc-finger domain-containing RBP that binds AU-rich elements of certain RNAs, resulting in

transcript destabilisation. Tristetraprolin is an established substrate of the p38-MAPK pathway, and tristetraprolin phosphorylation is reported to inhibit the destabilisation of transcripts including pro-inflammatory TNF $\alpha$  (Marderosian et al., 2006; Sun et al., 2007). Similarly, induction of Arid5a RNA by H<sub>2</sub>O<sub>2</sub> was inhibited by JNK-IN-8 (Appendix II, Table A16), suggesting upregulation by JNKs. Like tristetraprolin, Arid5a binds mRNAs and modulates their stability (Masuda et al., 2013). Although little is known about the regulation and function of Arid5a, it is associated with regulation of the pleiotropic cytokine interleukin-6 in non-cardiac systems (Masuda et al., 2013). Furthermore, despite the larger number of RNAs regulated by ERK1/2, several identified targets of ERK1/2 were also sensitive to JNK-IN-8 and/or SB203580, including Egr1 and Egr3 (Fig. 3.11, A and B) and Dusp2, Dusp4 and Dusp5 (Fig. 3.13), indicating overlapping functions of the different MAPK pathways in regulation of some genes.

Although the significance of individual genes is difficult to determine, by examining the RNAs regulated by the MAPKs in this study, it may be possible to begin to propose potential functional roles for the MAPK pathways in the cardiomyocyte RNA expression response to H<sub>2</sub>O<sub>2</sub>. Interestingly, several RNAs induced by H<sub>2</sub>O<sub>2</sub> were suppressed by all three MAPK inhibitors. One of these, Xirp1 (Appendix II, Tables A9, A17 and A20), encodes an actin-binding protein which localises to the myocardial intercalated disks and is upregulated in other cardiac stress conditions including in response to myocardial infarction, and is downregulated in failing hearts (Wang et al., 2014b; Harpster et al., 2006). Interestingly, Xirp1 is also upregulated in response to ischaemic preconditioning (Ashton et al., 2013), suggesting an association with cardioprotection. Accordingly, induction of Xirp1 by the MAPK pathways may represent a cytoprotective response to the insult caused by H<sub>2</sub>O<sub>2</sub>, although further investigation is required. Similarly, Kihl40, mutations of which are a common cause of autosomal-recessive nemaline myopathy (Ravenscroft et al., 2013), was also induced by H<sub>2</sub>O<sub>2</sub> and inhibited by all three MAPK inhibitors studied (Appendix II, Tables A9, A17 and A20)

Several “typical” Dusp family members [i.e. Dusps that contain a MAPK-binding domain (Huang and Tan, 2012)] were upregulated in response to H<sub>2</sub>O<sub>2</sub> (Fig. 3.13 and Appendix II, Table A4). The induction of Dusp2, Dusp4, Dusp5 and Dusp10 was identified using microarrays and/or qPCR as being sensitive to one or more the MAPK inhibitors investigated (Fig. 3.13) and baseline expression of Dusp8 was downregulated in response to JNK-IN-8 in isolation (Fig. 3.10A). These Dusps, named for their phosphatase activity against phosphorylated activation loop threonine and tyrosine residues negatively regulate the activation of MAPKs (Huang and Tan, 2012). Induction of Dusp2, Dusp4 and Dusp5 was inhibited by PD184352, JNK-IN-8 and SB203580 (Fig. 3.13, A – C) and upregulation of Dusp10 inhibited by JNK-IN-8 (Appendix II, Table A16). These data suggest that ERK1/2, JNKs and p38-MAPK $\alpha/\beta$  cooperatively function in negative feedback autoregulation during H<sub>2</sub>O<sub>2</sub>-induced cardiomyocyte apoptosis. Similar feedback loops have been reported previously, for example, the induction of Dusp2 by ERK1/2 activity in response to serum in CCL39 cells (Brondello et al., 1997).

Four antioxidation-associated mRNAs identified by microarrays as upregulated by H<sub>2</sub>O<sub>2</sub> were selected for further investigation using qPCR. Upregulation of Hmox1, Gclc, Nqo1 and Txnrd1 [as also previously reported (Clerk et al., 2007b)] was validated, as was the inhibition of Hmox1 by SB203580 and the inhibition of Gclc by both PD184352 and SB203580 (Fig. 3.12, A – D). These data indicate that ERK1/2 and p38-MAPK $\alpha/\beta$  regulate expression of (at least some) genes encoding antioxidant proteins in response to H<sub>2</sub>O<sub>2</sub>, thus presumably contributing to the cardiomyocyte response to increased oxidative stress, and potentially promoting cytoprotection. Similarly, H<sub>2</sub>O<sub>2</sub> induced upregulation of Cdkn1a, which encodes p21<sup>Cip1/Waf1</sup>, was found to be sensitive to SB203580 (Appendix II, Table A20), indicating a role for p38-MAPK $\alpha/\beta$  in regulation of this gene. In NIH 3T3 cells exposed to 0.25 mM H<sub>2</sub>O<sub>2</sub> (4 h), p21<sup>Cip1/Waf1</sup> is upregulated at both the RNA and protein level and is associated with transient cell cycle arrest, regarded to be a cytoprotective response to the encountered insult (Barnouin et al., 2002).

Gene Ontology analysis of the microarray expression profiles using the PANTHER GO-slim tool provided further insights into the potential roles of MAPKs in the cardiomyocyte gene expression response to H<sub>2</sub>O<sub>2</sub>. As might be expected, genes associated with cellular and metabolic processes, biological regulation and response to stimulus were most highly represented in the data for each of the MAPK inhibitors (Fig. 3.10). Gene Ontology analysis classifying genes by protein class indicated that genes associated with signalling molecules, transcription factors and nucleic acid binding were highly represented for all three of the MAPK inhibitors (Fig 3.11). This observation is consistent with the notion that, early in H<sub>2</sub>O<sub>2</sub>-induced apoptosis, the MAPK pathways are involved in establishing signalling networks and factors associated with regulation of transcription, potentially influencing the final cardiomyocyte response to the encountered stress. Interestingly, although genes encoding enzyme modulators were relatively highly represented in the data for PD184352 (15.8% of all genes, Fig. 3.11A) and JNK-IN-8 (11.9% of all genes, Fig. 3.11B) but less so in the data for SB203580 (<5%, Fig. 3.11C), and accordingly there is presumably divergence in the roles of the different MAPKs in this context. Similarly, 7.3% of the genes differentially regulated by SB203580 were classified as encoding oxidoreductases (Fig. 3.11C) compared to only 1.8% for PD184352 (Fig. 3.11A) and 0% for JNK-IN-8 (Fig. 3.11B). Accordingly, this may be reflective of a role for p38-MAPKs in defense against the encountered oxidative stress.

### **3.4.3 Nuclear localisation of activated MAPKs in response to H<sub>2</sub>O<sub>2</sub>**

One important aspect of the investigations in this chapter was to characterise the nuclear localisation of activated ERK1/2, JNKs and p38-MAPKs in response to H<sub>2</sub>O<sub>2</sub>. Since activated MAPKs phosphorylate nuclear-localised transcription factors, thereby modulating their transactivating activities, it is presumed that phosphorylated (i.e. activated) MAPKs are present in the nucleus following stimulation. To assess the nuclear localisation of activated MAPKs in response to H<sub>2</sub>O<sub>2</sub>, cardiomyocytes were exposed to H<sub>2</sub>O<sub>2</sub> and subcellular protein fractions subjected to immunoblotting for total and phosphorylated MAPKs; an approach successfully

adopted previously to assess localisation of activated ERK1/2 and RSKs in response to various GqPCR agonists (Amirak et al., 2013). These experiments indicated that activated ERK1/2 were substantially increased in the NPE fraction following 10 min H<sub>2</sub>O<sub>2</sub> stimulation (maximal at 20 – 30 min), suggesting that active ERK1/2 play a significant role in the nucleus (Fig. 3.1A and B). Interestingly, the degree and profiles of ERK1/2 activation were similar in the cytoplasmic and nuclear fractions (Fig. 3.1B), reinforcing the notion that the pathway plays important roles in both compartments. Perhaps surprisingly, there was an absence of net nuclear accumulation of total ERK1/2 protein following activation, as occurs in other cell types (Chen et al., 1992; Adachi et al., 1999), although it was also previously reported that exposure of cardiomyocytes to ET-1, phenylephrine or A61603 similarly resulted in increased detection of activated ERK1/2 in the nucleus in the absence of net nuclear accumulation (Amirak et al., 2013). Subcellular localisation of ERK1/2 is regulated by a number of factors including autodimerisation, interactions with scaffolding proteins or the cytoskeleton or by association with the upstream MKKs (Reszka et al., 1995; Adachi et al., 1999; Casar et al., 2009). However, these components and their regulation of ERK1/2 localisation in cardiomyocytes are yet to be elucidated.

p46- and p54-JNKs were maximally activated in the cytoplasmic fraction following 10 min 0.2 mM H<sub>2</sub>O<sub>2</sub> exposure, an earlier time than observed for maximal ERK1/2 activity (Fig. 3.1 A and B). Interestingly, cytoplasmic p38-MAPK activation in response to H<sub>2</sub>O<sub>2</sub> was extremely rapid, with a significant, ~5.8-fold stimulation by 2 min (Fig. 3.2 A and B). These data are largely consistent with previous observations, although p38-MAPK activation was previously investigated following ≥5 min 0.1 mM H<sub>2</sub>O<sub>2</sub> stimulation, thus activation at an earlier time-point is demonstrated here (Clerk et al., 1998b). In contrast with the data for ERK1/2, the increases in activated JNKs and p38-MAPKs in the cardiomyocyte nucleus following H<sub>2</sub>O<sub>2</sub> stimulation were smaller and not statistically significant (Figs. 3.2 and 3.3), although due to some variability in the response, an increased sample size would likely result in statistically significant observations. Nonetheless, activated JNKs and p38-MAPKs were indeed detected in the NPE

fraction following H<sub>2</sub>O<sub>2</sub> exposure, suggestive of a role for these pathways in the cardiomyocyte nucleus. In common with ERK1/2, net nuclear accumulation of JNKs or p38-MAPKs was not detected (Figs. 3.2 and 3.3). There are seemingly few studies examining the subcellular distribution of cardiac JNKs and p38-MAPKs, although JNK1 has previously been shown to translocate to cardiomyocyte nuclei upon ischaemia, where it is activated by MKK4 upon reperfusion (Mizukami et al., 1997). In other cell types, p38-MAPK does not exhibit redistribution to the nucleus upon activation, except in response to DNA damage, consistent with the observations here (Raingeaud et al., 1995; Wood et al., 2009).

The subcellular fractionation method used here relies on use of a hypotonic buffer to selectively isolate the cytosolic fraction followed by extraction and enrichment of nuclear proteins using a high salt buffer (Dignam et al., 1983). Although other effective approaches, such as exploiting differential solubility of subcellular components in detergents (Ramsby and Makowski, 2011), are available, the subcellular fractionation method used has been shown to reliably separate soluble cytoplasmic proteins from the nucleus; with negligible detectable cross-contamination (Amirak et al., 2013; Dignam et al., 1983).

#### **3.4.4 Conclusions and further work**

Considered together, the expression profiling and subcellular localisation data presented here indicate that ERK1/2, JNKs and p38-MAPKs play important roles in regulation of cardiomyocyte RNA expression in response to H<sub>2</sub>O<sub>2</sub>, and that these effects are mediated, at least in part, by activated MAPKs in the nucleus. Interestingly, of the MAPKs examined, ERK1/2 appear to play the largest role in terms of numbers of genes regulated and degree of activation in the nucleus, with somewhat lesser yet important contributions from JNKs and p38-MAPKs.

However, given that expression of a total of 214 of the 490 RNAs changed by H<sub>2</sub>O<sub>2</sub> was unaffected by any MAPK inhibitor, it is apparent that other regulatory pathways are implicated

in the modulation of RNA expression under these conditions. Although the identities of these pathways were not investigated during this study, it is possible that other oxidative stress-sensitive regulators of gene expression such as the transcription factor Nrf2 are involved in the cardiomyocyte response to H<sub>2</sub>O<sub>2</sub> (Zhou et al., 2014). Additional work is required to identify, and characterise the roles of, these pathways. Further investigations would also seek to assess the extent to which the contributions from the MAPK pathways to changes in RNA expression are reflected at the level of expressed protein. Of particular interest for further examination are the Dusps, due to their roles in negative regulation of MAPK activity. Zfp36/tristetraprolin is also a key gene of interest, due to its association with p38-MAPKs and modulation of pro-inflammatory transcripts.

**Chapter Four – Effects of pathophysiological stimuli on receptor-interacting protein kinases (RIPKs) in the heart**

## 4.1 Introduction

The data presented in Chapter Three demonstrate that the principal MAPK pathways, ERK1/2, JNKs and p38-MAPKs, play significant yet differential roles in regulation of cardiomyocyte mRNA expression during H<sub>2</sub>O<sub>2</sub>-induced apoptosis. Thus, these signalling pathways potentially contribute to the cardiomyocyte death response. However, it is clear that other pathways also play significant roles in modulating the balance between cardiomyocyte life and death. Rapidly emerging data in other systems have identified a novel form of cell death, necroptosis, mediated by a family of protein kinases, the RIPKs.

Interest in the RIPKs was piqued during efforts within Prof. Clerk's laboratory to delineate the cardiac kinome (i.e. the full complement of kinases expressed within the heart). These studies revealed that certain members of the RIPK family (RIPKs 1, 2 and 3) and other proteins implicated in necroptotic cell death (e.g. MLKL) are expressed at significant levels in the heart (Fuller et al., 2015). Considering the close association between cardiomyocyte death and cardiac pathologies such as HF and MI (Chiong et al., 2011), the RIPKs represent a promising field of investigation, since regulated cell death pathways have the potential to be targeted therapeutically. The pleiotropic roles of RIPK1 in both promotion of survival (through activation of NF $\kappa$ B and MAPKs) and induction of necroptotic death (Zhou and Yuan, 2014) make it a particularly salient target of scrutiny since developing an understanding of its function may highlight potential for therapeutic intervention both in inhibiting cell death responses and in promoting cardioprotection.

At the outset of this investigation, there were few published studies pertaining to the roles of RIPKs and necroptosis in the heart. Early studies subsequent to the observation that necrostatin-1 (Nec-1) has a protective effect against non-apoptotic death in ischaemic brain injury (Degterev et al., 2005), demonstrated that Nec-1 conferred protection against tertbutyl hydroperoxide-induced death of the cardiac-related H9c2 cell line and reduces infarct size following myocardial IR (Smith et al., 2007; Lim et al., 2007). The identification of RIPK1 kinase activity as the target of Nec-1 (Degterev et al., 2008) led to more focussed investigations. In

2012, Oerlemans and colleagues (Oerlemans et al., 2012) demonstrated that, in a mouse model of myocardial IR, administration of Nec-1 prior to onset of reperfusion inhibited RIPK1/3 phosphorylation and significantly reduced infarct size and necrotic cell death, with no effect on apoptotic death. A concomitant decrease in inflammatory and oxidative stress-associated transcripts (e.g. *Tnfa*, *Gab1*, *Nos2*, *Cox-2*) was also reported, reinforcing the importance of RIPK1 in mediating cardiac inflammatory and death responses. While these studies highlighted a key role for RIPK1 kinase activity in induction of necroptosis in the heart, Luedde *et al.* (Luedde et al., 2014) described upregulation of RIPK3 in the peri-infarct zone following ligation of the left anterior descending coronary artery. However, the study did not address whether this was localised to cardiomyocytes or non-myocytes. RIPK3 overexpression also induced necroptotic death of neonatal cardiomyocytes. More recently, Li and colleagues (Li et al., 2014) demonstrated that inhibition of TAK1 activity suppresses activation of JNKs and NF $\kappa$ B and sensitises cardiomyocytes to TNF $\alpha$ -induced necroptosis. The observation that cardiomyocytes could be rescued by RIPK1 inhibition with Nec-1, but not pan-caspase inhibition, reinforces the central role of RIPK1 kinase activity in necroptosis (Li et al., 2014).

Although the available studies indicate a key role for RIPKs and necroptosis in the heart, with potentially important consequences for development of cardiac pathologies, there remains a paucity of detail regarding the molecular regulation of these kinases in the heart. Furthermore, the pathway has been examined in the context of a relatively limited number of stimuli which may not adequately reflect the wide range of pathophysiological insults to which the heart is subjected. In this chapter, the aim was to investigate potential roles for RIPKs in the heart in response to a variety of agonists, achieved by adoption of a screening approach to assess the response of cardiac RIPKs to a range of pathophysiological stimuli.

## **4.2 Methods**

### **4.2.1 Neonatal rat ventricular cardiomyocytes and immunoblotting**

Primary cultures of neonatal rat ventricular cardiomyocytes (from 2 – 4 d Sprague-Dawley rats) were prepared as described in Chapter Two, section 2.3.1. Cardiomyocytes were treated with agonists and/or inhibitors (prepared as detailed in Chapter Two, section 2.2) as indicated. Unless stated otherwise, total protein extracts were prepared as in Chapter Two, section 2.5.1. Protein content in prepared extracts was quantified using a modification of the Bio-Rad Protein assay as described in Chapter Two, section 2.5.3. Extracts (20 – 100 µg) were separated by SDS-PAGE using 10% polyacrylamide gels and immunoblotted as described in Chapter Two, section 2.5.4 using the indicated antibodies.

### **4.2.2 Anion-exchange fast protein liquid chromatography (FPLC)**

Anion-exchange FPLC was performed in collaboration with Prof. Angela Clerk using a Mono Q HR 5/5 FPLC column and an Äkta FPLC system (both GE Healthcare) as described in Chapter Two, section 2.11. In summary, five 60 mm dishes of neonatal rat ventricular cardiomyocytes were treated as indicated, washed twice with ice-cold PBS and harvested into a total of 300 µl extraction buffer. The lysates were extracted on ice (10 min), centrifuged to remove cell debris (10,000×g, 5 min, 4°C), and the resulting supernatants removed to a clean tube. The extracts were further clarified with a second centrifugation (10,000×g, 5 min, 4°C) and the supernatant extracts removed to a clean tube. The extracts were loaded into a Mono Q HR 5/5 FPLC column pre-equilibrated with Mono Q Buffer A as described in Chapter Two section 2.11. Following a 5 ml isocratic wash, bound proteins were eluted from the column with a linear NaCl gradient (20 ml, 0 – 0.4 M) at a rate of 1 ml/min, formed by mixing Mono Q Buffer A with Mono Q Buffer B (Mono Q Buffer A containing 1 M NaCl). Fractions (0.5 ml) were collected with an automated fraction collector. Samples of each fraction were retained and boiled with 0.33 vol. 4× SDS-PAGE sample buffer (5 min).

Column fractions were immunoblotted using antibodies to RIPK1. Immunoreactive bands were analysed densitometrically and the values for each fraction normalised to the maximum value from each column.

### **4.3 Results**

#### **4.3.1 Effects of oxidative stress on RIPKs in neonatal rat cardiomyocytes and adult rat hearts**

Several studies have implicated RIPKs in regulation of cell death resulting from ischaemia and IR injury in systems including brain, kidney and heart (Degterev et al., 2005; Linkermann et al., 2012; Oerlemans et al., 2012; Luedde et al., 2014; Newton et al., 2016a). IR induces a wide range of responses in the cell, and is associated with an increase in oxidative stress and cell death. Directly applied oxidative stress (exemplified by H<sub>2</sub>O<sub>2</sub>) can induce cardiomyocyte apoptosis or necrosis, dependent on the concentration (Von Harsdorf et al., 1999; Cook et al., 1999b; Kwon et al., 2003). To examine the effects of oxidative stress on cardiac RIPK1, cardiomyocytes were exposed to H<sub>2</sub>O<sub>2</sub> (0.03 – 10 mM, 0.5 – 8h). Total protein extracts were produced and immunoblotted with antibodies to RIPK1.

In unstimulated cardiomyocytes, RIPK1 was detected as a band of ~70 kDa (rat RIPK1 predicted molecular weight, ~74.8 kDa) (Fig. 4.1) Exposure to H<sub>2</sub>O<sub>2</sub> concentrations of 0.2 mM and higher resulted in a reduction in electrophoretic mobility of RIPK1 (Fig. 4.1, A, B and C). At 0.2 mM, the response was transient, with a maximal band shift at 0.5 – 1 h, returning to baseline by 2 h. The response to 0.5 mM H<sub>2</sub>O<sub>2</sub> was of a greater magnitude, resulting in a band shift of the total RIPK1 complement of the cell at 0.5 – 1 h, with a partial reversal at 2 h (Fig 4.1A). A higher concentration, 1 mM H<sub>2</sub>O<sub>2</sub>, also resulted in reduction of RIPK1 mobility at 0.5 h. Maximal band shifting was observed at 1 – 2 h in response to 1 mM H<sub>2</sub>O<sub>2</sub>, although this subsided by 4 h. However, reduced mobility bands were detected following longer incubations of up to 8 h (Fig 4.1B).

Assessing the response of RIPK1 to exposure to various concentrations of H<sub>2</sub>O<sub>2</sub> for 1 h demonstrated that H<sub>2</sub>O<sub>2</sub> concentrations of 0.3 - 10 mM (Fig. 4.1C) resulted in reduced mobility of RIPK1, whilst concentrations of 0.1 and 0.03 mM had little or no effect. The response was maximal following exposure to 1 mM H<sub>2</sub>O<sub>2</sub> (Fig. 4.1C).

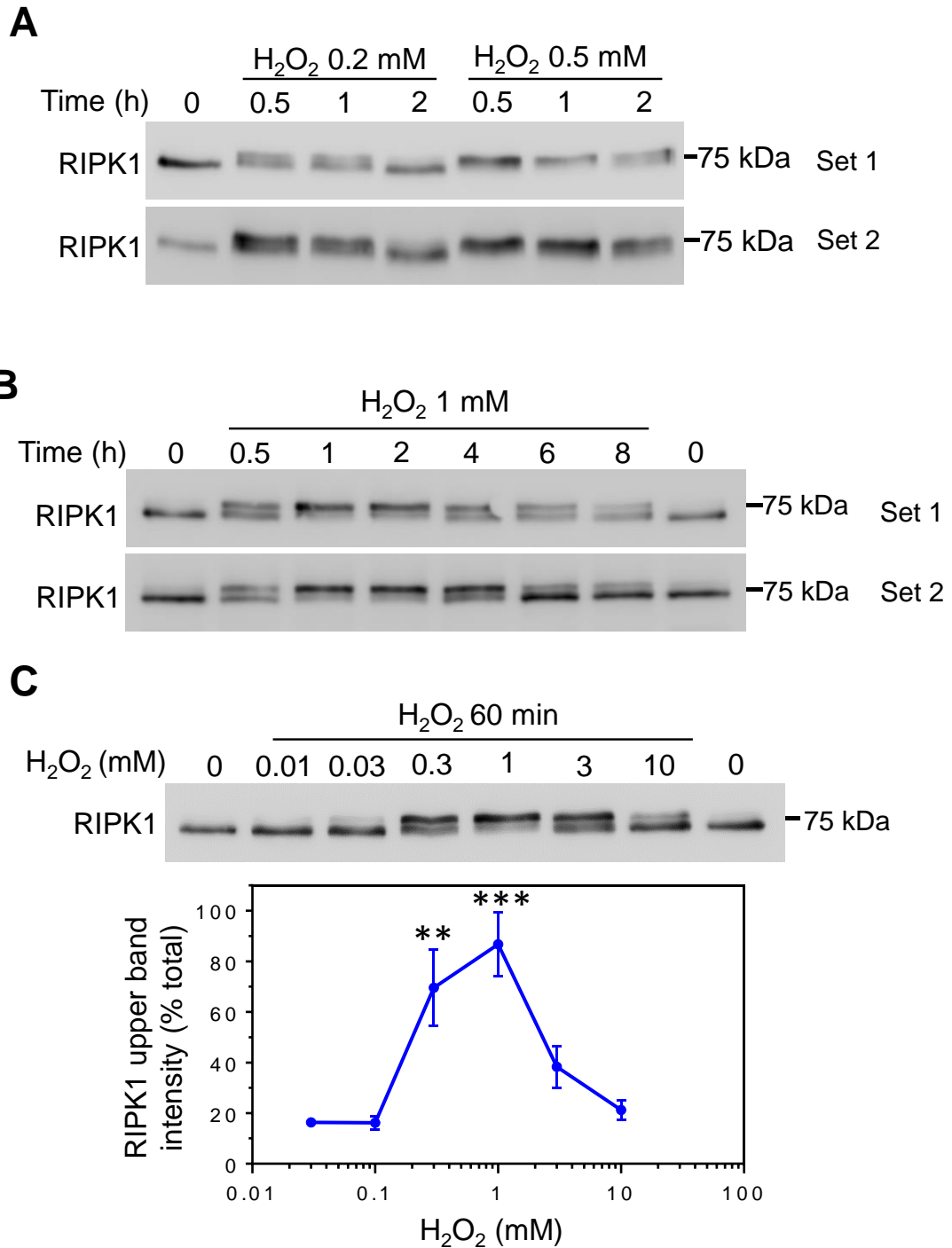


**Figure 4.1 Effects of oxidative stress on RIPK1 in cardiomyocytes.**

(**A** and **B**) Cardiomyocytes were exposed to 1 mM H<sub>2</sub>O<sub>2</sub> for 0 – 8 h (A) or 0.2 or 0.5 mM H<sub>2</sub>O<sub>2</sub> for 0 – 120 min (B). Total protein extracts (30 µg) were immunoblotted for RIPK1. Two experiments with independent cardiomyocyte preparations are shown. (**C**) Cardiomyocytes were exposed to 0 – 10 mM H<sub>2</sub>O<sub>2</sub> (60 min). Total protein extracts (30 µg) were immunoblotted for RIPK1 (upper panel). Densitometric analysis of the immunoblots is shown in the lower panel. Results shown are the percentages of the upper band relative to total RIPK1 immunoreactivity. Results are means ± SEM (n=3 independent cardiomyocyte preparations). \*\*, p<0.01; \*\*\*, p<0.001 (one-way ANOVA with Tukey post-test).

Having observed the effects of oxidative stress on RIPK1 in isolated neonatal cardiomyocytes, the effects of IR, which is associated with an increase in oxidative stress, on RIPKs in the mature whole organ were explored. Adult male rat hearts were subjected to IR (20 min ischaemia and 40 min reperfusion) and extracts were immunoblotted with antibodies to RIPK1 and RIPK3 (Fig. 4.2, A and C). IR resulted in a significant loss (>4-fold reduction relative to control) of RIPK1 protein, with no significant effects on the quantity of the related kinase, RIPK2 (Fig. 4.2, A and B) IR also resulted in the appearance of bands of reduced mobility for both RIPK1 and RIPK3 (Fig. 4.2C).

To determine whether the effects of directly applied oxidative stress on RIPKs in the isolated neonatal cardiomyocyte are reflected in the whole adult heart, adult male rat hearts were perfused under control conditions or with 0.2 mM H<sub>2</sub>O<sub>2</sub> for 1 h and extracts immunoblotted for RIPKs. H<sub>2</sub>O<sub>2</sub> induced the appearance of reduced mobility bands of both RIPK1 and RIPK3 (Fig. 4.2C).

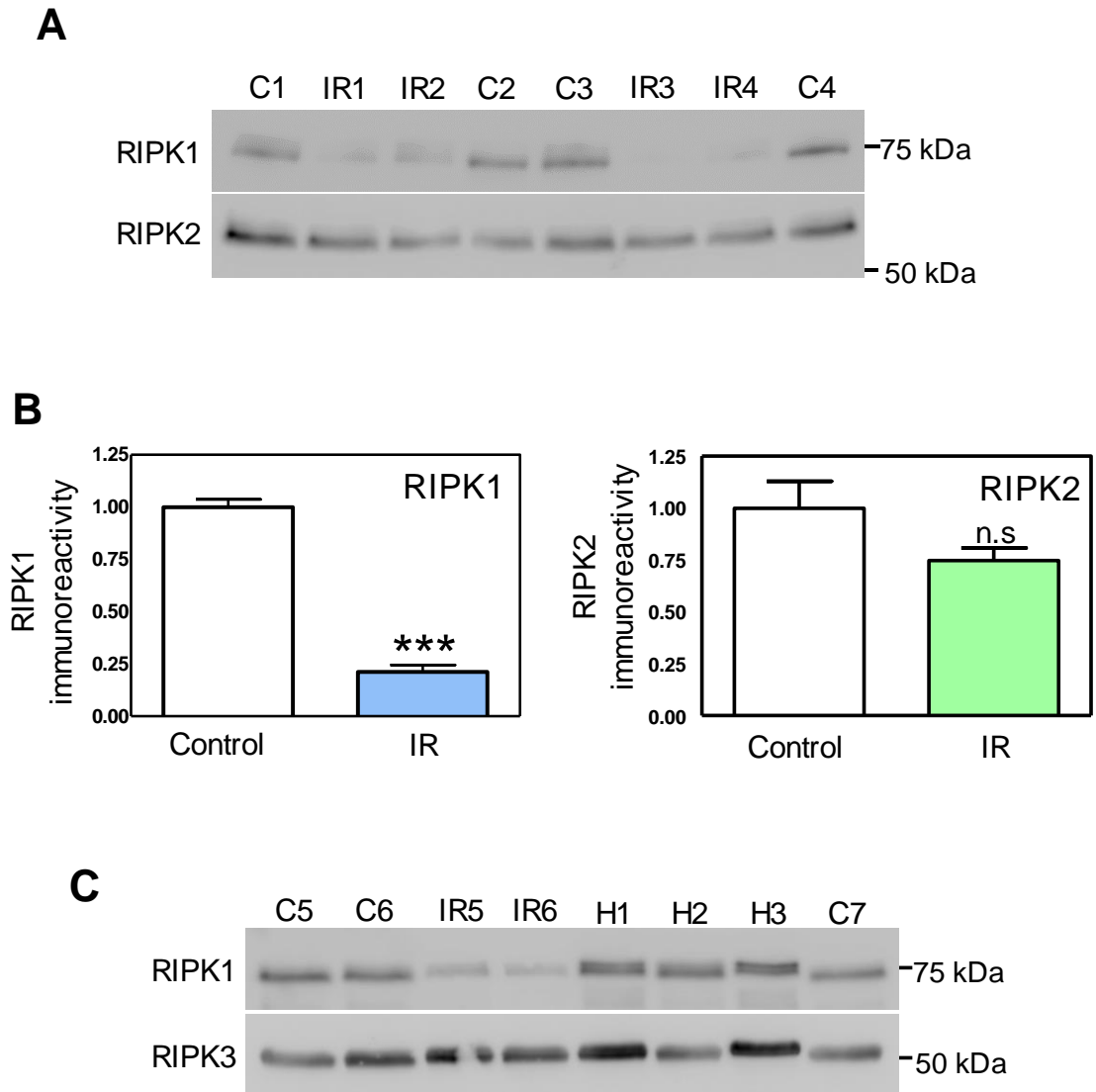


**Figure 4.2 Effects of ischaemia/reperfusion and H<sub>2</sub>O<sub>2</sub> on RIPKs in adult rat hearts.**

Isolated adult male rat hearts were perfused under control conditions (C, 60 min) or subjected to global ischaemia followed by reperfusion (IR, ischaemia 20 min; reperfusion 40 min) or were perfused with 0.2 mM H<sub>2</sub>O<sub>2</sub> (H, 60 min). **(A)** Total protein extracts (40 µg) were immunoblotted for RIPK1 and RIPK2, as indicated. **(B)** Densitometric analysis of the immunoblots in **(A)**. Results are means ± SEM (n=4) and are normalised to the mean of the controls. \*\*\*, p<0.0001 (Student's t-test). **(C)** Total protein extracts (100 µg) were immunoblotted for RIPK1 and RIPK3, as indicated. Each lane represents an individual heart.

### **4.3.2 Effects of pro-inflammatory cytokines (TNF $\alpha$ and IL1 $\beta$ ) on RIPK1 in neonatal rat cardiomyocytes**

#### **4.3.2.1 Effects of TNF $\alpha$ on RIPK1 in cardiomyocytes**

As discussed in Chapter One, section 1.4, pro-inflammatory cytokines such as TNF $\alpha$  and IL1 $\beta$  activate important signalling pathways such as the MAPKs in cardiomyocytes (Clerk et al., 1999), and are implicated in the regulation of both adaptive and maladaptive responses in the heart (Barrett et al., 2013; Hedayat et al., 2010). Historically, RIPKs and necroptosis have been characterised most extensively in the context of TNF $\alpha$  stimulation of immune and inflammatory cells. To determine whether RIPK1 responds to TNF $\alpha$  in cardiomyocytes, neonatal rat cardiomyocytes were exposed to TNF $\alpha$  (20 ng/ml) for 5 min – 8 h. Total protein extracts were separated using SDS-PAGE and immunoblotted with antibodies to RIPK1.

Exposure to TNF $\alpha$  induced the appearance of a reduced mobility band of ~75 kDa (Fig. 4.3A). The detection of the 75 kDa band was maximal at 15 min, representing  $51 \pm 0.015\%$  of the total detected RIPK1 protein at that time point (Fig. 4.3B). Notably, in addition to the maximally shifted 75 kDa band, a RIPK1 band exhibiting a small upshift relative to control was observed at 5 – 15 min (Fig. 4.3A). The maximal response was at 15 min and this subsided between 30 – 120 min (Fig. 4.3A). However, the presence of a reduced mobility band was still detectable following longer incubation of up to 6 h (Fig. 4.3C).

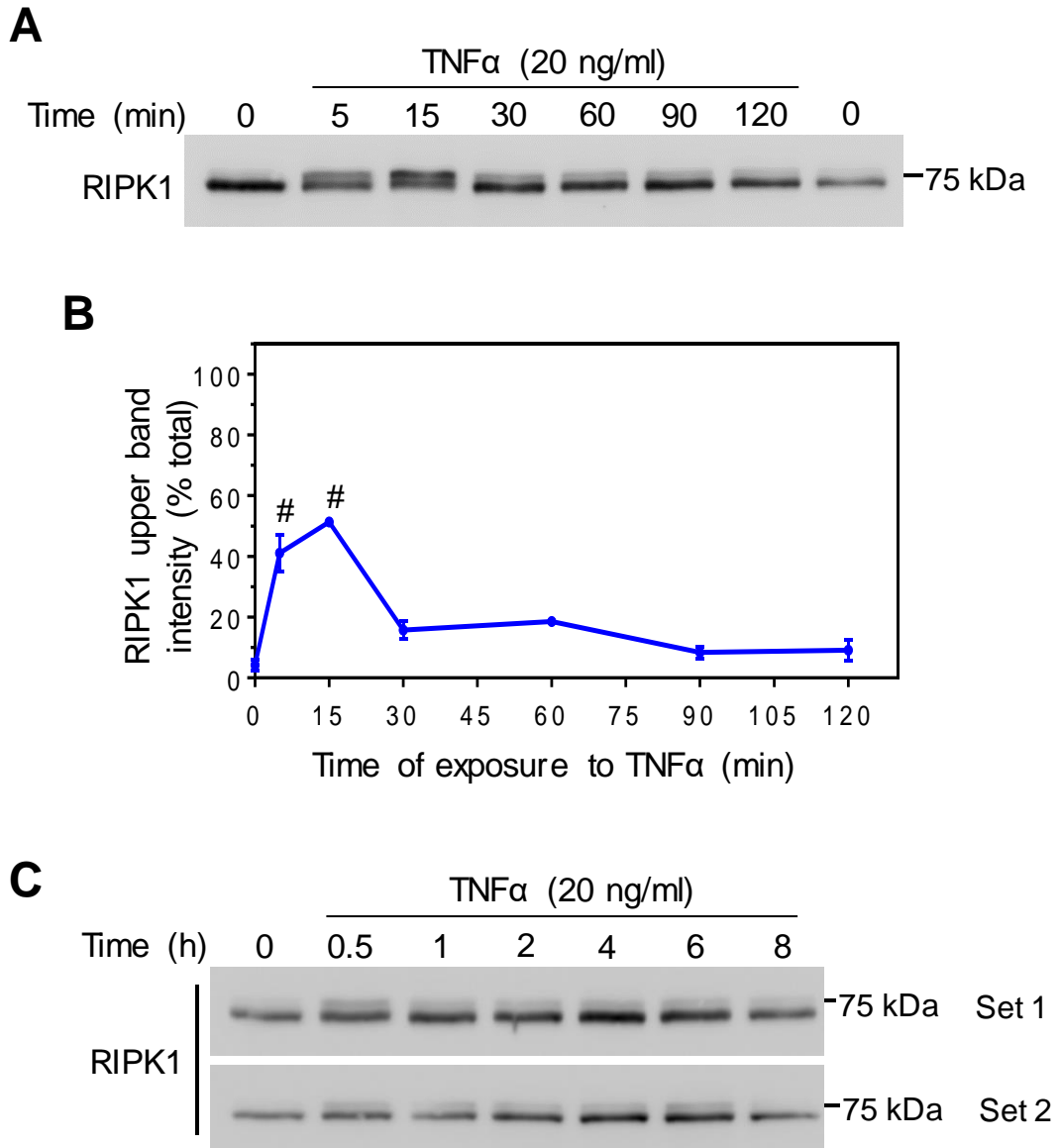


**Figure 4.3 Effects of TNF $\alpha$  on RIPK1 in cardiomyocytes.**

(A) Cardiomyocytes were untreated or exposed to TNF $\alpha$  (20 ng/ml) for 5 – 120 min. Total protein extracts (30  $\mu$ g) were immunoblotted for RIPK1. (B) Densitometric analysis of the RIPK1 immunoblots in (A). Results shown are the percentages of the upper band relative to total RIPK1 immunoreactivity and are means  $\pm$  SEM (n=3 independent cardiomyocyte preparations), normalised to the mean of the control values. #, p<0.0001 (one-way ANOVA with Tukey post-test). (C) Cardiomyocytes were untreated or exposed to TNF $\alpha$  (20 ng/ml) for 0.5 – 8 h. Total protein extracts were immunoblotted for RIPK1. The experiment was repeated and representative images from both cardiomyocyte preparations are shown.

#### **4.3.2.2 Effects of IL1 $\beta$ on RIPK1 in cardiomyocytes**

Having observed that RIPK1 responds to TNF $\alpha$  in cardiomyocytes, the immunoblotting approach described above was extended to cardiomyocytes exposed to a further important pro-inflammatory cytokine, IL1 $\beta$ . IL1 $\beta$  plays important roles in mediating pathophysiological responses in the heart (Yndestad et al., 2007). However, the response of RIPK1 to IL1 $\beta$  does not appear to have been assessed in the heart, or any other system. To assess the potential roles of IL1 $\beta$  in regulation of RIPK1 and necroptosis in cardiomyocytes, cardiomyocytes were unstimulated or exposed to IL1 $\beta$  (25 ng/ml, 5 min – 8 h). As with TNF $\alpha$  (Fig. 4.3), IL1 $\beta$  maximally induced the appearance of reduced mobility bands for RIPK1 within 5 – 15 min, with the 75 kDa band representing  $80\pm 0.15\%$  of total RIPK1 at 15 min (Fig. 4.4, A and B) Longer exposures up to 8 h also resulted in detection of a reduced mobility RIPK1 band (Fig. 4.4C) In common with TNF $\alpha$ , IL1 $\beta$  also induced a small upshift in RIPK1 relative to unstimulated cells at 5 – 15 min (Fig. 4.4A).

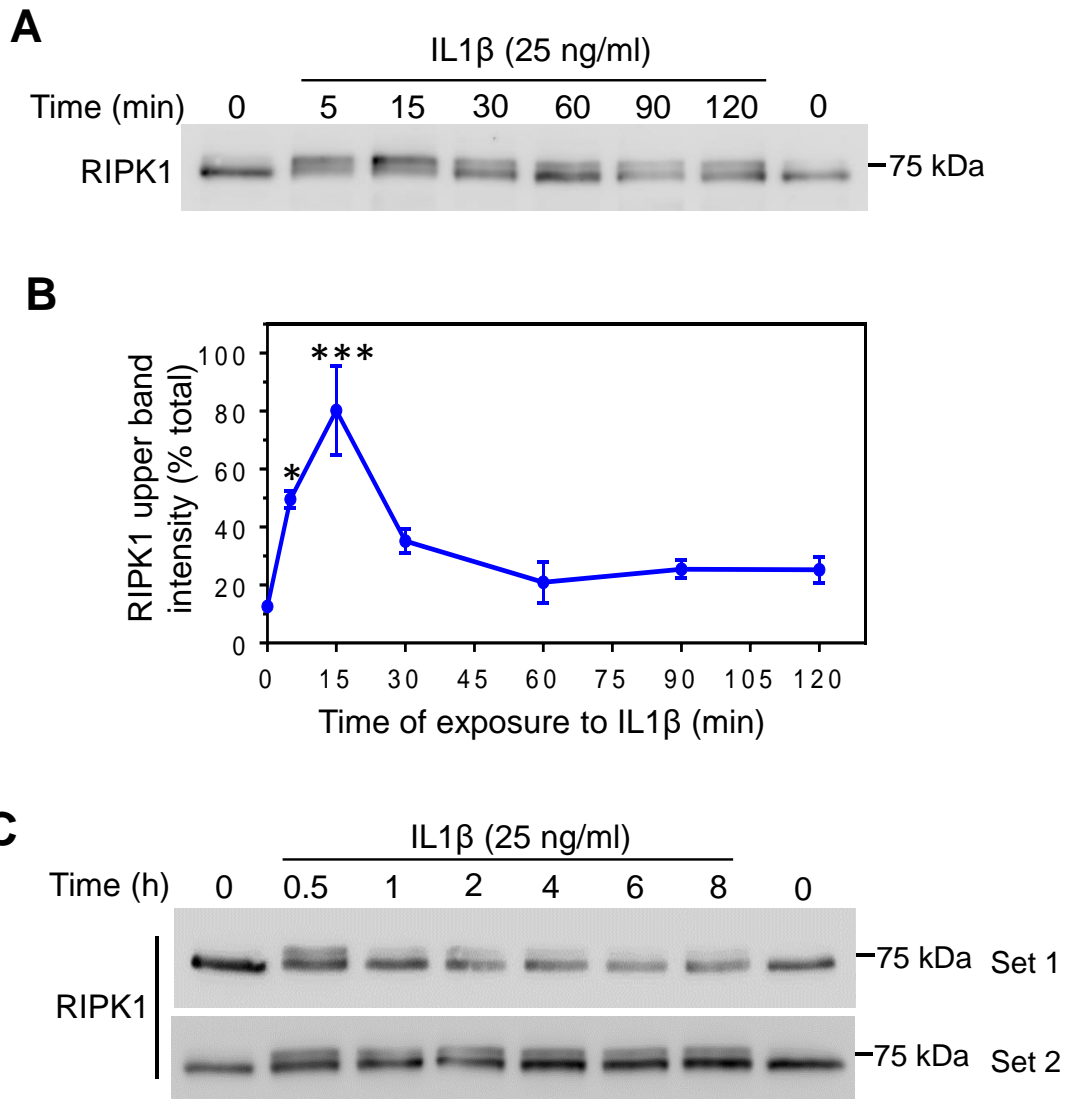


**Figure 4.4 Effects of IL1 $\beta$  on RIPK1 in cardiomyocytes**

(**A**) Cardiomyocytes were untreated or exposed to IL1 $\beta$  (25 ng/ml) for 5 – 120 min. Total protein extracts (30  $\mu$ g) were immunoblotted for RIPK1. (**B**) Densitometric analysis of the RIPK1 immunoblots in (**A**). Results shown are the percentages of the upper band relative to total RIPK1 immunoreactivity and are means  $\pm$  SEM (n=3 independent cardiomyocyte preparations), normalised to the mean of the control values. \*, p<0.05; \*\*\*, p<0.001 (one-way ANOVA with Tukey post-test). (**C**) Cardiomyocytes were untreated or exposed to IL1 $\beta$  (25 ng/ml) for 0.5 – 8 h. Total protein extracts were immunoblotted for RIPK. Representative images from two independent cardiomyocyte preparations are shown.

The reduction of protein electrophoretic mobility through SDS gels following phosphorylation has been documented extensively and is a well-established phenomenon (Wegener and Jones, 1984; Lozano et al., 1990; Fuller et al., 2012). Accordingly, to examine whether the reduction of RIPK1 mobility in response to IL1 $\beta$  might be caused by increased RIPK1 phosphorylation, protein extracts from unstimulated cardiomyocytes and from those exposed to IL1 $\beta$  (25 ng/ml, 15 min) were subjected to anion exchange FPLC using a Mono Q column. Mono Q columns contain a strong anion-exchange resin, which causes negatively charged residues on proteins to bind tightly. Increasing the phosphorylation status of a protein increases the number of negatively charged residues, resulting in tighter binding to the resin, and requiring a greater NaCl concentration to disrupt the association and elute the protein. Accordingly, more highly phosphorylated proteins typically elute in later fractions. The column fractions were immunoblotted for RIPK1. Densitometric analysis of the immunoblotted fractions demonstrated that RIPK1 in extracts from unstimulated cardiomyocytes eluted from the Mono Q column predominantly in a peak at ~0.19 – 0.2 M NaCl (fractions 19 – 20) (Fig. 4.5, A and B). However, exposure of cardiomyocytes to IL1 $\beta$  retarded the elution of RIPK1 from the Mono Q column, resulting in a peak of RIPK1 immunoreactivity eluting at ~0.21 – 0.22 M NaCl (fractions 21 – 22) (Fig. 4.5, A and B), consistent with a higher phosphorylation status of RIPK1 in response to IL1 $\beta$ .



#### **4.3.3 Effect of SB203580 on the RIPK1 response to IL1 $\beta$ in neonatal rat cardiomyocytes**

Previous investigations indicate that IL1 $\beta$  (10 ng/ml) potently activates p38-MAPKs in cardiomyocytes, with a maximal response at 5 – 15 min (Clerk et al., 1999). Having observed that IL1 $\beta$  (25 ng/ml) induces maximal band shifting of RIPK1 at 15 min (Fig. 4.4, A and B), it was hypothesised that the reduction in RIPK1 mobility might be due to phosphorylation by either p38-MAPKs or a p38-MAPK-activated kinase. To investigate this, the effects of the inhibitor of p38-MAPK $\alpha/\beta$  signalling, SB203580 (Cuenda et al., 1995), on the response of RIPK1 to IL1 $\beta$  were examined. Although SB203580 is widely used to inhibit activity of p38-MAPK $\alpha/\beta$ , it is also a more potent inhibitor of RIPK2 (Godl et al., 2003).

Cardiomyocytes were untreated or exposed to IL1 $\beta$  (25 ng/ml, 15 min) with or without pre-treatment with SB203580 (0.7  $\mu$ M, 15 min), or to SB203580 alone (30 min), and total protein extracts immunoblotted for RIPK1. As previously observed, IL1 $\beta$  induced a reduction of RIPK1 electrophoretic mobility and the appearance of higher molecular weight RIPK1 bands relative to control (Fig. 4.6). Exposure to SB203580 alone had no discernible effect on RIPK1 mobility. However, pre-treatment with SB203580 reduced the appearance of the higher molecular weight RIPK1 bands in response to IL1 $\beta$  (Fig. 4.6).

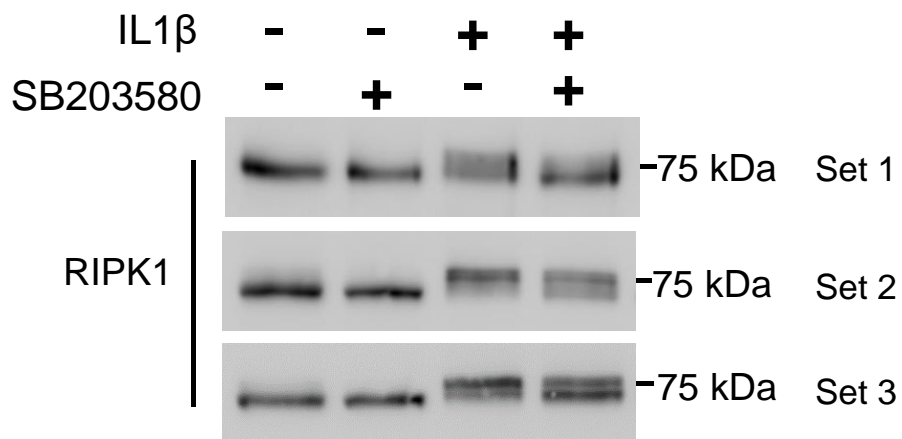


**Figure 4.6 Effects of SB203580 on the RIPK1 response to IL1 $\beta$  in cardiomyocytes.**

Cardiomyocytes were untreated or exposed to IL1 $\beta$  (25 ng/ml, 15 min) with or without pre-treatment with SB203580 (0.7  $\mu$ M, 15 min) or exposed to SB203580 alone (30 min). Total protein extracts (30  $\mu$ g) were immunoblotted for RIPK1. Images from three independent cardiomyocyte preparations are shown.

## **4.4 Discussion**

The data presented in this chapter provide novel insights into the regulation of RIPK1 in cardiomyocytes and the heart. The key findings are that exposure of cardiomyocytes to pro-inflammatory cytokines (TNF $\alpha$  and IL1 $\beta$ ) and H<sub>2</sub>O<sub>2</sub> promoted reduction of RIPK1 mobility on immunoblots (Figs. 4.2-4.4). Furthermore, electrophoretic mobility of RIPKs 1 and 3 was reduced in response to oxidative stress and IR in whole adult hearts (Fig. 4.3, A and C). These data indicate that RIPKs 1 and 3 in cardiomyocytes and/or hearts are differentially regulated in response to pathophysiological stimuli, reflecting post-translational modification of these proteins (Shirai et al., 2008) and suggesting important roles in mediation of the response of the cardiomyocyte to the encountered stimuli.

### **4.4.1 Differential signalling to RIPK1 by pro-inflammatory cytokines vs oxidative stress**

Although RIPK1 exhibited reduced mobility in response to all the stimuli examined, the extent and time courses of the responses differed. Reduction of RIPK1 mobility in response to both TNF $\alpha$  and IL-1 $\beta$  was rapid and transient, with maximal responses at 15 min, but the effect of TNF $\alpha$  on RIPK1 was of a lesser magnitude than that induced by IL1 $\beta$  at 15 min, with ~51% of the total RIPK1 content in the uppermost band, compared to ~80% of total RIPK1 in the uppermost band following the same duration of exposure to IL1 $\beta$  (Figs. 4.4 and 4.5). This observation implies that the signalling events initiated downstream of IL1 $\beta$  stimulation in this context result in modification of a larger pool of RIPK1 protein than in response to TNF $\alpha$ . However, the reasons for this and its potential implications are unclear and further investigation is required to elucidate the downstream signalling events occurring.

In contrast with the rapid maximal response to TNF $\alpha$  and IL1 $\beta$ , the reduction of RIPK1 mobility upon exposure to all H<sub>2</sub>O<sub>2</sub> concentrations was maximal at the later time of 60 min (Fig. 4.2, A and B). This disparity in the onset of the response is potentially explained by the fact that both TNF $\alpha$  and IL-1 $\beta$  exert their effects by binding to their respective receptors at the membrane,

while H<sub>2</sub>O<sub>2</sub> presumably modulates the activity of proteins intracellularly, rather than binding to a specific receptor. Indeed, rather than initiating assembly of specific signalling complexes, as do IL1 $\beta$  and TNF $\alpha$  (see Chapter One, Figs 1.4 and 1.5), H<sub>2</sub>O<sub>2</sub> may have a number of effects that potentially modulate signalling events, including (for example) inhibiting protein tyrosine phosphatases (Hecht and Zick, 1992; Gough and Cotter, 2011). It is also possible that exposure of cardiomyocytes to H<sub>2</sub>O<sub>2</sub> stimulates production or release of other signalling molecules or factors that may act in an autocrine or paracrine fashion to elicit the observed response, although Wang *et al.* reported that H<sub>2</sub>O<sub>2</sub>-induced necroptosis in H9c2 cells is independent of TNFR1, suggesting that TNF $\alpha$  is not implicated in the response to H<sub>2</sub>O<sub>2</sub> (Wang *et al.*, 2015). Although the data do not address the consequences of the observed effects on RIPK1, the rapidity and transience of their onset upon exposure to TNF $\alpha$  and IL1 $\beta$  may reflect an early initiating event in the cardiomyocyte response to these stimuli.

#### **4.4.2 Phosphorylation vs ubiquitinylation of RIPK1**

Differential electrophoretic mobility through SDS gels is a common result of post-translational modification of proteins (Shirai *et al.*, 2008). In other systems, RIPK1 undergoes phosphorylation and ubiquitinylation under different conditions (De Almagro *et al.*, 2017), and these modifications might result in reduced electrophoretic mobility of the protein. While ubiquitinylation of RIPK1 could result in reduced mobility of the protein, this is unlikely to be the cause here as the shift is of insufficient magnitude to reflect the modification of RIPK1 with even a single ubiquitin, a protein with a molecular weight of ~8.5 kDa (Chyan *et al.*, 2004). It is highly unlikely therefore that the observed band shifting is due to polyubiquitinylation, as such a modification would be expected to cause a shift of significantly greater magnitude than that observed here, producing high molecular weight “smears” of RIPK1 immunoreactivity on immunoblots (Lee *et al.*, 2004; Ea *et al.*, 2006).

The band shift response of RIPK1 to the various pathophysiological stimuli examined here is most consistent with phosphorylation. Reduction of protein mobility upon phosphorylation has been documented extensively and is particularly relevant in context of regulation of kinases such as RIPK1 (Wegener and Jones, 1984; Lozano et al., 1990; Fuller et al., 2012). Importantly, the increase in apparent molecular weight of a protein following phosphorylation is not a consequence of the relatively insignificant real-terms molecular weight increase caused by addition of a phosphate group (80 Da). Rather, it is a result of the reduced capacity for SDS to bind the protein due to the increase in negatively charged residues induced by phosphorylation (Peck, 2006; Lee et al., 2004). Accordingly, the detection of multiple bands of RIPK1 immunoreactivity in response to the various stimuli examined is suggestive of phosphorylation on multiple residues. Evidence from other investigators supports the notion that the reduction of RIPK1 mobility is caused by phosphorylation. The RIPK1 response to TNF $\alpha$  observed here in cardiomyocytes is qualitatively similar to the effects observed by Lee and colleagues (Lee et al., 2004) in mouse embryonic fibroblasts. In these cells, TNF $\alpha$  led to a reduction in RIPK1 mobility following 5 – 10 min exposure (closely resembling that observed in (Fig. 4.4A) and this was sensitive to treatment with lambda phosphatase, restoring shifted RIPK1 bands to the original position on immunoblots (Lee et al., 2004).

Further evidence that the observed RIPK1 band shift is due to phosphorylation was obtained by subjecting extracts from IL1 $\beta$ -treated cardiomyocytes to fractionation on a Mono Q column (Fig 4.5). Immunoblotting of fractions showed that IL1 $\beta$  led to a retardation in RIPK1 elution from the Mono Q column relative to that in unstimulated cardiomyocytes (Fig 4.5, A and B). This is indicative of a higher phosphorylation status, as increasing the number of negatively charged residues results in tighter binding of proteins to the anion-exchange resin, thus requiring a greater NaCl concentration to disrupt the association and leading to elution in later fractions. Additionally, the RIPK1 band exhibiting the greatest shift in response to IL1 $\beta$  eluted in a later fraction bands exhibiting a smaller shift (Fig. 4.5A), further suggesting that the shift is due to phosphorylation.

The p38-MAPK $\alpha/\beta$  inhibitor SB203580 was also observed to reduce some of the response of RIPK1 to IL1 $\beta$  (Fig. 4.6), representing a further line of evidence that the observed reduction of electrophoretic mobility is a consequence of phosphorylation. This observation also provides novel preliminary evidence that RIPK1 may be a substrate for phosphorylation by either p38-MAPK $\alpha/\beta$  or a p38-MAPK $\alpha/\beta$ -activated kinase, such as MAPKAPK2 or MAPKAPK3 (Cargnello and Roux, 2011), an observation that has not previously been reported. However, SB203580 is not entirely selective for p38-MAPK $\alpha/\beta$  and inhibits RIPK2 with greater potency (Godl et al., 2003). Therefore it will be necessary to conduct further investigations in order to determine whether the observed effect of SB203580 on the RIPK1 response to IL1 $\beta$  is due to inhibition of p38-MAPK $\alpha/\beta$  or as a result of off-target effects. One potential approach is to examine whether the observed effects can be replicated using structurally unrelated p38-MAPK inhibitors that do not inhibit RIPK2, for example the allosteric inhibitor BIRB 796 (Bain et al., 2007).

The catalytic activity of kinases is itself frequently regulated by phosphorylation, and they are generally strongly activated by phosphorylation of specific residues within a segment of the kinase domain known as the activation loop (Adams, 2003). Indeed, the small initial RIPK1 upshift observed in response to the various stimuli examined is consistent with phosphorylation at a single site, and potentially reflects the activation loop phosphorylation site as for Thr197 of PKA as seen in Cauthron *et al.* (Cauthron et al., 1998). This observation is potentially relevant to cardiomyocyte death in response to pathophysiological stimuli as a wide range of studies implicate RIPK1 kinase activity in induction of necroptotic cell death, a response inhibited by pharmacological inhibition of RIPK1 or expression of kinase-inactive RIPK1 mutants (Degterev et al., 2008; Berger et al., 2014; Newton et al., 2014; Newton et al., 2016a).

#### 4.4.3 Significance of observations for cardiomyocyte death

The response of RIPK1 in cardiomyocytes to various H<sub>2</sub>O<sub>2</sub> concentrations supports the notion that RIPK1 moderates cardiomyocyte death. RIPK1 mobility was largely unaffected by non-toxic and sub-apoptotic doses of H<sub>2</sub>O<sub>2</sub> (0.03 and 0.1 mM, respectively) (Fig. 4.2C) but exhibited reduced mobility in response to concentrations that induce apoptosis and/or necrosis ( $\geq 0.3$  mM) with a maximal response upon exposure to 1 mM H<sub>2</sub>O<sub>2</sub> (Fig. 4.2C). Notably, densitometric analysis of the reduced mobility RIPK1 bands produced “bell-shaped” dose-dependency curves, as observed for a number of other responses induced by H<sub>2</sub>O<sub>2</sub> in cardiomyocytes [e.g. expression of Mdm2 (Pikkarainen et al., 2009), phosphorylation of Ndr2 (Fuller et al., 2008)]. However, since the multiple bands of RIPK1 immunoreactivity are probably due to phosphorylation at multiple sites, it is possible that the modifications have different functions and may, amongst other effects, both promote and inhibit activity, as in other systems. For example, mutation of Ser89 to alanine results in a robust increase in RIPK1 catalytic activity and therefore Ser89 most likely represents an inhibitory phosphorylation site (Mcquade et al., 2013).

Phosphorylations may also affect function independently of changes in RIPK1 catalytic activity and interpretation of the data is further complicated by the observation that in some contexts in non-cardiac systems, increased RIPK1 phosphorylation is associated with sequestration of RIPK1 in pro-survival complex I, preventing RIPK1 from forming pro-apoptotic or pro-necroptotic complexes and thus inhibiting cell death (Dondelinger et al., 2015). Direct comparison of the observations pertaining to H<sub>2</sub>O<sub>2</sub> and RIPK1 described here to those presented in other studies is problematic due to different model systems and approaches. Despite this, a previous study by Wang *et al.* (Wang et al., 2013) employed siRNA-mediated knockdown of RIPK1 (and RIPK3) expression in neonatal mouse cardiomyocytes, conferring a protective effect against necrosis induced by 0.5 mM H<sub>2</sub>O<sub>2</sub>. In these cells, H<sub>2</sub>O<sub>2</sub> also induced an increase in RIPK1 and RIPK3 protein expression. In Wang *et al.*, H<sub>2</sub>O<sub>2</sub> exposure had the greatest effect on RIPK1 protein expression at 12 – 24 h, a later time than examined here, with

a more minor increase at 6 h. There was, however, no observable change in RIPK1 electrophoretic mobility. (Wang et al., 2013). The same research group subsequently reported that RIPK1/3 knockdown protected H9c2 cells against necrosis in response to a 24 h exposure to 0.5 mM H<sub>2</sub>O<sub>2</sub> (Wang et al., 2015), although caution should be exercised in comparing results generated using the H9c2 cardiomyoblast cell line to those employing primary cardiomyocytes, as used in this study.

Having observed regulation of RIPK1 in response to pathophysiological stimuli in isolated neonatal cardiomyocytes, it was important to investigate the effects of stresses on RIPKs in the intact adult heart. Although ischaemia results in extensive cardiomyocyte death and must be reversed to rescue damaged tissue and preserve life, reperfusion *per se* can, paradoxically, result in significant injury to the myocardium and may prove lethal (Hausenloy and Yellon, 2013). Accordingly, it is imperative to develop a deeper understanding of the mechanisms underlying IR injury, with a view to identification of novel therapeutic targets and treatment options.

Here, IR and oxidative stress in the form of H<sub>2</sub>O<sub>2</sub> promoted reduced electrophoretic mobility of both RIPK1 and RIPK3 in samples from perfused adult rat hearts and led to a significant reduction in full-length RIPK1 protein (Fig. 4.3, A and B). The reduction of detected RIPK1 protein may be due to caspase cleavage, a response that suppresses necroptosis in other systems (Van Raam et al., 2013), or to other forms of degradation. It is also possible that IR causes RIPK1 to undergo a conformational change or other modification such that the epitope is masked and cannot be detected by the anti-RIPK1 antibodies used, as observed by Fuller and colleagues in a study of a different kinase, MST3 (Fuller et al., 2012). The reduction in detected RIPK1 appears to contrast with the results presented in Oerlemans *et al.*, (Oerlemans et al., 2012) in which there is an apparent increase in RIPK1 expression following myocardial IR. However, this may be explained by inherent differences between the model systems and protocols employed. Here, zero-flow global ischaemia (20 min) was induced in isolated rat hearts by cessation of perfusion whereas Oerlemans and colleagues subjected

adult mouse hearts to 30 min ischaemia *in vivo* using left coronary artery ligation. Importantly, in this thesis, the hearts were only reperfused for 40 min prior to cessation of the protocol, while Oerlemans and colleagues permitted reperfusion for 24 h. Thus, it is possible that the effects leading to reduced RIPK1 immunoreactivity in Fig. 4.3 are reversed during the significantly longer reperfusion time employed in the Oerlemans study. A further possibility is that the contrasting result is due to the antibodies used to detect the protein. This investigation used an antibody to RIPK1 supplied by Cell Signalling Technology (CST, cat. no. 3493) while Oerlemans and colleagues used an antibody supplied by BD Biosciences (cat. no. 610459). The CST antibody used here is raised to Leu190 in the N-terminal kinase domain of human RIPK1 while BD Bioscience list the respective immunogen as residues 385-650 of human RIPK1. Thus, as discussed above, the discrepant observations may also be due to differential accessibility of the respective epitopes following stimulation (Oerlemans et al., 2012). Future investigations might benefit from using more than one anti-RIPK1 antibody, raised to different epitopes, to further characterise the effects of the stimuli on RIPK1.

In contrast with RIPKs 1 and 3, IR had no effect on the position or intensity of RIPK2 bands (Fig. 4.3, A and B). While related to RIPKs 1 and 3, RIPK2 is not thought to be associated with the necroptotic death pathway (Cho et al., 2009), further suggesting a specific role for RIPK1s and 3 in mediating death responses in the heart. Although both IR and H<sub>2</sub>O<sub>2</sub> promoted reduction of RIPK3 mobility in adult perfused rat hearts, none of the stimuli examined had any effect on the mobility or abundance of RIPK3 in neonatal cardiomyocytes (data not shown). This observation might be explained in part by differences between the sensitivities to the various stimuli examined of adult heart cells compared to cardiomyocytes cultured from neonatal rats. Furthermore, the cellular composition of the two experimental systems differs, as neonatal cell cultures are ~95% cardiomyocytes (Fuller et al., 2015) whereas whole perfused adult hearts are composed of both cardiomyocytes and a heterogeneous population of other non-myocyte cell types, possibly leading to differences in observations between the two systems. It is also possible that any modifications to RIPK3 in neonatal myocytes were

simply not detected by separation with SDS-PAGE, as not all phosphoproteins exhibit differential migration patterns (Peck, 2006).

The data presented in this chapter provide novel insight into the regulation and roles of RIPK1 in the heart in response to pathophysiological stimuli. In addition to responses to TNF $\alpha$ , IR and oxidative stress as observed in other systems, data here demonstrate that cardiac RIPK1 responds to IL1 $\beta$ , an effect yet to be reported elsewhere. Furthermore, preliminary evidence indicates that RIPK1 in cardiomyocytes may be phosphorylated by p38-MAPK $\alpha/\beta$ , a p38-MAPK $\alpha/\beta$ -activated kinase, or RIPK2, in response to IL1 $\beta$ . However, further investigation is necessary to determine if the observed reduction of RIPK1 electrophoretic mobility is indeed caused by phosphorylation and, if so, to identify the sites responsible and their functional implications. Initially, the emphasis will be on phosphorylation sites that potentially regulate RIPK1 kinase activity and on ubiquitinylation sites linked to MAPK activation and cell survival.

**Chapter Five - Generation of adenoviruses for expression of RIPK1 in  
cardiomyocytes**

## 5.1 Introduction

RIPK1 represents a key node in the regulation of a number of signalling pathways that variously promote cell survival, inflammation and cell death through apoptosis or necroptosis (Ofengeim and Yuan, 2013). RIPK1 undergoes numerous post-translational modifications, most notably ubiquitinylation and phosphorylation (see section 1.5.2) (Zhou and Yuan, 2014), and these modifications influence whether the cell survives or dies. The data presented in Chapter Four demonstrate that RIPK1 in cardiomyocytes and hearts exhibits a reduction in electrophoretic mobility in response to diverse pathophysiological stimuli including pro-inflammatory cytokines (TNF $\alpha$  and IL1 $\beta$ ), oxidative stress (exemplified by H<sub>2</sub>O<sub>2</sub>) and IR; and that this is likely to be caused by phosphorylation. To adequately investigate the effects of these stimuli on RIPK1, and to further elucidate the roles of RIPK1 in the heart, it is necessary to establish whether this phenomenon is indeed caused by phosphorylation (or by other post-translational modifications) and to identify the sites at which these modifications occur. Numerous RIPK1 phosphorylation sites have been identified using mass spectrometry (Degterev et al., 2008; Dondelinger et al., 2015) although relatively few (Ser14/15, Ser89, Ser161 and Ser166) have been confirmed using site-specific experimental means such as mutational analysis or specific antibodies (Mcquade et al., 2013; Ofengeim et al., 2015; Newton et al., 2016b).

One strategy to determine if the reduction of RIPK1 mobility observed in Chapter Four is due to phosphorylation is to mutate individual potential phosphorylation sites and assess whether these mutations abolish RIPK1 band shifting in response to the various treatments examined. Furthermore, epitope-tagged wild-type proteins may be immunoprecipitated from treated cells and treated with exogenous phosphatase to assess whether reduced mobility is due to phosphorylation. As cardiomyocytes are terminally differentiated, they are not amenable to genetic manipulation using techniques such as the CRISPR-Cas9 system (Ran et al., 2013) and as a result it is necessary to express mutant proteins exogenously. Cardiomyocytes have low transfection efficiencies (Djurovic et al., 2004), although adenoviruses represent a highly

efficient means of expressing exogenous proteins. This chapter describes the generation of adenoviruses expressing FLAG-tagged wild-type and phosphorylation/ubiquitinylation site mutant RIPK1. The principal aim in this chapter is to use FLAG-tagged RIPK1 constructs to assess whether the effects, detailed in Chapter Four, of the pathophysiological stimuli on RIPK1 are a result of phosphorylation. A further aim is to use mutational analysis to formally identify the RIPK1 activation loop phosphorylation site (ALPS).

## **5.2 Methods**

### **5.2.1 Identification of candidate RIPK1 activation loop phosphorylation and ubiquitinylation sites**

Evolutionarily conserved serine, threonine and lysine residues were identified using protein sequence alignment using the BLAST blastp suite (<https://blast.ncbi.nlm.nih.gov>), in conjunction with the PhosphoSitePlus<sup>®</sup> resource (<http://www.phosphosite.org/>). RIPK1 sequences from human (accession no. NP\_003795.2), rat (accession no. NP\_001100820.1) and mouse (accession no. NP\_033094.3) were aligned.

### **5.2.2 Generation of shuttle vectors expressing FLAG-tagged RIPK1 constructs**

#### **5.2.2.1 Generation of shuttle vectors expressing FLAG-tagged wild-type RIPK1 (FLAG-RIPK1-Shut)**

The shuttle vector expressing FLAG-tagged wild-type RIPK1 (FLAG-RIPK1-Shut) was generated by inserting the DNA sequence encoding mouse RIPK1 between the KpnI and HindIII sites of the FLAG-pShuttle-CMV plasmid. FLAG-pShuttle-CMV plasmids were supplied by Dr. Stephen J. Fuller. The sequence encoding the FLAG-tag (DYKDDDDK) (Fig. 5.1) was inserted between the BglII and NotI sites in the multiple cloning site of the pShuttle-CMV vector (Fig. 5.1). The wild-type mouse RIPK1 sequence (accession no. NM\_009068.3) was amplified

from a cDNA open reading frame clone purchased from Origene (cat. no. MR209813). In order to permit insertion of the construct into the KpnI and HindIII sites of the FLAG-pShuttle-CMV vector (Fig. 5.2), primers were designed to amplify the RIPK1 sequence flanked by the respective restriction sites.

**Forward oligonucleotide sequence:**

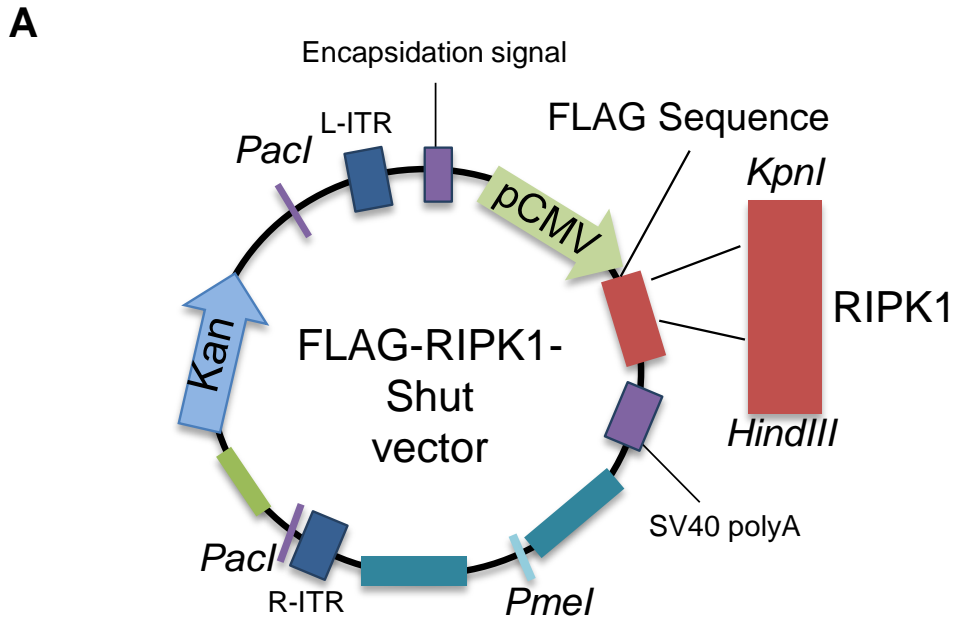
5'-**GATCT**ACC**ATG****GACTACAAAGACGATGACGACAAG**GGTACCGTCGACGC-3';  
*BglII* FLAG sequence

**Reverse oligonucleotide sequence :**

5'-**GGCCGC**GTTCGACGGTACC**CTTGTCGTCATCGTCTTTGTAGTC****CAT**GGTA-3'  
*NotI* FLAG sequence

**Figure 5.1 Construction of the oligonucleotide cassette encoding the FLAG-tag**

The BglII site in forward and NotI site in reverse are highlighted in yellow. Initiation codons are highlighted in green and the sequences encoding the FLAG-tag are underlined and emboldened.



**B**

**FLAG-RIPK1-Shut multiple cloning site region sequence (positions 888 – 1031):**

ShutF sequence (888 – 907) BglIII  
GGTCTATATAAGCAGAGCTGGTTTAGTGAACCGTCAGATCCGCTAG**AGATCTACCATG**

FLAG sequence KpnI RIPK1 sequence  
**GACTACAAAGACGATGACGACAAG****GGTACC**ATGCAACCAGACATGTCC**TTGGAC**...

-----RIPK1 SEQUENCE-----

RIPK1 sequence HindIII  
 ...ATTCGTGCCAGCCAGAGC**TAGAAGCTT**CTAGATAAGATATC...

ShutR sequence 1009 – 1031  
 ...CGATCCACCGGATCTAGATAACTGATCATAATCAGCCATACCAC

**Figure 5.2 Plasmid map of the FLAG-RIPK1-Shut vector**

(A) Cloned full-length wild-type and mutant RIPK1 DNA constructs were ligated into the KpnI and HindIII sites of the FLAG-pShuttle-CMV plasmid. Restriction enzyme sites are italicized. Kan denotes the kanamycin resistance gene. pCMV denotes the cytomegalovirus promoter. R-ITR and L-ITR denote the right- and left- inverted terminal repeats, respectively. (B) Sequence for the FLAG-RIPK1-Shut multiple cloning site region showing the positions of the FLAG and RIPK1 sequences. Positions and sequences of the ShutF and ShutR primers and restriction sites are indicated.

The mouse RIPK1 sequence contains an internal KpnI restriction enzyme site (GGTACC) 564 bp downstream of the initiation codon. To prevent undesired digestion of the construct at this site, a conservative point mutation was introduced during cloning; yielding a site that is not recognized by KpnI. The point mutation was introduced using PCR, using the strategy detailed in (Fig. 5.3) A complementary forward and reverse primer pair was designed to contain the desired mutation (GGTACC→GGAACC) flanked by 15 bases on each side. Initially, two PCR reactions were performed. The first, to produce the 594 bp N-terminal RIPK1 fragment containing the mutated KpnI site, used the RIPK1\_Fwd and KpnI\_Rev primers (see Table 5.1 for details). The second, to produce the 1429 bp C-terminal RIPK1 fragment containing the mutated KpnI site, used the KpnI\_Fwd and RIPK1\_Rev primers (see Table 5.1 for details). The purchased RIPK1 open reading frame clone was used as template in both reactions. Each PCR reaction (50 µl) contained *Pfu* polymerase (1.5 units, 0.5 µl), 10 × *Pfu* reaction buffer (5 µl), dNTP mixture (2 mM of each nucleotide, 5 µl), forward and reverse primers (2 µM, 0.5 µl of each primer), Origene RIPK1 clone (2 µl, 50 ng) and nuclease-free water (36.5 µl). PCR cycling conditions are indicated in (Fig 5.4A).

Following PCR, the 594 bp N-terminal and 1429 bp C-terminal RIPK1 DNA fragments were purified by electrophoresis through a 1% agarose gel as described in Chapter Two section 2.9 followed by spin column purification as described in Chapter Two section 2.10.3. A mixture of the purified N- and C-terminal products from the first two PCR reactions was used as template for a third PCR, to produce the full-length wild-type RIPK1 construct. The reaction (50 µl) consisted of *Pfu* polymerase (1.5 units, 0.5 µl), 10× *Pfu* reaction buffer (5 µl), dNTP mixture (2 mM of each nucleotide, 5 µl), template (2 µl of each product from the first two PCRs) and nuclease free water (34.5 µl). The assembled reactions were transferred to a thermocycler and denatured at 94°C for 5 min, followed by four cycles of 94°C (30 s), 60°C (30 s) and 72°C (5 min) to allow annealing and extension from the overlapping complementary regions of the template products (Fig 5.4B). Following this, the reaction was paused and the flanking RIPK1\_Fwd and RIPK1\_Rev primers were added (2 µM, 0.5 µl of each primer) in order to

produce the full-length RIPK1 sequence, flanked by KpnI and HindIII sites. This was achieved by 42 cycles of 94°C (30 s), 55°C (30 s) and 72°C (5 min) followed by a final extension phase at 72°C (7 min) (Fig 5.4B). Following PCR, the full-length RIPK1 construct was electrophoresed through a 1% agarose gel and then column purified.

The purified full-length RIPK1 construct (35 µl), flanked by KpnI and HindIII sites, was cut in a double digest reaction (50 µl) containing 10x CutSmart® Buffer (5 µl), KpnI (10 units, 1 µl), HindIII (10 units, 1 µl) and nuclease-free water (8 µl). The reactions were incubated for 2 h at 37°C. Following digestion, the cut DNA was column purified as described and eluted in 35 µl elution buffer. The purified KpnI/HindIII-digested RIPK1 DNA was then ligated into the KpnI and HindIII sites of the FLAG-pShuttle-CMV vector MCS to produce the wild-type FLAG-RIPK1-Shut plasmid (See Fig. 5.2 for plasmid map). Prior to ligation, the FLAG-pShuttle-CMV vector was subjected to double digestion (37°C, 16 h) with KpnI and HindIII as detailed for the RIPK1 construct. The ligation reaction (20 µl) contained the purified digested RIPK1 DNA (10 µl), FLAG-pShuttle-CMV plasmid (50 ng, 0.5 µl), 5x T4 ligase buffer (4 µl), T4 DNA ligase (0.5 units, 0.5 µl) and nuclease-water (4 µl). Ligations were carried out at 14°C for 1 h followed by 26°C for 1 h.

The ligated FLAG-RIPK1-Shut plasmid was subsequently amplified by heat-shock transformation into ultracompetent XL10-Gold *E. coli* cells, as described in Chapter Two, section 2.10.1. The cells were spread onto LB agar plates containing kanamycin (50 µg/ml) and incubated overnight at 37°C. Resulting bacterial colonies were PCR screened using the RIPK1\_Fwd and KpnI\_Rev primers as described in Chapter Two, section 2.10.2 to verify presence of the FLAG-RIPK1-Shut plasmid, with an expected product size of 594 bp. Positive colonies (i.e. those in which amplification of the expected 594 bp product had taken place) were inoculated into 5 ml LB containing kanamycin (50 µg/ml) and incubated in a rotary shaker overnight (37°C, 250 rpm) and the FLAG-RIPK1-Shut plasmids isolated using the alkaline lysis minipreparation method, as described in Chapter Two, section 2.10.4. Plasmids were sequenced as described in Chapter Two, section 2.10.6 to verify the presence of the intended

mutation and to ensure no undesired mutations were incorporate during PCR. Sequence verified plasmids were subsequently amplified as described and isolated using the alkaline lysis maxipreparation method, as described in Chapter Two section 2.10.5. The plasmids were stored at -20°C.

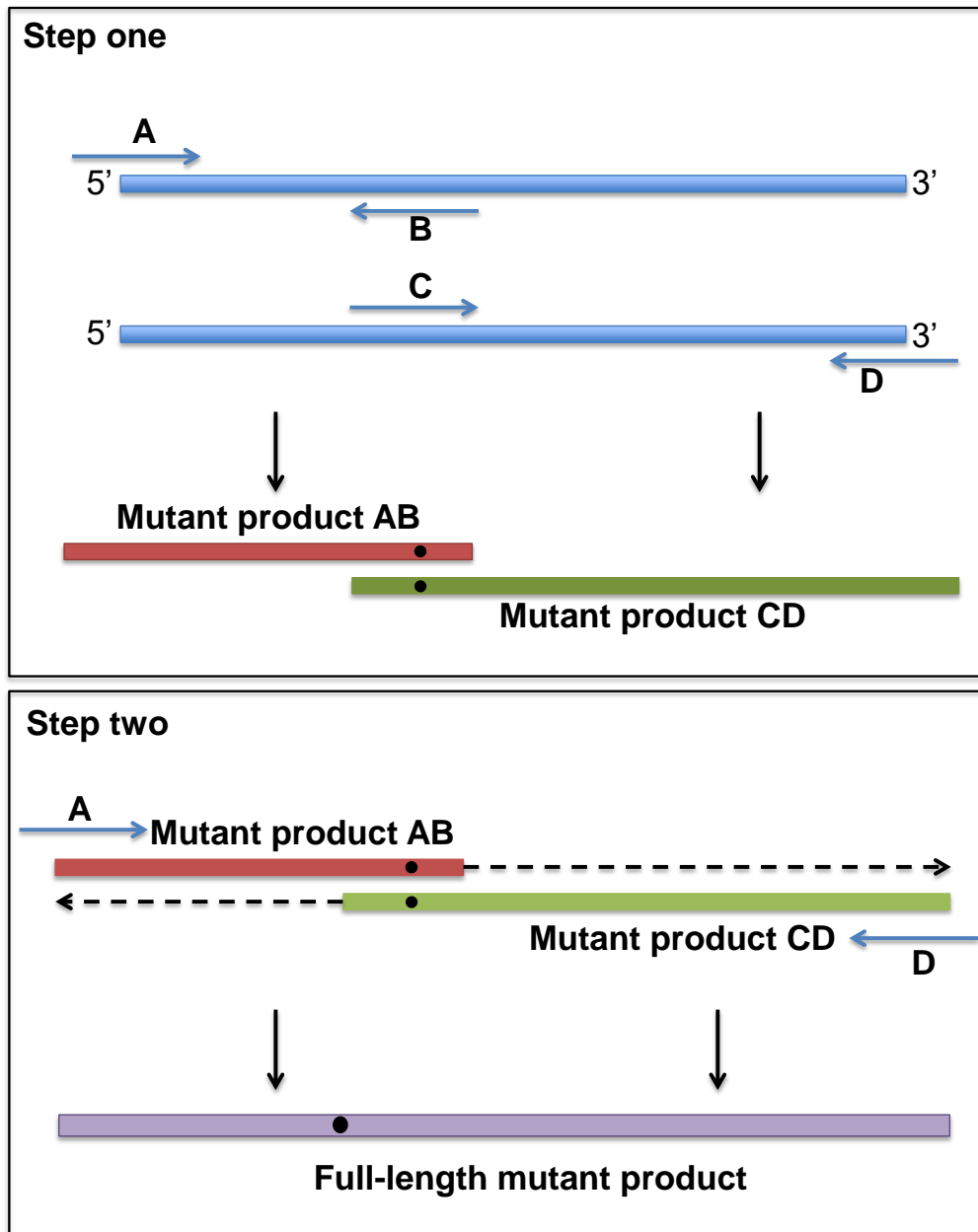


**Figure 5.3 General strategy for introducing mutations using PCR**

DNA constructs containing mutations were produced in two steps using PCR. Step one consisted of two reactions to produce fragments containing the desired mutations within a 23 – 31 bp overlapping region; which were then used as template in the second PCR step to produce the full-length mutant constructs. In the first PCR step, the forward flanking primer (A) and reverse mutagenic primer (B) were used to produce the N-terminal mutant fragment (Product AB). The forward mutagenic primer (C) and reverse flanking primer (D) were used to produce the C-terminal mutant fragment (Product CD). Primers A and D were designed to introduce N-terminal KpnI and C-terminal HindIII restriction sites. In step two, a mixture of the mutant products AB and CD was used as template and the PCR reaction was initiated in the absence of primers to allow annealing and extension at the complementary overlapping region. The flanking primers (primers A and D) were then added and the reaction continued to amplify the full-length mutant product.

### **5.2.2.2 Generation of shuttle vectors expressing FLAG-tagged S161A mutant RIPK1 (FLAG-S161A-Shut)**

Site-directed mutagenesis was used to mutate Ser161 of RIPK1 to an unphosphorylatable alanine residue, using the same strategy as for the mutation of the internal KpnI site for the FLAG-RIPK1-Shut plasmid. The strategy is detailed in Fig 5.3. Two separate reactions were performed to produce the N- and C- terminal fragments, each containing the desired point mutation (**TCC**→**GCC**); using the wild-type FLAG-RIPK1-Shut plasmid (described in section 5.2.2.1) as template. A further reaction was then conducted to produce full-length RIPK1 constructs carrying the desired S161A mutation, using a mixture of products from the first two reactions as template. Using the FLAG-RIPK1-Shut plasmid as template in the first two reactions allowed production of mutant RIPK1 constructs flanked by the required N-terminal KpnI and C-terminal HindIII sites.

For the 582 bp N-terminal fragment of the S161A mutant, the ShutF and mutagenic S161A\_Rev primer were used while for the 1567 bp C-terminal S161A mutant fragment, the mutagenic S161A\_Fwd primer and ShutR primers were used. Details of primers are found in Table 5.1. The primers (2 μM, 0.5 μl each primer) were used in 50 μl *Pfu* reactions, as described in section 5.2.2.1. The FLAG-RIPK1-Shut plasmid (50 ng) was used as template for both reactions. PCR cycling conditions are indicated in Fig. 5.4C.

The S161A N- and C-terminal products electrophoresed on a 1% agarose gel as described in Chapter Two, section 2.9 and column purified as described in Chapter Two section 2.10.3. A third PCR reaction was established to produce the full-length S161A construct, as described for the wild-type construct in section 5.2.2.1, using the purified S161A N- and C-terminal fragments (2 ul of each) as template. This reaction used the flanking ShutF and ShutR primers, using PCR cycling conditions as indicated in Fig. 5B. The resulting PCR products were run on a 1% agarose gel and column purified. The purified products were digested with KpnI and HindIII and ligated into the respective sites in the pShuttle-CMV multiple cloning site as described in section 5.2.2.1 to produce the FLAG-S161A-Shut plasmid. The FLAG-S161A-

Shut plasmids were heat-shock transformed into XL10-Gold cells as described and resulting colonies PCR screened as described in Chapter Two, section 2.10.2 using the ShutF and S166A\_Rev primers, with an expected product size of 597 bp. Positive colonies were inoculated into 5 ml LB containing kanamycin and plasmids isolated using the alkaline lysis minipreparation method, as described. Samples of the purified plasmids were sequenced as described in Chapter Two, section 2.10.6 using the RIPK1\_Fwd primer. Sequence verified plasmids were amplified as described and isolated using the alkaline lysis maxipreparation method, as described in Chapter Two section 2.10.5. The plasmids were stored at -20°C.

### **5.2.2.3 Generation of shuttle vectors expressing FLAG-tagged S166A mutant RIPK1 (FLAG-S166A-Shut)**

Site-directed mutagenesis was used to mutate Ser166 of RIPK1 to an unphosphorylatable alanine residue (**AGC**→**GCC**), using the strategy detailed in Fig 5.3. Two separate reactions were performed to produce the N- and C- terminal fragments each containing the desired point mutation; using the wild-type FLAG-RIPK1-Shut plasmid (described in section 5.2.2.1) as template.

For the 597 bp N-terminal fragment of the S166A mutant, the ShutF and mutagenic S166A\_Rev primer were used while for the 1552 bp C-terminal S166A mutant fragment, the mutagenic S166A\_Fwd primer and ShutR primers were used. Details of primers are found in Table 5.1. The primers (2 µM, 0.5 µl each primer) were used in 50 µl *Pfu* reactions, as described in section 5.2.2.1. The FLAG-RIPK1-Shut plasmid (50 ng) was used as template for both reactions. PCR cycling conditions are indicated in Fig. 5.4C.

The S166A N- and C-terminal products electrophoresed on a 1% agarose gel as described in Chapter Two, section 2.9 and column purified as described in Chapter Two section 2.10.3. A third PCR reaction was established to produce the full-length S166A construct, as described for the wild-type construct in section 5.2.2.1, using the purified S166A N- and C-terminal

fragments (2 ul of each) as template. This reaction used the flanking ShutF and ShutR primers, using PCR cycling conditions as indicated in Fig. 5.4B. The resulting PCR products were run on a 1% agarose gel and column purified. The purified products were digested with KpnI and HindIII and ligated into the respective sites in the pShuttle-CMV multiple cloning site as described in section 5.2.2.1 to produce the FLAG-S166A-Shut plasmid. The FLAG-S166A-Shut plasmids were heat-shock transformed into XL10-Gold cells as described and resulting colonies PCR screened as described in Chapter Two, section 2.10.2 using the ShutF and S166A\_Rev primers, with an expected product size of 597 bp. Positive colonies were inoculated into 5 ml LB containing kanamycin and plasmids isolated using the alkaline lysis minipreparation method, as described. Samples of the purified plasmids were sequenced as described in Chapter Two, section 2.10.6 using the RIPK1\_Fwd primer. Sequence verified plasmids were amplified as described and isolated using the alkaline lysis maxipreparation method, as described in Chapter Two section 2.10.5. The plasmids were stored at -20°C.

#### **5.2.2.4 Generation of shuttle vectors expressing FLAG-tagged T183A mutant RIPK1 (FLAG-T183A-Shut)**

Site-directed mutagenesis was used to mutate Thr183 of RIPK1 to an unphosphorylatable alanine residue (**ACT**→**GCT**), using the strategy detailed in Fig 5.3. Two separate reactions were performed to produce the N- and C- terminal fragments each containing the desired point mutation; using the wild-type FLAG-RIPK1-Shut plasmid (described in section 5.2.2.1) as template.

For the 648 bp N-terminal fragment of the T183A mutant, the ShutF and mutagenic T183A\_Rev primer were used whilst for the 1501 bp C-terminal T183A mutant fragment, the mutagenic T183A\_Fwd primer and ShutR primers were used. Details of primers are found in Table 5.1. The primers (2 µM, 0.5 µl each primer) were used in 50 µl *Pfu* reactions, as

described in section 5.2.2.1. The FLAG-RIPK1-Shut plasmid (50 ng) was used as template for both reactions. PCR cycling conditions are indicated in Fig. 5.4C.

The T183A N- and C-terminal products electrophoresed on a 1% agarose gel as described in Chapter Two, section 2.9 and column purified as described in Chapter Two section 2.10.3. A third PCR reaction was established to produce the full-length T183A construct, as described for the wild-type construct in section 5.2.2.1, using the purified T183A N- and C-terminal fragments (2 ul of each) as template. This reaction used the flanking ShutF and ShutR primers, using PCR cycling conditions as indicated in Fig. 5.4B. The resulting PCR products were run on a 1% agarose gel and column purified. The purified products were digested with KpnI and HindIII and ligated into the respective sites in the pShuttle-CMV multiple cloning site as described in section 5.2.2.1 to produce the FLAG-T183A-Shut plasmid. The FLAG-T183A-Shut plasmids were heat-shock transformed into XL10-Gold cells as described and resulting colonies PCR screened as described in Chapter Two, section 2.10.2 using the ShutF and S166A\_Rev primers, with an expected product size of 597 bp. Positive colonies were inoculated into 5 ml LB containing kanamycin and plasmids isolated using the minipreparation method, as described. Samples of the purified plasmids were sequenced as described in Chapter Two, section 2.10.6 using the RIPK1\_Fwd primer. Sequence verified plasmids were amplified as described and isolated using the alkaline lysis maxipreparation method, as described in Chapter Two section 2.10.5. The plasmids were stored at -20°C.

#### **5.2.2.5 Generation of shuttle vectors expressing FLAG-tagged K376R mutant RIPK1 (FLAG-K376R-Shut)**

Site-directed mutagenesis was used to mutate Lys376 of RIPK1 to an arginine residue (AAG→AGG), using the strategy detailed in Fig 5.3. Mutation of lysine to arginine prevents ubiquitinylation at that site (Xu and Jaffrey, 2013). Arginine is a particularly suitable substitute, as, like lysine, it carries a positive charge at physiological pH and has a relatively large side

chain, thus diminishing the likelihood of destabilising effects of the mutation on protein structure and conformation. Two separate reactions were performed to produce the N- and C- terminal fragments each containing the desired point mutation; using the wild-type FLAG-RIPK1-Shut plasmid (described in section 5.2.2.1) as template.

For the 1225 bp N-terminal fragment of the K376R mutant, the ShutF and mutagenic K376R\_Rev primer were used whilst for the 920 bp C-terminal K376R mutant fragment, the mutagenic K376R\_Fwd primer and ShutR primers were used. Details of primers are found in Table 5.1. The primers (2  $\mu$ M, 0.5  $\mu$ l each primer) were used in 50  $\mu$ l *Pfu* reactions, as described in section 5.2.2.1. The FLAG-RIPK1-Shut plasmid (50 ng) was used as template for both reactions. PCR cycling conditions are indicated in Fig. 5.4C.

The K376R N- and C-terminal products electrophoresed on a 1% agarose gel as described in Chapter Two, section 2.9 and column purified as described in Chapter Two section 2.10.3. A third PCR reaction was established to produce the full-length K376R construct, as described for the wild-type construct in section 5.2.2.1, using the purified K376R N- and C-terminal fragments (2  $\mu$ l of each) as template. This reaction used the flanking ShutF and ShutR primers, using PCR cycling conditions as indicated in Fig. 5.4B. The resulting PCR products were run on a 1% agarose gel and column purified. The purified products were digested with KpnI and HindIII and ligated into the respective sites in the pShuttle-CMV multiple cloning site as described in section 5.2.2.1 to produce the FLAG-K376R-Shut plasmid. The ligated FLAG-K376R-Shut plasmids were heat-shock transformed into XL10-Gold cells as described and resulting colonies PCR screened as described in Chapter Two, section 2.10.2 using the K376R\_Fwd and ShutR primers, with an expected product size of 920 bp. Positive colonies were inoculated into 5 ml LB containing kanamycin and plasmids isolated using the alkaline lysis minipreparation method, as described. Samples of the purified plasmids were sequenced as described in Chapter Two, section 2.10.6 using the T183A\_Fwd primer. Sequence verified plasmids were amplified as described and isolated using the alkaline lysis maxipreparation method, as described in Chapter Two section 2.10.5. The plasmids were stored at -20°C.

**Table 5.1 Primers used in generation of wild-type and mutant FLAG-tagged RIPK1 constructs**

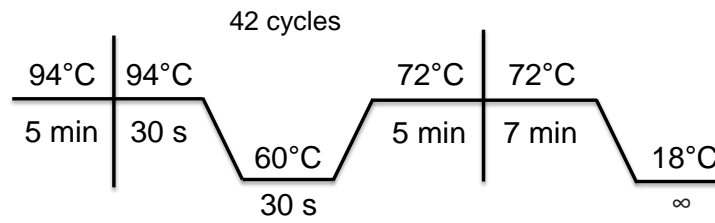
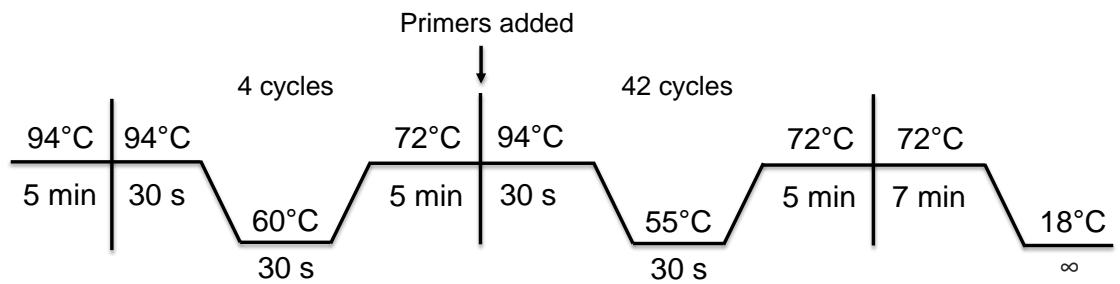
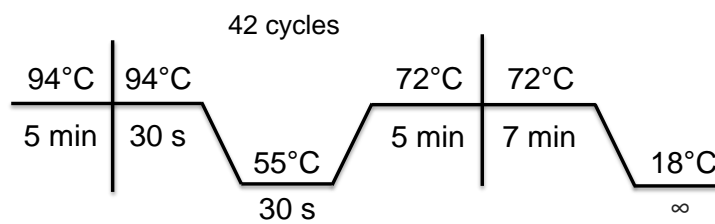
(A) Sequences of primers used in generation of wild-type and mutant FLAG-tagged RIPK1 constructs. Restriction sites are emboldened and italicised. Codons containing mutated bases are emboldened and the mutated bases highlighted in red text. Full mouse RIPK1 DNA and protein sequences with positions of mutations are found in Appendices III and IV, respectively. (B) Details of primer pairs used to generate wild-type and mutant RIPK1 fragments and full-length constructs.

**A**

Primer	Sequence (5' – 3')	Length (bp)	Tm (°C)
RIPK1_Fwd	GACAAG <b>GGTACC</b> ATGCAACCAGACATGTCCTTGGAC	36	67.9
RIPK1_Rev	ATCTAG <b>AAGCTT</b> CTAGCTCTGGCTGGCAGCAATCA	35	65.6
KpnI_Fwd	GAAGAACAATGGT <b>GG</b> AACCCTTTACTACATG	31	60.4
KpnI_Rev	CATGTAGTAAAGGG <b>TCC</b> ACCATTGTTCTTC	31	60.4
S161A_Fwd	CTTGGTGTGGCT <b>GC</b> CTTTAAGACATGG	27	61.3
S161A_Rev	CCATGTCTTAAAG <b>GC</b> AGCCACACCAAG	27	61.3
S166A_Fwd	TTTAAGACATGG <b>CC</b> AAACTGACTAAG	27	56.7
S166A_Rev	CTTAGTCAGTTT <b>GC</b> CCATGTCTTAAA	27	56.7
T183A_Fwd	GTGAGCAGCACCC <b>GCT</b> AAGAAGAACAAT	27	59.7
T183A_Rev	ATTGTTCTTCTT <b>AGC</b> GGTGCTGCTCAC	27	59.7
K376R_Fwd	TGTGCAGGCT <b>AGG</b> CTGCAAGAGG	23	60.6
K376R_Rev	CCTCTTGCAG <b>CT</b> AGCCTGCACA	23	60.6
ShutF	GGTCTATATAAGCAGAGCTG	20	55.3
ShutR	GTGGTATGGCTGATTATGATCAG	23	58.9

**B**

Construct	N-terminal fragment		C-terminal fragment		Full-length construct	
	Forward primer	Reverse primer	Forward primer	Reverse primer	Forward primer	Reverse primer
<b>RIPK1</b>	RIPK1_Fwd	KpnI_Rev	KpnI_Fwd	RIPK1_Rev	RIPK1_Fwd	RIPK1_Rev
<b>S161A</b>	ShutF	S161A_Rev	S161A_Fwd	ShutR	ShutF	ShutR
<b>S166A</b>	ShutF	S166A_Rev	S166A_Fwd	ShutR	ShutF	ShutR
<b>T183A</b>	ShutF	T183A_Rev	T183A_Fwd	ShutR	ShutF	ShutR
<b>K376R</b>	ShutF	K376R_Rev	K376R_Fwd	ShutR	ShutF	ShutR

**A****B****C**

**Figure 5.4 PCR conditions for generation of wild-type and mutant RIPK1 constructs**

PCR conditions for (A) amplification of wild-type RIPK1 N- and C-terminal fragments, (B) generation of full-length wild-type and mutant constructs and (C) generation of S161A, S166A, T183A and K376R mutant RIPK1 N- and C-terminal fragments.

### 5.2.3 Generation of adenoviruses expressing FLAG-tagged RIPK1 constructs

Shuttle vector plasmids, generated as described in section 5.2.2, were used to produce adenoviruses expressing wild-type and S161A, S166A, T183A and K376R mutant RIPK1 constructs. To produce the recombinant adenoviral plasmids, the FLAG-RIPK1-Shut, FLAG-S161A-Shut, FLAG-S166A-Shut, FLAG-T183A-Shut and FLAG-K376R-Shut plasmids were linearised by digestion with PmeI and transformed into BJ5183-AD-1 *E. coli* as described in Chapter Two, section 2.10.7.1, to undergo homologous recombination with the pAdeasy-1 plasmid.

The transformed BJ5183-AD-1 cells were spread onto warm LB agar containing kanamycin (50 µg/µl) and grown overnight at 37°C. Resulting colonies were PCR screened for the presence of recombinant adenoviral plasmids as described in Chapter Two, section 2.10.2 using the AdV\_184F/AdV\_184R and AdV\_300F/AdV\_300R primer pairs (details of primers are found in Chapter Two, Table 2.3. The AdV\_184F/AdV\_184R primer pair is designed to span a sequence common to both the pShuttle-CMV and pAdeasy1 plasmids producing a product of 184 bp. The second primer pair, AdV\_300F/AdV\_300R spans a region that is present in the pShuttle-CMV plasmid, producing a 300 bp product, but is absent in the pAdeasy-1 plasmid if homologous recombination has occurred. Thus, PCR using these primer pairs will lead to a single 184 bp product if homologous recombination has occurred and the respective recombinant RIPK1 constructs are present. Conversely, production of two products, of sizes 184 and 300 bp, indicates presence of the shuttle vector construct and that recombination was unsuccessful. Colonies positive for the recombinant adenoviral plasmids were inoculated into LB and plasmids isolated using the alkaline lysis minipreparation method as described in Chapter Two, section 2.10.4. Purified plasmids (0.1 µg) were amplified by heat shock transformation into XL10-Gold cells and isolated using the alkaline lysis maxipreparation method as described in Chapter Two, sections 2.10.1 and 2.10.5. The recombinant adenoviral plasmids were linearised by digestion with PacI and transfected into HEK 293 cells for

production of adenoviruses, which were then propagated as described in Chapter Two, section 2.10.8.

#### **5.2.4 Transfection of HEK 293 cell cultures**

For expression of FLAG-tagged RIPK1 proteins using shuttle vectors, plasmids were transfected into HEK 293 cells using jetPRIME<sup>®</sup> transfection reagent. HEK 293 cells were cultured in 60 mm dishes in HEK 293 growth medium [DMEM containing 10% FCS (v/v), 1% (v/v) glutamine and 50 units/ml penicillin and streptomycin] and grown to confluence. The shuttle vector plasmid (1 – 5 µg, as indicated) was gently mixed into 100 – 200 µl jetPRIME<sup>®</sup> buffer followed by addition of jetPRIME<sup>®</sup> reagent (2 – 10 µl). The mixture was vortex mixed (10 s) followed by incubation at room temperature (20°C, 10 min). The mixture was then added dropwise to the HEK 293 cultures with gentle rocking. The transfected cultures were incubated to permit expression of proteins (48 h, 37°C, 5% CO<sub>2</sub>). Serum-containing medium was withdrawn 24 h prior to experimentation and replaced with HEK 293 maintenance medium [DMEM containing 1% (v/v) glutamine and 50 units/ml penicillin and streptomycin].

#### **5.2.5 Infection of cardiomyocytes with adenoviruses**

Cultures of neonatal rat cardiomyocytes were prepared as described in Chapter Two section 2.3.1. Cardiomyocytes were infected with stocks of adenoviruses expressing FLAG-tagged RIPK1 proteins (10 – 50 µl) at the time of plating and the infected cultures incubated to permit expression of proteins (18 – 48 h, 37°C, 5% CO<sub>2</sub>). Serum-containing medium was withdrawn 24 h prior to experimentation and replaced with maintenance medium [(DMEM)/Medium 199 4:1 (v/v), 100 units/ml penicillin and streptomycin].

### **5.2.6 Immunoprecipitations**

Immunoprecipitation of FLAG-tagged RIPK1 proteins was performed as described in Chapter Two, section 2.6. Cardiomyocytes or HEK 293 cells were treated as indicated and washed twice with ice-cold 1× PBS. Cells were extracted by scraping into 150 µl ice-cold immunoprecipitation buffer. Lysates were vortex mixed and extracted on ice (10 min) followed by centrifugation (5 min, 10000×g, 4°C). A portion (30 µl) of the lysates was boiled with 2× SDS-PAGE sample buffer (5 min) for immunoblotting to assess protein input. A sample of supernatant (5 µl) was also retained for protein quantification as described in Chapter Two, section 2.5.3.

For immunoprecipitations, 100 µl total cell lysate was removed to a clean pre-chilled tube containing EZview™ red anti-FLAG M2 affinity gel beads (20 µl of a 1:1 slurry in immunoprecipitation buffer) and immunoprecipitations performed on a rotating mixer (18 h, 4°C). Following immunoprecipitation, the samples were centrifuged (5 min, 10000×g, 4°C) and the supernatants retained and boiled with 2× SDS-PAGE sample buffer (5 min). The pelleted anti-FLAG beads were washed with immunoprecipitation buffer (3×, 0.7 ml per wash) and the final pellets boiled with 2× SDS-PAGE sample buffer (5 min). Samples were stored at -20°C.

## **5.3 Results**

### **5.3.1 Identification of candidate RIPK1 activation loop phosphorylation sites and ubiquitylation sites**

Previous investigations indicate that phosphorylation is a key regulator of RIPK1 signalling, and that RIPK1 kinase activity is essential for formation of the necrosome (Degterev et al., 2008; Cho et al., 2009; Mcquade et al., 2013). The catalytic activity of many kinases is strongly activated by phosphorylation of key residues within a region known as the activation loop (Adams, 2003), although the activation loop phosphorylation site (ALPS) for RIPK1 has yet to be formally identified. To identify candidate ALPSs, protein sequences from human (accession

no. NP\_003795.2), rat (accession no. NP\_001100820.1) and mouse (accession no. NP\_033094.3) RIPK1 were aligned to identify evolutionarily conserved phosphorylatable residues in the kinase activation loop. Three such residues were wholly conserved from human to mouse and rat: Ser161, Ser166 and Thr182 (Thr182 refers to the human sequence, the equivalent residue is Thr183 in mouse and rat) (Fig. 5.5, A and C). Other potentially phosphorylatable residues were conserved in mouse and rat but not in human (i.e. Ser169, Ser180/181) and therefore are unlikely to play important roles in regulation of RIPK1 kinase activity. Although Ser161 and Ser166 are established phosphorylation sites (McQuade et al., 2013; Ofengeim et al., 2015), there appears to be no reference to Thr183 in the literature or in information curated by the PhosphositePlus® resource. Sequence alignment also confirmed that Lys377, a site required for IKK, NF $\kappa$ B and MAPK activation by TNF $\alpha$  in non-cardiac cells (associated with cytoprotection) (Ea et al., 2006; Duprez et al., 2012), is conserved in both rat (Lys375) and mouse (Lys376) (Fig. 5.5, B and C).

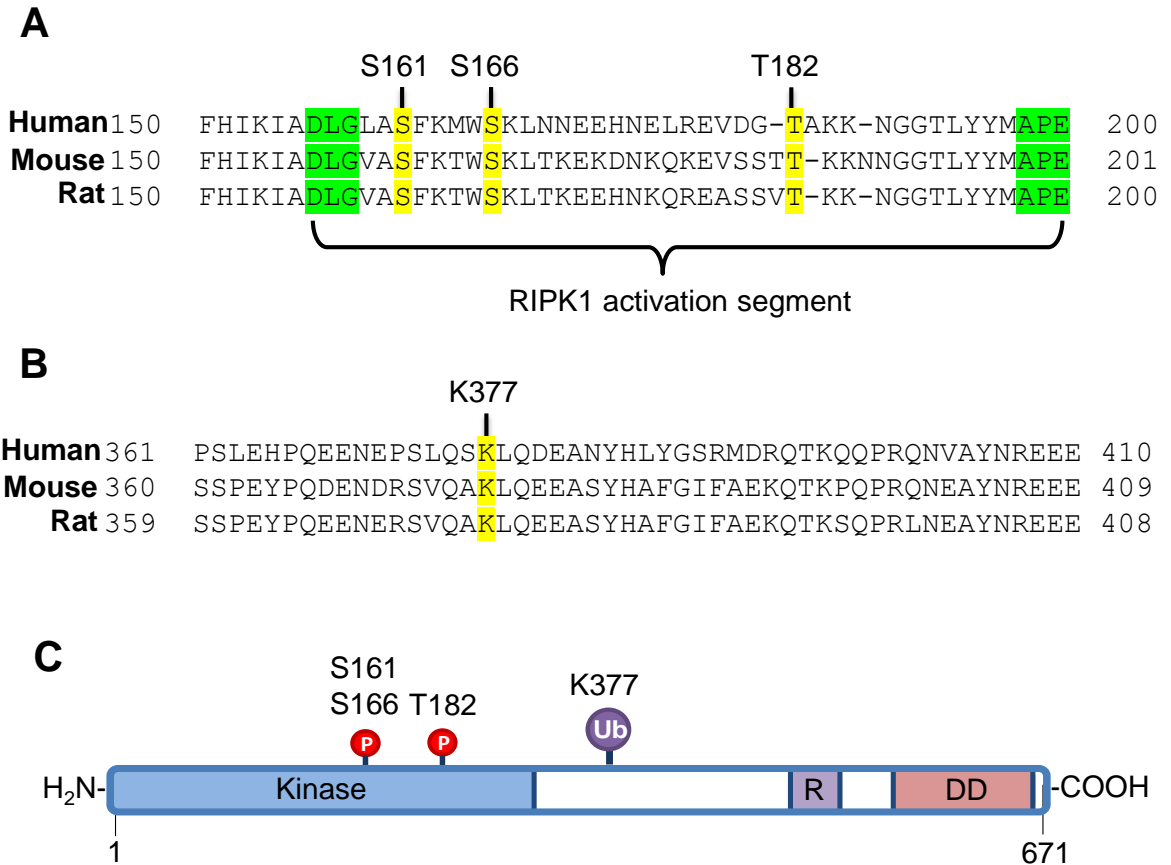


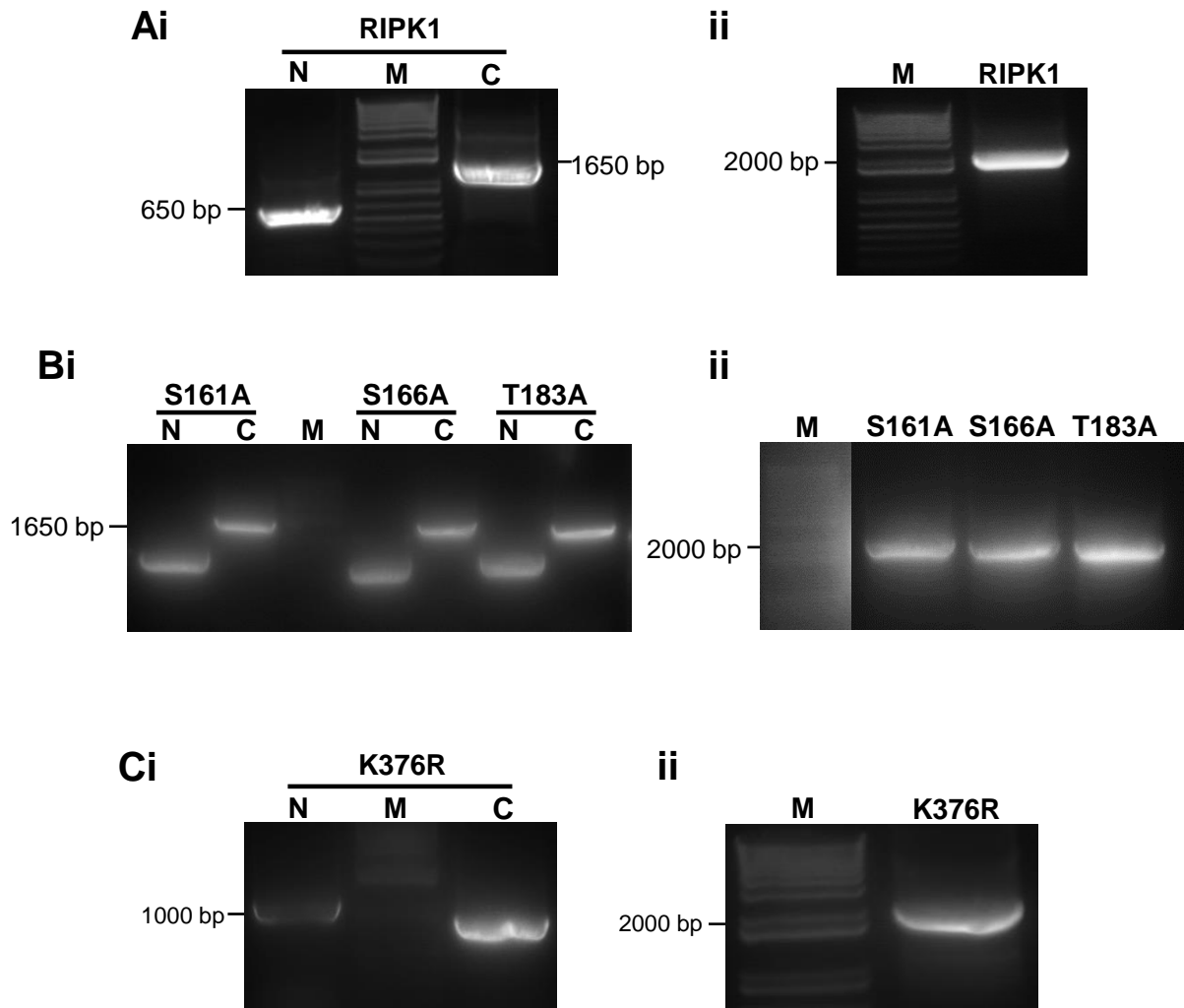
**Figure 5.5 Identification of conserved RIPK1 phosphorylation and ubiquitinylation sites**

Protein sequences for human, rat and mouse RIPK1 were aligned using blastp. **(A)** Identification of conserved phosphorylatable residues. Essential kinase subdomain VIII motifs are highlighted in green and conserved serine and threonine residues in the activation loop are highlighted in yellow. **(B)** Conserved lysine residue in the RIPK1 intermediate domain. **(C)** Schematic of the RIPK1 domain structure. Positions of the identified conserved residues are indicated. Residue numbers are for human RIPK1. P denotes a potentially phosphorylatable site and Ub denotes a ubiquitinylatable lysine residue. R denotes the RIP-homotypic interaction motif. DD denotes the death domain.

### **5.3.2 Generation of shuttle vectors expressing FLAG-tagged wild-type and mutant RIPK1**

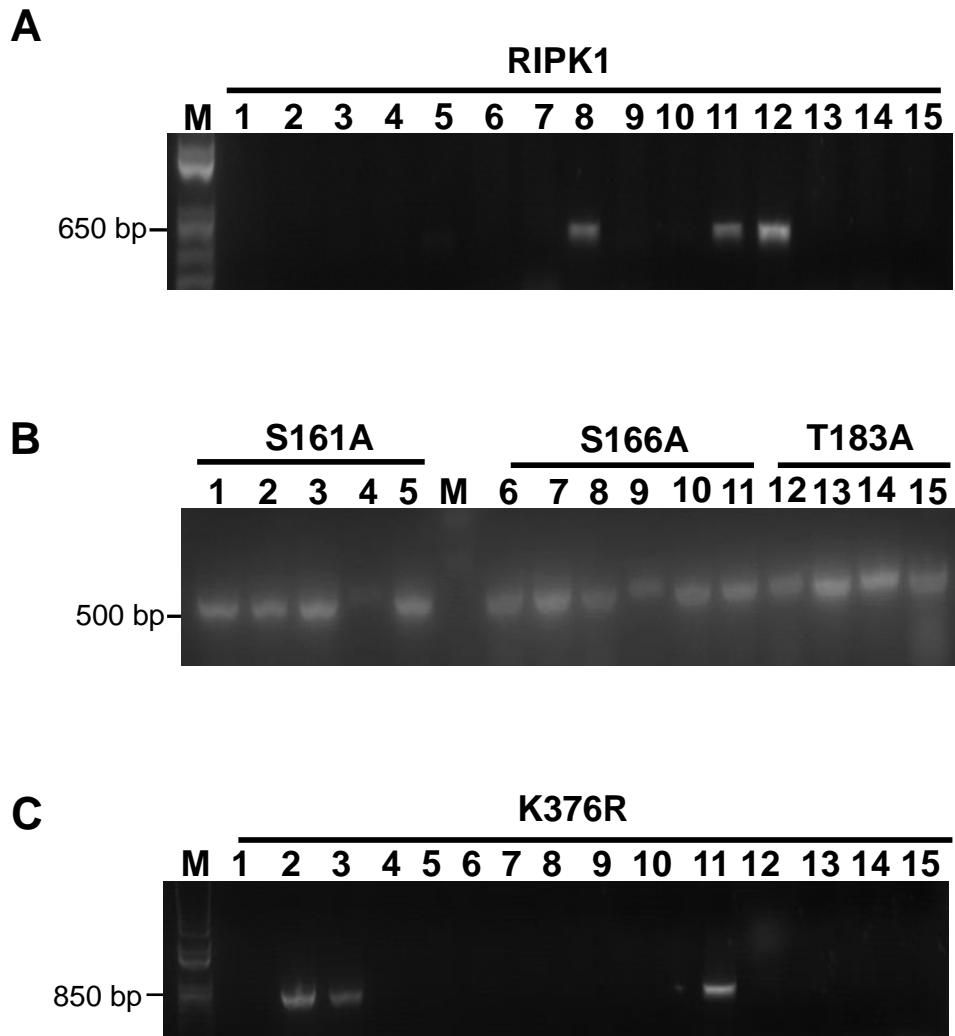
Using protein sequence alignment, Ser161, Ser166 and Thr183 were identified as potential ALPSs, and Lys376 was identified as a ubiquitylation site of interest. To facilitate investigation of the importance of these sites in cardiomyocytes, and to establish whether these sites contribute to the reduced RIPK1 mobility in response to pathophysiological stimuli described in Chapter Four, shuttle vector plasmids expressing FLAG-tagged mouse wild-type RIPK1 (FLAG-RIPK1-Shut) and mutant RIPK1 (FLAG-S161A-Shut, FLAG-S166A-Shut, FLAG-T183A-Shut and FLAG-K376R-Shut) were produced as described in section 5.2.2. The DNA constructs encoding wild-type and mutant RIPK1 were generated using the PCR strategy described in Fig. 5.3 and specific primers, as detailed in Table 5.1. Agarose gel electrophoresis of the resulting PCR products confirmed successful amplification of the N- and C-terminal fragments (Fig. 5.6, Ai, Bi and Ci) and successful generation of the full-length constructs using the N- and C-terminal fragments as template (Fig. 5.6. Aii, Bii and Cii).

The full-length constructs were digested with KpnI and HindIII and ligated into the respective restriction sites of the FLAG-pShuttle-CMV plasmid. The shuttle vectors expressing the FLAG-tagged RIPK1 constructs were then transformed into XL10-Gold *E. coli* and resulting colonies PCR screened to confirm the presence of the RIPK1 constructs (Fig. 5.7). The shuttle vector plasmids were subsequently amplified and the presence of the intended mutations verified by sequencing (Fig. 5.8).



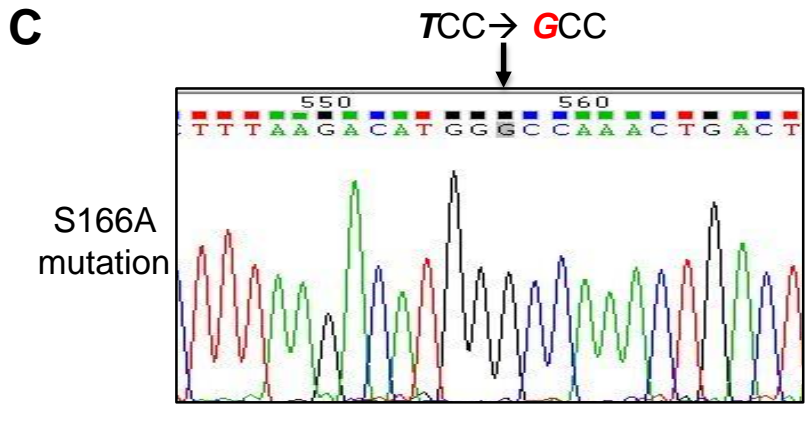
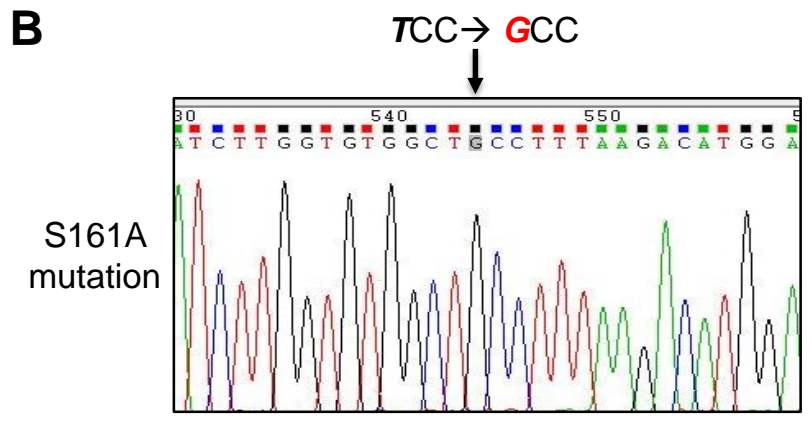
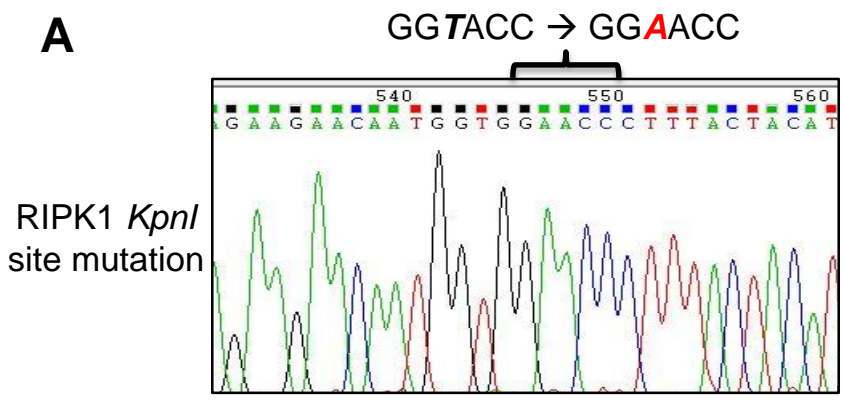
**Figure 5.6 Generation of the wild-type and mutant RIPK1 DNA constructs**

Agarose gel (1%) electrophoresis of RIPK1 DNA constructs. **(Ai)** Wild-type RIPK1 was amplified from an open reading frame clone as a 594 bp N-terminal fragment (N) using the RIPK1\_Fwd and KpnI\_Rev primers and a 1429 bp C-terminal fragment (C) using the KpnI\_Fwd and RIPK1\_Rev primers. **(Aii)** The full-length 2023 bp construct was produced using a mixture of the N- and C-terminal products as template using the RIPK1\_Fwd and RIPK1\_Rev primers. **(Bi)** S161A, S166A and T183A N-terminal fragments were produced using the ShutF primer and the respective reverse mutagenic primers. C-terminal fragments were produced using the respective forward mutagenic primers and the ShutR primer. **(Bii)** full-length S161A, S166A and T183A constructs were produced using the ShutR and ShutF primers and a mixture of the respective N- and C-terminal products as template. **(Ci)** The 1225 bp K376R N-terminal fragment was produced using the ShutF and K376R\_Rev primers and the 920 bp C-terminal fragment used the K376R\_Fwd and ShutR primers. **(Cii)** The full-length K376R construct was produced using the ShutF and ShutR primers and a mixture of the N- and C-terminal products as template. M denotes the 1 kb Plus DNA Ladder marker. Full details of primers used are found in Table 5.1.



**Figure 5.7 Colony screening for shuttle vectors expressing FLAG-tagged wild-type and mutant RIPK1 constructs**

Full-length wild-type (RIPK1) and mutant (S161A, S166A, T183A and K376R) constructs were digested with KpnI/HindIII, ligated into the FLAG-pShuttle-CMV plasmid and amplified in XL10-Gold *E. coli*. Transformed bacteria were spread on kanamycin plates and resulting colonies PCR screened for the presence of the RIPK1 plasmids. Products were electrophoresed on 1% agarose gels (**A**) Colonies were PCR screened for the FLAG-RIPK1-Shut plasmid using the RIPK1\_Fwd and KpnI-Rev primers. (**B**) Colonies were screened for the plasmids containing the S161A, S166A and T183A constructs using the ShutF and S166A-Rev primers. (**C**) Colonies were screened for the FLAG-K376R-Shut plasmid using the K376R\_Fwd and the ShutR primers. M denotes the 1 kb Plus DNA Ladder marker.



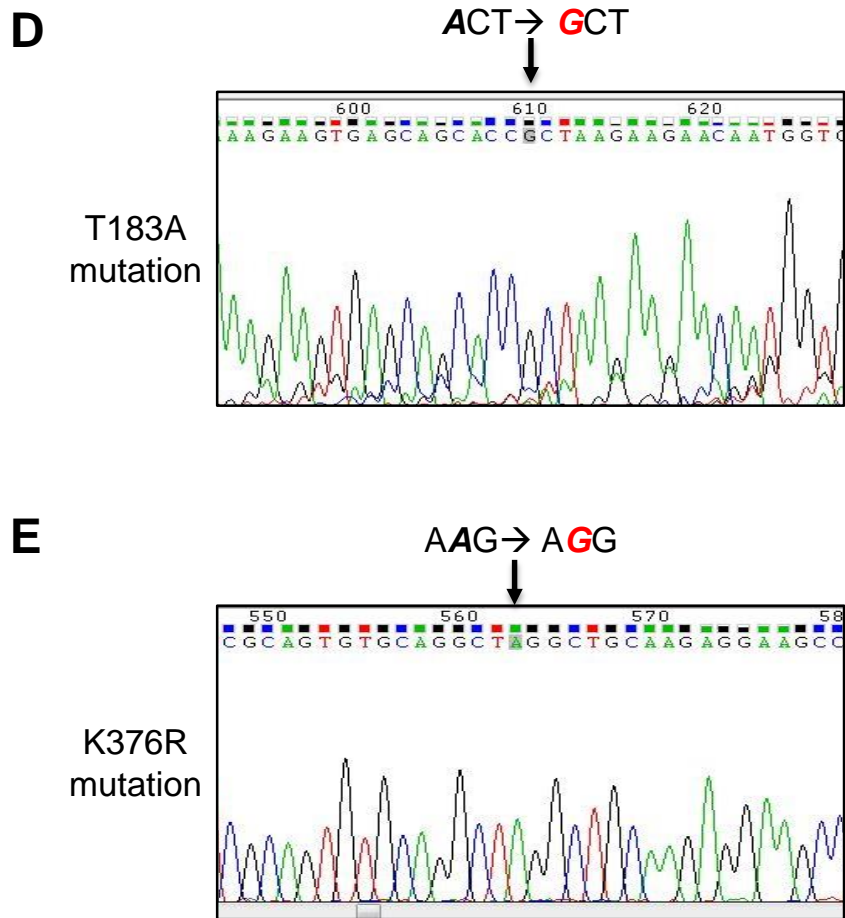


**Figure 5.8 FLAG-tagged wild-type and mutant RIPK1 shuttle vector sequence chromatograms**

Shuttle vector plasmids expressing wild-type and mutant RIPK1 constructs were sequenced to verify the presence of the desired mutations. Sequence chromatograms showing the relevant mutations are shown. Sequencing for (A – C) used the RIPK1\_Fwd primer. Sequencing for (E) used the T183A\_Fwd primer. Details of primers are found in Table 5.1.

### **5.3.3 Expression of shuttle vectors expressing FLAG-tagged wild-type and mutant RIPK1 in HEK 293 cells**

To assess whether the FLAG-tagged wild-type and mutant RIPK1 proteins could be expressed successfully using the shuttle vectors, the FLAG-RIPK1-Shut, FLAG-S161A-Shut and FLAG-S166A-shut plasmids were transfected into HEK 293 cells, as described in section 5.2.4. The proteins were immunoprecipitated using antibodies to the FLAG-tag and detected by immunoblotting for the FLAG-tag (Fig. 5.9).

Initially, the expression of wild-type RIPK1 using the FLAG-RIPK1-Shut plasmids was assessed. Immunoblotting of immunoprecipitates resulted in detection of two dominant bands of FLAG immunoreactivity (of ~74 and ~79 kDa) (Fig. 5.9A). Although it is not clear why the transfected shuttle vector resulted in expression of two bands, immunoblotting of the total cell lysates with antibodies to RIPK1 also detected both bands in transfected cells, and it is therefore possible that one of the bands represents a RIPK1 species that has undergone post-translational modification. In Chapter Four, exposure of cardiomyocytes to TNF $\alpha$  resulted in reduced mobility of endogenous RIPK1 (Fig. 4.3). To assess whether the exogenously expressed FLAG-tagged RIPK1 construct responds to TNF $\alpha$  stimulation in the same manner, transfected HEK cells were exposed to TNF $\alpha$  (20 ng/ml, 5 min). However, there was no apparent effect on the mobility of either of the detected bands (Fig. 5.9A).

Transfection of HEK 293 cells with the FLAG-S166A-Shut and FLAG-S161A-Shut plasmids also resulted in detection of multiple bands of FLAG and RIPK1 immunoreactivity (Fig. 5.9, B and C). In contrast with the effects of IL1 $\beta$  on endogenous RIPK1 in cardiomyocytes observed in Chapter Four (Fig. 4.4), exposure of HEK 293 cells expressing FLAG-RIPK1-Shut or FLAG-S166A-Shut to IL1 $\beta$  (25 ng/ml, 15 min) had no effect on the mobility of the detected RIPK1 bands (Fig. 5.9B). Although neither TNF $\alpha$  nor IL1 $\beta$  had any effect on the electrophoretic mobility of the expressed constructs, exposure of HEK 293 cells transfected with the FLAG-RIPK1-Shut, FLAG-S161A-Shut and FLAG-S166A-Shut plasmids to the potent PP1/PP2A inhibitor calyculin A (Garcia et al., 2002) resulted in detection of reduced mobility bands of all

three proteins (Fig. 5.9C). This is likely a result of increased Ser/Thr phosphorylation as previously observed in investigations of other kinases (Fuller et al., 2008; Fuller et al., 2012).

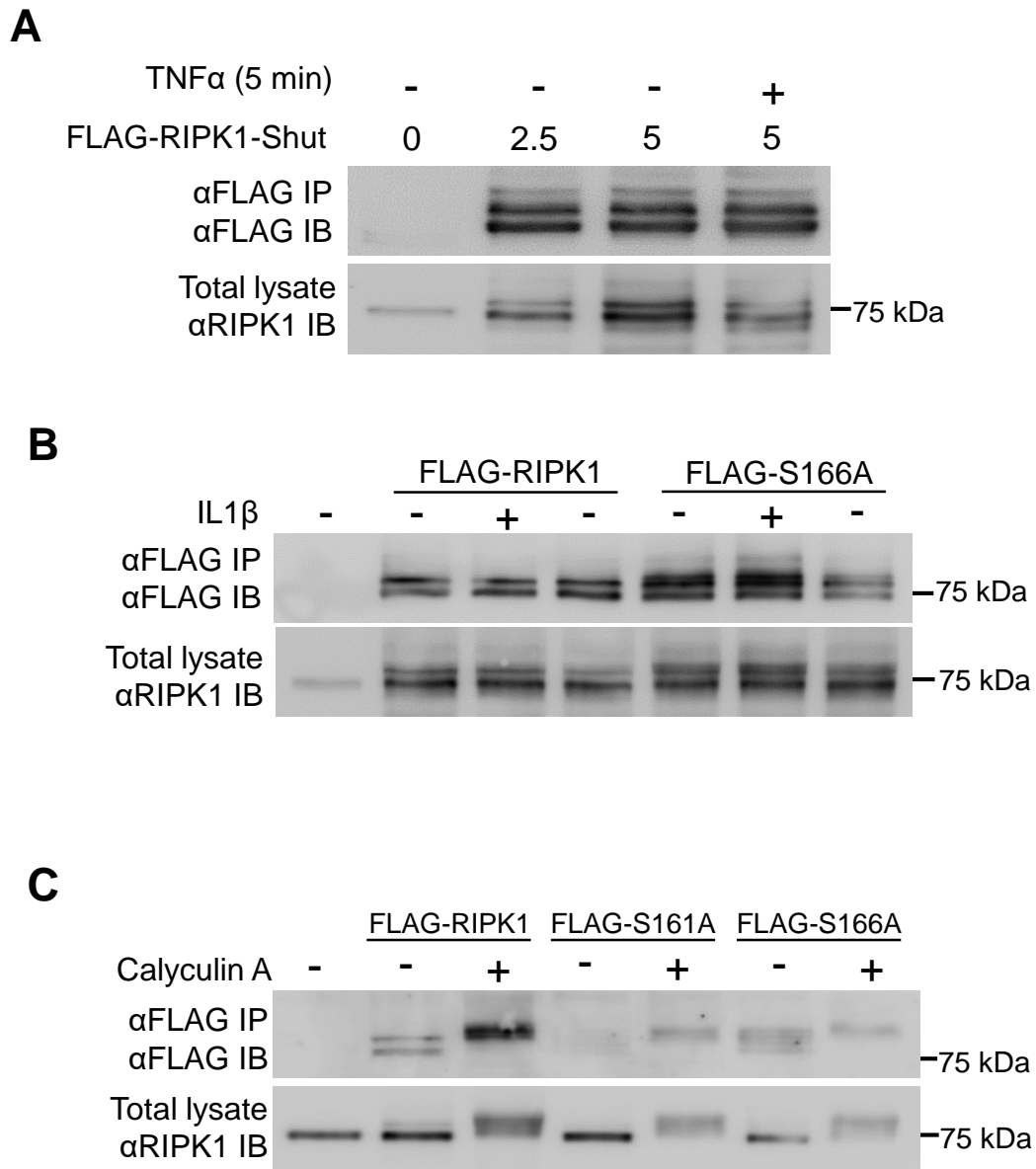


**Figure 5.9 Expression of FLAG-tagged wild-type and mutant RIPK1 shuttle vectors in HEK 293 cells**

(A) HEK 293 cells were untransfected or transfected with different quantities of FLAG-RIPK1-Shut plasmid as indicated. Cells were untreated or exposed to TNF $\alpha$  (20 ng/ml, 5 min). FLAG-tagged constructs were immunoprecipitated and immunoblotted for FLAG (upper blot) or total lysates (30  $\mu$ g protein) immunoblotted for RIPK1 (lower blot). (B) HEK 293 cells were untransfected or transfected with 1.25  $\mu$ g shuttle vector plasmid as indicated. Cells were untreated or exposed to IL1 $\beta$  (25 ng/ml, 15 min). FLAG-tagged constructs were immunoprecipitated and immunoblotted for FLAG (upper blot) or total lysates (30  $\mu$ g protein) immunoblotted for RIPK1 (lower blot). (C) HEK 293 cells were untransfected or transfected with 1.25  $\mu$ g shuttle vector plasmid as indicated. Cells were untreated or exposed to calyculin A (100 nM, 10 min). FLAG-tagged constructs were immunoprecipitated and immunoblotted for FLAG (upper blot) or total lysates (30  $\mu$ g protein) immunoblotted for RIPK1 (lower blot).

#### **5.3.4 Generation of adenoviruses expressing wild-type and mutant RIPK1**

Transfection of HEK 293 cells with shuttle vectors confirmed that the FLAG-tagged RIPK1 proteins could be expressed, although the exogenously expressed RIPK1 constructs did not respond to TNF $\alpha$  and IL1 $\beta$  treatment of HEK 293 cells in the same manner as endogenous RIPK1 in cardiomyocytes. To facilitate further investigation of RIPK1 in cardiomyocytes, shuttle vectors expressing wild-type and mutant RIPK1 were used to produce adenoviruses. Shuttle vectors were linearised by digestion with PacI and transformed into BJ5183-AD-1 *E. coli* to undergo homologous recombination with the pAdeasy-1 plasmid, producing recombinant adenoviral plasmids expressing the FLAG-tagged RIPK1 constructs. The bacteria were spread onto LB agar and resulting colonies screened for the presence of the recombinant adenoviral plasmid as described in Chapter Two, section 2.10.2 and section 5.2.3. Agarose gel electrophoresis of products from the PCR screens resulted in detection of single 184 bp bands for each of the constructs (Fig 5.10), indicating successful homologous recombination and the presence of the recombinant adenoviral plasmid. Plasmids were isolated from positive colonies and amplified. The purified plasmids were sequence verified and used to produce and propagate adenoviruses in HEK 293 cells, as described in Chapter Two, section 2.10.8.

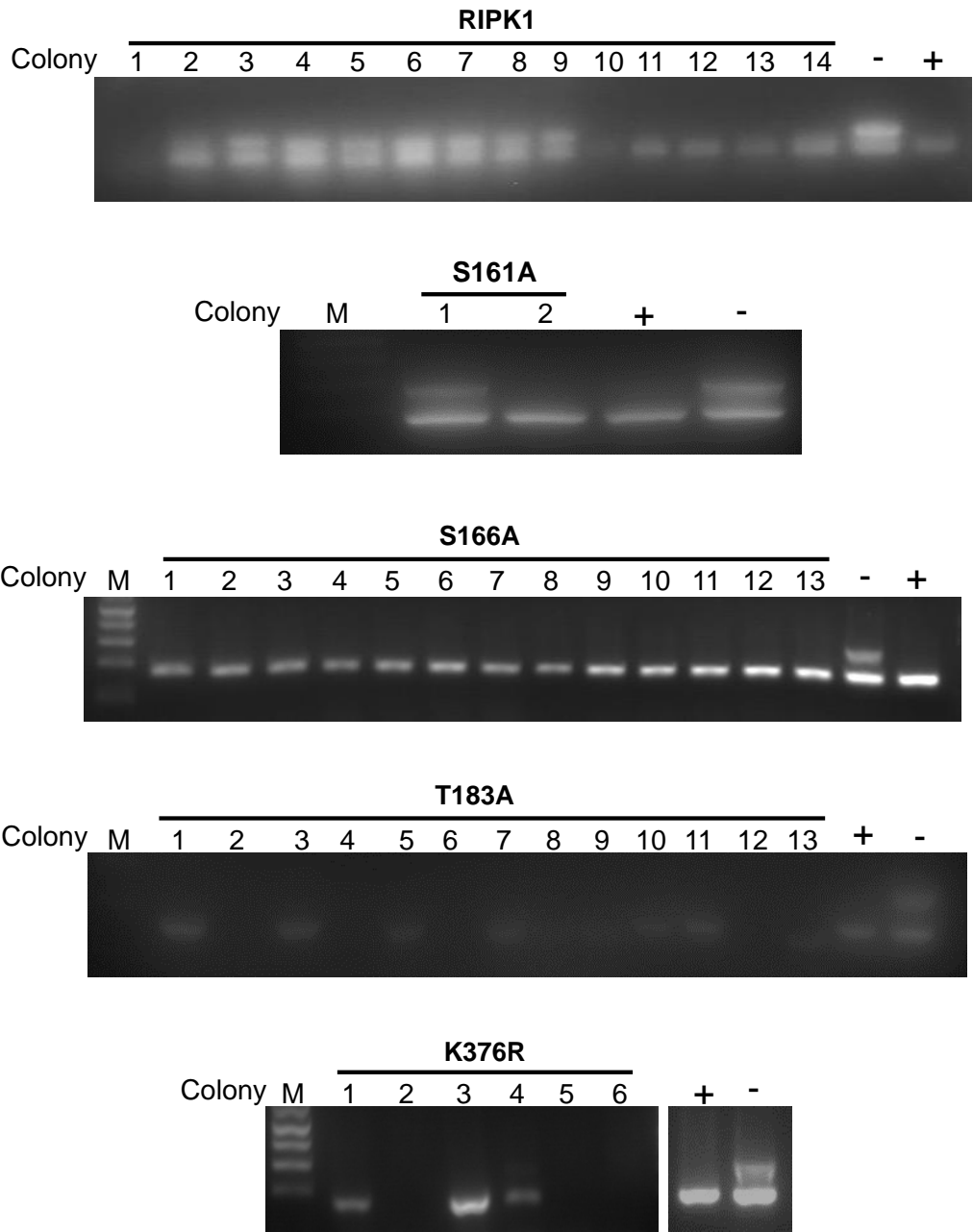


**Figure 5.10 Colony screening for adenoviral plasmids expressing FLAG-tagged wild-type and mutant RIPK1**

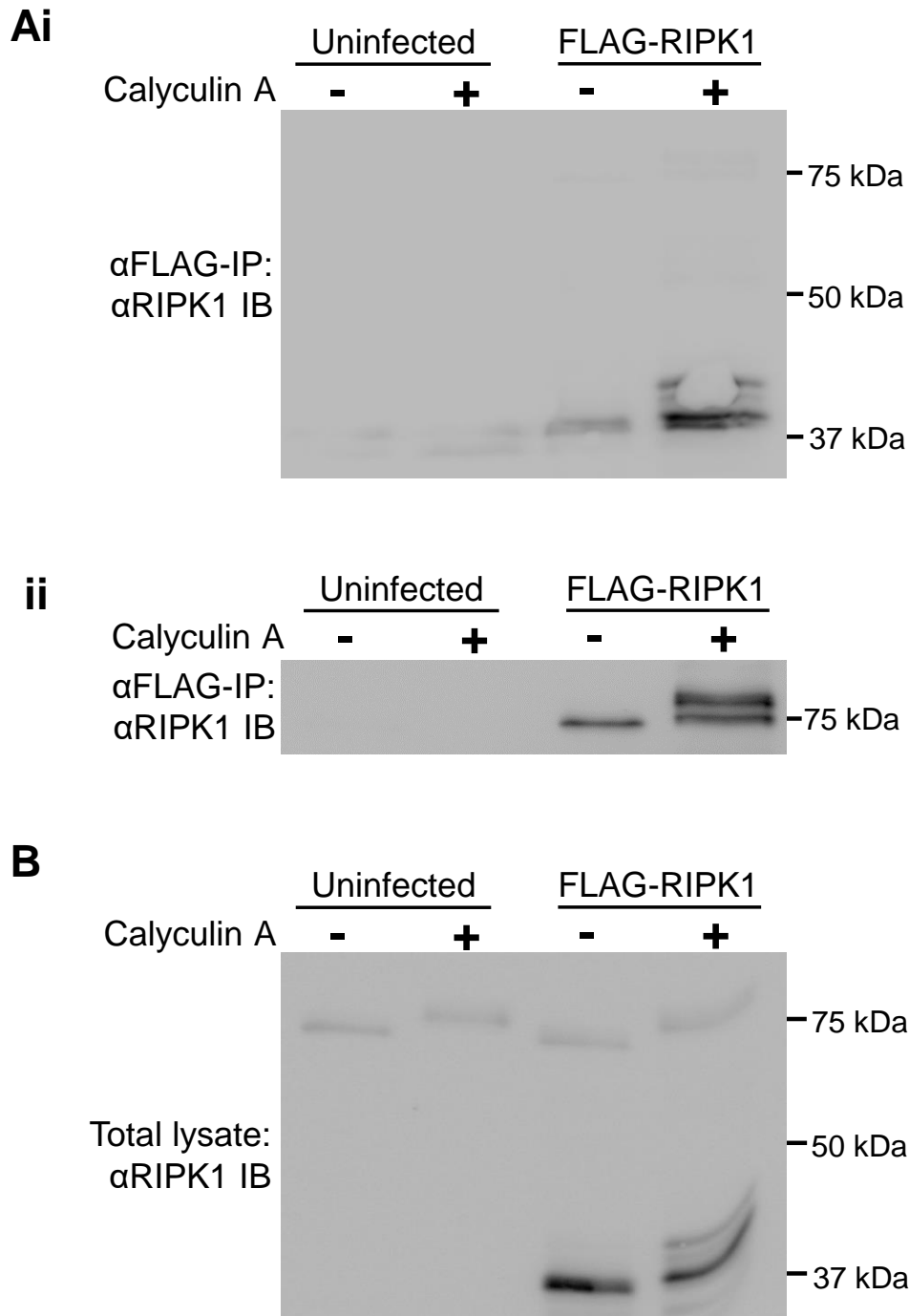
BJ5183-AD-1 colonies transformed with linearised wild-type (RIPK1) and mutant (S161A, S166A, T183A and K376R) RIPK1 shuttle vector constructs, as indicated, were PCR screened to determine if homologous recombination to produce the adenoviral plasmid had occurred. The AdV184\_F/AdV\_184R and AdV\_300F/AdV\_300R primer pairs were used. Products were electrophoresed on a 2% agarose gel. A single 184 bp band indicates that homologous recombination has occurred and the presence of the adenoviral plasmid. Two bands (of 184 and 300 bp) indicates the presence of the shuttle vector. FLAG-pShuttle-CMV was used as a negative control (-) and FLAG-PKN1 adenoviral plasmid was used as a positive control (+). M denotes the 1 kb Plus Ladder marker.

### 5.3.5 Adenoviral expression of FLAG-tagged RIPK1 proteins in cardiomyocytes

Experiments were conducted to assess whether the FLAG-tagged RIPK1 constructs could be expressed in cardiomyocytes using adenoviral transduction. Cardiomyocytes were uninfected or infected with adenoviruses expressing wild-type FLAG-RIPK1 (30  $\mu$ l adenoviral stock). The cardiomyocytes were incubated for 48 h prior to serum withdrawal (24 h). FLAG-tagged proteins were immunoprecipitated and immunoblotted for RIPK1. In immunoprecipitates from unstimulated cells, FLAG-RIPK1 was detected as a dominant band of immunoreactivity of ~36 kDa and as a less intense band of ~72 kDa (Fig. 5.11Ai), approximately corresponding to the expected molecular weight for full-length FLAG-RIPK1 (75.8 kDa). Longer exposure times facilitated enhanced visualisation of the 72 kDa bands (Fig. 5.11Aii). Previous experiments indicated that FLAG-RIPK1, FLAG-S161A and FLAG-S166A expressed using shuttle vectors in HEK 293 cells exhibited a reduction in mobility in response to treatment with the PP1/PP2A inhibitor calyculin A (Fig. 5.9C). Exposure of infected cardiomyocytes expressing FLAG-RIPK1 to calyculin A (100 nM, 10 min) also resulted in detection of reduced mobility FLAG-RIPK1 bands of >37 kDa and >74 kDa (Fig. 5.11, Ai and Aii).

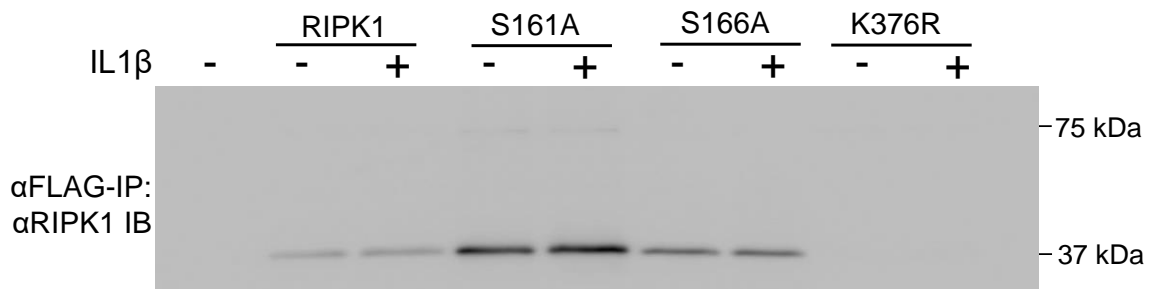
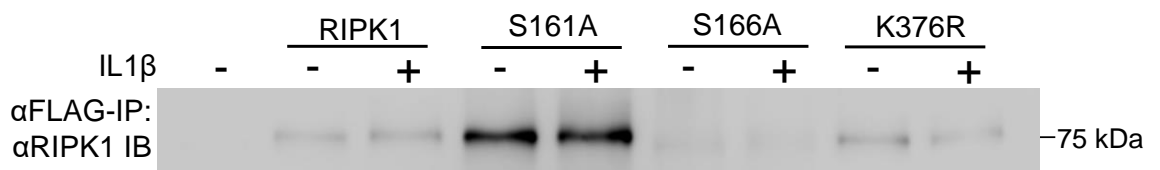
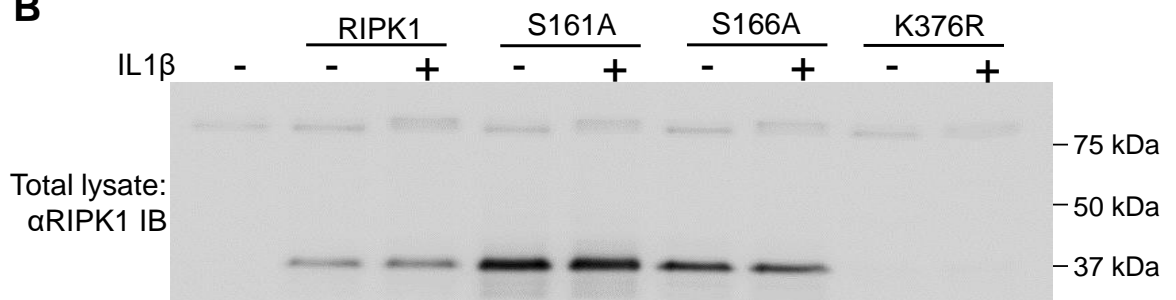
Previously, IL1 $\beta$  treatment had no effect on FLAG-RIPK1, FLAG-S161A or FLAG-S166A constructs expressed using shuttle vectors in HEK 293 cells (Fig. 5.9B). To investigate whether the constructs respond to IL1 $\beta$  in cardiomyocytes, cardiomyocytes were uninfected or infected with adenoviruses expressing FLAG-RIPK1 (30  $\mu$ l) FLAG-S161A (10  $\mu$ l), FLAG-S166A (30  $\mu$ l) or FLAG-K376R (50  $\mu$ l). The cardiomyocytes were incubated for 24 h to permit expression of the FLAG-tagged proteins and then serum-containing medium was withdrawn for a further 24 h. The cardiomyocytes were either untreated or exposed to IL1 $\beta$  (25 ng/ml, 15 min) and FLAG-tagged proteins immunoprecipitated and immunoblotted for RIPK1. As observed in Fig. 5.11, in unstimulated cardiomyocytes, the FLAG-RIPK1, FLAG-S161A, and FLAG-S166A constructs were detected as dominant bands of ~36 kDa and less intense bands of ~72 kDa (Fig. 5.12Ai), although there was little or none detected FLAG-K376R. A longer exposure time permitted enhanced detection of the less intense bands migrating at ~72 kDa, and also allowed

detection of ~72 kDa bands for the FLAG-K376R construct (Fig. 5.12Aii). However, exposure to IL1 $\beta$  did not appear to have a substantial effect on the mobility of any RIPK1 construct (Fig. 5.12, Ai and Aii).



**Figure 5.11 Expression of FLAG-tagged RIPK1 in cardiomyocytes**

Cardiomyocytes were uninfected or infected with adenoviruses expressing FLAG-RIPK1, as indicated, and either untreated or exposed to calyculin A (100 nM, 10 min) (**Ai**) FLAG-tagged proteins were immunoprecipitated and immunoblotted for RIPK1 (**ii**) The immunoblot in (**Ai**) subjected to a longer exposure time. (**B**) Total cell lysates (30 µg protein) were immunoblotted for RIPK1.

**Ai****ii****B**

**Figure 5.12 Effects of IL1 $\beta$  on FLAG-tagged RIPK1 constructs in cardiomyocytes**

Cardiomyocytes were either uninfected or infected with adenoviruses expressing FLAG-tagged RIPK1 constructs, as indicated. Cardiomyocytes were untreated or exposed to IL1 $\beta$  (25 ng/ml, 15 min) **(Ai)** FLAG-tagged proteins were immunoprecipitated and immunoblotted for RIPK1. **(Aii)** The immunoblot in **(Ai)** subjected to a longer exposure time. **(B)** Total cell lysates (30  $\mu$ g protein) were immunoblotted for RIPK1.

## 5.4 Discussion

This chapter details the production of adenoviruses expressing N-terminally FLAG-tagged wild-type and mutant RIPK1 constructs, with the intention of using these constructs to further investigate the roles and regulation of RIPK1 in cardiomyocytes. Initially, multispecies protein sequence alignment was conducted to identify conserved phosphorylatable residues in the RIPK1 kinase activation segment (Fig. 5.5A). Sequence alignments indicated that three potentially phosphorylatable activation segment residues, Ser161, Ser166 and Thr183 are wholly conserved from human to mouse and rat, and thus are of prime interest in identification of the RIPK1 ALPS (Fig. 5.5A). A further residue in the RIPK1 intermediate domain, Lys376, is also conserved (Fig. 5.5B) and polyubiquitinylation at this residue is implicated in activation of NF $\kappa$ B and MAPKs downstream of RIPK1 in other cell types (Ea et al., 2006; Li et al., 2006; Duprez et al., 2012). Accordingly, adenoviruses expressing wild-type and S161A, S166A, T183A and K376R mutant RIPK1 were generated.

### 5.4.1 Expression of FLAG-tagged RIPK1 constructs

The wild-type and mutant constructs were first sub-cloned into the FLAG-pShuttle-CMV plasmid, and expression of the FLAG-RIPK1, FLAG-S161A and FLAG-S166A proteins assessed in HEK 293 (Fig. 5.9). FLAG-RIPK1-Shut was detected in HEK 293 cells as two bands of ~74 kDa and ~79 kDa (Fig. 5.9A). Detection of the 74 kDa band is largely in agreement with expected molecular weight of mouse FLAG-RIPK1 (~75.8 kDa). The reason for the detection of a 79 kDa band is unknown although since the band was not detected in untransfected total cell lysates (Fig. 5.9A), this may represent a FLAG-RIPK1 species that has undergone post-translational modification. It is also possible that the 79 kDa band is the full-length FLAG-RIPK1 construct, in which case detection of the 74 kDa band may reflect the presence of a truncated FLAG-RIPK1 species. Although the FLAG-RIPK1 constructs did not respond to exposure of HEK 293 cells to TNF $\alpha$  or IL1 $\beta$  (Fig. 5.9, A and B), PP1/PP2A inhibition

with calyculin A resulted in reduced mobility of the FLAG-RIPK1, FLAG-S161A and FLAG-S166A constructs (Fig. 5.9, A and C) confirming that modification of the exogenously expressed constructs could be detected.

To further investigate the regulation of RIPK1 in cardiomyocytes, the shuttle vectors were used to produce FLAG-RIPK1, FLAG-S161A, FLAG-S166A, FLAG-T183A and K376R adenoviruses. However, due to time limitations, FLAG-T183A had not undergone the final amplification in HEK 293 cells to produce the final, high-titre adenoviral stock. Adenovirally mediated expression of FLAG-RIPK1 was first tested by infecting cardiomyocytes and immunoprecipitating the proteins with antibodies to the FLAG-tag (Fig. 5.11). Immunoblotting of the immunoprecipitated proteins with anti-RIPK1 antibodies detected dominant bands of ~36 kDa (Fig. 5.11Ai) and less intense bands of ~72 kDa (Fig. 5.11Ai). Visualisation of the ~72 kDa bands was enhanced by exposing the membrane for a longer duration (Fig. 5.11Aii). The ~72 kDa bands approximately correspond to the expected molecular weight of mouse RIPK1, allowing for the limitations in the sensitivity of the technique, although immunoblotting of total lysates indicated that detection of the full-length RIPK1 constructs was considerably lower than that of the ~36 kDa bands (Figs. 5.11B and 5.12B)

It is possible that the ~36 kDa bands are a RIPK1 cleavage product produced in response to overexpression of the protein. A previous study by Lin and colleagues (Lin et al., 1999) reported that TNF $\alpha$  treatment of HeLa cells leads to caspase-8 mediated cleavage of RIPK1 at Asp324, resulting in a C-terminal RIPK1 product with an apparent molecular weight of 42 kDa, and a smaller N-terminal product containing the kinase domain. In this context, cleavage of RIPK1 at Asp324 was reported to promote apoptosis (Lin et al., 1999). A further study using Jurkat cell extracts exposed to cytochrome *c* indicated that RIPK1 is cleaved by caspase-6, also producing a <40 kDa RIPK1 product, as observed here (Figs. 5.11 and 5.12) (Van Raam et al., 2013). Zhang *et al.* (Zhang et al., 2015) similarly reported production of a 37 kDa N-terminal RIPK1 cleavage fragment by caspase-8 and indicated that RIPK1 cleavage at Asp324 protects Jurkat cells against TRAIL-induced death. Cleavage of mouse RIPK1 at the equivalent

residue, Asp325, would produce an N-terminal fragment with a predicted molecular weight of ~37.5 kDa. This, considered together with the observations of the studies discussed, strongly suggests that the FLAG-tagged RIPK1 proteins are cleaved following expression in cardiomyocytes, resulting in the observed ~36 kDa bands.

As observed in HEK 293 cells, exposure of cardiomyocytes to calyculin A resulted in detection of reduced mobility FLAG-RIPK1 bands of >74 kDa (Fig. 5.11, Ai and Aii). As calyculin A is a potent inhibitor of PP1/PP2A (Garcia et al., 2002), it is probable that the observed reduction of RIPK1 mobility is caused by phosphorylation of multiple Ser/Thr residues. Although Ser/Thr phosphorylation is the most likely explanation for the observed reduction of mobility, further experiments are required to confirm this. Although calyculin A resulted in detection of reduced mobility FLAG-RIPK1 bands in both cardiomyocytes and HEK 293 cells (Figs. 5.9A and 5.11), IL1 $\beta$  exposure had no effect on any of the FLAG-tagged RIPK1 constructs in either cell type (Figs. 5.9B and 5.12). It is possible that the responses to the different stimuli are dependent on localisation of the expressed protein to specific cellular regions or compartments. For example, the modification of endogenous RIPK1 in response to IL1 $\beta$  detailed in Chapter Four may occur in specific complexes, and it is possible that the exogenously expressed FLAG-tagged RIPK1 constructs were not incorporated into these complexes.

Further experimentation may allow identification of conditions for the successful use of the RIPK1 adenoviruses, although due to the apparent cleavage of the exogenously expressed constructs and the lack of response to IL1 $\beta$ , it may not be possible to use the adenoviruses for investigation of regulation of RIPK1 in cardiomyocytes.

#### **5.4.2 Investigating the causes of reduced RIPK1 electrophoretic mobility**

The data presented in Chapter Four demonstrate that RIPK1 in cardiomyocytes exhibits reduced mobility in response to pro-inflammatory cytokines (i.e. TNF $\alpha$  and IL1 $\beta$ ) (Chapter Four, Fig. 4.3 and 4.4) and H<sub>2</sub>O<sub>2</sub> (Chapter Four, Fig. 4.1). It was hypothesised that this

phenomenon is due to phosphorylation, most likely at multiple different sites. Further evidence indicating that RIPK1 undergoes phosphorylation in response to IL1 $\beta$  was obtained using anion-exchange FPLC (Chapter Four, Fig. 4.5). However, to further investigate the response of RIPK1 to these stimuli, it is necessary to confirm that the observed reduction in mobility is in fact caused by phosphorylation. This can be investigated by conducting dephosphorylation experiments using exogenous PP2A. While it is possible to incubate total cell lysates with PP2A, this approach may be inefficient due to the large number of endogenous PP2A targets within the cell (Slupe et al., 2011), and thus an approach using exogenously expressed FLAG-RIPK1 is favoured.

Accordingly, the principal aim in this chapter was to produce adenoviruses expressing FLAG-tagged RIPK1 which can be immunoprecipitated for use in experiments to assess RIPK1 phosphorylation in response to the various stimuli examined. The intention was to infect cardiomyocytes with FLAG-RIPK1 adenoviruses followed by exposure to TNF $\alpha$  (20 ng/ml, 15 min), IL1 $\beta$  (25 ng/ml, 15 min) or H<sub>2</sub>O<sub>2</sub> (1 mM, 60 min) in an attempt to stimulate the maximal RIPK1 response, as determined by the experiments in Chapter Four. The constructs would be immunoprecipitated using antibodies to the FLAG-tag, as described in section 5.2.6, and dephosphorylation initiated with the addition of recombinant PP2A catalytic domain, in the presence or absence of okadaic acid, a PP2A inhibitor (Garcia et al., 2002). Treated immunoprecipitates would subsequently be separated using SDS-PAGE, followed by immunoblotting for FLAG and/or RIPK1. The expectation is that the stimulated FLAG-RIPK1 constructs would exhibit reduced mobility as in Chapter Four and that incubation with PP2A would result in the bands migrating at the same position as the untreated constructs if the reduced mobility is caused by phosphorylation. The inclusion of okadaic acid should then lead to the treated FLAG-RIPK1 bands exhibiting reduced mobility, due to inhibition of dephosphorylation by PP2A. This strategy was adopted successfully in a previous study by Fuller and colleagues (Fuller et al., 2012). However, due to unforeseen problems with

expressing full-length FLAG-RIPK1 in cardiomyocytes and the lack of response to IL1 $\beta$ , these experiments were not possible.

#### **5.4.3 Identification of the RIPK1 activation loop phosphorylation site (ALPS)**

RIPK1 is a key mediator of cell survival and death responses in certain contexts, and ample evidence in both non-cardiac systems and the heart indicates that RIPK1 kinase activity is obligatory for its pro-necrotic function (Degterev et al., 2008; McQuade et al., 2013; Newton et al., 2016a; Oerlemans et al., 2012; Wang et al., 2015). Previously, structural modelling and sequence alignment comparing B-Raf and RIPK1 indicated homology between the activation loops of these kinases. Specifically, the important regulatory autophosphorylation site of B-Raf, Thr598 (Zhang and Guan, 2000), was found to be homologous to Ser161 in the RIPK1 activation loop (Degterev et al., 2008). This led other investigators to propose Ser161 as the RIPK1 ALPS. However, substitution of non-phosphorylatable alanine at Ser161 does not fully abolish kinase activity and only led to minimal attenuation of induction of necroptosis (Degterev et al., 2008; McQuade et al., 2013). Accordingly, while Ser161 may contribute to RIPK1 kinase activity, it is not the ALPS and phosphorylation at other site(s) is required for efficient catalysis. Although mutation of Ser161 to alanine does not block kinase activity or functional competence to induce necroptosis, it substantially attenuates sensitivity of RIPK1 to Nec-1, indicating that this residue is implicated in the interaction between RIPK1 and this inhibitor (Degterev et al., 2008; McQuade et al., 2013). Some studies have used autophosphorylation of RIPK1 at Ser166 as a marker of activation (Berger et al., 2014; Ofengeim et al., 2015; Newton et al., 2016b). However, it has yet to be definitively demonstrated and reported that Ser166 is the RIPK1 ALPS. McQuade and colleagues (McQuade et al., 2013) mutated Ser166 to alanine, resulting in a ~71% decrease in RIPK1 autophosphorylation in an *in vitro* kinase assay, although the authors did not acknowledge this observation (McQuade et al., 2013).

A major aim in this chapter was to definitively identify the RIPK1 ALPS. Here, sequence alignment revealed that three RIPK1 kinase domain Ser/Thr residues, Ser161, Ser166 and Thr183, are absolutely conserved from human to rat and mouse (Fig. 5.5), potentially indicating important roles in regulation of RIPK1 kinase activity. Ser161 and Ser166 are established phosphorylation sites, as discussed above, although there does not appear to be any published information pertaining to potential roles of Thr183. To investigate the importance of these sites in regulation of RIPK1 function, adenoviruses expressing FLAG-tagged wild-type (FLAG-RIPK1), S161A, S166A and T183A RIPK1 were generated. As discussed in section 5.4.1, the T183A adenoviruses had not undergone the final amplification in HEK 293 cells to produce a sufficiently infective titre. A kinase-deficient RIPK1 variant in which the critical lysine residue required for ATP binding and phosphotransfer (Carrera et al., 1993), Lys45, was mutated to alanine as in Berger *et al.* (Berger et al., 2014) was also produced (FLAG-K45A, data not shown) but similarly had not undergone sufficient amplification for use. Final adenoviral stocks of the wild-type FLAG-RIPK1, FLAG-S161A and FLAG-S166A adenoviruses were produced and their expression tested in cardiomyocytes. However, as demonstrated in Figs. 5.11 and 5.12, and discussed in section 5.4.1, the overexpressed FLAG-tagged constructs appear to undergo cleavage in cardiomyocytes.

Despite the problems experienced with expression of the full-length constructs, it may still be possible to use the adenoviruses in kinase assays to identify the ALPS. In further investigations, cardiomyocytes would be infected with FLAG-RIPK1, FLAG-S161A, FLAG-S166A, FLAG-T183A and FLAG-K45A adenoviruses and exposed to putative agonists (for example calyculin A, TNF $\alpha$ , IL1 $\beta$ , H<sub>2</sub>O<sub>2</sub>). The various RIPK1 constructs would be immunoprecipitated using antibodies to the FLAG-tag and subjected to kinase assays *in vitro*, assessing the incorporation of radioactively labelled [ $\gamma$ -<sup>32</sup>P]ATP into an appropriate substrate using Čerenkov counting. It may be necessary to conduct initial experiments to identify the most suitable substrate. Previous studies have used autophosphorylation as an indication of RIPK1 kinase activity (Degterev et al., 2008; Cho et al., 2009; Mcquade et al., 2013) although

it may be more appropriate to use alternative substrates such as exogenously expressed RIPK3 or the widely used generic phosphoacceptor substrate, myelin basic protein (Clerk and Sugden, 1997a). The results of these experiments should indicate the phosphorylation site(s) required for RIPK1 kinase activity in response to the various stimuli in cardiomyocytes, with the expectation that the constructs containing the mutated ALPS will exhibit significantly reduced kinase activity relative to the wild-type.

#### **5.4.4 RIPK1 signalling to NF $\kappa$ B and MAPKs in cardiomyocytes**

In addition to its role in regulation of cell death, in non-cardiac cell types, RIPK1 is required for TNF $\alpha$ -mediated activation of cytoprotective NF $\kappa$ B signalling (Hsu et al., 1996) (Kelliher et al., 1998) and the three principal MAPK pathways, ERK1/2, JNKs and p38-MAPKs (Liu et al., 1996; Devin et al., 2003; Lee et al., 2004). Interestingly, RIPK1 catalytic activity is required for activation of ERK1/2 but not JNKs or p38-MAPKs (Devin et al., 2003; Lee et al., 2004; Zhang et al., 2013). Activation of NF $\kappa$ B and MAPKs downstream of RIPK1 is dependent on K63-linked polyubiquitinylation of RIPK1 at Lys377, resulting in the recruitment of the TAK1 complex and activation of IKKs (Ea et al., 2006; Li et al., 2006). To begin to investigate the roles of RIPK1 in activation of NF $\kappa$ B and MAPKs in cardiomyocytes, adenoviruses expressing FLAG-tagged mouse RIPK1 containing a mutation of the conserved K376 residue (FLAG-K376R) were produced (Fig. 5.10), although the effects of the mutation on NF $\kappa$ B and MAPK activation were not examined due to time limitations. Future investigations would seek to express FLAG-K376R and wild-type FLAG-RIPK1 in cardiomyocytes followed by exposure to TNF $\alpha$  or other agonists. The effects on activation of NF $\kappa$ B would be investigated by assessing activation of IKKs and phosphorylation of their substrate, I $\kappa$ B $\alpha$ , as in Ea *et al.* (Ea et al., 2006). Effects on the activation of MAPKs would be investigated by immunoblotting for phosphorylated (i.e. activated) ERK1/2, JNKs and p38-MAPKs.

## **Chapter Six – Summary, discussion and future work**

## **6.1 Overview and summary of results**

One of the major aims for this thesis, detailed in Chapter Three, was to characterise the roles of three well-established signalling pathways, the ERK1/2, JNK and p38-MAPK cascades, in regulation of cardiomyocyte RNA expression during H<sub>2</sub>O<sub>2</sub>-induced apoptosis. Chapters Four and Five focused on the regulation of cardiac RIPK1, which mediates the novel necroptotic cell death pathway, and is also involved in cytoprotection, potentially through JNK and p38-MAPK signalling.

### **6.1.1 Regulation of cardiomyocyte RNA expression by MAPKs in response to oxidative stress**

- H<sub>2</sub>O<sub>2</sub> (0.2 mM) promoted activation of MAPKs in the nucleus with no net nuclear accumulation of total protein. ERK1/2 were activated to a similar extent in nucleus and cytoplasm, whilst activation of JNKs and p38-MAPKs was greater in the cytoplasm than in the nucleus.
- ERK1/2 play a substantial role in regulation of basal cardiomyocyte RNA expression, with lesser contributions by JNKs and p38-MAPK $\alpha/\beta$ . H<sub>2</sub>O<sub>2</sub> induced substantial changes in cardiomyocyte RNA expression, and ERK1/2 played the largest role in terms of numbers of RNAs regulated (~35% of RNAs), with relatively smaller contributions by JNKs (~26% of RNAs) and p38-MAPK $\alpha/\beta$  (~31% of RNAs). Approximately 44% of RNAs were regulated through alternative mechanisms.

### **6.1.2 Effects of pathophysiological stimuli on cardiac RIPKs**

- In cardiomyocytes, moderate and high concentrations of H<sub>2</sub>O<sub>2</sub> induced appearance of reduced mobility RIPK1 bands on immunoblots, consistent with multiple phosphorylations.

Similarly, in adult rat perfused hearts, 0.2 mM H<sub>2</sub>O<sub>2</sub> resulted in reduced electrophoretic mobility RIPK1 also consistent with increased phosphorylation. Following ischaemia/reperfusion in perfused hearts, RIPK1 exhibited reduced electrophoretic mobility, but this was associated with decreased RIPK1 immunoreactivity, suggestive of either degradation or conformational changes resulting in epitope masking.

- Exposure of cardiomyocytes to pro-inflammatory cytokines (TNF $\alpha$  and IL1 $\beta$ ) resulted in reduction of RIPK1 electrophoretic mobility on immunoblots, consistent with phosphorylation. This was supported by RIPK1 analysis using anion-exchange FPLC.
- The p38-MAPK $\alpha/\beta$  inhibitor SB203580 reduced the rate of appearance of reduced mobility RIPK1 bands in cardiomyocytes exposed to IL1 $\beta$ , suggesting that RIPK1 might be phosphorylated by p38-MAPK $\alpha/\beta$  or a p38-MAPK $\alpha/\beta$ -activated kinase.
- Shuttle vectors for expression of FLAG-tagged wild-type RIPK1 (FLAG-RIPK1) and phosphorylation/ubiquitinylation site mutant RIPK1 (FLAG-S161A, FLAG-S166A, FLAG-T183A and FLAG-K376R) were produced. The FLAG-RIPK1, FLAG-S161A and FLAG-S166A constructs did not exhibit reduced mobility in response to IL1 $\beta$  when expressed in HEK 293 cells but exhibited reduced mobility in response to calyculin A. Adenoviruses were generated for expression of FLAG-tagged constructs in neonatal rat cardiomyocytes, but much of the expressed RIPK1 protein appeared to have undergone cleavage.
- Exposure of neonatal rat cardiomyocytes infected with FLAG-RIPK1 adenoviruses to the PP1/PP2A inhibitor calyculin A resulted in reduced mobility FLAG-RIPK1 bands, but the FLAG-RIPK1, FLAG-S161A, FLAG-S166A or FLAG-K376R constructs did not respond to IL1 $\beta$  in cardiomyocytes.

## **6.2 Discussion**

### **6.2.1 Stress signalling in cardiomyocytes and the heart**

The heart and its constituent cardiomyocytes are subjected to a wide range of pathophysiological stresses. Exposure to such stresses can result in activation of intracellular signalling pathways, leading to varied responses including differential regulation of gene expression and modulation of the balance between cardiomyocyte life and death (Clerk et al., 2007a). Extensive research in recent decades has focussed on identification of the pathophysiological stimuli responsible for these effects and on elucidating the signalling pathways that might be involved in eliciting them. Amongst the most significant pathophysiological stresses encountered by the heart and cardiomyocytes are oxidative stress and pro-inflammatory cytokines, which are associated with activation of various intracellular signalling pathways and a wide range of adaptive and maladaptive responses (Tsutsui et al., 2011; Hedayat et al., 2010).

Oxidative stress, exemplified by  $H_2O_2$ , is a key regulator of the balance between life and death of cardiomyocytes, and is associated with the pathogenesis and progression of cardiac diseases such as HF. It has been well-established through numerous investigations that exposure to moderate levels of  $H_2O_2$  induces cardiomyocyte apoptosis (Aikawa et al., 1997; Von Harsdorf et al., 1999; Cook et al., 1999b; Kwon et al., 2003) and, as confirmed in Chapter Three, promotes substantial changes in cardiomyocyte RNA expression (Kemp et al., 2003; Clerk et al., 2007b). These changes are assumed to influence the progression of cardiomyocyte apoptosis.  $H_2O_2$  also activates the three principal MAPK cascades, which regulate gene expression in other cell types (Clerk et al., 1998b; Turjanski et al., 2007). The investigations detailed in Chapter Three sought to establish the importance of MAPKs in eliciting global changes in cardiomyocyte RNA expression during  $H_2O_2$ -induced apoptosis. The results presented indicate that the MAPKs do indeed contribute substantially, yet differentially, to global changes in cardiomyocyte RNA expression in this context and accordingly to the overall response of the cardiomyocyte. As observed in previous investigations examining

cardiomyocyte gene expression in response to other agonists (i.e. the  $\alpha$ -adrenergic agonists phenylephrine, ET-1 and A61603) (Kennedy et al., 2006; Marshall et al., 2010; Amirak et al., 2013), ERK1/2 represents a major node in signalling to RNA expression in cardiomyocytes exposed to  $H_2O_2$  (Chapter Three, Fig. 3.9). Although the data indicate that JNKs and p38-MAPKs also make contributions, these were found to be somewhat smaller than that of ERK1/2 (Chapter Three, Fig. 3.9). Since, like in other systems, cardiac JNKs and p38-MAPKs are particularly activated by  $H_2O_2$  and other cellular stresses (Clerk et al., 1998a; Clerk et al., 1998b; Clerk and Sugden, 1997b; Laderoute and Webster, 1997) and also by IR (Bogoyevitch et al., 1996) it is perhaps surprising that these pathways did not dominate over ERK1/2 in regulation of cardiomyocyte RNA expression induced by  $H_2O_2$ . However, while ERK1/2 were found to regulate a larger number of RNAs than either the JNKs or p38-MAPK $\alpha/\beta$ , many RNAs induced by  $H_2O_2$  were differentially regulated by more than one MAPK inhibitor (e.g. Klf4, Xirp1, Egr1 and Egr3, Dusp2, Dusp4, Dusp5) (Appendix II, Tables A9, A16 and A20), indicative of overlapping contributions by the different MAPK pathways. Assuming the mRNAs are translated into protein, the products of many of the mRNAs promoted by the JNKs (e.g. Atf3) (Appendix II, Table A16) or p38-MAPK $\alpha/\beta$  (e.g. Hmox1, Gclc, Cdkn1a, Zfp36) (Appendix II, Table A20) may potentially have important effects on the overall response of the cardiomyocyte, and therefore the heart, to the encountered stress. However, although the data presented indicate that the three principal MAPK pathways make substantial contributions in this context, ~44% of the RNAs differentially regulated by  $H_2O_2$  were unaffected by any MAPK inhibitor (Appendix II, Tables A6 and A7). It is therefore apparent that other  $H_2O_2$ -responsive signalling pathways or regulatory mechanisms are involved in regulation of cardiomyocyte RNA expression, with a potentially important impact on the response of the heart to oxidative stress. Although the identity of these mechanisms is not immediately clear, established redox-sensitive transcriptional regulators such as the transcription factor Nrf2 (Zhou et al., 2014) may be involved. Further work is required to examine these mechanisms.

While the data presented in Chapter Three provide further insights into the regulation of cardiomyocyte responses to oxidative stress by the extensively investigated MAPK pathways, other, less well-characterised pathways are also likely to make important contributions to cardiomyocyte signalling under stress conditions, potentially with important consequences for the heart as a whole organ. Cardiomyocyte cell death in response to varied insults is a key contributor to the pathogenesis of heart diseases such as HF, although the relative significance of apoptosis vs necrosis in the development of HF continues to be debated (Clerk et al., 2003; Van Empel et al., 2005; Konstantinidis et al., 2012). Since necrosis has conventionally been conceptualised as a passive and unregulated process in response to overwhelming stress, it was largely assumed that necrotic death was refractory to targeted therapy. However, the recent identification of necroptosis as a regulated form of necrosis (Degterev et al., 2005) and a possible contributor to pathologies has highlighted new potential for therapeutic intervention (Zhou and Yuan, 2014). Necroptotic death is centrally regulated by RIPK1 (Cho et al., 2009). However, RIPK1 also executes important functions in signalling to cytoprotection in non-cardiac systems, including through signalling to the activation of MAPKs. RIPK1 is required for recruitment and activation of TAK1 and IKKs, resulting in stimulation of NF $\kappa$ B-dependent gene expression (Kelliher et al., 1998; Ea et al., 2006) and also activation of JNKs and p38-MAPKs (Liu et al., 1996; Lee et al., 2004; Devin et al., 2003). Accordingly, RIPK1 and its roles in the heart are of particular interest, both in examining the fundamental processes underlying development of cardiovascular diseases associated with increased cardiomyocyte death, and in identifying potential therapeutic targets aiming to either diminish this fallout of cardiomyocytes or otherwise to increase cytoprotective mechanisms. It was therefore hypothesised that the RIPK1 has significant functions in modulating cardiomyocyte responses to stress stimuli, potentially in mediating cardiac cell death, as well as in activation of other important signalling pathway such as the MAPKs.

In Chapter Four, exposure of cardiomyocytes or hearts to a range of important pathophysiological agonists, including pro-inflammatory cytokines or oxidative stress, resulted

in reduction of RIPK1 electrophoretic mobility on immunoblots (Chapter Four, Figs. 4.1 – 4.4). IR and H<sub>2</sub>O<sub>2</sub> also resulted in reduced mobility of RIPK1 in extracts from whole adult rat hearts (Chapter Four, Fig. 4.2). As discussed, this effect is consistent with increased phosphorylation of RIPK1 in response to the respective stimuli. Investigations in non-cardiac systems, such as that of Cho *et al.* (Cho *et al.*, 2009), indicate that RIPK1 phosphorylation and kinase activity are required for formation of the necrosome and induction of necroptotic cell death. Similarly, pharmacological inhibition, or genetic disruption, of RIPK1 catalytic activity protects cells against necroptotic death (Degterev *et al.*, 2005; Berger *et al.*, 2014; Shutinoski *et al.*, 2016; Newton *et al.*, 2016a). Investigations examining the roles of RIPK1 and RIPK3 in the heart also demonstrate that increased phosphorylation is associated with necrotic death of cardiomyocytes and negative impacts on cardiac function (Oerlemans *et al.*, 2012; Luedde *et al.*, 2014). Increased RIPK1 phosphorylation is also associated with necroptotic death, which potentially contributes to pathologies, in other organ systems (Degterev *et al.*, 2005; Ofengeim *et al.*, 2015) Accordingly, if the observed reduction of RIPK1 electrophoretic mobility is indeed caused by phosphorylation, this may be reflective of a role in mediating cardiomyocyte death in response to pathophysiological stresses, with potential impacts on the development of pathologies associated with increased cardiac cell death, such as MI or HF (Konstantinidis *et al.*, 2012).

Despite the association between increased RIPK1 phosphorylation and cell death, phosphorylation of RIPK1 by IKKs is also associated with preventing RIPK1 from integrating the pro-apoptotic complex II and the necrosome (Dondelinger *et al.*, 2015). While Dondelinger *et al.* (Dondelinger *et al.*, 2015) demonstrated that phosphorylation of RIPK1 by IKKs protects against cell death, and also identified some of the targeted phosphorylation sites, the physiological and functional relevance of RIPK1 phosphorylation in eliciting cytoprotection is yet to be established. Further work is required to establish the importance of RIPK1 phosphorylation and kinase activity in eliciting either cell death or cytoprotection, to investigate

its relevance in cardiomyocytes and the heart and to investigate whether RIPK1 is a viable therapeutic target in the treatment of cardiovascular diseases.

As discussed above, in addition to its functions in mediating cell death, RIPK1 is also involved in activation of cytoprotective mechanisms (Kelliher et al., 1998). Site-specific K63-linked polyubiquitinylation of RIPK1 at Lys377 (Lys 376 in mouse, see Chapter Five Fig. 5.5B) results in recruitment of IKKs and TAK1 (Ea et al., 2006). IKKs mediate activation of NF $\kappa$ B leading to upregulation of pro-survival proteins (Kreuz et al., 2001) while TAK1 signals to activation of JNKs and p38-MAPKs (Liu et al., 1996; Lee et al., 2004; Devin et al., 2003). An investigation by Li *et al.* (Li et al., 2014) demonstrated that TAK1 inhibition renders cardiomyocytes susceptible to necroptosis in response to TNF $\alpha$ , and is associated with defective activation of NF $\kappa$ B and JNKs. Accordingly, JNKs may confer cytoprotection in this context, and their activation by TAK1 might lie downstream of RIPK1. Chapter Five details the production of adenoviruses expressing FLAG-tagged mouse RIPK1 in which Lys376 was mutated to arginine (FLAG-K376R) to prevent ubiquitinylation. The intention was to use the adenoviruses to express the mutated form of RIPK1 in cardiomyocytes in order to examine the effects on activation of MAPKs in cardiomyocytes. Cardiomyocytes infected with FLAG-K376R adenoviruses would have been treated with various pathophysiological stimuli (e.g. TNF $\alpha$ , IL1 $\beta$  or H<sub>2</sub>O<sub>2</sub>) and the effects of the mutation on activation of MAPKs assessed by immunoblotting with antibodies to phosphorylated (i.e. activated) MAPKs. This approach could also be extended to further investigate the still poorly defined roles of different MAP3Ks, for example MEKKs, ASK1 and TAK1, in signalling to activation of MAPKs in cardiomyocytes. However, unforeseen difficulties with expressing the full-length mutant and wild-type RIPK1 constructs combined with time limitations resulted in an inability to conduct the experiments required, and accordingly further work is needed to establish the potential roles and significance of RIPK1 in signalling to MAPKs in cardiomyocytes.

In Chapter Four (Fig. 4.6), it was observed that RIPK1 in cardiomyocytes may be phosphorylated by p38-MAPK $\alpha/\beta$  [or a p38-MAPK $\alpha/\beta$ -activated kinase such as MAPKAPK2

or 3 (Cargnello and Roux, 2011)] in response to IL1 $\beta$ . As discussed, the presence of RIPK1 is required for TNF $\alpha$ -induced activation of p38-MAPK (Lee et al., 2004) although there do not appear to be any published studies indicating that RIPK1 is a substrate of the p38-MAPK pathway and therefore this is a novel observation. Further investigation will be required to determine whether RIPK1 is indeed a *bona fide* substrate of the p38-MAPK $\alpha/\beta$  pathway, to establish which sites are phosphorylated, and to determine the functional relevance of these phosphorylation events (see section 6.3.2). The activation of MAPKs, particularly JNKs and p38-MAPKs, in response to pro-inflammatory cytokines in cardiomyocytes (Clerk et al., 1999) and other systems (Bird et al., 1994; Raingeaud et al., 1995) is well established. RIPK1 was observed to respond to TNF $\alpha$  and IL1 $\beta$  treatment in cardiomyocytes (Chapter Four, Fig. 4.3 and 4.4), with inhibition of the response to IL1 $\beta$  by SB203580 (Chapter Four, Fig. 4.6). These observations may be indicative of crosstalk between the RIPK1 and MAPK pathways, with potentially important consequences for development and progression of cardiovascular diseases associated with increased cell death, cytokine expression and inflammation, such as MI and HF (Jacobs et al., 1999; Hedayat et al., 2010; Konstantinidis et al., 2012).

## **6.2.2 Study limitations**

### **6.2.2.1 Use of pharmacological inhibitors**

Pharmacological inhibitors were employed to implicate the MAPK cascades in regulation of cardiomyocyte RNA expression (see Chapter Three). Since no pharmacological inhibitor is entirely selective, attempts were made to optimise the use of the inhibitors employed. In Chapter Three, section 3.3.2, experiments were performed to confirm the potency and selectivity of PD1854352 (to inhibit ERK1/2 activation) (Sebolt-Leopold et al., 1999), JNK-IN-8 (to inhibit JNKs) (Zhang et al., 2012) and SB203580 (to inhibit p38-MAPK $\alpha/\beta$  signalling) (Cuenda et al., 1995). Despite limitations in their use, pharmacological inhibitors remain invaluable in identifying potential roles of different signalling pathways, are relatively

economical and easily manipulable. Ideally, inhibitor experiments should be repeated using other inhibitors with unrelated structures and/or mechanisms of action to verify that results can be replicated. Genetic manipulation of pathways, for example knockdown of signalling protein expression with siRNA or using tissues from transgenic animals, is also a potentially useful approach. However, these methods are still subject to limitations, particularly with respect to terminally-differentiated cardiomyocytes where genetic approaches may prove technically problematic. Furthermore, unlike pharmacological inhibitors, genetic approaches relying on knockdown or overexpression of proteins may result in disruption of the delicate stoichiometry of signalling molecules and thus have unintended consequences. Ideally, a range of complementary approaches should be adopted to interrogate the pathways of interest. Nonetheless, the results from experiments using pharmacological inhibitors, such as those reported here, are still valuable in elucidating the roles of different pathways in eliciting different cellular responses.

#### **6.2.2.2 Use of neonatal rat cardiomyocytes**

Cultured neonatal rat ventricular cardiomyocytes were the primary experimental system used in this thesis. Since the ultimate aim of biomedical research is to elucidate the biological mechanisms regulating health and disease processes in humans, human cardiomyocytes would be the most desirable model system. However, due to practical and ethical reasons, it is necessary to use cardiomyocytes from other animals. Neonatal rat cardiomyocytes are a well-characterised, relatively standardised, and widely employed model, thus facilitating comparison of results from different experiments both within research groups and from external investigators. Crucially, the studies examining cardiomyocyte gene expression in response to H<sub>2</sub>O<sub>2</sub> that directly informed this investigation (Kemp et al., 2003; Clerk et al., 2007b) were conducted using neonatal rat cardiomyocytes, and thus it was essential to continue to use the system for consistency.

Since many cardiac pathologies (such as HF and MI) predominantly affect adults, it is arguable that adult rat cardiomyocyte cultures are more reflective of the adult phenotype and should therefore be the preferred experimental system. However, neonatal cardiomyocytes are more amenable to formation of stable, confluent, synchronised cultures than are adult cardiomyocytes (Chlopcikova et al., 2001), which also undergo substantial morphological changes in culture (Chlopcikova et al., 2001; Bugaisky and Zak, 1989). Furthermore, adult cardiomyocytes are sensitive to environmental perturbations and thus the success of such preparations is highly dependent on factors including the concentration of  $\text{Ca}^{2+}$  in the digestion medium and also batch-to-batch variability of digestion enzymes (Chlopcikova et al., 2001; Bugaisky and Zak, 1989). Crucially, the procedure for isolation of adult rat cardiomyocytes may result in stimulation of stress-responsive signalling pathways (Clerk et al., 2007b), which may have undesired consequences such as modulation of gene expression, thus making them substantially less suitable for experiments such as those detailed here. Nonetheless, it is important to assess the extent to which the observations made in the neonatal system are recapitulated in the adult animal. Here, the effects of a pro-apoptotic  $\text{H}_2\text{O}_2$  concentration on RIPK1 in neonatal cardiomyocytes were observed to be similar in the whole adult heart (see Chapter Four, Figs. 4.1 and 4.2). Furthermore, the effects of  $\text{IL1}\beta$  on RIPK1 in neonatal cardiomyocytes reported here (see Chapter Four, Fig. 4.6) were subsequently replicated in whole adult hearts, as was the effect of SB203580 on the RIPK1 response  $\text{IL1}\beta$  (KA Rostron and A Clerk, unpublished data). Accordingly, while it is not possible to directly compare the isolated neonatal cardiomyocyte system to the whole adult organ, many of the responses observed in neonatal cardiomyocytes are similar to those occurring in adult hearts, and neonatal cardiomyocytes are therefore a valid and valuable model.

### **6.3 Future work**

The research presented in this thesis has provided novel insights into some of the intracellular signalling pathways involved in regulation of gene expression and cell death in the heart, and has highlighted areas of interest for future investigations.

#### **6.3.1 Regulation of cardiomyocyte gene expression by MAPKs in response to H<sub>2</sub>O<sub>2</sub>**

The results reported in Chapter Three indicate that ERK1/2, and to a lesser extent, JNKs and p38-MAPKs, play important roles in regulation of global RNA expression during cardiomyocyte apoptosis in response to H<sub>2</sub>O<sub>2</sub>. Initially, it will be important to establish whether the observed changes in RNA expression are reflected at the level of protein expression. Genes upregulated in response to H<sub>2</sub>O<sub>2</sub> and found to be differentially regulated by the MAPK pathways would be selected for further examination. Key genes of interest include the Dusps, as a result of their roles in negative regulation of MAPK signalling (Huang and Tan, 2012). Other genes of interest include Zfp36 (tristetraprolin) due to its association with post-transcriptional regulation of important pro-inflammatory genes such as TNF $\alpha$  in other cell types (Brooks and Blackshear, 2013) and the fact that the roles of tristetraprolin in the heart have not been investigated extensively. Assessment of the extent to which changes in RNA expression are reflected at the level of protein could be achieved by exposing cardiomyocytes to H<sub>2</sub>O<sub>2</sub> in the presence or absence of the MAPK inhibitors used in Chapter Three, followed by immunoblotting of protein extracts with antibodies to the relevant proteins. Further studies may also seek to examine the contributions of MAPKs to cardiomyocyte gene expression in the context of oxidative stress. These experiments would employ selective inhibitors of downstream kinases such as RSKs to further dissect the roles of the MAPK cascades in regulation of global RNA expression, as employed successfully in previous cardiomyocyte studies such as that of Amirak and colleagues (Amirak et al., 2013).

It will also be important to assess the extent to which the changes in gene expression observed in neonatal cardiomyocytes occur in the whole adult heart. To investigate this, adult male rat

hearts would be perfused *ex vivo* with H<sub>2</sub>O<sub>2</sub>, in the presence or absence of MAPK inhibitors in the perfusate. This approach would provide sufficient material to permit analysis of RNA expression of selected genes using qPCR, as well as assessment of the effects of H<sub>2</sub>O<sub>2</sub> and the MAPK inhibitors on protein expression using immunoblotting.

Since ~44% of the RNAs differentially regulated in response to H<sub>2</sub>O<sub>2</sub> were unaffected by any of the MAPK inhibitors, other signalling pathways and regulatory mechanisms are clearly involved in regulation of cardiomyocyte gene expression in response oxidative stress. Further work might seek to identify the pathways and mechanisms responsible, with an initial focus on transcriptional regulators known to be responsive to oxidative stress, such as the transcription factor Nrf2 (Zhou et al., 2014).

### **6.3.2 Regulation and roles of RIPK1 in the heart**

The results of the experiments detailed in Chapter Four indicate that RIPK1 in cardiomyocytes and hearts exhibits reduced mobility in response to a number of important pathophysiological stimuli, most likely reflecting increased phosphorylation. Attempts to further investigate whether the observed effects were due to phosphorylation using adenoviruses were hindered by unforeseen difficulties in expressing full-length exogenous FLAG-tagged RIPK1 constructs. However, it may still prove possible to use the adenoviruses (detailed in Chapter Five) to identify the RIPK1 ALPS by assessing the effects of the various mutations on RIPK1 activity in *in vitro* kinase assays.

It will also be important to conduct further investigation into the regulation of RIPK1 in response to IL1 $\beta$ , a novel observation detailed in Chapter Four. Of particular interest is further examination of the potential roles of p38-MAPKs in phosphorylation of RIPK1 in response to IL1 $\beta$  stimulation. This phenomenon does not appear to have been previously reported in any system and, as a result, initial approaches using non-cardiac cell lines that are amenable to genetic manipulation are justified. For example, expression of p38-MAPK and MAPKAPKs 2

and 3 could be knocked down using siRNA or other approaches such as CRISPR-Cas9, to establish if these interventions affect the response of RIPK1 to IL1 $\beta$ . Mutational analysis, in which phosphorylatable serine or threonine residues are systematically mutated to alanine, could also be employed to determine the RIPK1 residue(s) targeted for phosphorylation by p38-MAPKs. The effect could be further investigated in cardiac cells by using an inducible cardiac-specific p38-MAPK $\alpha$  knockout mouse model, such as that described by Nishida *et al.* (Nishida et al., 2004).

## References

- Acehan, D., Jiang, X., Morgan, D. G., Heuser, J. E., Wang, X. & Akey, C. W. (2002). Three-dimensional structure of the apoptosome: implications for assembly, procaspase-9 binding, and activation. *Mol Cell*, 9, 423-32.
- Adachi, M., Fukuda, M. & Nishida, E. (1999). Two co-existing mechanisms for nuclear import of MAP kinase: passive diffusion of a monomer and active transport of a dimer. *EMBO J*, 18, 5347-58.
- Adams, J. A. (2003). Activation loop phosphorylation and catalysis in protein kinases: is there functional evidence for the autoinhibitor model? *Biochemistry*, 42, 601-7.
- Aggeli, I. K., Beis, I. & Gaitanaki, C. (2010). ERKs and JNKs mediate hydrogen peroxide-induced Egr-1 expression and nuclear accumulation in H9c2 cells. *Physiol Res*, 59, 443-54.
- Ahuja, P., Sdek, P. & Maclellan, W. R. (2007). Cardiac myocyte cell cycle control in development, disease, and regeneration. *Physiol Rev*, 87, 521-44.
- Aikawa, R., Komuro, I., Yamazaki, T., Zou, Y., Kudoh, S., Tanaka, M., Shiojima, I., Hiroi, Y. & Yazaki, Y. (1997). Oxidative stress activates extracellular signal-regulated kinases through Src and Ras in cultured cardiac myocytes of neonatal rats. *J Clin Invest*, 100, 1813-21.
- Al-Mehdi, A. B., Pastukh, V. M., Swiger, B. M., Reed, D. J., Patel, M. R., Bardwell, G. C., Pastukh, V. V., Alexeyev, M. F. & Gillespie, M. N. (2012). Perinuclear mitochondrial clustering creates an oxidant-rich nuclear domain required for hypoxia-induced transcription. *Sci Signal*, 5, ra47.
- Amirak, E., Fuller, S. J., Sugden, P. H. & Clerk, A. (2013). p90 ribosomal S6 kinases play a significant role in early gene regulation in the cardiomyocyte response to G(q)-protein-coupled receptor stimuli, endothelin-1 and alpha(1)-adrenergic receptor agonists. *Biochem J*, 450, 351-63.
- Arend, W. P., Malyak, M., Guthridge, C. J. & Gabay, C. (1998). Interleukin-1 receptor antagonist: role in biology. *Annu Rev Immunol*, 16, 27-55.
- Arola, O. J., Saraste, A., Pulkki, K., Kallajoki, M., Parvinen, M. & Voipio-Pulkki, L. M. (2000). Acute doxorubicin cardiotoxicity involves cardiomyocyte apoptosis. *Cancer Res*, 60, 1789-92.
- Ashton, K. J., Tupicoff, A., Williams-Pritchard, G., Kiessling, C. J., See Hoe, L. E., Headrick, J. P. & Peart, J. N. (2013). Unique transcriptional profile of sustained ligand-activated preconditioning in pre- and post-ischemic myocardium. *PLoS One*, 8, e72278.
- Azad, N. & Lemay, G. (2014). Management of chronic heart failure in the older population. *J Geriatr Cardiol*, 11, 329-37.
- Babior, B. M. (1984). Oxidants from phagocytes: agents of defense and destruction. *Blood*, 64, 959-66.
- Bae, Y. S., Kang, S. W., Seo, M. S., Baines, I. C., Tekle, E., Chock, P. B. & Rhee, S. G. (1997). Epidermal growth factor (EGF)-induced generation of hydrogen peroxide. Role in EGF receptor-mediated tyrosine phosphorylation. *J Biol Chem*, 272, 217-21.

- Bain, J., Plater, L., Elliott, M., Shpiro, N., Hastie, C. J., Mclauchlan, H., Klevernic, I., Arthur, J. S., Alessi, D. R. & Cohen, P. (2007). The selectivity of protein kinase inhibitors: a further update. *Biochem J*, 408, 297-315.
- Balaban, R. S., Nemoto, S. & Finkel, T. (2005). Mitochondria, oxidants, and aging. *Cell*, 120, 483-95.
- Barnouin, K., Dubuisson, M. L., Child, E. S., Fernandez De Mattos, S., Glassford, J., Medema, R. H., Mann, D. J. & Lam, E. W. (2002). H<sub>2</sub>O<sub>2</sub> induces a transient multi-phase cell cycle arrest in mouse fibroblasts through modulating cyclin D and p21Cip1 expression. *J Biol Chem*, 277, 13761-70.
- Barrett, O. P., Yndestad, A., Marshall, A. K., Sugden, P. H. & Clerk, A. (2013). The early transcriptomic response to interleukin 1beta and interleukin 33 in rat neonatal cardiomyocytes. *Cytokine*, 61, 340-4.
- Bartz, R. R. & Piantadosi, C. A. (2010). Clinical review: oxygen as a signaling molecule. *Crit Care*, 14, 234.
- Becker, L. B., Vanden Hoek, T. L., Shao, Z. H., Li, C. Q. & Schumacker, P. T. (1999). Generation of superoxide in cardiomyocytes during ischemia before reperfusion. *Am J Physiol*, 277, H2240-6.
- Beltrami, A. P., Barlucchi, L., Torella, D., Baker, M., Limana, F., Chimenti, S., Kasahara, H., Rota, M., Musso, E., Urbanek, K., Leri, A., Kajstura, J., Nadal-Ginard, B. & Anversa, P. (2003). Adult cardiac stem cells are multipotent and support myocardial regeneration. *Cell*, 114, 763-76.
- Bennett, B. L., Sasaki, D. T., Murray, B. W., O'leary, E. C., Sakata, S. T., Xu, W., Leisten, J. C., Motiwala, A., Pierce, S., Satoh, Y., Bhagwat, S. S., Manning, A. M. & Anderson, D. W. (2001). SP600125, an anthrapyrazolone inhibitor of Jun N-terminal kinase. *Proc Natl Acad Sci U S A*, 98, 13681-6.
- Berger, S. B., Kasparcova, V., Hoffman, S., Swift, B., Dare, L., Schaeffer, M., Capriotti, C., Cook, M., Finger, J., Hughes-Earle, A., Harris, P. A., Kaiser, W. J., Mocarski, E. S., Bertin, J. & Gough, P. J. (2014). Cutting Edge: RIP1 kinase activity is dispensable for normal development but is a key regulator of inflammation in SHARPIN-deficient mice. *J Immunol*, 192, 5476-80.
- Bergmann, M. W., Loser, P., Dietz, R. & Von Harsdorf, R. (2001). Effect of NF-kappa B Inhibition on TNF-alpha-induced apoptosis and downstream pathways in cardiomyocytes. *J Mol Cell Cardiol*, 33, 1223-32.
- Bertrand, M. J., Milutinovic, S., Dickson, K. M., Ho, W. C., Boudreault, A., Durkin, J., Gillard, J. W., Jaquith, J. B., Morris, S. J. & Barker, P. A. (2008). cIAP1 and cIAP2 facilitate cancer cell survival by functioning as E3 ligases that promote RIP1 ubiquitination. *Mol Cell*, 30, 689-700.
- Bird, T. A., Kyriakis, J. M., Tyshler, L., Gayle, M., Milne, A. & Virca, G. D. (1994). Interleukin-1 activates p54 mitogen-activated protein (MAP) kinase/stress-activated protein kinase by a pathway that is independent of p21ras, Raf-1, and MAP kinase kinase. *J Biol Chem*, 269, 31836-44.
- Bogoyevitch, M. A., Gillespie-Brown, J., Ketterman, A. J., Fuller, S. J., Ben-Levy, R., Ashworth, A., Marshall, C. J. & Sugden, P. H. (1996). Stimulation of the stress-activated mitogen-activated protein kinase subfamilies in perfused heart. p38/RK mitogen-activated protein

kinases and c-Jun N-terminal kinases are activated by ischemia/reperfusion. *Circ Res*, 79, 162-73.

Bogoyevitch, M. A., Glennon, P. E., Andersson, M. B., Clerk, A., Lazou, A., Marshall, C. J., Parker, P. J. & Sugden, P. H. (1994). Endothelin-1 and fibroblast growth factors stimulate the mitogen-activated protein kinase signaling cascade in cardiac myocytes. The potential role of the cascade in the integration of two signaling pathways leading to myocyte hypertrophy. *J Biol Chem*, 269, 1110-9.

Bradford, M. M. (1976). A rapid and sensitive method for the quantitation of microgram quantities of protein utilizing the principle of protein-dye binding. *Anal Biochem*, 72, 248-54.

Brikos, C., Wait, R., Begum, S., O'Neill, L. A. & Saklatvala, J. (2007). Mass spectrometric analysis of the endogenous type I interleukin-1 (IL-1) receptor signaling complex formed after IL-1 binding identifies IL-1RAcP, MyD88, and IRAK-4 as the stable components. *Mol Cell Proteomics*, 6, 1551-9.

Brondello, J. M., Brunet, A., Pouyssegur, J. & McKenzie, F. R. (1997). The dual specificity mitogen-activated protein kinase phosphatase-1 and -2 are induced by the p42/p44MAPK cascade. *J Biol Chem*, 272, 1368-76.

Brooks, S. A. & Blackshear, P. J. (2013). Tristetraprolin (TTP): interactions with mRNA and proteins, and current thoughts on mechanisms of action. *Biochim Biophys Acta*, 1829, 666-79.

Bryant, D., Becker, L., Richardson, J., Shelton, J., Franco, F., Peshock, R., Thompson, M. & Giroir, B. (1998). Cardiac failure in transgenic mice with myocardial expression of tumor necrosis factor-alpha. *Circulation*, 97, 1375-81.

Bugaisky, L. B. & Zak, R. (1989). Differentiation of adult rat cardiac myocytes in cell culture. *Circ Res*, 64, 493-500.

Buja, L. M. & Vela, D. (2008). Cardiomyocyte death and renewal in the normal and diseased heart. *Cardiovasc Pathol*, 17, 349-74.

Bujak, M., Dobaczewski, M., Chatila, K., Mendoza, L. H., Li, N., Reddy, A. & Frangogiannis, N. G. (2008). Interleukin-1 receptor type I signaling critically regulates infarct healing and cardiac remodeling. *Am J Pathol*, 173, 57-67.

Burgoyne, J. R., Mongue-Din, H., Eaton, P. & Shah, A. M. (2012). Redox signaling in cardiac physiology and pathology. *Circ Res*, 111, 1091-106.

Cai, Z., Jitkaew, S., Zhao, J., Chiang, H. C., Choksi, S., Liu, J., Ward, Y., Wu, L. G. & Liu, Z. G. (2014). Plasma membrane translocation of trimerized MLKL protein is required for TNF-induced necroptosis. *Nat Cell Biol*, 16, 55-65.

Cao, Z., Xiong, J., Takeuchi, M., Kurama, T. & Goeddel, D. V. (1996). TRAF6 is a signal transducer for interleukin-1. *Nature*, 383, 443-6.

Cargnello, M. & Roux, P. P. (2011). Activation and function of the MAPKs and their substrates, the MAPK-activated protein kinases. *Microbiol Mol Biol Rev*, 75, 50-83.

Carrera, A. C., Alexandrov, K. & Roberts, T. M. (1993). The conserved lysine of the catalytic domain of protein kinases is actively involved in the phosphotransfer reaction and not required for anchoring ATP. *Proc Natl Acad Sci U S A*, 90, 442-6.

- Casar, B., Pinto, A. & Crespo, P. (2009). ERK dimers and scaffold proteins: unexpected partners for a forgotten (cytoplasmic) task. *Cell Cycle*, 8, 1007-13.
- Cauthron, R. D., Carter, K. B., Liauw, S. & Steinberg, R. A. (1998). Physiological phosphorylation of protein kinase A at Thr-197 is by a protein kinase A kinase. *Mol Cell Biol*, 18, 1416-23.
- Cavigelli, M., Dolfi, F., Claret, F. X. & Karin, M. (1995). Induction of c-fos expression through JNK-mediated TCF/Elk-1 phosphorylation. *EMBO J*, 14, 5957-64.
- Chen, Q. M., Tu, V. C., Wu, Y. & Bahl, J. J. (2000). Hydrogen peroxide dose dependent induction of cell death or hypertrophy in cardiomyocytes. *Arch Biochem Biophys*, 373, 242-8.
- Chen, R. H., Sarnecki, C. & Blenis, J. (1992). Nuclear localization and regulation of erk- and rsk-encoded protein kinases. *Mol Cell Biol*, 12, 915-27.
- Childs, A. C., Phaneuf, S. L., Dirks, A. J., Phillips, T. & Leeuwenburgh, C. (2002). Doxorubicin treatment in vivo causes cytochrome C release and cardiomyocyte apoptosis, as well as increased mitochondrial efficiency, superoxide dismutase activity, and Bcl-2:Bax ratio. *Cancer Res*, 62, 4592-8.
- Chiong, M., Wang, Z. V., Pedrozo, Z., Cao, D. J., Troncoso, R., Ibacache, M., Criollo, A., Nemchenko, A., Hill, J. A. & Lavandero, S. (2011). Cardiomyocyte death: mechanisms and translational implications. *Cell Death Dis*, 2, e244.
- Chlopcikova, S., Psotova, J. & Miketova, P. (2001). Neonatal rat cardiomyocytes--a model for the study of morphological, biochemical and electrophysiological characteristics of the heart. *Biomed Pap Med Fac Univ Palacky Olomouc Czech Repub*, 145, 49-55.
- Cho, Y. S., Challa, S., Moquin, D., Genga, R., Ray, T. D., Guildford, M. & Chan, F. K. (2009). Phosphorylation-driven assembly of the RIP1-RIP3 complex regulates programmed necrosis and virus-induced inflammation. *Cell*, 137, 1112-23.
- Chyan, C. L., Lin, F. C., Peng, H., Yuan, J. M., Chang, C. H., Lin, S. H. & Yang, G. (2004). Reversible mechanical unfolding of single ubiquitin molecules. *Biophys J*, 87, 3995-4006.
- Clerk, A., Aggeli, I. K., Stathopoulou, K. & Sugden, P. H. (2006). Peptide growth factors signal differentially through protein kinase C to extracellular signal-regulated kinases in neonatal cardiomyocytes. *Cell Signal*, 18, 225-35.
- Clerk, A., Cole, S. M., Cullingford, T. E., Harrison, J. G., Jormakka, M. & Valks, D. M. (2003). Regulation of cardiac myocyte cell death. *Pharmacol Ther*, 97, 223-61.
- Clerk, A., Cullingford, T. E., Fuller, S. J., Giraldo, A., Markou, T., Pikkarainen, S. & Sugden, P. H. (2007a). Signaling pathways mediating cardiac myocyte gene expression in physiological and stress responses. *J Cell Physiol*, 212, 311-22.
- Clerk, A., Fuller, S. J., Michael, A. & Sugden, P. H. (1998a). Stimulation of "stress-regulated" mitogen-activated protein kinases (stress-activated protein kinases/c-Jun N-terminal kinases and p38-mitogen-activated protein kinases) in perfused rat hearts by oxidative and other stresses. *J Biol Chem*, 273, 7228-34.
- Clerk, A., Harrison, J. G., Long, C. S. & Sugden, P. H. (1999). Pro-inflammatory cytokines stimulate mitogen-activated protein kinase subfamilies, increase phosphorylation of c-Jun and

- ATF2 and upregulate c-Jun protein in neonatal rat ventricular myocytes. *J Mol Cell Cardiol*, 31, 2087-99.
- Clerk, A., Kemp, T. J., Harrison, J. G., Mullen, A. J., Barton, P. J. & Sugden, P. H. (2002). Up-regulation of c-jun mRNA in cardiac myocytes requires the extracellular signal-regulated kinase cascade, but c-Jun N-terminal kinases are required for efficient up-regulation of c-Jun protein. *Biochem J*, 368, 101-10.
- Clerk, A., Kemp, T. J., Zoumpoulidou, G. & Sugden, P. H. (2007b). Cardiac myocyte gene expression profiling during H<sub>2</sub>O<sub>2</sub>-induced apoptosis. *Physiol Genomics*, 29, 118-27.
- Clerk, A., Michael, A. & Sugden, P. H. (1998b). Stimulation of multiple mitogen-activated protein kinase sub-families by oxidative stress and phosphorylation of the small heat shock protein, HSP25/27, in neonatal ventricular myocytes. *Biochem J*, 333 ( Pt 3), 581-9.
- Clerk, A. & Sugden, P. H. (1997a). Activation of p21-activated protein kinase alpha (alpha PAK) by hyperosmotic shock in neonatal ventricular myocytes. *FEBS Lett*, 403, 23-5.
- Clerk, A. & Sugden, P. H. (1997b). Cell stress-induced phosphorylation of ATF2 and c-Jun transcription factors in rat ventricular myocytes. *Biochem J*, 325 ( Pt 3), 801-10.
- Clerk, A. & Sugden, P. H. (1998). The p38-MAPK inhibitor, SB203580, inhibits cardiac stress-activated protein kinases/c-Jun N-terminal kinases (SAPKs/JNKs). *FEBS Lett*, 426, 93-6.
- Clerk, A. & Sugden, P. H. (1999). Activation of protein kinase cascades in the heart by hypertrophic G protein-coupled receptor agonists. *Am J Cardiol*, 83, 64h-69h.
- Cook, S. A., Sugden, P. H. & Clerk, A. (1999a). Activation of c-Jun N-terminal kinases and p38-mitogen-activated protein kinases in human heart failure secondary to ischaemic heart disease. *J Mol Cell Cardiol*, 31, 1429-34.
- Cook, S. A., Sugden, P. H. & Clerk, A. (1999b). Regulation of bcl-2 family proteins during development and in response to oxidative stress in cardiac myocytes: association with changes in mitochondrial membrane potential. *Circ Res*, 85, 940-9.
- Cuadrado, A. & Nebreda, A. R. (2010). Mechanisms and functions of p38 MAPK signalling. *Biochem J*, 429, 403-17.
- Cuenda, A., Rouse, J., Doza, Y. N., Meier, R., Cohen, P., Gallagher, T. F., Young, P. R. & Lee, J. C. (1995). SB 203580 is a specific inhibitor of a MAP kinase homologue which is stimulated by cellular stresses and interleukin-1. *FEBS Lett*, 364, 229-33.
- Cullingford, T. E., Butler, M. J., Marshall, A. K., Tham El, L., Sugden, P. H. & Clerk, A. (2008a). Differential regulation of Kruppel-like factor family transcription factor expression in neonatal rat cardiac myocytes: effects of endothelin-1, oxidative stress and cytokines. *Biochim Biophys Acta*, 1783, 1229-36.
- Cullingford, T. E., Markou, T., Fuller, S. J., Giraldo, A., Pikkarainen, S., Zoumpoulidou, G., Alsafi, A., Ekere, C., Kemp, T. J., Dennis, J. L., Game, L., Sugden, P. H. & Clerk, A. (2008b). Temporal regulation of expression of immediate early and second phase transcripts by endothelin-1 in cardiomyocytes. *Genome Biol*, 9, R32.
- Czabotar, P. E., Lessene, G., Strasser, A. & Adams, J. M. (2014). Control of apoptosis by the BCL-2 protein family: implications for physiology and therapy. *Nat Rev Mol Cell Biol*, 15, 49-63.

- Davis, R. J. (1993). The mitogen-activated protein kinase signal transduction pathway. *J Biol Chem*, 268, 14553-6.
- Davis, R. J. (2000). Signal transduction by the JNK group of MAP kinases. *Cell*, 103, 239-52.
- De Almagro, M. C., Goncharov, T., Izrael-Tomasevic, A., Duttler, S., Kist, M., Varfolomeev, E., Wu, X., Lee, W. P., Murray, J., Webster, J. D., Yu, K., Kirkpatrick, D. S., Newton, K. & Vucic, D. (2017). Coordinated ubiquitination and phosphorylation of RIP1 regulates necroptotic cell death. *Cell Death Differ*, 24, 26-37.
- De Almagro, M. C., Goncharov, T., Newton, K. & Vucic, D. (2015). Cellular IAP proteins and LUBAC differentially regulate necrosome-associated RIP1 ubiquitination. *Cell Death Dis*, 6, e1800.
- Dean, J. L., Brook, M., Clark, A. R. & Saklatvala, J. (1999). p38 mitogen-activated protein kinase regulates cyclooxygenase-2 mRNA stability and transcription in lipopolysaccharide-treated human monocytes. *J Biol Chem*, 274, 264-9.
- Degterev, A., Hitomi, J., Gernscheid, M., Ch'en, I. L., Korkina, O., Teng, X., Abbott, D., Cuny, G. D., Yuan, C., Wagner, G., Hedrick, S. M., Gerber, S. A., Lugovskoy, A. & Yuan, J. (2008). Identification of RIP1 kinase as a specific cellular target of necrostatins. *Nat Chem Biol*, 4, 313-21.
- Degterev, A., Huang, Z., Boyce, M., Li, Y., Jagtap, P., Mizushima, N., Cuny, G. D., Mitchison, T. J., Moskowitz, M. A. & Yuan, J. (2005). Chemical inhibitor of nonapoptotic cell death with therapeutic potential for ischemic brain injury. *Nat Chem Biol*, 1, 112-9.
- Devin, A., Lin, Y. & Liu, Z. G. (2003). The role of the death-domain kinase RIP in tumour-necrosis-factor-induced activation of mitogen-activated protein kinases. *EMBO Rep*, 4, 623-7.
- Dewald, O., Ren, G., Duerr, G. D., Zoerlein, M., Klemm, C., Gersch, C., Tincey, S., Michael, L. H., Entman, M. L. & Frangogiannis, N. G. (2004). Of mice and dogs: species-specific differences in the inflammatory response following myocardial infarction. *Am J Pathol*, 164, 665-77.
- Dignam, J. D., Lebovitz, R. M. & Roeder, R. G. (1983). Accurate transcription initiation by RNA polymerase II in a soluble extract from isolated mammalian nuclei. *Nucleic Acids Res*, 11, 1475-89.
- Djurovic, S., Iversen, N., Jeansson, S., Hoover, F. & Christensen, G. (2004). Comparison of nonviral transfection and adeno-associated viral transduction on cardiomyocytes. *Mol Biotechnol*, 28, 21-32.
- Dondelinger, Y., Declercq, W., Montessuit, S., Roelandt, R., Goncalves, A., Bruggeman, I., Hulpiau, P., Weber, K., Sehon, C. A., Marquis, R. W., Bertin, J., Gough, P. J., Savvides, S., Martinou, J. C., Bertrand, M. J. & Vandenabeele, P. (2014). MLKL compromises plasma membrane integrity by binding to phosphatidylinositol phosphates. *Cell Rep*, 7, 971-81.
- Dondelinger, Y., Jouan-Lanhouet, S., Divert, T., Theatre, E., Bertin, J., Gough, P. J., Giansanti, P., Heck, A. J., Dejardin, E., Vandenabeele, P. & Bertrand, M. J. (2015). NF-kappaB-Independent Role of IKKalpha/IKKbeta in Preventing RIPK1 Kinase-Dependent Apoptotic and Necroptotic Cell Death during TNF Signaling. *Mol Cell*, 60, 63-76.
- Dorn, G. W., 2nd, Robbins, J. & Sugden, P. H. 2003. Phenotyping hypertrophy: eschew obfuscation. *Circ Res*, 92, 1171-5.

- Doroshov, J. H. (1983). Effect of anthracycline antibiotics on oxygen radical formation in rat heart. *Cancer Res*, 43, 460-72.
- Dumitru, C. D., Ceci, J. D., Tsatsanis, C., Kontoyiannis, D., Stamatakis, K., Lin, J. H., Patriotis, C., Jenkins, N. A., Copeland, N. G., Kollias, G. & Tsichlis, P. N. (2000). TNF-alpha induction by LPS is regulated posttranscriptionally via a Tpl2/ERK-dependent pathway. *Cell*, 103, 1071-83.
- Duprez, L., Bertrand, M. J., Vanden Berghe, T., Dondelinger, Y., Festjens, N. & Vandenabeele, P. (2012). Intermediate domain of receptor-interacting protein kinase 1 (RIPK1) determines switch between necroptosis and RIPK1 kinase-dependent apoptosis. *J Biol Chem*, 287, 14863-72.
- Ea, C. K., Deng, L., Xia, Z. P., Pineda, G. & Chen, Z. J. (2006). Activation of IKK by TNFalpha requires site-specific ubiquitination of RIP1 and polyubiquitin binding by NEMO. *Mol Cell*, 22, 245-57.
- Ellederova, Z., Cais, O., Susor, A., Uhlirva, K., Kovarova, H., Jelinkova, L., Tomek, W. & Kubelka, M. (2008). ERK1/2 map kinase metabolic pathway is responsible for phosphorylation of translation initiation factor eIF4E during in vitro maturation of pig oocytes. *Mol Reprod Dev*, 75, 309-17.
- Enslin, H., Raingeaud, J. & Davis, R. J. (1998). Selective activation of p38 mitogen-activated protein (MAP) kinase isoforms by the MAP kinase kinases MKK3 and MKK6. *J Biol Chem*, 273, 1741-8.
- Favata, M. F., Horiuchi, K. Y., Manos, E. J., Daulerio, A. J., Stradley, D. A., Feeser, W. S., Van Dyk, D. E., Pitts, W. J., Earl, R. A., Hobbs, F., Copeland, R. A., Magolda, R. L., Scherle, P. A. & Trzaskos, J. M. (1998). Identification of a novel inhibitor of mitogen-activated protein kinase kinase. *J Biol Chem*, 273, 18623-32.
- Finkel, T. (2011). Signal transduction by reactive oxygen species. *J Cell Biol*, 194, 7-15.
- Finn, S. G., Dickens, M. & Fuller, S. J. (2001). c-Jun N-terminal kinase-interacting protein 1 inhibits gene expression in response to hypertrophic agonists in neonatal rat ventricular myocytes. *Biochem J*, 358, 489-95.
- Foltz, I. N., Gerl, R. E., Wieler, J. S., Luckach, M., Salmon, R. A. & Schrader, J. W. (1998). Human mitogen-activated protein kinase kinase 7 (MKK7) is a highly conserved c-Jun N-terminal kinase/stress-activated protein kinase (JNK/SAPK) activated by environmental stresses and physiological stimuli. *J Biol Chem*, 273, 9344-51.
- Frantz B, Klatt T, Pang M, Parsons J, Rolando A, Williams H, Tocci M. J., O'Keefe S. J. & O'Neill E. A. (1998). The activation state of p38 mitogen-activated protein kinase determines the efficiency of ATP competition for pyridinylimidazole inhibitor binding. *Biochemistry* 37, 13846-53.
- Fuchs, S. Y., Adler, V., Buschmann, T., Yin, Z., Wu, X., Jones, S. N. & Ronai, Z. (1998). JNK targets p53 ubiquitination and degradation in nonstressed cells. *Genes Dev*, 12, 2658-63.
- Fuller, S. J., McGuffin, L. J., Marshall, A. K., Giraldo, A., Pikkarainen, S., Clerk, A. & Sugden, P. H. (2012). A novel non-canonical mechanism of regulation of MST3 (mammalian Sterile20-related kinase 3). *Biochem J*, 442, 595-610.

- Fuller, S. J., Osborne, S. A., Leonard, S. J., Hardyman, M. A., Vaniotis, G., Allen, B. G., Sugden, P. H. & Clerk, A. (2015). Cardiac protein kinases: the cardiomyocyte kinome and differential kinase expression in human failing hearts. *Cardiovasc Res*, 108, 87-98.
- Fuller, S. J., Pikkarainen, S., Tham El, L., Cullingford, T. E., Molkentin, J. D., Cornils, H., Hergovich, A., Hemmings, B. A., Clerk, A. & Sugden, P. H. (2008). Nuclear Dbf2-related protein kinases (NDRs) in isolated cardiac myocytes and the myocardium: activation by cellular stresses and by phosphoprotein serine-/threonine-phosphatase inhibitors. *Cell Signal*, 20, 1564-77.
- Gaillard, P., Jeanclaude-Etter, I., Ardisson, V., Arkinstall, S., Cambet, Y., Camps, M., Chabert, C., Church, D., Cirillo, R., Gretener, D., Halazy, S., Nichols, A., Szyndralewicz, C., Vitte, P. A. & Gotteland, J. P. (2005). Design and synthesis of the first generation of novel potent, selective, and in vivo active (benzothiazol-2-yl)acetonitrile inhibitors of the c-Jun N-terminal kinase. *J Med Chem*, 48, 4596-607.
- Gandhi, M. S., Kamalov, G., Shahbaz, A. U., Bhattacharya, S. K., Ahokas, R. A., Sun, Y., Gerling, I. C. & Weber, K. T. (2011). Cellular and molecular pathways to myocardial necrosis and replacement fibrosis. *Heart Fail Rev*, 16, 23-34.
- Garcia-Santamarina, S., Boronat, S. & Hidalgo, E. (2014). Reversible cysteine oxidation in hydrogen peroxide sensing and signal transduction. *Biochemistry*, 53, 2560-80.
- Garcia, L., Garcia, F., Llorens, F., Unzeta, M., Itarte, E. & Gomez, N. (2002). PP1/PP2A phosphatases inhibitors okadaic acid and calyculin A block ERK5 activation by growth factors and oxidative stress. *FEBS Lett*, 523, 90-4.
- Garlanda, C., Dinarello, C. A. & Mantovani, A. (2013). The interleukin-1 family: back to the future. *Immunity*, 39, 1003-18.
- Gerlach, B., Cordier, S. M., Schmukle, A. C., Emmerich, C. H., Rieser, E., Haas, T. L., Webb, A. I., Rickard, J. A., Anderton, H., Wong, W. W., Nachbur, U., Gangoda, L., Warnken, U., Purcell, A. W., Silke, J. & Walczak, H. (2011). Linear ubiquitination prevents inflammation and regulates immune signalling. *Nature*, 471, 591-6.
- Godl, K., Wissing, J., Kurtenbach, A., Habenberger, P., Blencke, S., Gutbrod, H., Salassidis, K., Stein-Gerlach, M., Missio, A., Cotten, M. & Daub, H. (2003). An efficient proteomics method to identify the cellular targets of protein kinase inhibitors. *Proc Natl Acad Sci U S A*, 100, 15434-9.
- Gough, D. R. & Cotter, T. G. (2011). Hydrogen peroxide: a Jekyll and Hyde signalling molecule. *Cell Death Dis*, 2, e213.
- Haas, T. L., Emmerich, C. H., Gerlach, B., Schmukle, A. C., Cordier, S. M., Rieser, E., Feltham, R., Vince, J., Warnken, U., Wenger, T., Koschny, R., Komander, D., Silke, J. & Walczak, H. (2009). Recruitment of the linear ubiquitin chain assembly complex stabilizes the TNF-R1 signaling complex and is required for TNF-mediated gene induction. *Mol Cell*, 36, 831-44.
- Halestrap, A. P., Clarke, S. J. & Javadov, S. A. (2004). Mitochondrial permeability transition pore opening during myocardial reperfusion--a target for cardioprotection. *Cardiovasc Res*, 61, 372-85.
- Hall-Jackson, C. A., Goedert, M., Hedge, P. & Cohen, P. (1999). Effect of SB 203580 on the activity of c-Raf in vitro and in vivo. *Oncogene*, 18, 2047-54.

- Hamid, T., Gu, Y., Ortines, R. V., Bhattacharya, C., Wang, G., Xuan, Y. T. & Prabhu, S. D. (2009). Divergent tumor necrosis factor receptor-related remodeling responses in heart failure: role of nuclear factor-kappaB and inflammatory activation. *Circulation*, 119, 1386-97.
- Haq, S., Choukroun, G., Lim, H., Tymitz, K. M., Del Monte, F., Gwathmey, J., Grazette, L., Michael, A., Hajjar, R., Force, T. & Molkenin, J. D. (2001). Differential activation of signal transduction pathways in human hearts with hypertrophy versus advanced heart failure. *Circulation*, 103, 670-7.
- Harman, D. (1956). Aging: a theory based on free radical and radiation chemistry. *J Gerontol*, 11, 298-300.
- Harpster, M. H., Bandyopadhyay, S., Thomas, D. P., Ivanov, P. S., Keele, J. A., Pineguina, N., Gao, B., Amarendran, V., Gomelsky, M., McCormick, R. J. & Stayton, M. M. (2006). Earliest changes in the left ventricular transcriptome postmyocardial infarction. *Mamm Genome*, 17, 701-15.
- Haudek, S. B., Taffet, G. E., Schneider, M. D. & Mann, D. L. (2007). TNF provokes cardiomyocyte apoptosis and cardiac remodeling through activation of multiple cell death pathways. *J Clin Invest*, 117, 2692-701.
- Hausenloy, D. J. & Yellon, D. M. (2013). Myocardial ischemia-reperfusion injury: a neglected therapeutic target. *J Clin Invest*, 123, 92-100.
- Hazzalin, C. A., Cano, E., Cuenda, A., Barratt, M. J., Cohen, P. & Mahadevan, L. C. (1996). p38/RK is essential for stress-induced nuclear responses: JNK/SAPKs and c-Jun/ATF-2 phosphorylation are insufficient. *Curr Biol*, 6, 1028-31.
- He, S., Liang, Y., Shao, F. & Wang, X. (2011). Toll-like receptors activate programmed necrosis in macrophages through a receptor-interacting kinase-3-mediated pathway. *Proc Natl Acad Sci U S A*, 108, 20054-9.
- He, S., Wang, L., Miao, L., Wang, T., Du, F., Zhao, L. & Wang, X. (2009). Receptor interacting protein kinase-3 determines cellular necrotic response to TNF-alpha. *Cell*, 137, 1100-11.
- Hearse, D. J., Humphrey, S. M. & Chain, E. B. (1973). Abrupt reoxygenation of the anoxic potassium-arrested perfused rat heart: a study of myocardial enzyme release. *J Mol Cell Cardiol*, 5, 395-407.
- Hecht, D. & Zick, Y. (1992). Selective inhibition of protein tyrosine phosphatase activities by H<sub>2</sub>O<sub>2</sub> and vanadate in vitro. *Biochem Biophys Res Commun*, 188, 773-9.
- Hedayat, M., Mahmoudi, M. J., Rose, N. R. & Rezaei, N. (2010). Proinflammatory cytokines in heart failure: double-edged swords. *Heart Fail Rev*, 15, 543-62.
- Herskowitz, A., Choi, S., Ansari, A. A. & Wesselingh, S. (1995). Cytokine mRNA expression in postischemic/reperfused myocardium. *Am J Pathol*, 146, 419-28.
- Hibi, M., Lin, A., Smeal, T., Minden, A. & Karin, M. (1993). Identification of an oncoprotein- and UV-responsive protein kinase that binds and potentiates the c-Jun activation domain. *Genes Dev*, 7, 2135-48.
- Higuchi, Y., Mctiernan, C. F., Frye, C. B., MCGowan, B. S., Chan, T. O. & Feldman, A. M. (2004). Tumor necrosis factor receptors 1 and 2 differentially regulate survival, cardiac

dysfunction, and remodeling in transgenic mice with tumor necrosis factor-alpha-induced cardiomyopathy. *Circulation*, 109, 1892-7.

Hildebrand, J. M., Tanzer, M. C., Lucet, I. S., Young, S. N., Spall, S. K., Sharma, P., Pierotti, C., Garnier, J. M., Dobson, R. C., Webb, A. I., Tripaydonis, A., Babon, J. J., Mulcair, M. D., Scanlon, M. J., Alexander, W. S., Wilks, A. F., Czabotar, P. E., Lessene, G., Murphy, J. M. & Silke, J. (2014). Activation of the pseudokinase MLKL unleashes the four-helix bundle domain to induce membrane localization and necroptotic cell death. *Proc Natl Acad Sci U S A*, 111, 15072-7.

Hitti, E., Iakovleva, T., Brook, M., Deppenmeier, S., Gruber, A. D., Radzioch, D., Clark, A. R., Blackshear, P. J., Kotlyarov, A. & Gaestel, M. (2006). Mitogen-activated protein kinase-activated protein kinase 2 regulates tumor necrosis factor mRNA stability and translation mainly by altering tristetraprolin expression, stability, and binding to adenine/uridine-rich element. *Mol Cell Biol*, 26, 2399-407.

Ho, C. Y., Lopez, B., Coelho-Filho, O. R., Lakdawala, N. K., Cirino, A. L., Jarolim, P., Kwong, R., Gonzalez, A., Colan, S. D., Seidman, J. G., Diez, J. & Seidman, C. E. (2010). Myocardial fibrosis as an early manifestation of hypertrophic cardiomyopathy. *N Engl J Med*, 363, 552-63.

Holler, N., Zaru, R., Micheau, O., Thome, M., Attinger, A., Valitutti, S., Bodmer, J. L., Schneider, P., Seed, B. & Tschopp, J. (2000). Fas triggers an alternative, caspase-8-independent cell death pathway using the kinase RIP as effector molecule. *Nat Immunol*, 1, 489-95.

Hong, F., Kwon, S. J., Jhun, B. S., Kim, S. S., Ha, J., Kim, S. J., Sohn, N. W., Kang, C. & Kang, I. (2001). Insulin-like growth factor-1 protects H9c2 cardiac myoblasts from oxidative stress-induced apoptosis via phosphatidylinositol 3-kinase and extracellular signal-regulated kinase pathways. *Life Sci*, 68, 1095-105.

Hsu, H., Huang, J., Shu, H. B., Baichwal, V. & Goeddel, D. V. (1996). TNF-dependent recruitment of the protein kinase RIP to the TNF receptor-1 signaling complex. *Immunity*, 4, 387-96.

Huang, C. Y. & Tan, T. H. (2012). DUSPs, to MAP kinases and beyond. *Cell Biosci*, 2, 24.

Huttemann, M., Pecina, P., Rainbolt, M., Sanderson, T. H., Kagan, V. E., Samavati, L., Doan, J. W. & Lee, I. (2011). The multiple functions of cytochrome c and their regulation in life and death decisions of the mammalian cell: From respiration to apoptosis. *Mitochondrion*, 11, 369-81.

Jacobs, M., Staufenberger, S., Gergs, U., Meuter, K., Brandstatter, K., Hafner, M., Ertl, G. & Schorb, W. (1999). Tumor necrosis factor-alpha at acute myocardial infarction in rats and effects on cardiac fibroblasts. *J Mol Cell Cardiol*, 31, 1949-59.

Jouan-Lanhouet, S., Arshad, M. I., Piquet-Pellorce, C., Martin-Chouly, C., Le Moigne-Muller, G., Van Herreweghe, F., Takahashi, N., Sergent, O., Lagadic-Gossmann, D., Vandenabeele, P., Samson, M. & Dimanche-Boitrel, M. T. (2012). TRAIL induces necroptosis involving RIPK1/RIPK3-dependent PARP-1 activation. *Cell Death Differ*, 19, 2003-14.

Kaludercic, N., Deshwal, S. & Di Lisa, F. (2014). Reactive oxygen species and redox compartmentalization. *Front Physiol*, 5, 285.

- Kanayama, A., Seth, R. B., Sun, L., Ea, C. K., Hong, M., Shaito, A., Chiu, Y. H., Deng, L. & Chen, Z. J. (2004). TAB2 and TAB3 activate the NF-kappaB pathway through binding to polyubiquitin chains. *Mol Cell*, 15, 535-48.
- Kang, P. M., Haunstetter, A., Aoki, H., Usheva, A. & Izumo, S. (2000). Morphological and molecular characterization of adult cardiomyocyte apoptosis during hypoxia and reoxygenation. *Circ Res*, 87, 118-25.
- Kaya, A., Lee, B. C. & Gladyshev, V. N. (2015). Regulation of protein function by reversible methionine oxidation and the role of selenoprotein MsrB1. *Antioxid Redox Signal*, 23, 814-22.
- Kelliher, M. A., Grimm, S., Ishida, Y., Kuo, F., Stanger, B. Z. & Leder, P. (1998). The death domain kinase RIP mediates the TNF-induced NF-kappaB signal. *Immunity*, 8, 297-303.
- Kemp, T. J., Causton, H. C. & Clerk, A. (2003). Changes in gene expression induced by H(2)O(2) in cardiac myocytes. *Biochem Biophys Res Commun*, 307, 416-21.
- Kennedy, R. A., Kemp, T. J., Sugden, P. H. & Clerk, A. (2006). Using U0126 to dissect the role of the extracellular signal-regulated kinase 1/2 (ERK1/2) cascade in the regulation of gene expression by endothelin-1 in cardiac myocytes. *J Mol Cell Cardiol*, 41, 236-47.
- Kim, H. A. & Song, Y. W. (2002). TNF-alpha-mediated apoptosis in chondrocytes sensitized by MG132 or actinomycin D. *Biochem Biophys Res Commun*, 295, 937-44.
- Konstantinidis, K., Whelan, R. S. & Kitsis, R. N. (2012). Mechanisms of cell death in heart disease. *Arterioscler Thromb Vasc Biol*, 32, 1552-62.
- Koshinuma, S., Miyamae, M., Kaneda, K., Kotani, J. & Figueredo, V. M. (2014). Combination of necroptosis and apoptosis inhibition enhances cardioprotection against myocardial ischemia-reperfusion injury. *J Anesth*, 28, 235-41.
- Kotamraju, S., Konorev, E. A., Joseph, J. & Kalyanaraman, B. (2000). Doxorubicin-induced apoptosis in endothelial cells and cardiomyocytes is ameliorated by nitron spin traps and ebselen. Role of reactive oxygen and nitrogen species. *J Biol Chem*, 275, 33585-92.
- Koudstaal, S., Oerlemans, M. I., Van Der Spoel, T. I., Janssen, A. W., Hofer, I. E., Doevendans, P. A., Sluijter, J. P. & Chamuleau, S. A. (2015). Necrostatin-1 alleviates reperfusion injury following acute myocardial infarction in pigs. *Eur J Clin Invest*, 45, 150-9.
- Kovalenko, A., Chable-Bessia, C., Cantarella, G., Israel, A., Wallach, D. & Courtois, G. (2003). The tumour suppressor CYLD negatively regulates NF-kappaB signalling by deubiquitination. *Nature*, 424, 801-5.
- Krenning, G., Zeisberg, E. M. & Kalluri, R. (2010). The origin of fibroblasts and mechanism of cardiac fibrosis. *J Cell Physiol*, 225, 631-7.
- Kreuz, S., Siegmund, D., Scheurich, P. & Wajant, H. (2001). NF-kappaB inducers upregulate cFLIP, a cycloheximide-sensitive inhibitor of death receptor signaling. *Mol Cell Biol*, 21, 3964-73.
- Krown, K. A., Page, M. T., Nguyen, C., Zechner, D., Gutierrez, V., Comstock, K. L., Glembotski, C. C., Quintana, P. J. & Sabbadini, R. A. (1996). Tumor necrosis factor alpha-induced apoptosis in cardiac myocytes. Involvement of the sphingolipid signaling cascade in cardiac cell death. *J Clin Invest*, 98, 2854-65.

- Kubota, T., Mctiernan, C. F., Frye, C. S., Demetris, A. J. & Feldman, A. M. (1997a). Cardiac-specific overexpression of tumor necrosis factor-alpha causes lethal myocarditis in transgenic mice. *J Card Fail*, 3, 117-24.
- Kubota, T., Mctiernan, C. F., Frye, C. S., Slawson, S. E., Lemster, B. H., Koretsky, A. P., Demetris, A. J. & Feldman, A. M. (1997b). Dilated cardiomyopathy in transgenic mice with cardiac-specific overexpression of tumor necrosis factor-alpha. *Circ Res*, 81, 627-35.
- Kumar, S., Mcdonnell, P. C., Gum, R. J., Hand, A. T., Lee, J. C. & Young, P. R. (1997). Novel homologues of CSBP/p38 MAP kinase: activation, substrate specificity and sensitivity to inhibition by pyridinyl imidazoles. *Biochem Biophys Res Commun*, 235, 533-8.
- Kwon, S. H., Pimentel, D. R., Remondino, A., Sawyer, D. B. & Colucci, W. S. (2003). H(2)O(2) regulates cardiac myocyte phenotype via concentration-dependent activation of distinct kinase pathways. *J Mol Cell Cardiol*, 35, 615-21.
- Kyriakis, J. M. & Avruch, J. (1990). pp54 microtubule-associated protein 2 kinase. A novel serine/threonine protein kinase regulated by phosphorylation and stimulated by poly-L-lysine. *J Biol Chem*, 265, 17355-63.
- Laderoute, K. R. & Webster, K. A. (1997). Hypoxia/reoxygenation stimulates Jun kinase activity through redox signaling in cardiac myocytes. *Circ Res*, 80, 336-44.
- Laflamme, M. A. & Murry, C. E. (2011). Heart regeneration. *Nature*, 473, 326-35.
- Lambeth, J. D. (2004). NOX enzymes and the biology of reactive oxygen. *Nat Rev Immunol*, 4, 181-9.
- Lawler, S., Fleming, Y., Goedert, M. & Cohen, P. (1998). Synergistic activation of SAPK1/JNK1 by two MAP kinase kinases in vitro. *Curr Biol*, 8, 1387-90.
- Lazou, A., Sugden, P. H. & Clerk, A. (1998). Activation of mitogen-activated protein kinases (p38-MAPKs, SAPKs/JNKs and ERKs) by the G-protein-coupled receptor agonist phenylephrine in the perfused rat heart. *Biochem J*, 332 ( Pt 2), 459-65.
- Lee, J. D., Ulevitch, R. J. & Han, J. (1996) Primary structure of BMK1: a new mammalian map kinase. *Biochem Biophys Res Commun*. 213(2) 515-24.
- Lee, K. & Esselman, W. J. (2002). Inhibition of PTPs by H(2)O(2) regulates the activation of distinct MAPK pathways. *Free Radic Biol Med*, 33, 1121-32.
- Lee, S. R., Kwon, K. S., Kim, S. R. & Rhee, S. G. (1998). Reversible inactivation of protein-tyrosine phosphatase 1B in A431 cells stimulated with epidermal growth factor. *J Biol Chem*, 273, 15366-72.
- Lee, T. H., Shank, J., Cusson, N. & Kelliher, M. A. (2004). The kinase activity of Rip1 is not required for tumor necrosis factor-alpha-induced I kappa B kinase or p38 MAP kinase activation or for the ubiquitination of Rip1 by Traf2. *J Biol Chem*, 279, 33185-91.
- Levine, B., Kalman, J., Mayer, L., Fillit, H. M. & Packer, M. (1990). Elevated circulating levels of tumor necrosis factor in severe chronic heart failure. *N Engl J Med*, 323, 236-41.
- Li, H., Kobayashi, M., Blonska, M., You, Y. & Lin, X. (2006). Ubiquitination of RIP is required for tumor necrosis factor alpha-induced NF-kappaB activation. *J Biol Chem*, 281, 13636-43.

- Li, J., Mcquade, T., Siemer, A. B., Napetschnig, J., Moriwaki, K., Hsiao, Y. S., Damko, E., Moquin, D., Walz, T., Mcdermott, A., Chan, F. K. & Wu, H. (2012). The RIP1/RIP3 necrosome forms a functional amyloid signaling complex required for programmed necrosis. *Cell*, 150, 339-50.
- Li, L., Chen, Y., Doan, J., Murray, J., Molkentin, J. D. & Liu, Q. (2014). Transforming growth factor beta-activated kinase 1 signaling pathway critically regulates myocardial survival and remodeling. *Circulation*, 130, 2162-72.
- Li, M. & Beg, A. A. (2000). Induction of necrotic-like cell death by tumor necrosis factor alpha and caspase inhibitors: novel mechanism for killing virus-infected cells. *J Virol*, 74, 7470-7.
- Li, X., Moody, M. R., Engel, D., Walker, S., Clubb, F. J., Jr., Sivasubramanian, N., Mann, D. L. & Reid, M. B. (2000). Cardiac-specific overexpression of tumor necrosis factor-alpha causes oxidative stress and contractile dysfunction in mouse diaphragm. *Circulation*, 102, 1690-6.
- Liang, Q., Bueno, O. F., Wilkins, B. J., Kuan, C. Y., Xia, Y. & Molkentin, J. D. (2003). c-Jun N-terminal kinases (JNK) antagonize cardiac growth through cross-talk with calcineurin-NFAT signaling. *EMBO J*, 22, 5079-89.
- Liang, Q. & Molkentin, J. D. (2003). Redefining the roles of p38 and JNK signaling in cardiac hypertrophy: dichotomy between cultured myocytes and animal models. *J Mol Cell Cardiol*, 35, 1385-94.
- Liao, P., Georgakopoulos, D., Kovacs, A., Zheng, M., Lerner, D., Pu, H., Saffitz, J., Chien, K., Xiao, R. P., Kass, D. A. & Wang, Y. (2001). The in vivo role of p38 MAP kinases in cardiac remodeling and restrictive cardiomyopathy. *Proc Natl Acad Sci U S A*, 98, 12283-8.
- Lim, S. Y., Davidson, S. M., Mocanu, M. M., Yellon, D. M. & Smith, C. C. (2007). The cardioprotective effect of necrostatin requires the cyclophilin-D component of the mitochondrial permeability transition pore. *Cardiovasc Drugs Ther*, 21, 467-9.
- Lin, Y., Devin, A., Rodriguez, Y. & Liu, Z. G. (1999). Cleavage of the death domain kinase RIP by caspase-8 prompts TNF-induced apoptosis. *Genes Dev*, 13, 2514-26.
- Lingel, A., Weiss, T. M., Niebuhr, M., Pan, B., Appleton, B. A., Wiesmann, C., Bazan, J. F. & Fairbrother, W. J. (2009). Structure of IL-33 and its interaction with the ST2 and IL-1RACp receptors--insight into heterotrimeric IL-1 signaling complexes. *Structure*, 17, 1398-410.
- Linkermann, A., Brasen, J. H., Himmerkus, N., Liu, S., Huber, T. B., Kunzendorf, U. & Krautwald, S. (2012). Rip1 (receptor-interacting protein kinase 1) mediates necroptosis and contributes to renal ischemia/reperfusion injury. *Kidney Int*, 81, 751-61.
- Liu, Q., Sabnis, Y., Zhao, Z., Zhang, T., Buhrlage, S. J., Jones, L. H. & Gray, N. S. (2013). Developing irreversible inhibitors of the protein kinase cysteinome. *Chem Biol*, 20, 146-59.
- Liu, Z. G., Hsu, H., Goeddel, D. V. & Karin, M. (1996). Dissection of TNF receptor 1 effector functions: JNK activation is not linked to apoptosis while NF-kappaB activation prevents cell death. *Cell*, 87, 565-76.
- Locksley, R. M., Killeen, N. & Lenardo, M. J. (2001). The TNF and TNF receptor superfamilies: integrating mammalian biology. *Cell*, 104, 487-501.
- Lozano, F., Alberola-Ila, J., Places, L., Gallart, T. & Vives, J. (1990). Phosphorylation-mediated changes in the electrophoretic mobility of CD5 molecules. *Eur J Biochem*, 193, 469-77.

- Luedde, M., Lutz, M., Carter, N., Sosna, J., Jacoby, C., Vucur, M., Gautheron, J., Roderburg, C., Borg, N., Reisinger, F., Hippe, H.-J., Linkermann, A., Wolf, M. J., Rose-John, S., Lüllmann-Rauch, R., Adam, D., Flögel, U., Heikenwalder, M., Luedde, T. & Frey, N. (2014). RIP3, a kinase promoting necroptotic cell death, mediates adverse remodelling after myocardial infarction. *Cardiovasc Res*, 103, 206-16
- Luheshi, N. M., Rothwell, N. J. & Brough, D. (2009). Dual functionality of interleukin-1 family cytokines: implications for anti-interleukin-1 therapy. *Br J Pharmacol*, 157, 1318-29.
- Marber, M. S., Rose, B. & Wang, Y. (2011). The p38 mitogen-activated protein kinase pathway—a potential target for intervention in infarction, hypertrophy, and heart failure. *J Mol Cell Cardiol*, 51, 485-90.
- Marderosian, M., Sharma, A., Funk, A. P., Vartanian, R., Masri, J., Jo, O. D. & Gera, J. F. (2006). Tristetraprolin regulates Cyclin D1 and c-Myc mRNA stability in response to rapamycin in an Akt-dependent manner via p38 MAPK signaling. *Oncogene*, 25, 6277-90.
- Marshall, A. K., Barrett, O. P., Cullingford, T. E., Shanmugasundram, A., Sugden, P. H. & Clerk, A. (2010). ERK1/2 signaling dominates over RhoA signaling in regulating early changes in RNA expression induced by endothelin-1 in neonatal rat cardiomyocytes. *PLoS One*, 5, e10027.
- Martel, G., Berube, J. & Rousseau, S. (2013). The protein kinase TPL2 is essential for ERK1/ERK2 activation and cytokine gene expression in airway epithelial cells exposed to pathogen-associated molecular patterns (PAMPs). *PLoS One*, 8, e59116.
- Martin, J. L., Avkiran, M., Quinlan, R. A., Cohen, P. & Marber, M. S. (2001). Antiischemic effects of SB203580 are mediated through the inhibition of p38alpha mitogen-activated protein kinase: Evidence from ectopic expression of an inhibition-resistant kinase. *Circ Res*, 89, 750-2.
- Masuda, K., Ripley, B., Nishimura, R., Mino, T., Takeuchi, O., Shioi, G., Kiyonari, H. & Kishimoto, T. (2013). Arid5a controls IL-6 mRNA stability, which contributes to elevation of IL-6 level in vivo. *Proc Natl Acad Sci U S A*, 110, 9409-14.
- Matsui, T., Nagoshi, T. & Rosenzweig, A. (2003). Akt and PI 3-kinase signaling in cardiomyocyte hypertrophy and survival. *Cell Cycle*, 2, 220-3.
- May, G. H., Allen, K. E., Clark, W., Funk, M. & Gillespie, D. A. (1998). Analysis of the interaction between c-Jun and c-Jun N-terminal kinase in vivo. *J Biol Chem*, 273, 33429-35.
- Mccully, J. D., Wakiyama, H., Hsieh, Y. J., Jones, M. & Levitsky, S. (2004). Differential contribution of necrosis and apoptosis in myocardial ischemia-reperfusion injury. *Am J Physiol Heart Circ Physiol*, 286, H1923-35.
- Mcilwain, D. R., Berger, T. & Mak, T. W. (2013). Caspase functions in cell death and disease. *Cold Spring Harb Perspect Biol*, 5, a008656.
- Mcmurray, J., Abdullah, I., Dargie, H. J. & Shapiro, D. (1991). Increased concentrations of tumour necrosis factor in "cachectic" patients with severe chronic heart failure. *Br Heart J*, 66, 356-8.
- Mcquade, T., Cho, Y. & Chan, F. K. (2013). Positive and negative phosphorylation regulates RIP1- and RIP3-induced programmed necrosis. *Biochem J*, 456, 409-15.

- Medzhitov, R. & Horng, T. (2009). Transcriptional control of the inflammatory response. *Nat Rev Immunol*, 9, 692-703.
- Meng, T. C., Fukada, T. & Tonks, N. K. (2002). Reversible oxidation and inactivation of protein tyrosine phosphatases in vivo. *Mol Cell*, 9, 387-99.
- Mi, H., Muruganujan, A., Casagrande, J.T. & Thomas, P.D. (2013). Large-scale gene function analysis with the PANTHER classification system. *Nat Protoc*, 8, 1551-66.
- Micheau, O., Lens, S., Gaide, O., Alevizopoulos, K. & Tschopp, J. (2001). NF-kappaB signals induce the expression of c-FLIP. *Mol Cell Biol*, 21, 5299-305.
- Micheau, O. & Tschopp, J. (2003). Induction of TNF receptor I-mediated apoptosis via two sequential signaling complexes. *Cell*, 114, 181-90.
- Mizukami, Y., Yoshioka, K., Morimoto, S. & Yoshida, K. (1997). A novel mechanism of JNK1 activation. Nuclear translocation and activation of JNK1 during ischemia and reperfusion. *J Biol Chem*, 272, 16657-62.
- Mody, N., Leitch, J., Armstrong, C., Dixon, J. & Cohen, P. (2001). Effects of MAP kinase cascade inhibitors on the MKK5/ERK5 pathway. *FEBS Lett*, 502, 21-4.
- Monden, Y., Kubota, T., Inoue, T., Tsutsumi, T., Kawano, S., Ide, T., Tsutsui, H. & Sunagawa, K. (2007). Tumor necrosis factor-alpha is toxic via receptor 1 and protective via receptor 2 in a murine model of myocardial infarction. *Am J Physiol Heart Circ Physiol*, 293, H743-53.
- Montezano, A. C. & Touyz, R. M. (2012). Reactive oxygen species and endothelial function--role of nitric oxide synthase uncoupling and Nox family nicotinamide adenine dinucleotide phosphate oxidases. *Basic Clin Pharmacol Toxicol*, 110, 87-94.
- Murry, C. E., Jennings, R. B. & Reimer, K. A. (1986). Preconditioning with ischemia: a delay of lethal cell injury in ischemic myocardium. *Circulation*, 74, 1124-36.
- Nadruz, W. (2015). Myocardial remodeling in hypertension. *J Hum Hypertens*, 29, 1-6.
- Newton, K., Dugger, D. L., Maltzman, A., Greve, J. M., Hedehus, M., Martin-McNulty, B., Carano, R. A., Cao, T. C., Van Bruggen, N., Bernstein, L., Lee, W. P., Wu, X., Devoss, J., Zhang, J., Jeet, S., Peng, I., Mckenzie, B. S., Roose-Girma, M., Caplazi, P., Diehl, L., Webster, J. D. & Vucic, D. (2016a). RIPK3 deficiency or catalytically inactive RIPK1 provides greater benefit than MLKL deficiency in mouse models of inflammation and tissue injury. *Cell Death Differ*, 23, 1565-76.
- Newton, K., Dugger, D. L., Wickliffe, K. E., Kapoor, N., De Almagro, M. C., Vucic, D., Komuves, L., Ferrando, R. E., French, D. M., Webster, J., Roose-Girma, M., Warming, S. & Dixit, V. M. (2014). Activity of protein kinase RIPK3 determines whether cells die by necroptosis or apoptosis. *Science*, 343, 1357-60.
- Newton, K., Wickliffe, K. E., Maltzman, A., Dugger, D. L., Strasser, A., Pham, V. C., Lill, J. R., Roose-Girma, M., Warming, S., Solon, M., Ngu, H., Webster, J. D. & Dixit, V. M. (2016b). RIPK1 inhibits ZBP1-driven necroptosis during development. *Nature*, 540, 129-133.
- Nishida, K., Yamaguchi, O., Hirotani, S., Hikoso, S., Higuchi, Y., Watanabe, T., Takeda, T., Osuka, S., Morita, T., Kondoh, G., Uno, Y., Kashiwase, K., Taniike, M., Nakai, A., Matsumura, Y., Miyazaki, J., Sudo, T., Hongo, K., Kusakari, Y., Kurihara, S., Chien, K. R., Takeda, J., Hori, M. & Otsu, K. (2004). p38alpha mitogen-activated protein kinase plays a critical role in

- cardiomyocyte survival but not in cardiac hypertrophic growth in response to pressure overload. *Mol Cell Biol*, 24, 10611-20.
- O'donnell, M. A., Legarda-Addison, D., Skountzos, P., Yeh, W. C. & Ting, A. T. (2007). Ubiquitination of RIP1 regulates an NF-kappaB-independent cell-death switch in TNF signaling. *Curr Biol*, 17, 418-24.
- Oberpriller, J. O. & Oberpriller, J. C. (1974). Response of the adult newt ventricle to injury. *J Exp Zool*, 187, 249-53.
- Oerlemans, M. I., Liu, J., Arslan, F., Den Ouden, K., Van Middelaar, B. J., Doevendans, P. A. & Sluijter, J. P. (2012). Inhibition of RIP1-dependent necrosis prevents adverse cardiac remodeling after myocardial ischemia-reperfusion in vivo. *Basic Res Cardiol*, 107, 270.
- Ofengeim, D., Ito, Y., Najafov, A., Zhang, Y., Shan, B., Dewitt, J. P., Ye, J., Zhang, X., Chang, A., Vakifahmetoglu-Norberg, H., Geng, J., Py, B., Zhou, W., Amin, P., Berlink Lima, J., Qi, C., Yu, Q., Trapp, B. & Yuan, J. (2015). Activation of necroptosis in multiple sclerosis. *Cell Rep*, 10, 1836-49.
- Ofengeim, D. & Yuan, J. (2013). Regulation of RIP1 kinase signalling at the crossroads of inflammation and cell death. *Nat Rev Mol Cell Biol*, 14, 727-36.
- Ohren, J. F., Chen, H., Pavlovsky, A., Whitehead, C., Zhang, E., Kuffa, P., Yan, C., Mcconnell, P., Spessard, C., Banotai, C., Mueller, W. T., Delaney, A., Omer, C., Sebolt-Leopold, J., Dudley, D. T., Leung, I. K., Flamme, C., Warmus, J., Kaufman, M., Barrett, S., Tecle, H. & Hasemann, C. A. (2004). Structures of human MAP kinase kinase 1 (MEK1) and MEK2 describe novel noncompetitive kinase inhibition. *Nat Struct Mol Biol*, 11, 1192-7.
- Oppenheim, J. J. (2001). Cytokines: past, present, and future. *Int J Hematol*, 74, 3-8.
- Pai, V. B. & Nahata, M. C. (2000). Cardiotoxicity of chemotherapeutic agents: incidence, treatment and prevention. *Drug Saf*, 22, 263-302.
- Pandya, K. & Smithies, O. 2011. beta-MyHC and cardiac hypertrophy: size does matter. *Circ Res*, 109, 609-10
- Pashkow, F. J. (2011). Oxidative Stress and Inflammation in Heart Disease: Do Antioxidants Have a Role in Treatment and/or Prevention? *Int J Inflam*, 2011, 514623.
- Pavlosky, A., Lau, A., Su, Y., Lian, D., Huang, X., Yin, Z., Haig, A., Jevnikar, A. M. & Zhang, Z. X. (2014). RIPK3-mediated necroptosis regulates cardiac allograft rejection. *Am J Transplant*, 14, 1778-90.
- Payne, D. M., Rossomando, A. J., Martino, P., Erickson, A. K., Her, J. H., Shabanowitz, J., Hunt, D. F., Weber, M. J. & Sturgill, T. W. (1991). Identification of the regulatory phosphorylation sites in pp42/mitogen-activated protein kinase (MAP kinase). *EMBO J*, 10, 885-92.
- Pearce, L. R., Komander, D. & Alessi, D. R. (2010). The nuts and bolts of AGC protein kinases. *Nat Rev Mol Cell Biol*, 11, 9-22.
- Peck, S. C. (2006). Analysis of protein phosphorylation: methods and strategies for studying kinases and substrates. *Plant J*, 45, 512-22.

- Peng, J., Schwartz, D., Elias, J. E., Thoreen, C. C., Cheng, D., Marsischky, G., Roelofs, J., Finley, D. & Gygi, S. P. (2003). A proteomics approach to understanding protein ubiquitination. *Nat Biotechnol*, 21, 921-6.
- Petersen, J. W. & Felker, G. M. (2006). Inflammatory biomarkers in heart failure. *Congest Heart Fail*, 12, 324-8.
- Petrich, B. G., Gong, X., Lerner, D. L., Wang, X., Brown, J. H., Saffitz, J. E. & Wang, Y. (2002). c-Jun N-terminal kinase activation mediates downregulation of connexin43 in cardiomyocytes. *Circ Res*, 91, 640-7.
- Petrich, B. G., Molkentin, J. D. & Wang, Y. (2003). Temporal activation of c-Jun N-terminal kinase in adult transgenic heart via cre-loxP-mediated DNA recombination. *FASEB J*, 17, 749-51.
- Pikkarainen, S., Kennedy, R. A., Marshall, A. K., Tham El, L., Lay, K., Kriz, T. A., Handa, B. S., Clerk, A. & Sugden, P. H. (2009). Regulation of expression of the rat orthologue of mouse double minute 2 (MDM2) by H<sub>2</sub>O<sub>2</sub>-induced oxidative stress in neonatal rat cardiac myocytes. *J Biol Chem*, 284, 27195-210.
- Pinto, A. R., Ilinykh, A., Ivey, M. J., Kuwabara, J. T., D'antoni, M. L., Debuque, R., Chandran, A., Wang, L., Arora, K., Rosenthal, N. A. & Tallquist, M. D. (2016). Revisiting Cardiac Cellular Composition. *Circ Res*, 118, 400-9.
- Pittman, K. & Kubes, P. (2013). Damage-associated molecular patterns control neutrophil recruitment. *J Innate Immun*, 5, 315-23.
- Plotnikov, A., Zehorai, E., Procaccia, S. & Seger, R. (2011). The MAPK cascades: signaling components, nuclear roles and mechanisms of nuclear translocation. *Biochim Biophys Acta*, 1813, 1619-33.
- Poss, K. D., Wilson, L. G. & Keating, M. T. (2002). Heart regeneration in zebrafish. *Science*, 298, 2188-90.
- Qin, D., Wang, X., Li, Y., Yang, L., Wang, R., Peng, J., Essandoh, K., Mu, X., Peng, T., Han, Q., Yu, K. J. & Fan, G. C. (2016). MicroRNA-223-5p and -3p Cooperatively Suppress Necroptosis in Ischemic/Reperused Hearts. *J Biol Chem*, 291, 20247-59.
- Raedschelders, K., Ansley, D. M. & Chen, D. D. (2012). The cellular and molecular origin of reactive oxygen species generation during myocardial ischemia and reperfusion. *Pharmacol Ther*, 133, 230-55.
- Raingeaud, J., Gupta, S., Rogers, J. S., Dickens, M., Han, J., Ulevitch, R. J. & Davis, R. J. (1995). Pro-inflammatory cytokines and environmental stress cause p38 mitogen-activated protein kinase activation by dual phosphorylation on tyrosine and threonine. *J Biol Chem*, 270, 7420-6.
- Ramsby, M. & Makowski, G. (2011). Differential detergent fractionation of eukaryotic cells. *Cold Spring Harb Protoc*, 2011, prot5592.
- Ran, F. A., Hsu, P. D., Wright, J., Agarwala, V., Scott, D. A. & Zhang, F. (2013). Genome engineering using the CRISPR-Cas9 system. *Nat Protoc*, 8, 2281-308.
- Ravenscroft, G., Miyatake, S., Lehtokari, V. L., Todd, E. J., Vornanen, P., Yau, K. S., Hayashi, Y. K., Miyake, N., Tsurusaki, Y., Doi, H., Saito, H., Osaka, H., Yamashita, S., Ohya, T.,

- Sakamoto, Y., Koshimizu, E., Imamura, S., Yamashita, M., Ogata, K., Shiina, M., Bryson-Richardson, R. J., Vaz, R., Ceyhan, O., Brownstein, C. A., Swanson, L. C., Monnot, S., Romero, N. B., Amthor, H., Kresoje, N., Sivadorai, P., Kiraly-Borri, C., Haliloglu, G., Talim, B., Orhan, D., Kale, G., Charles, A. K., Fabian, V. A., Davis, M. R., Lammens, M., Sewry, C. A., Manzur, A., Muntoni, F., Clarke, N. F., North, K. N., Bertini, E., Nevo, Y., Willichowski, E., Silberg, I. E., Topaloglu, H., Beggs, A. H., Allcock, R. J., Nishino, I., Wallgren-Pettersson, C., Matsumoto, N. & Laing, N. G. (2013). Mutations in KLHL40 are a frequent cause of severe autosomal-recessive nemaline myopathy. *Am J Hum Genet*, 93, 6-18.
- Re, D. B., Le Verche, V., Yu, C., Amoroso, M. W., Politi, K. A., Phani, S., Ikiz, B., Hoffmann, L., Koolen, M., Nagata, T., Papadimitriou, D., Nagy, P., Mitsumoto, H., Kariya, S., Wichterle, H., Henderson, C. E. & Przedborski, S. (2014). Necroptosis drives motor neuron death in models of both sporadic and familial ALS. *Neuron*, 81, 1001-8.
- Reszka, A. A., Seger, R., Diltz, C. D., Krebs, E. G. & Fischer, E. H. (1995). Association of mitogen-activated protein kinase with the microtubule cytoskeleton. *Proc Natl Acad Sci U S A*, 92, 8881-5.
- Reyskens, K. & Arthur, J. S. C. (2016). Emerging Roles of the Mitogen and Stress Activated Kinases MSK1 and MSK2. *Front Cell Dev Biol*, 4, 56.
- Rizvi, A., Tang, X. L., Qiu, Y., Xuan, Y. T., Takano, H., Jadoon, A. K. & Bolli, R. (1999). Increased protein synthesis is necessary for the development of late preconditioning against myocardial stunning. *Am J Physiol*, 277, H874-84.
- Robinson, N., McComb, S., Mulligan, R., Dudani, R., Krishnan, L. & Sad, S. (2012). Type I interferon induces necroptosis in macrophages during infection with *Salmonella enterica* serovar Typhimurium. *Nat Immunol*, 13, 954-62.
- Rose, B. A., Force, T. & Wang, Y. (2010). Mitogen-activated protein kinase signaling in the heart: angels versus demons in a heart-breaking tale. *Physiol Rev*, 90, 1507-46.
- Roskoski, R., Jr. (2012). ERK1/2 MAP kinases: structure, function, and regulation. *Pharmacol Res*, 66, 105-43.
- Rouse, J., Cohen, P., Trigon, S., Morange, M., Alonso-Llamazares, A., Zamanillo, D., Hunt, T. & Nebreda, A. R. (1994). A novel kinase cascade triggered by stress and heat shock that stimulates MAPKAP kinase-2 and phosphorylation of the small heat shock proteins. *Cell*, 78, 1027-37.
- Roux, P. P. & Blenis, J. (2004). ERK and p38 MAPK-activated protein kinases: a family of protein kinases with diverse biological functions. *Microbiol Mol Biol Rev*, 68, 320-44.
- Saitoh, M., Nishitoh, H., Fujii, M., Takeda, K., Tobiume, K., Sawada, Y., Kawabata, M., Miyazono, K. & Ichijo, H. (1998). Mammalian thioredoxin is a direct inhibitor of apoptosis signal-regulating kinase (ASK) 1. *EMBO J*, 17, 2596-606.
- Sanchez, I., Hughes, R. T., Mayer, B. J., Yee, K., Woodgett, J. R., Avruch, J., Kyriakis, J. M. & Zon, L. I. (1994). Role of SAPK/ERK kinase-1 in the stress-activated pathway regulating transcription factor c-Jun. *Nature*, 372, 794-8.
- Saurin, A. T., Martin, J. L., Heads, R. J., Foley, C., Mockridge, J. W., Wright, M. J., Wang, Y. & Marber, M. S. (2000). The role of differential activation of p38-mitogen-activated protein kinase in preconditioned ventricular myocytes. *FASEB J*, 14, 2237-46.

- Sawyer, D. B., Siwik, D. A., Xiao, L., Pimentel, D. R., Singh, K. & Colucci, W. S. (2002). Role of oxidative stress in myocardial hypertrophy and failure. *J Mol Cell Cardiol*, 34, 379-88.
- Scaffidi, P., Misteli, T. & Bianchi, M. E. (2002). Release of chromatin protein HMGB1 by necrotic cells triggers inflammation. *Nature*, 418, 191-5.
- Schieber, M. & Chandel, N. S. (2014). ROS function in redox signaling and oxidative stress. *Curr Biol*, 24, R453-62.
- Schlessinger, J. (2000). Cell signaling by receptor tyrosine kinases. *Cell*, 103, 211-25.
- Schulz, R., Gres, P., Skyschally, A., Duschin, A., Belosjorow, S., Konietzka, I. & Heusch, G. (2003). Ischemic preconditioning preserves connexin 43 phosphorylation during sustained ischemia in pig hearts in vivo. *FASEB J*, 17, 1355-7.
- Sebolt-Leopold, J. S., Dudley, D. T., Herrera, R., Van Becelaere, K., Wiland, A., Gowan, R. C., Tecle, H., Barrett, S. D., Bridges, A., Przybranowski, S., Leopold, W. R. & Saltiel, A. R. (1999). Blockade of the MAP kinase pathway suppresses growth of colon tumors in vivo. *Nat Med*, 5, 810-6.
- Shiozaki, E. N., Chai, J. & Shi, Y. (2002). Oligomerization and activation of caspase-9, induced by Apaf-1 CARD. *Proc Natl Acad Sci U S A*, 99, 4197-202.
- Shirai, A., Matsuyama, A., Yashiroda, Y., Hashimoto, A., Kawamura, Y., Arai, R., Komatsu, Y., Horinouchi, S. & Yoshida, M. (2008). Global analysis of gel mobility of proteins and its use in target identification. *J Biol Chem*, 283, 10745-52.
- Shutinoski, B., Alturki, N. A., Rijal, D., Bertin, J., Gough, P. J., Schlossmacher, M. G. & Sad, S. (2016). K45A mutation of RIPK1 results in poor necroptosis and cytokine signaling in macrophages, which impacts inflammatory responses in vivo. *Cell Death Differ*, 23, 1628-37.
- Shveygert, M., Kaiser, C., Bradrick, S. S. & Gromeier, M. (2010). Regulation of eukaryotic initiation factor 4E (eIF4E) phosphorylation by mitogen-activated protein kinase occurs through modulation of Mnk1-eIF4G interaction. *Mol Cell Biol*, 30, 5160-7.
- Sivasubramanian, N., Coker, M. L., Kurrelmeyer, K. M., Maclellan, W. R., Demayo, F. J., Spinale, F. G. & Mann, D. L. (2001). Left ventricular remodeling in transgenic mice with cardiac restricted overexpression of tumor necrosis factor. *Circulation*, 104, 826-31.
- Slezak, J., Tribulova, N., Pristacova, J., Uhrik, B., Thomas, T., Khaper, N., Kaul, N. & Singal, P. K. (1995). Hydrogen peroxide changes in ischemic and reperfused heart. Cytochemistry and biochemical and X-ray microanalysis. *Am J Pathol*, 147, 772-81.
- Slupe, A. M., Merrill, R. A. & Strack, S. (2011). Determinants for Substrate Specificity of Protein Phosphatase 2A. *Enzyme Res*, 2011, 398751.
- Smith, C. C., Davidson, S. M., Lim, S. Y., Simpkin, J. C., Hothersall, J. S. & Yellon, D. M. (2007). Necrostatin: a potentially novel cardioprotective agent? *Cardiovasc Drugs Ther*, 21, 227-33.
- Souders, C. A., Bowers, S. L. & Baudino, T. A. (2009). Cardiac fibroblast: the renaissance cell. *Circ Res*, 105, 1164-76.

- Stokoe, D., Engel, K., Campbell, D. G., Cohen, P. & Gaestel, M. (1992). Identification of MAPKAP kinase 2 as a major enzyme responsible for the phosphorylation of the small mammalian heat shock proteins. *FEBS Lett*, 313, 307-13.
- Sugden, P. H. & Clerk, A. (1997). Regulation of the ERK subgroup of MAP kinase cascades through G protein-coupled receptors. *Cell Signal*, 9, 337-51.
- Sugden, P. H. & Clerk, A. (1998). Cellular mechanisms of cardiac hypertrophy. *J Mol Med (Berl)*, 76, 725-46.
- Sun, J. Z., Tang, X. L., Park, S. W., Qiu, Y., Turrens, J. F. & Bolli, R. (1996). Evidence for an essential role of reactive oxygen species in the genesis of late preconditioning against myocardial stunning in conscious pigs. *J Clin Invest*, 97, 562-76.
- Sun, L., Stoecklin, G., Van Way, S., Hinkovska-Galcheva, V., Guo, R. F., Anderson, P. & Shanley, T. P. (2007). Tristetraprolin (TTP)-14-3-3 complex formation protects TTP from dephosphorylation by protein phosphatase 2a and stabilizes tumor necrosis factor-alpha mRNA. *J Biol Chem*, 282, 3766-77.
- Sun, L., Wang, H., Wang, Z., He, S., Chen, S., Liao, D., Wang, L., Yan, J., Liu, W., Lei, X. & Wang, X. (2012). Mixed lineage kinase domain-like protein mediates necrosis signaling downstream of RIP3 kinase. *Cell*, 148, 213-27.
- Sun, X., Yin, J., Starovasnik, M. A., Fairbrother, W. J. & Dixit, V. M. (2002). Identification of a novel homotypic interaction motif required for the phosphorylation of receptor-interacting protein (RIP) by RIP3. *J Biol Chem*, 277, 9505-11.
- Sundaresan, M., Yu, Z. X., Ferrans, V. J., Irani, K. & Finkel, T. (1995). Requirement for generation of H<sub>2</sub>O<sub>2</sub> for platelet-derived growth factor signal transduction. *Science*, 270, 296-9.
- Suzuki, K., Murtuza, B., Smolenski, R. T., Sammut, I. A., Suzuki, N., Kaneda, Y. & Yacoub, M. H. (2001). Overexpression of interleukin-1 receptor antagonist provides cardioprotection against ischemia-reperfusion injury associated with reduction in apoptosis. *Circulation*, 104, 1308-13.
- Takaesu, G., Kishida, S., Hiyama, A., Yamaguchi, K., Shibuya, H., Irie, K., Ninomiya-Tsuji, J. & Matsumoto, K. (2000). TAB2, a novel adaptor protein, mediates activation of TAK1 MAPKKK by linking TAK1 to TRAF6 in the IL-1 signal transduction pathway. *Mol Cell*, 5, 649-58.
- Tenev, T., Bianchi, K., Darding, M., Broemer, M., Langlais, C., Wallberg, F., Zachariou, A., Lopez, J., Macfarlane, M., Cain, K. & Meier, P. (2011). The Ripoptosome, a signaling platform that assembles in response to genotoxic stress and loss of IAPs. *Mol Cell*, 43, 432-48.
- Tong, L., Pav, S., White, D. M., Rogers, S., Crane, K. M., Cywin, C. L., Brown, M. L. & Pargellis, C. A. (1997). A highly specific inhibitor of human p38 MAP kinase binds in the ATP pocket. *Nat Struct Biol*, 4, 311-6.
- Torre-Amione, G., Kapadia, S., Lee, J., Durand, J. B., Bies, R. D., Young, J. B. & Mann, D. L. (1996). Tumor necrosis factor-alpha and tumor necrosis factor receptors in the failing human heart. *Circulation*, 93, 704-11.
- Tristao, V. R., Goncalves, P. F., Dalboni, M. A., Batista, M. C., Durao Mde, S., Jr. & Monte, J. C. (2012). Nec-1 protects against nonapoptotic cell death in cisplatin-induced kidney injury. *Ren Fail*, 34, 373-7.

- Tsutsui, H., Kinugawa, S. & Matsushima, S. (2011). Oxidative stress and heart failure. *Am J Physiol Heart Circ Physiol*, 301, H2181-90.
- Turjanski, A. G., Vaque, J. P. & Gutkind, J. S. (2007). MAP kinases and the control of nuclear events. *Oncogene*, 26, 3240-53.
- Valen, G., Starkopf, J., Takeshima, S., Kullisaar, T., Vihalemm, T., Kengsepp, A. T., Lowbeer, C., Vaage, J. & Zilmer, M. (1998). Preconditioning with hydrogen peroxide (H<sub>2</sub>O<sub>2</sub>) or ischemia in H<sub>2</sub>O<sub>2</sub>-induced cardiac dysfunction. *Free Radic Res*, 29, 235-45.
- Valgimigli, M., Merli, E., Malagutti, P., Soukhomovskaia, O., Cicchitelli, G., Antelli, A., Canistro, D., Francolini, G., Macri, G., Mastroianni, F., Paolini, M. & Ferrari, R. (2004). Hydroxyl radical generation, levels of tumor necrosis factor- $\alpha$ , and progression to heart failure after acute myocardial infarction. *J Am Coll Cardiol*, 43, 2000-8.
- Van Berlo, J. H., Maillet, M. & Molkentin, J. D. (2013). Signaling effectors underlying pathologic growth and remodeling of the heart. *J Clin Invest*, 123, 37-45.
- Van Empel, V. P., Bertrand, A. T., Hofstra, L., Crijns, H. J., Doevendans, P. A. & De Windt, L. J. (2005). Myocyte apoptosis in heart failure. *Cardiovasc Res*, 67, 21-9.
- Van Raam, B. J., Ehrnhoefer, D. E., Hayden, M. R. & Salvesen, G. S. (2013). Intrinsic cleavage of receptor-interacting protein kinase-1 by caspase-6. *Cell Death Differ*, 20, 86-96.
- Van Tassell, B. W., Seropian, I. M., Toldo, S., Mezzaroma, E. & Abbate, A. (2013). Interleukin-1 $\beta$  induces a reversible cardiomyopathy in the mouse. *Inflamm Res*, 62, 637-40.
- Varfolomeev, E., Blankenship, J. W., Wayson, S. M., Fedorova, A. V., Kayagaki, N., Garg, P., Zobel, K., Dynek, J. N., Elliott, L. O., Wallweber, H. J., Flygare, J. A., Fairbrother, W. J., Deshayes, K., Dixit, V. M. & Vucic, D. (2007). IAP antagonists induce autoubiquitination of c-IAPs, NF- $\kappa$ B activation, and TNF $\alpha$ -dependent apoptosis. *Cell*, 131, 669-81.
- Varfolomeev, E., Goncharov, T., Fedorova, A. V., Dynek, J. N., Zobel, K., Deshayes, K., Fairbrother, W. J. & Vucic, D. (2008). c-IAP1 and c-IAP2 are critical mediators of tumor necrosis factor  $\alpha$  (TNF $\alpha$ )-induced NF- $\kappa$ B activation. *J Biol Chem*, 283, 24295-9.
- Vince, J. E., Wong, W. W., Khan, N., Feltham, R., Chau, D., Ahmed, A. U., Benetatos, C. A., Chunduru, S. K., Condon, S. M., Mckinlay, M., Brink, R., Leverkus, M., Tergaonkar, V., Schneider, P., Callus, B. A., Koentgen, F., Vaux, D. L. & Silke, J. (2007). IAP antagonists target cIAP1 to induce TNF $\alpha$ -dependent apoptosis. *Cell*, 131, 682-93.
- Von Harsdorf, R., Li, P. F. & Dietz, R. (1999). Signaling pathways in reactive oxygen species-induced cardiomyocyte apoptosis. *Circulation*, 99, 2934-41.
- Wang, H., Sun, L., Su, L., Rizo, J., Liu, L., Wang, L. F., Wang, F. S. & Wang, X. (2014a). Mixed lineage kinase domain-like protein MLKL causes necrotic membrane disruption upon phosphorylation by RIP3. *Mol Cell*, 54, 133-46.
- Wang, J. X., Zhang, X. J., Li, Q., Wang, K., Wang, Y., Jiao, J. Q., Feng, C., Teng, S., Zhou, L. Y., Gong, Y., Zhou, Z. X., Liu, J., Wang, J. L. & Li, P. F. (2015). MicroRNA-103/107 Regulate Programmed Necrosis and Myocardial Ischemia/Reperfusion Injury Through Targeting FADD. *Circ Res*, 117, 352-63.

- Wang, K., Liu, F., Zhou, L. Y., Ding, S. L., Long, B., Liu, C. Y., Sun, T., Fan, Y. Y., Sun, L. & Li, P. F. (2013). miR-874 regulates myocardial necrosis by targeting caspase-8. *Cell Death Dis*, 4, e709.
- Wang, L., Du, F. & Wang, X. (2008). TNF-alpha induces two distinct caspase-8 activation pathways. *Cell*, 133, 693-703.
- Wang, Q., Lin, J. L., Erives, A. J., Lin, C. I. & Lin, J. J. (2014b). New insights into the roles of Xin repeat-containing proteins in cardiac development, function, and disease. *Int Rev Cell Mol Biol*, 310, 89-128.
- Wang, X., Li, Y., Liu, S., Yu, X., Li, L., Shi, C., He, W., Li, J., Xu, L., Hu, Z., Yu, L., Yang, Z., Chen, Q., Ge, L., Zhang, Z., Zhou, B., Jiang, X., Chen, S. & He, S. (2014c). Direct activation of RIP3/MLKL-dependent necrosis by herpes simplex virus 1 (HSV-1) protein ICP6 triggers host antiviral defense. *Proc Natl Acad Sci U S A*, 111, 15438-43.
- Wang, Y., Huang, S., Sah, V. P., Ross, J., Jr., Brown, J. H., Han, J. & Chien, K. R. (1998a). Cardiac muscle cell hypertrophy and apoptosis induced by distinct members of the p38 mitogen-activated protein kinase family. *J Biol Chem*, 273, 2161-8.
- Wang, Y., Su, B., Sah, V. P., Brown, J. H., Han, J. & Chien, K. R. (1998b). Cardiac hypertrophy induced by mitogen-activated protein kinase kinase 7, a specific activator for c-Jun NH2-terminal kinase in ventricular muscle cells. *J Biol Chem*, 273, 5423-6.
- Weber, A., Wasiliew, P. & Kracht, M. (2010). Interleukin-1 (IL-1) pathway. *Sci Signal*, 3(105): cm1.
- Wegener, A. D. & Jones, L. R. (1984). Phosphorylation-induced mobility shift in phospholamban in sodium dodecyl sulfate-polyacrylamide gels. Evidence for a protein structure consisting of multiple identical phosphorylatable subunits. *J Biol Chem*, 259, 1834-41.
- Wertz, I. E., O'rourke, K. M., Zhou, H., Eby, M., Aravind, L., Seshagiri, S., Wu, P., Wiesmann, C., Baker, R., Boone, D. L., Ma, A., Koonin, E. V. & Dixit, V. M. (2004). De-ubiquitination and ubiquitin ligase domains of A20 downregulate NF-kappaB signalling. *Nature*, 430, 694-9.
- Whitmarsh, A. J., Yang, S. H., Su, M. S., Sharrocks, A. D. & Davis, R. J. (1997). Role of p38 and JNK mitogen-activated protein kinases in the activation of ternary complex factors. *Mol Cell Biol*, 17, 2360-71.
- Widmann, C., Gibson, S., Jarpe, M. B. & Johnson, G. L. (1999). Mitogen-activated protein kinase: conservation of a three-kinase module from yeast to human. *Physiol Rev*, 79, 143-80.
- Winston, B. W., Chan, E. D., Johnson, G. L. & Riches, D. W. (1997). Activation of p38mapk, MKK3, and MKK4 by TNF-alpha in mouse bone marrow-derived macrophages. *J Immunol*, 159, 4491-7.
- Wood, C. D., Thornton, T. M., Sabio, G., Davis, R. A. & Rincon, M. (2009). Nuclear localization of p38 MAPK in response to DNA damage. *Int J Biol Sci*, 5, 428-37.
- Wortzel, I. & Seger, R. (2011). The ERK Cascade: Distinct Functions within Various Subcellular Organelles. *Genes Cancer*, 2, 195-209.

- Wu, J., Huang, Z., Ren, J., Zhang, Z., He, P., Li, Y., Ma, J., Chen, W., Zhang, Y., Zhou, X., Yang, Z., Wu, S. Q., Chen, L. & Han, J. (2013). Mkl1 knockout mice demonstrate the indispensable role of Mkl1 in necroptosis. *Cell Res*, 23, 994-1006.
- Xu, G. & Jaffrey, S. R. (2013). Proteomic identification of protein ubiquitination events. *Biotechnol Genet Eng Rev*, 29, 73-109.
- Xu, Y., Ma, H., Shao, J., Wu, J., Zhou, L., Zhang, Z., Wang, Y., Huang, Z., Ren, J., Liu, S., Chen, X. & Han, J. (2015). A Role for Tubular Necroptosis in Cisplatin-Induced AKI. *J Am Soc Nephrol*, 26, 2647-58.
- Yamamoto, S., Seta, K., Morisco, C., Vatner, S. F. & Sadoshima, J. (2001). Chelerythrine rapidly induces apoptosis through generation of reactive oxygen species in cardiac myocytes. *J Mol Cell Cardiol*, 33, 1829-48.
- Yano, M., Kim, S., Izumi, Y., Yamanaka, S. & Iwao, H. (1998). Differential activation of cardiac c-jun amino-terminal kinase and extracellular signal-regulated kinase in angiotensin II-mediated hypertension. *Circ Res*, 83, 752-60.
- Yndestad, A., Damas, J. K., Oie, E., Ueland, T., Gullestad, L. & Aukrust, P. (2007). Role of inflammation in the progression of heart failure. *Curr Cardiol Rep*, 9, 236-41.
- Young P. R., McLaughlin M. M., Kumar S, Kassis S, Doyle M. L., McNulty D, Gallagher T. F., Fisher S, McDonnell P. C., Carr S. A., Huddleston M. J., Seibel G, Porter T. G., Livi G. P., Adams J. L. & Lee J.C. (1997). Pyridinyl imidazole inhibitors of p38 mitogen-activated protein kinase bind in the ATP site. *J Biol Chem*, 272, 12116-21.
- Ytrehus, K., Walsh, R. S., Richards, S. C. & Downey, J. M. (1995). Hydrogen peroxide as a protective agent during reperfusion. A study in the isolated perfused rabbit heart subjected to regional ischemia. *Cardiovasc Res*, 30, 1033-7.
- Yue, P., Massie, B. M., Simpson, P. C. & Long, C. S. (1998). Cytokine expression increases in nonmyocytes from rats with postinfarction heart failure. *Am J Physiol*, 275, H250-8.
- Zarubin, T. & Han, J. (2005). Activation and signaling of the p38 MAP kinase pathway. *Cell Res*, 15, 11-8.
- Zhang, B. H. & Guan, K. L. (2000). Activation of B-Raf kinase requires phosphorylation of the conserved residues Thr598 and Ser601. *EMBO J*, 19, 5429-39.
- Zhang, L., Blackwell, K., Workman, L. M., Chen, S., Pope, M. R., Janz, S. & Habelhah, H. (2015). RIP1 Cleavage in the Kinase Domain Regulates TRAIL-Induced NF-kappaB Activation and Lymphoma Survival. *Mol Cell Biol*, 35, 3324-38.
- Zhang, M., Li, J., Geng, R., Ge, W., Zhou, Y., Zhang, C., Cheng, Y. & Geng, D. (2013). The inhibition of ERK activation mediates the protection of necrostatin-1 on glutamate toxicity in HT-22 cells. *Neurotox Res*, 24, 64-70.
- Zhang, T., Inesta-Vaquera, F., Niepel, M., Zhang, J., Ficarro, S. B., Machleidt, T., Xie, T., Marto, J. A., Kim, N., Sim, T., Laughlin, J. D., Park, H., Lograsso, P. V., Patricelli, M., Nomanbhoy, T. K., Sorger, P. K., Alessi, D. R. & Gray, N. S. (2012). Discovery of potent and selective covalent inhibitors of JNK. *Chem Biol*, 19, 140-54.
- Zhang, T., Zhang, Y., Cui, M., Jin, L., Wang, Y., Lv, F., Liu, Y., Zheng, W., Shang, H., Zhang, J., Zhang, M., Wu, H., Guo, J., Zhang, X., Hu, X., Cao, C. M. & Xiao, R. P. (2016). CaMKII is

a RIP3 substrate mediating ischemia- and oxidative stress-induced myocardial necroptosis. *Nat Med*, 22, 175-82.

Zhang, W. & Liu, H. T. (2002). MAPK signal pathways in the regulation of cell proliferation in mammalian cells. *Cell Res*, 12, 9-18.

Zhou, S., Sun, W., Zhang, Z. & Zheng, Y. (2014). The role of Nrf2-mediated pathway in cardiac remodeling and heart failure. *Oxid Med Cell Longev*, 2014, 260429.

Zhou, W. & Yuan, J. (2014). Necroptosis in health and diseases. *Semin Cell Dev Biol*, 35, 14-23.

Zou, H., Henzel, W. J., Liu, X., Lutschg, A. & Wang, X. (1997). Apaf-1, a human protein homologous to *C. elegans* CED-4, participates in cytochrome c-dependent activation of caspase-3. *Cell*, 90, 405-13.

Zweier, J. L., Flaherty, J. T. & Weisfeldt, M. L. (1987). Direct measurement of free radical generation following reperfusion of ischemic myocardium. *Proc Natl Acad Sci U S A*, 84, 1404-7.

## APPENDIX I: SDS-PAGE GEL RECIPES

### **6% stacking gels (for 10 ml gel mixture):**

Acrylamide 30% - 2.0 ml

Bisacrylamide 2% - 0.8 ml

20% SDS - 50  $\mu$ l

Tris 1M pH 6.8 - 1.25 ml

H<sub>2</sub>O - 5.87 ml

TEMED - 10  $\mu$ l

APS 25% - 75  $\mu$ l

### **10% resolving gels (for 10 ml gel mixture):**

Acrylamide 30% 3.33 ml

Bisacrylamide 2% - 1.33 ml

20% SDS - 50  $\mu$ l

Tris 1M pH 8.8 - 3.75 ml

H<sub>2</sub>O - 1.45 ml

TEMED - 10  $\mu$ l

APS 25% - 75  $\mu$ l

## **APPENDIX II: MICROARRAY DATA TABLES**

**Table A1 Changes in transcript expression induced by PD184352**

Cardiomyocytes were unstimulated (Control) or exposed to PD184352 (2  $\mu$ M) for 2 h 15 min. Changes in RNA expression were determined using Affymetrix Rat Gene 2.0 ST microarrays, using GeneSpring 14.5 analysis to identify RNAs with significant changes in expression (>1.5-fold relative to control) and a significant effect of the inhibitor (one-way ANOVA with SNK post-test and Benjamini-Hochberg FDR correction,  $p < 0.05$ ). Raw values are given for controls and results are the mean fold change relative to controls (n=3 independent hybridisations).

**RNAs upregulated in response to PD184352**

Transcript ID	Gene Symbol	Control	PD184352
		(Raw values)	(Relative to control)
17807283	Abca1	416	1.66
17850744	Adams15	216	1.93
17754293	Adarb1	141	1.73
17723725	Apcdd1	97	1.57
17687609	Atf3	132	1.81
17653231	Baiap2	212	1.64
17719938	Bambi	142	1.60
17766015	Bcl2l11	160	1.70
17845173	Cilp	182	1.75
17819669	Cyp1b1	512	1.77
17845877	Fam214a	156	1.58
17738055	Fat4	277	1.51
17695522	Fgfr3	108	1.65
17777751	Flrt3	87	1.83
17860796	Kcne4	319	1.54
17710605	Klf2	153	1.68
17622657	Mrgprf	194	1.75
17715072	Nedd9	392	1.51
17789572	Pdk4	315	2.69
17823303	Pgf	306	1.90
17690991	Pik3ip1	330	1.87
17623967	Rab3il1	166	1.60
17679974	Rab7b	122	1.51
17821038	Rhob	597	1.60
17821293	Rsad2	75	1.67
17844592	Sema7a	293	1.67
17864290	Slc40a1	246	1.72
17797024	Sox17	178	1.98
17864503	Stk17b	258	1.62
17813989	Ston1	363	1.62
17719481	Unknown	81	1.56
17631450	Zfp74	242	1.50

**Table A1 cont.****RNAs downregulated in response to PD184352**

<b>Transcript ID</b>	<b>Gene Symbol</b>	<b>Control (Raw values)</b>	<b>PD184352 (Relative to control)</b>
17709074	Angpt2	551	<b>0.61</b>
17879104	Apln	574	<b>0.57</b>
17725828	Arap3	171	<b>0.65</b>
17627604	Arhgap18	651	<b>0.61</b>
17659402	Ccl3	681	<b>0.51</b>
17638903	Ccnd1	373	<b>0.56</b>
17808573	Cdkn2b	257	<b>0.60</b>
17682154	Cfap45	139	<b>0.65</b>
17641660	Ch25h	313	<b>0.30</b>
17764202	Chst1	268	<b>0.54</b>
17637749	Chst15	253	<b>0.54</b>
17650883	Csf3	113	<b>0.37</b>
17693465	Cxcl1	643	<b>0.66</b>
17693459	Cxcl2	208	<b>0.46</b>
17683912	Cxcr4	418	<b>0.47</b>
17708195	Dlc1	1574	<b>0.60</b>
17765071	Dll4	285	<b>0.28</b>
17712103	Dusp4	267	<b>0.27</b>
17626435	Dusp5	197	<b>0.45</b>
17827855	Dusp6	273	<b>0.10</b>
17722348	Egr1	1291	<b>0.05</b>
17758189	Egr2	135	<b>0.41</b>
17803896	Epha2	112	<b>0.52</b>
17815588	Etv1	226	<b>0.60</b>
17666684	Etv5	156	<b>0.43</b>
17801898	Fhl3	411	<b>0.51</b>
17774919	Fjx1	136	<b>0.47</b>
17623115	Fosl1	115	<b>0.44</b>
17778359	Foxs1	225	<b>0.66</b>
17720816	Frmd4a	592	<b>0.41</b>
17793546	Frmd4b	221	<b>0.51</b>
17745332	Fst	181	<b>0.64</b>
17783411	Gimap4	231	<b>0.66</b>
17646620	Grap	124	<b>0.65</b>
17728750	Ier2	191	<b>0.63</b>
17777184	Il1a	228	<b>0.28</b>
17858700	Il1r1	1510	<b>0.37</b>
17709452	Irs2	475	<b>0.42</b>
17728243	Irx3	172	<b>0.57</b>
17618664	Kcne3	453	<b>0.33</b>
17652361	Kcnj2	303	<b>0.53</b>
17691166	Lif	167	<b>0.42</b>
17765032	LOC691418	237	<b>0.51</b>
17676301	Mafk	362	<b>0.66</b>

**Table A1 cont.****RNAs downregulated in response to PD184352 cont.**

<b>Transcript ID</b>	<b>Gene Symbol</b>	<b>Control (Raw values)</b>	<b>PD184352 (Relative to control)</b>
17751179	Ndst3	229	<b>0.54</b>
17759817	Nrarp	172	<b>0.66</b>
17731247	Nrp1	1316	<b>0.60</b>
17666273	Nrros	114	<b>0.59</b>
17827193	Nuak1	388	<b>0.53</b>
17799362	Pappa	688	<b>0.66</b>
17828155	Phlda1	306	<b>0.15</b>
17821531	Pik3cg	141	<b>0.56</b>
17700983	Plau	275	<b>0.41</b>
17611428	Plekhg1	248	<b>0.64</b>
17735703	Plk2	1381	<b>0.61</b>
17809625	Plk3	127	<b>0.57</b>
17712060	Pragmin	239	<b>0.58</b>
17759401	Prdm1	121	<b>0.52</b>
17774894	Prr5l	91	<b>0.62</b>
17844430	Ptpn9	570	<b>0.66</b>
17621742	Ptpre	126	<b>0.65</b>
17739018	Ptx3	586	<b>0.65</b>
17745872	Rai14	626	<b>0.47</b>
17819479	Rapgef5	164	<b>0.66</b>
17681025	Rgs16	369	<b>0.64</b>
17684906	Rgs2	370	<b>0.40</b>
17857692	Runx2	160	<b>0.57</b>
17779204	Sdc4	1184	<b>0.52</b>
17681477	Sele	84	<b>0.54</b>
17831678	Shank3	140	<b>0.64</b>
17613677	Slc1a5	358	<b>0.64</b>
17813885	Socs5	594	<b>0.65</b>
17699557	Sox7	183	<b>0.61</b>
17764824	Spred1	404	<b>0.37</b>
17691731	Spred2	433	<b>0.27</b>
17631334	Spred3	173	<b>0.60</b>
17738042	Spry1	164	<b>0.56</b>
17705145	Spry2	507	<b>0.30</b>
17725883	Spry4	281	<b>0.17</b>
17665170	St3gal6	468	<b>0.63</b>
17789522	Tfpi2	101	<b>0.44</b>
17799396	Tlr4	301	<b>0.59</b>
17624534	Tmem2	888	<b>0.54</b>
17681381	Tnfsf18	50	<b>0.65</b>
17829670	Trib1	363	<b>0.54</b>
17821133	Trib2	346	<b>0.43</b>
17851432	Ubash3b	149	<b>0.54</b>
17737832	Unknown	79	<b>0.65</b>
17726303	Zfp608	468	<b>0.57</b>
17728781	Zswim4	180	<b>0.62</b>

**Table A2 Changes in transcript expression induced by JNK-IN-8**

Cardiomyocytes were unstimulated (Control) or exposed to JNK-IN-8 (1  $\mu$ M) for 2 h 15 min. Changes in RNA expression were determined using Affymetrix Rat Gene 2.0 ST microarrays, using GeneSpring 14.5 analysis to identify RNAs with significant changes in expression (>1.5-fold relative to control) and a significant effect of the inhibitor (one-way ANOVA with SNK post-test and Benjamini-Hochberg FDR correction,  $p < 0.05$ ). Raw values are given for controls and results are the mean fold change relative to controls (n=3 independent hybridisations).

**RNAs downregulated in response to JNK-IN-8**

<b>Transcript ID</b>	<b>Gene Symbol</b>	<b>Control (Raw values)</b>	<b>JNK-IN-8 (Relative to control)</b>
17627697	Ctgf	1463	<b>0.39</b>
17751869	Cyr61	872	<b>0.50</b>
17795854	Dusp16	286	<b>0.60</b>
17638514	Dusp8	279	<b>0.35</b>
17656333	Gla1	59	<b>0.62</b>
17725668	Hbegf	363	<b>0.47</b>
17808683	Jun	422	<b>0.64</b>
17775303	Olr776	65	<b>0.62</b>
17620947	Unknown	191	<b>0.66</b>
17803987	Unknown	136	<b>0.62</b>
17815738	Unknown	336	<b>0.63</b>
17820179	Unknown	99	<b>0.61</b>

**RNAs upregulated in response to JNK-IN-8**

<b>Transcript ID</b>	<b>Gene Symbol</b>	<b>Control (Raw values)</b>	<b>JNK-IN-8 (Relative to control)</b>
17819669	Cyp1b1	512	<b>1.98</b>
17795409	Olr1	1395	<b>1.60</b>

**Table A3 Changes in transcript expression induced by SB203580**

Cardiomyocytes were unstimulated (Control) or exposed to SB203580 (0.7  $\mu$ M) for 2 h 15 min. Changes in RNA expression were determined using Affymetrix Rat Gene 2.0 ST microarrays, using GeneSpring 14.5 analysis to identify RNAs with significant changes in expression (>1.5-fold relative to control) and a significant effect of the inhibitor (one-way ANOVA with SNK post-test and Benjamini-Hochberg FDR correction,  $p < 0.05$ ). Raw values are given for controls and results are the mean fold change relative to controls ( $n=3$  independent hybridisations).

**RNAs downregulated in response to SB203580**

<b>Transcript ID</b>	<b>Gene Symbol</b>	<b>Control (Raw values)</b>	<b>SB203580 (Relative to control)</b>
17820179	Unknown	99	<b>0.57</b>

**RNAs upregulated in response to SB203580**

<b>Transcript ID</b>	<b>Gene Symbol</b>	<b>Control (Raw values)</b>	<b>SB203580 (Relative to control)</b>
17681128	LOC680254	152	<b>1.51</b>
17652341	Map2k6	72	<b>1.68</b>
17843221	Olr1196	36	<b>1.51</b>
17679974	Rab7b	122	<b>1.56</b>
17612614	Unknown	40	<b>1.59</b>

**Table A4 Transcripts upregulated in response to H<sub>2</sub>O<sub>2</sub>**

Cardiomyocytes were unstimulated (Control) or exposed to H<sub>2</sub>O<sub>2</sub> (0.2 mM, 2 h). Changes in RNA expression were determined using Affymetrix Rat Gene 2.0 ST microarrays, using GeneSpring 14.5 analysis to identify RNAs with significant increase in expression in response to H<sub>2</sub>O<sub>2</sub> (>1.5-fold change relative to control; moderated t-test with Benjamini-Hochberg FDR correction, p<0.05). Raw values are given for controls and results are the mean fold change relative to controls (n=4 independent hybridisations).

Transcript ID	Gene Symbol	Control	H <sub>2</sub> O <sub>2</sub>
		(Raw values)	(Relative to controls)
17781129	Abcb1a	541	3.48
17810550	Adprh12	153	1.53
17617581	Aen	113	3.48
17782314	Akr1b8	564	2.33
17693425	Areg	82	1.61
17705843	Arhgef3	189	2.09
17858347	Arid5a	218	2.18
17821662	Arl4a	120	1.57
17717253	Arl5b	261	1.90
17652634	Armc7	131	2.20
17759590	Arrdc3	1034	1.58
17670615	Arvcf	113	1.53
17687609	Atf3	132	7.45
17673406	Atp5j2	65	1.51
17726777	Atp8b1	277	1.53
17861066	B3gnt7	67	1.58
17664484	Bach1	517	2.21
17621224	Bag3	801	1.58
17653231	Baiap2	212	1.75
17632894	Bax	143	1.76
17796337	Bcat1	357	1.55
17766015	Bcl2l11	160	1.76
17818164	Bdkrb2	181	2.83
17766552	Bmp2	193	2.06
17753161	Brd2	722	1.70
17636338	Btbd10	136	1.65
17684316	Btg2	308	2.91
17826458	Cbarp	109	1.51
17664770	Cbr1	246	2.84
17664759	Cbr1	1116	1.51
17664780	Cbr3	105	1.64
17655535	Ccng1	2202	1.51
17747788	Ccnl1	471	1.52
17630241	Cd3eap	85	1.50
17774921	Cd44	663	1.66
17868794	Cd80	54	5.22
17669098	Cd80	104	5.00
17753672	Cdkn1a	604	5.59
17808573	Cdkn2b	257	1.56
17765084	Chac1	119	3.03
17748939	Chrb2	70	1.58
17847383	Cish	357	2.15
17610582	Cited2	1010	1.68

**Table A4 cont.**

Transcript ID	Gene Symbol	Control	H <sub>2</sub> O <sub>2</sub>
		(Raw values)	(Relative to controls)
17708936	Ckap2	81	1.81
17859270	Coq10b	187	1.72
17716200	Crem	139	1.93
17750384	Csf1	1259	1.58
17856536	Csrnp1	120	3.28
17727278	Ctdp1	247	1.64
17751869	Cyr61	872	1.50
17628832	Dact2	146	1.85
17634960	Ddias	67	1.75
17828625	Ddit3	227	2.07
17769238	Dok5	182	1.64
17833617	Dot1l	431	2.12
17850594	Dpy19l2	39	1.55
17682903	Dusp10	353	1.61
17765931	Dusp2	145	3.21
17712103	Dusp4	267	1.85
17626435	Dusp5	197	2.70
17706222	Eaf1	208	1.82
17877966	Eda2r	204	3.65
17705094	Ednrb	836	1.70
17748848	Efna1	336	1.86
17722348	Egr1	1291	1.68
17699889	Egr3	90	1.69
17834736	Eid3	82	3.13
17734860	Ell2	198	1.80
17735400	Enc1	549	1.50
17803896	Epha2	112	2.95
17693433	Ereg	68	4.14
17804459	Errfi1	1256	1.94
17735859	Esm1	217	1.82
17664927	Ets2	517	1.93
17739583	Etv3	287	1.60
17815275	Fam110c	100	3.24
17741698	Fam212b	82	2.51
17806608	Fam219a	115	1.52
17669931	Fam43a	306	1.59
17610500	Fbxo30	329	1.72
17852444	Fdx1	196	1.57
17817508	Fos	121	2.25
17630236	Fosb	59	6.02
17623115	Fosl1	115	5.16
17716029	Gabpb1l	215	1.57
17791733	Gadd45a	695	2.40
17718415	Gadd45g	412	3.17
17846065	Gclc	634	2.69
17742399	Gclm	337	1.69
17707117	Gdf15	116	15.19
17797288	Gem	317	1.98
17654535	Gfer	173	1.71

**Table A4 cont.**

<b>Transcript ID</b>	<b>Gene Symbol</b>	<b>Control</b>	<b>H<sub>2</sub>O<sub>2</sub></b>
		<b>(Raw values)</b>	<b>(Relative to controls)</b>
17645401	Gfpt2	1557	<b>1.83</b>
17693015	Gpat3	105	<b>3.32</b>
17815053	Grhl1	87	<b>1.67</b>
17730641	Gse1	202	<b>1.58</b>
17716626	Gtpbp4	176	<b>1.66</b>
17831416	Gtse1	101	<b>2.45</b>
17628982	Has1	81	<b>1.69</b>
17837405	Has2	286	<b>2.05</b>
17725668	Hbegf	363	<b>2.19</b>
17669934	Hes1	471	<b>1.70</b>
17715718	Hist1h2bh	527	<b>1.65</b>
17715802	Hist1h4b	153	<b>1.66</b>
17610557	Hivep2	489	<b>1.71</b>
17753387	Hmga1	774	<b>1.66</b>
17728071	Hmox1	1149	<b>3.41</b>
17752874	Hspa1a/b	103	<b>2.07</b>
17816804	Hspa2	112	<b>1.59</b>
17674382	Hspb8	908	<b>1.65</b>
17718644	Id4	107	<b>1.83</b>
17728750	Ier2	191	<b>1.98</b>
17756250	Ier3	782	<b>1.93</b>
17685432	Ier5	332	<b>1.90</b>
17858730	Il1rl1	430	<b>2.14</b>
17788345	Il6	108	<b>1.99</b>
17719769	Inhba	220	<b>2.47</b>
17681323	Intron to Gas5	133	<b>1.61</b>
17769167	Intron to LOC100911177	311	<b>1.53</b>
17769169	Intron to LOC100911177	73	<b>1.54</b>
17623687	Intron to Snhg1	78	<b>1.51</b>
17700736	Ipo5	764	<b>1.58</b>
17617588	Isg20	64	<b>5.97</b>
17710887	Jund	470	<b>1.62</b>
17840711	Kansl2	389	<b>1.54</b>
17654269	Kctd5	233	<b>1.55</b>
17836999	Klf10	245	<b>1.66</b>
17807351	Klf4	345	<b>1.91</b>
17880605	Klf5	333	<b>1.72</b>
17700455	Klf5	270	<b>1.53</b>
17707169	Klhl26	148	<b>1.60</b>
17856642	Klhl40	98	<b>3.05</b>
17691166	Lif	167	<b>3.09</b>
17785906	Lmcd1	441	<b>2.38</b>
17739110	LOC100910449	80	<b>2.02</b>
17807593	LOC102550203	284	<b>1.86</b>
17692310	LOC102551714	57	<b>1.84</b>
17637453	LOC102554302	229	<b>1.66</b>
17787531	LOC689800	59	<b>1.90</b>
17663983	Mafg	204	<b>1.77</b>
17708402	Mak16	229	<b>1.56</b>

**Table A4 cont.**

Transcript ID	Gene Symbol	Control	H <sub>2</sub> O <sub>2</sub>
		(Raw values)	(Relative to controls)
17646559	Map2k3	364	1.93
17836020	Mdm2	366	5.14
17711465	Mfap3l	169	1.62
17700626	Mir18a	37	1.57
17700628	Mir19a	39	1.69
17648510	Mir22	147	1.77
17732589	Mir27a	55	1.56
17714890	Mirlet7f-1	38	2.09
17749411	Mllt11	412	1.57
17792604	Mthfd2	348	1.54
17792855	Mxd1	231	1.86
17796946	Mybl1	70	3.00
17829696	Myc	264	2.41
17659041	NF1	142	1.86
17714621	Nfil3	203	1.68
17741409	Ngf	102	1.68
17869377	Nid2	146	1.66
17733371	Nob1	441	1.58
17738403	Noct	206	2.53
17733363	Nqo1	347	2.83
17832476	Nr4a1	178	4.78
17772385	Nr4a2	165	1.70
17798725	Nr4a3	63	11.10
17645338	Olr1387	40	2.12
17619333	Olr230	36	1.73
17779084	Oser1	444	1.62
17730529	Osgin1	76	3.12
17717422	Otud1	152	1.69
17769225	Pard6b	74	2.74
17634940	Pcf11	359	1.50
17745324	Pelo	489	1.83
17716849	Pfkfb3	397	1.50
17828155	Phlda1	306	2.35
17680418	Phlda3	220	2.84
17614190	Plaur	252	1.68
17844002	Plet1	62	5.15
17735703	Plk2	1381	1.55
17723942	Pmaip1	45	1.86
17842335	Ppan	192	1.57
17756153	Ppp1r10	465	1.57
17632926	Ppp1r15a	311	1.78
17666316	Ppp1r2	470	1.74
17712060	Pragmin	239	2.18
17793342	Prickle2	230	1.76
17719280	Prl6a1	31	1.92
17775140	Prrg4	582	1.52
17771568	Psmc5	183	1.56
17680795	Ptgs2	712	2.22
17859412	Ptp4a1	1544	1.72

**Table A4 cont.**

Transcript ID	Gene Symbol	Control	H <sub>2</sub> O <sub>2</sub>
		(Raw values)	(Relative to controls)
17863629	Ptp4a1	1246	1.76
17630418	PVR	516	2.32
17679974	Rab7b	122	1.84
17738821	Rap2b	152	1.63
17734548	Rbm34	180	1.52
17689820	Rbm47	84	1.55
17668004	Rcan1	1895	1.52
17805250	Rdh10	153	1.57
17861997	RGD1562136	96	1.73
17834704	RGD1563365	120	1.51
17774787	RGD1564664	158	1.84
17684906	Rgs2	370	3.29
17821038	Rhob	597	1.65
17649347	Rhot1	42	1.53
17721512	Riok3	590	1.50
17806037	Ripk2	421	1.68
17840784	Rnd1	444	2.00
17730862	Rpl13	206	1.58
17766170	Rpl22l2	54	1.72
17614756	Rpl28	41	1.53
17610687	Rps13	40	1.69
17772976	Rps3	53	1.56
17857692	Runx2	160	1.67
17639867	Sac3d1	89	1.83
17814680	Sdc1	560	1.58
17679473	Serpib2	251	6.69
17676856	Serpine1	764	2.76
17614694	Sertad1	176	1.62
17802844	Sesn2	163	3.65
17751449	Sgms2	152	2.73
17747564	Siah2	355	1.56
17757468	Sik1	457	1.67
17652327	Slc16a6	203	2.23
17681552	Slc19a2	147	2.74
17696492	Slc1a4	361	1.86
17777498	Slc23a2	197	1.69
17801572	Slc2a1	1520	1.61
17683239	Slc30a1	236	2.19
17836034	Slc35e3	537	1.56
17725180	Slc39a6	603	1.62
17864290	Slc40a1	246	1.62
17671549	Slc7a1	575	1.67
17747235	Slc7a11	99	4.32
17649532	Slnf2	280	1.57
17770731	Snhg7	1268	1.70
17735293	Snora47	63	1.56
17793995	Snora7a	295	1.61
17844990	Snord16a	100	1.53
17709866	Snord19	121	1.55

**Table A4 cont.**

<b>Transcript ID</b>	<b>Gene Symbol</b>	<b>Control</b>	<b>H<sub>2</sub>O<sub>2</sub></b>
		<b>(Raw values)</b>	<b>(Relative to controls)</b>
17623689	Snord22	111	<b>1.59</b>
17736124	Snord72	43	<b>1.52</b>
17645306	Snord95	137	<b>1.51</b>
17745308	Snx18	693	<b>1.60</b>
17663683	Socs3	503	<b>1.57</b>
17655823	Sqstm1	609	<b>1.95</b>
17819714	Srsf7	158	<b>1.57</b>
17767319	Srxn1	94	<b>8.55</b>
17712330	Star	109	<b>1.80</b>
17737660	Terc	118	<b>1.86</b>
17789522	Tfpi2	101	<b>1.78</b>
17777978	Thbd	107	<b>1.55</b>
17758158	Tmem26	160	<b>1.53</b>
17654148	Tnfrsf12a	877	<b>1.87</b>
17638748	Tnfrsf22	170	<b>2.15</b>
17650292	Tob1	871	<b>1.76</b>
17797247	Tp53inp1	549	<b>2.97</b>
17778298	Trib3	100	<b>1.89</b>
17646726	Trim16	182	<b>1.51</b>
17738669	Tsc22d2	425	<b>1.52</b>
17652422	Ttyh2	285	<b>1.63</b>
17723990	Tubb6	1014	<b>1.74</b>
17834717	Txnrd1	630	<b>2.68</b>
17686443	Uap1	169	<b>6.08</b>
17814012	Uap1l2	64	<b>3.74</b>
17673512	Ubc	1018	<b>1.84</b>
17691637	Unknown	63	<b>1.62</b>
17674327	Unknown	235	<b>1.59</b>
17808103	Unknown	119	<b>1.58</b>
17873757	Unknown	145	<b>1.79</b>
17624595	Unknown	175	<b>1.52</b>
17831177	Unknown	130	<b>1.67</b>
17844970	Unknown	130	<b>1.67</b>
17862391	Unknown	106	<b>2.62</b>
17769925	Unknown	201	<b>1.55</b>
17719481	Unknown	81	<b>1.82</b>
17862387	Unknown	214	<b>1.86</b>
17862389	Unknown	192	<b>1.83</b>
17868712	Unknown	58	<b>1.53</b>
17868967	Unknown	190	<b>1.63</b>
17857041	Unknown	195	<b>1.53</b>
17761562	Unknown	189	<b>1.69</b>
17881046	Unknown	268	<b>1.57</b>
17825181	Unknown	295	<b>1.61</b>
17612614	Unknown	40	<b>1.53</b>
17848154	Unknown	73	<b>1.75</b>
17709357	Unknown	414	<b>1.52</b>

**Table A4 cont.**

<b>Transcript ID</b>	<b>Gene Symbol</b>	<b>Control</b>	<b>H<sub>2</sub>O<sub>2</sub></b>
		<b>(Raw values)</b>	<b>(Relative to controls)</b>
17820466	Wdr43	598	<b>1.50</b>
17856543	Xirp1	1051	<b>2.79</b>
17628094	Zbtb2	134	<b>1.59</b>
17852451	Zc3h12c	302	<b>1.87</b>
17672229	Zfand2a	306	<b>3.57</b>
17624514	Zfand5	1288	<b>1.66</b>
17631103	Zfp36	617	<b>2.06</b>
17614769	Zfp626	95	<b>1.55</b>
17737682	Zmat3	198	<b>1.94</b>

**Table A5 Transcripts downregulated in response to H<sub>2</sub>O<sub>2</sub>**

Cardiomyocytes were unstimulated (Control) or exposed to H<sub>2</sub>O<sub>2</sub> (0.2 mM, 2 h). Changes in RNA expression were determined using Affymetrix Rat Gene 2.0 ST microarrays, using GeneSpring 14.5 analysis to identify RNAs with significant decrease in expression in response to H<sub>2</sub>O<sub>2</sub> (>1.5-fold change relative to control; moderated t-test with Benjamini-Hochberg FDR correction, p<0.05). Raw values are given for controls and results are the mean fold change relative to controls (n=4 independent hybridisations).

<b>Transcript ID</b>	<b>Gene Symbol</b>	<b>Control (Raw values)</b>	<b>H<sub>2</sub>O<sub>2</sub> (Relative to controls)</b>
17799707	Acer2	313	<b>0.47</b>
17667628	Adamts5	510	<b>0.58</b>
17719191	Agtr1a	357	<b>0.66</b>
17815851	Akap6	742	<b>0.66</b>
17789297	Akap9	477	<b>0.67</b>
17846985	Amotl2	396	<b>0.66</b>
17837080	Angpt1	232	<b>0.60</b>
17796393	Antisense to Rassf8	129	<b>0.66</b>
17763560	Aplnr	199	<b>0.65</b>
17845894	Arpp19	97	<b>0.66</b>
17680619	Aspm	97	<b>0.57</b>
17792236	Atoh8	268	<b>0.59</b>
17878335	Atrx	629	<b>0.65</b>
17673260	Auts2l	238	<b>0.64</b>
17680721	B3galt2	333	<b>0.59</b>
17843642	Bcl9l	503	<b>0.57</b>
17764983	Casc5	125	<b>0.62</b>
17880642	Ccdc141	132	<b>0.62</b>
17744890	Ccnb1	118	<b>0.58</b>
17843026	Cdon	918	<b>0.49</b>
17742771	Cenpe	140	<b>0.61</b>
17687536	Cenpf	178	<b>0.58</b>
17854478	Cep162	112	<b>0.63</b>
17782474	Chrm2	1605	<b>0.58</b>
17777174	Ckap2l	90	<b>0.60</b>
17872611	Dmd	954	<b>0.58</b>
17858146	Dst	1133	<b>0.66</b>

**Table A5 cont.**

<b>Transcript ID</b>	<b>Gene Symbol</b>	<b>Control (Raw values)</b>	<b>H<sub>2</sub>O<sub>2</sub> (Relative to controls)</b>
17699765	Ebf2	122	<b>0.62</b>
17637939	Ebf3	321	<b>0.59</b>
17746602	Ect2	112	<b>0.64</b>
17865182	Erbb4	159	<b>0.66</b>
17815588	Etv1	226	<b>0.65</b>
17611079	Eya4	111	<b>0.63</b>
17771237	Fam78a	231	<b>0.64</b>
17768463	Fam83d	136	<b>0.62</b>
17776634	Fbn1	1963	<b>0.62</b>
17772756	Figf	139	<b>0.64</b>
17696327	Figf1	167	<b>0.64</b>
17808333	Frem1	241	<b>0.62</b>
17675438	Fry	645	<b>0.66</b>
17687729	G0s2	527	<b>0.49</b>
17815757	G2e3	171	<b>0.67</b>
17821495	Gpr22	156	<b>0.60</b>
17655129	Hba1	972	<b>0.28</b>
17655107	Hba1/2	155	<b>0.30</b>
17655118	Hba-a1	221	<b>0.33</b>
17635606	Hbb	308	<b>0.24</b>
17635600	Hbb-b1	97	<b>0.42</b>
17635616	Hbb-b1	315	<b>0.33</b>
17715833	Hist1h1b	299	<b>0.59</b>
17700037	Htr2a	367	<b>0.66</b>
17762176	Intron to Cacnb4	235	<b>0.60</b>
17759530	Intron to Ebf3	79	<b>0.66</b>
17748808	Intron to Fdps	173	<b>0.59</b>
17855024	Intron to Ppp2r3a	166	<b>0.66</b>
17755547	Intron to Rev3l	59	<b>0.66</b>
17711829	Intron to Sorbs2	217	<b>0.60</b>
17837524	Intron to Tmem65	116	<b>0.66</b>
17865965	Irs1	279	<b>0.61</b>
17717602	Irx4	418	<b>0.60</b>
17764518	Kcna4	96	<b>0.64</b>
17618664	Kcne3	453	<b>0.61</b>
17860796	Kcne4	319	<b>0.64</b>
17796225	Kcnj8	466	<b>0.67</b>
17625128	Kif20b	69	<b>0.61</b>
17853237	Kif23	132	<b>0.65</b>
17809656	Kif2c	103	<b>0.67</b>
17748476	Kirrel	682	<b>0.66</b>
17785455	Klf15	128	<b>0.56</b>
17837495	Klhl38	160	<b>0.56</b>
17813889	Kpna2	2186	<b>0.59</b>
17662569	Kpna2	1843	<b>0.63</b>
17736233	Lifr	841	<b>0.56</b>

**Table A5 cont.**

<b>Transcript ID</b>	<b>Gene Symbol</b>	<b>Control (Raw values)</b>	<b>H<sub>2</sub>O<sub>2</sub> (Relative to controls)</b>
17686320	LOC685351	118	<b>0.39</b>
17728554	LOC685411	104	<b>0.66</b>
17669287	LOC689217	70	<b>0.58</b>
17714742	LOC689587	55	<b>0.67</b>
17836590	Lrp1	1961	<b>0.62</b>
17828320	Lrrc10	260	<b>0.59</b>
17810315	Macf1	1159	<b>0.61</b>
17735024	Mef2c	392	<b>0.66</b>
17782472	Mir490	64	<b>0.63</b>
17822197	Mis18bp1	86	<b>0.66</b>
17637913	Mki67	646	<b>0.50</b>
17720028	MPP7	383	<b>0.58</b>
17720030	Mpp7	858	<b>0.67</b>
17704998	Mycbp2	491	<b>0.63</b>
17721099	Nabl	1255	<b>0.65</b>
17808303	Nfib	1999	<b>0.62</b>
17835031	Nr1h4	128	<b>0.62</b>
17633908	Nr2f2	574	<b>0.66</b>
17731247	Nrp1	1316	<b>0.65</b>
17877478	Obp1f	68	<b>0.62</b>
17849828	Olr1115	83	<b>0.59</b>
17645356	Olr1397	206	<b>0.64</b>
17840683	Olr1877	64	<b>0.53</b>
17635740	Olr194	58	<b>0.66</b>
17618063	Olr20	63	<b>0.60</b>
17747228	Pcdh18	332	<b>0.56</b>
17694650	Pcdh7	765	<b>0.66</b>
17711915	Pcm1	687	<b>0.65</b>
17694084	Pdgfra	2983	<b>0.58</b>
17665547	Phldb2	1041	<b>0.66</b>
17690991	Pik3ip1	330	<b>0.51</b>
17620368	Plk1	372	<b>0.45</b>
17690210	Ppargc1a	581	<b>0.55</b>
17670970	Prkdc	212	<b>0.64</b>
17687572	Prox1	247	<b>0.57</b>
17659777	Prr11	74	<b>0.58</b>
17845217	Rasl12	190	<b>0.59</b>
17795994	Rerg	393	<b>0.59</b>
17766923	Rin2	354	<b>0.65</b>
17800088	Ror1	519	<b>0.64</b>
17797354	Runx1t1	347	<b>0.55</b>
17716433	Ryr2	1853	<b>0.61</b>
17789488	Samd9l	382	<b>0.54</b>
17789483	Samd9l	211	<b>0.66</b>

**Table A5 cont.**

<b>Transcript ID</b>	<b>Gene Symbol</b>	<b>Control (Raw values)</b>	<b>H<sub>2</sub>O<sub>2</sub> (Relative to controls)</b>
17856909	Sgol1	65	<b>0.64</b>
17859327	Sgol2	62	<b>0.61</b>
17737579	Slc2a2	147	<b>0.63</b>
17854985	Slc35g2	103	<b>0.65</b>
17649522	Slfn5	528	<b>0.60</b>
17853413	Smad6	564	<b>0.53</b>
17738567	Smad9	208	<b>0.60</b>
17852869	Snx33	406	<b>0.53</b>
17636071	St5	431	<b>0.51</b>
17699814	Stc1	1401	<b>0.49</b>
17813989	Ston1	363	<b>0.62</b>
17807544	Svep1	360	<b>0.63</b>
17795793	Tas2r113	54	<b>0.64</b>
17850618	Tbx20	3376	<b>0.62</b>
17611107	Tcf21	281	<b>0.58</b>
17758246	Tet1	386	<b>0.63</b>
17688028	Tgfbr3	1314	<b>0.63</b>
17827700	Tmcc3	125	<b>0.56</b>
17798353	Tmem8b	107	<b>0.51</b>
17865381	Tnp1	64	<b>0.66</b>
17830802	Tnrc6b	610	<b>0.66</b>
17660863	Top2a	326	<b>0.53</b>
17767437	Tpx2	179	<b>0.62</b>
17821133	Trib2	346	<b>0.60</b>
17748341	Trim2	262	<b>0.63</b>
17846281	Ttk	97	<b>0.66</b>
17628672	Ttll2	70	<b>0.64</b>
17773733	Ttn	283	<b>0.46</b>
17773418	Ttn	2498	<b>0.53</b>
17824838	Unknown	49	<b>0.59</b>
17869552	Unknown	72	<b>0.62</b>
17846920	Unknown	146	<b>0.67</b>
17683590	Unknown	95	<b>0.61</b>
17778194	Unknown	80	<b>0.62</b>
17688837	Unknown	97	<b>0.62</b>
17696705	Unknown	72	<b>0.61</b>
17739289	Unknown	212	<b>0.66</b>
17834493	Unknown	131	<b>0.66</b>
17870224	Unknown	89	<b>0.64</b>
17681386	Unknown	77	<b>0.65</b>
17669427	Unknown	276	<b>0.62</b>
17673323	Unknown	555	<b>0.58</b>
17784265	Unknown	291	<b>0.62</b>
17617825	Unknown	105	<b>0.59</b>
17867695	Unknown	95	<b>0.67</b>
17748455	Unknown	209	<b>0.65</b>
17725000	Unknown	227	<b>0.62</b>
17702423	Unknown	109	<b>0.66</b>
17719529	Unknown	98	<b>0.66</b>
17618570	Unknown	77	<b>0.60</b>
17735950	Unknown	67	<b>0.59</b>
17851236	Unknown	74	<b>0.62</b>

**Table A5 cont.**

<b>Transcript ID</b>	<b>Gene Symbol</b>	<b>Control (Raw values)</b>	<b>H<sub>2</sub>O<sub>2</sub> (Relative to controls)</b>
17862549	Unknown	113	<b>0.65</b>
17686829	Unknown	71	<b>0.61</b>
17676207	Unknown	94	<b>0.65</b>
17824985	Unknown	75	<b>0.66</b>
17640505	Unknown	72	<b>0.64</b>
17755940	Unknown	66	<b>0.63</b>
17667572	Unknown	249	<b>0.63</b>
17734970	Unknown	110	<b>0.65</b>
17824511	Unknown	121	<b>0.66</b>
17815738	Unknown	336	<b>0.55</b>
17867308	Unknown	1570	<b>0.48</b>
17867314	Unknown	2176	<b>0.56</b>
17690416	Unknown	59	<b>0.62</b>
17878327	Unknown	233	<b>0.63</b>
17867296	Unknown	85	<b>0.63</b>
17612467	Vom1r19	80	<b>0.67</b>
17628732	Vom2r-ps18	80	<b>0.64</b>
17709537	Zcchc24	834	<b>0.62</b>
17791192	Zfp467	201	<b>0.57</b>
17726303	Zfp608	468	<b>0.61</b>
17829163	Zfpm2	348	<b>0.67</b>

**Table A6 Transcripts upregulated by H<sub>2</sub>O<sub>2</sub> and unaffected by any MAPK inhibitor**

Cardiomyocytes were unstimulated or exposed to H<sub>2</sub>O<sub>2</sub> (0.2 mM, 2 h) with or without pre-treatment (15 min) with 2 μM PD184352, 1 μM JNK-IN-8 or 0.7 μM SB203580, or exposed to the inhibitors alone (2 h 15 min). Changes in RNA expression were determined using Affymetrix Rat Gene 2.0 ST microarrays, using GeneSpring 14.5 analysis to identify RNAs with significant increase in expression in response to H<sub>2</sub>O<sub>2</sub> (>1.5-fold change relative to control; moderated t-test with Benjamini-Hochberg FDR correction, p<0.05) without a significant effect of the inhibitors. Raw values are given for controls and results are the mean fold changes relative to controls (n=3/4 independent hybridisations). PD, PD184352. JI8, JNK-IN-8. SB, SB203580.

Transcript ID	Gene Symbol	Control	PD	JI8	SB	H <sub>2</sub> O <sub>2</sub>	PD+H <sub>2</sub> O <sub>2</sub>	JI8+H <sub>2</sub> O <sub>2</sub>	SB+H <sub>2</sub> O <sub>2</sub>
		(Raw values)	(Relative to controls)						
17810550	Adprhl2	153	0.97	1.01	1.01	<b>1.53</b>	1.41	1.37	1.39
17617581	Aen	113	1.01	1.16	1.01	<b>3.48</b>	3.49	3.34	3.20
17717253	Arl5b	261	1.03	1.10	1.03	<b>1.90</b>	1.62	1.82	1.93
17726777	Atp8b1	277	1.06	1.00	1.03	<b>1.53</b>	1.89	1.36	1.49
17664484	Bach1	517	0.77	1.12	1.09	<b>2.21</b>	1.78	2.16	2.03
17653231	Baiap2	212	1.64	1.28	1.23	<b>1.75</b>	2.04	1.84	1.72
17796337	Bcat1	357	0.95	1.04	0.98	<b>1.55</b>	1.59	1.52	1.56
17766015	Bcl2l11	160	1.70	1.31	1.09	<b>1.76</b>	1.69	1.93	1.49
17636338	Btbd10	136	1.13	1.21	1.11	<b>1.65</b>	2.01	1.71	1.63
17826458	Cbarp	109	0.86	0.93	0.94	<b>1.51</b>	1.24	1.61	1.54
17664759	Cbr1	1116	1.02	1.06	1.00	<b>1.51</b>	1.19	1.80	1.40
17664780	Cbr3	105	1.17	1.05	1.10	<b>1.64</b>	1.35	1.76	1.49
17655535	Ccng1	2202	1.11	1.10	1.10	<b>1.51</b>	1.66	1.56	1.59
17774921	Cd44	663	0.80	1.07	1.04	<b>1.66</b>	1.61	1.70	1.59
17669098	Cd80	104	1.15	1.06	1.08	<b>5.00</b>	5.95	5.09	5.13

**Table A6 cont.**

Transcript ID	Gene Symbol	Control	PD	Jl8	SB	H <sub>2</sub> O <sub>2</sub>	PD+H <sub>2</sub> O <sub>2</sub>	Jl8+H <sub>2</sub> O <sub>2</sub>	SB+H <sub>2</sub> O <sub>2</sub>
		(Raw values)	(Relative to controls)						
17765084	Chac1	119	1.25	1.13	0.91	<b>3.03</b>	2.44	3.18	2.79
17748939	Chrn2	70	1.14	1.10	1.07	<b>1.58</b>	1.52	1.56	1.70
17859270	Coq10b	187	1.19	1.17	1.09	<b>1.72</b>	2.08	1.49	1.40
17716200	Crem	139	1.25	1.24	1.25	<b>1.93</b>	2.08	1.76	1.78
17750384	Csf1	1259	1.30	1.08	1.25	<b>1.58</b>	1.92	1.61	1.74
17727278	Ctdp1	247	1.14	1.14	1.03	<b>1.64</b>	1.39	1.61	1.35
17828625	Ddit3	227	1.31	1.20	1.25	<b>2.07</b>	1.91	1.90	2.43
17850594	Dpy19l2	39	1.13	1.03	1.06	<b>1.55</b>	1.37	1.70	1.66
17877966	Eda2r	204	1.44	1.49	1.37	<b>3.65</b>	3.49	3.68	3.76
17834736	Eid3	82	1.02	1.25	1.18	<b>3.13</b>	3.00	3.13	2.73
17734860	Ell2	198	1.19	1.22	1.03	<b>1.80</b>	2.24	1.74	1.56
17735400	Enc1	549	0.92	1.05	0.90	<b>1.50</b>	1.35	1.56	1.40
17735859	Esm1	217	1.50	1.47	1.14	<b>1.82</b>	2.00	1.89	1.49
17741698	Fam212b	82	1.39	1.12	1.16	<b>2.51</b>	2.96	2.41	2.42
17806608	Fam219a	115	1.08	1.03	1.10	<b>1.52</b>	1.44	1.32	1.43
17610500	Fbxo30	329	0.86	0.99	0.90	<b>1.72</b>	1.82	1.70	1.53
17852444	Fdx1	196	0.97	1.14	1.01	<b>1.57</b>	1.32	1.50	1.32
17817508	Fos	121	0.73	1.05	1.28	<b>2.25</b>	2.13	2.12	2.35
17623115	Fosl1	115	0.44	1.11	1.10	<b>5.16</b>	4.42	4.15	4.85
17791733	Gadd45a	695	1.06	1.07	1.43	<b>2.40</b>	1.98	2.27	2.63
17742399	Gclm	337	1.32	1.38	1.30	<b>1.69</b>	1.95	1.71	1.67

**Table A6 cont.**

Transcript ID	Gene Symbol	Control	PD	JI8	SB	H <sub>2</sub> O <sub>2</sub>	PD+H <sub>2</sub> O <sub>2</sub>	JI8+H <sub>2</sub> O <sub>2</sub>	SB+H <sub>2</sub> O <sub>2</sub>
		(Raw values)	(Relative to controls)						
17654535	Gfer	173	1.15	1.12	1.07	<b>1.71</b>	1.89	1.73	1.68
17645401	Gfpt2	1557	0.91	1.27	1.04	<b>1.83</b>	2.27	2.12	1.68
17815053	Grhl1	87	1.22	1.24	1.10	<b>1.67</b>	1.42	1.67	1.68
17669934	Hes1	471	0.86	1.17	0.96	<b>1.70</b>	1.38	1.73	1.41
17715802	Hist1h4b	153	1.30	1.27	1.25	<b>1.66</b>	1.90	1.72	1.52
17610557	Hivep2	489	0.98	1.11	1.04	<b>1.71</b>	1.55	1.67	1.58
17816804	Hspa2	112	1.10	0.89	0.88	<b>1.59</b>	1.89	1.53	1.35
17617588	Isg20	64	1.25	1.48	1.66	<b>5.97</b>	6.37	6.41	6.07
17840711	Kansl2	389	1.05	1.11	1.03	<b>1.54</b>	1.39	1.28	1.24
17654269	Kctd5	233	1.05	1.08	1.04	<b>1.55</b>	1.25	1.50	1.46
17836999	Klf10	245	0.99	1.04	1.17	<b>1.66</b>	1.70	1.42	1.69
17707169	Klhl26	148	1.19	1.08	0.94	<b>1.60</b>	1.62	1.74	1.58
17807593	LOC102550203	284	1.16	1.20	1.13	<b>1.86</b>	2.24	2.24	1.99
17637453	LOC102554302	229	1.04	0.93	0.88	<b>1.66</b>	1.60	1.64	1.80
17663983	Mafg	204	0.89	1.13	1.14	<b>1.77</b>	1.70	1.72	1.77
17708402	Mak16	229	1.02	1.22	0.99	<b>1.56</b>	1.58	1.58	1.40
17836020	Mdm2	366	1.14	1.10	0.95	<b>5.14</b>	5.35	4.66	4.55
17648510	Mir22	147	1.23	1.41	1.19	<b>1.77</b>	1.95	1.87	1.49
17792604	Mthfd2	348	1.19	1.29	1.15	<b>1.54</b>	1.88	1.81	1.67
17796946	Mybl1	70	0.88	1.11	0.98	<b>3.00</b>	3.03	2.83	2.82
17659041	NF1	142	1.14	1.23	1.07	<b>1.86</b>	1.76	1.79	1.90

**Table A6 cont.**

Transcript ID	Gene Symbol	Control	PD	JI8	SB	H <sub>2</sub> O <sub>2</sub>	PD+H <sub>2</sub> O <sub>2</sub>	JI8+H <sub>2</sub> O <sub>2</sub>	SB+H <sub>2</sub> O <sub>2</sub>
		(Raw values)	(Relative to controls)						
17714621	Nfil3	203	1.14	0.81	0.85	<b>1.68</b>	1.99	1.37	1.40
17733371	Nob1	441	1.11	1.18	1.13	<b>1.58</b>	1.38	1.43	1.37
17733363	Nqo1	347	1.12	1.25	0.94	<b>2.83</b>	3.29	3.32	2.50
17779084	Oser1	444	1.08	1.12	1.05	<b>1.62</b>	1.93	1.70	1.62
17730529	Osgin1	76	1.11	1.18	1.21	<b>3.12</b>	3.41	3.04	2.91
17716849	Pfkfb3	397	1.27	0.91	1.00	<b>1.50</b>	1.27	1.26	1.29
17735703	Plk2	1381	0.61	0.71	1.00	<b>1.55</b>	1.62	1.29	1.42
17723942	Pmaip1	45	0.89	0.95	0.92	<b>1.86</b>	2.26	1.62	1.63
17842335	Ppan	192	0.88	1.11	1.02	<b>1.57</b>	1.53	1.66	1.46
17756153	Ppp1r10	465	1.03	0.97	0.88	<b>1.57</b>	1.66	1.59	1.61
17632926	Ppp1r15a	311	1.05	0.90	1.12	<b>1.78</b>	1.98	1.50	1.71
17793342	Prickle2	230	0.70	1.02	1.01	<b>1.76</b>	1.75	1.78	1.78
17775140	Prrg4	582	0.89	0.85	0.98	<b>1.52</b>	1.29	1.39	1.49
17771568	Psmc5	183	1.24	1.12	1.15	<b>1.56</b>	1.61	1.48	1.83
17859412	Ptp4a1	1544	1.09	1.14	1.08	<b>1.72</b>	1.83	1.84	1.65
17863629	Ptp4a1	1246	1.11	1.16	1.11	<b>1.76</b>	1.87	1.85	1.66
17738821	Rap2b	152	1.09	1.21	1.17	<b>1.63</b>	1.90	1.67	1.60
17734548	Rbm34	180	0.95	1.21	1.26	<b>1.52</b>	1.47	1.59	1.61
17689820	Rbm47	84	0.89	1.05	0.91	<b>1.55</b>	1.34	1.42	1.28
17805250	Rdh10	153	1.02	1.17	1.17	<b>1.57</b>	1.76	1.61	1.49
17861997	RGD1562136	96	0.98	1.32	1.36	<b>1.73</b>	1.40	1.63	1.67

**Table A6 cont.**

Transcript ID	Gene Symbol	Control	PD	JI8	SB	H <sub>2</sub> O <sub>2</sub>	PD+H <sub>2</sub> O <sub>2</sub>	JI8+H <sub>2</sub> O <sub>2</sub>	SB+H <sub>2</sub> O <sub>2</sub>
		(Raw values)	(Relative to controls)						
17834704	RGD1563365	120	0.90	1.18	1.16	<b>1.51</b>	1.21	1.53	1.43
17774787	RGD1564664	158	1.87	1.24	1.16	<b>1.84</b>	2.51	1.60	1.67
17721512	Riok3	590	0.93	1.04	0.96	<b>1.50</b>	1.55	1.56	1.42
17806037	Ripk2	421	1.02	1.07	1.02	<b>1.68</b>	1.36	1.59	1.52
17639867	Sac3d1	89	1.04	1.04	0.94	<b>1.83</b>	1.90	1.79	1.76
17614694	Sertad1	176	1.06	1.04	0.98	<b>1.62</b>	1.46	1.51	1.68
17802844	Sesn2	163	1.45	1.47	1.24	<b>3.65</b>	4.20	3.62	3.35
17747564	Siah2	355	1.09	1.17	1.13	<b>1.56</b>	1.38	1.44	1.40
17681552	Slc19a2	147	1.00	1.08	1.12	<b>2.74</b>	2.78	3.13	2.96
17696492	Slc1a4	361	1.06	1.18	1.31	<b>1.86</b>	1.99	1.89	1.92
17777498	Slc23a2	197	1.05	1.19	1.17	<b>1.69</b>	1.48	1.61	1.67
17683239	Slc30a1	236	1.21	1.06	1.05	<b>2.19</b>	2.19	1.97	1.99
17836034	Slc35e3	537	1.03	0.97	1.08	<b>1.56</b>	1.37	1.40	1.50
17725180	Slc39a6	603	0.94	0.93	0.86	<b>1.62</b>	1.77	1.59	1.53
17864290	Slc40a1	246	1.72	1.29	1.22	<b>1.62</b>	1.50	1.90	1.60
17671549	Slc7a1	575	0.90	1.10	1.02	<b>1.67</b>	1.72	1.66	1.51
17735293	Snora47	63	1.11	1.24	1.08	<b>1.56</b>	1.77	1.52	1.50
17793995	Snora7a	295	0.97	1.03	0.96	<b>1.61</b>	1.81	1.60	1.49
17844990	Snord16a	100	1.19	1.27	1.08	<b>1.53</b>	1.82	1.57	1.32
17709866	Snord19	121	1.13	1.26	1.19	<b>1.55</b>	1.86	1.84	1.35
17736124	Snord72	43	1.14	1.39	1.09	<b>1.52</b>	1.71	1.51	1.29
17645306	Snord95	137	1.11	1.28	1.06	<b>1.51</b>	1.41	1.66	1.48

**Table A6 cont.**

Transcript ID	Gene Symbol	Control	PD	JI8	SB	H <sub>2</sub> O <sub>2</sub>	PD+H <sub>2</sub> O <sub>2</sub>	JI8+H <sub>2</sub> O <sub>2</sub>	SB+H <sub>2</sub> O <sub>2</sub>
		(Raw values)	(Relative to controls)						
17745308	Snx18	693	0.69	0.93	0.97	<b>1.60</b>	1.34	1.44	1.48
17663683	Socs3	503	0.89	0.85	0.90	<b>1.57</b>	1.76	1.42	1.27
17655823	Sqstm1	609	1.36	1.20	1.09	<b>1.95</b>	2.15	2.14	1.73
17819714	Srsf7	158	1.22	1.19	1.03	<b>1.57</b>	1.81	1.57	1.34
17712330	Star	109	0.93	1.05	1.05	<b>1.80</b>	1.58	1.78	1.48
17638748	Tnfrsf22	170	0.85	0.96	0.94	<b>2.15</b>	1.91	2.08	2.01
17797247	Tp53inp1	549	1.09	0.98	1.00	<b>2.97</b>	3.54	2.90	2.69
17778298	Trib3	100	0.95	0.98	0.96	<b>1.89</b>	1.54	1.96	1.78
17652422	Ttyh2	285	0.83	1.21	1.13	<b>1.63</b>	1.50	2.01	1.78
17723990	Tubb6	1014	0.94	0.95	1.07	<b>1.74</b>	1.60	1.46	1.62
17834717	Txnrd1	630	1.00	1.11	0.97	<b>2.68</b>	2.38	2.70	2.35
17673512	Ubc	1018	1.22	0.99	0.92	<b>1.84</b>	2.16	1.84	1.49
17868712	Unknown	58	1.04	0.96	1.04	<b>1.53</b>	1.53	1.47	1.69
17868967	Unknown	190	0.96	0.86	1.02	<b>1.63</b>	1.56	1.54	1.70
17857041	Unknown	195	1.10	1.19	1.03	<b>1.53</b>	1.33	1.52	1.54
17761562	Unknown	189	1.22	1.37	1.36	<b>1.69</b>	1.89	1.70	1.66
17881046	Unknown	268	0.98	1.16	1.04	<b>1.57</b>	1.69	1.58	1.52
17825181	Unknown	295	0.97	1.03	0.96	<b>1.61</b>	1.81	1.60	1.49
17612614	Unknown	40	1.33	1.42	1.59	<b>1.53</b>	1.25	1.27	1.33
17848154	Unknown	73	1.13	1.32	1.01	<b>1.75</b>	1.67	1.66	1.42
17709357	Unknown	414	1.47	1.35	1.45	<b>1.52</b>	1.66	1.35	1.22

**Table A6 cont.**

Transcript ID	Gene Symbol	Control	PD	Jl8	SB	H <sub>2</sub> O <sub>2</sub>	PD+H <sub>2</sub> O <sub>2</sub>	Jl8+H <sub>2</sub> O <sub>2</sub>	SB+H <sub>2</sub> O <sub>2</sub>
		(Raw values)	(Relative to controls)						
17820466	Wdr43	598	0.84	1.01	0.96	<b>1.50</b>	1.41	1.47	1.37
17628094	Zbtb2	134	0.96	1.07	1.04	<b>1.59</b>	1.45	1.50	1.59
17852451	Zc3h12c	302	1.17	1.20	1.14	<b>1.87</b>	1.64	2.28	2.02
17672229	Zfand2a	306	1.06	1.10	1.00	<b>3.57</b>	3.85	3.49	2.86
17624514	Zfand5	1288	1.10	1.00	0.98	<b>1.66</b>	1.47	1.61	1.56
17614769	Zfp626	95	1.38	1.37	1.19	<b>1.55</b>	1.28	1.74	1.58
17737682	Zmat3	198	1.08	1.01	0.99	<b>1.94</b>	1.68	1.78	1.75

**Table A7 Transcripts downregulated by H<sub>2</sub>O<sub>2</sub> and unaffected by any MAPK inhibitor**

Cardiomyocytes were unstimulated or exposed to H<sub>2</sub>O<sub>2</sub> (0.2 mM, 2 h) with or without pre-treatment (15 min) with 2 μM PD184352, 1 μM JNK-IN-8 or 0.7 μM SB203580, or exposed to the inhibitors alone (2 h 15 min). Changes in RNA expression were determined using Affymetrix Rat Gene 2.0 ST microarrays, using GeneSpring 14.5 analysis to identify RNAs with significant decrease in expression in response to H<sub>2</sub>O<sub>2</sub> (>1.5-fold change relative to control; moderated t-test with Benjamini-Hochberg FDR correction, p<0.05) without a significant effect of the inhibitors. Raw values are given for controls and results are the mean fold changes relative to controls (n=3/4 independent hybridisations). PD, PD184352. JI8, JNK-IN-8. SB, SB203580. PD, PD184352. JI8, JNK-IN-8. SB, SB203580.

Transcript ID	Gene Symbol	Control	PD	JI8	SB	H <sub>2</sub> O <sub>2</sub>	PD+H <sub>2</sub> O <sub>2</sub>	JI8+H <sub>2</sub> O <sub>2</sub>	SB+H <sub>2</sub> O <sub>2</sub>
		(Raw values)	(Relative to controls)						
17815851	Akap6	742	0.91	0.98	0.99	<b>0.66</b>	0.55	0.64	0.72
17789297	Akap9	477	0.91	0.98	0.96	<b>0.67</b>	0.70	0.72	0.78
17846985	Amotl2	396	0.93	0.98	0.93	<b>0.66</b>	0.73	0.63	0.74
17837080	Angpt1	232	0.88	0.88	1.01	<b>0.60</b>	0.71	0.64	0.70
17845894	Arpp19	97	1.17	1.17	0.95	<b>0.66</b>	0.59	0.56	0.70
17878335	Atrx	629	0.91	1.01	0.99	<b>0.65</b>	0.71	0.74	0.80
17673260	Auts2l	238	0.97	0.97	0.96	<b>0.64</b>	0.67	0.69	0.72
17680721	B3galt2	333	1.06	1.12	1.06	<b>0.59</b>	0.51	0.62	0.61
17744890	Ccnb1	118	1.06	1.15	1.03	<b>0.58</b>	0.69	0.65	0.66
17742771	Cenpe	140	0.87	1.02	0.92	<b>0.61</b>	0.67	0.72	0.72
17687536	Cenpf	178	0.88	0.98	0.98	<b>0.58</b>	0.64	0.68	0.69
17782474	Chrm2	1605	0.93	1.06	0.93	<b>0.58</b>	0.55	0.64	0.64
17872611	Dmd	954	0.91	0.98	0.97	<b>0.58</b>	0.46	0.55	0.63
17858146	Dst	1133	0.98	1.00	1.00	<b>0.66</b>	0.64	0.69	0.74
17699765	Ebf2	122	0.88	1.04	1.00	<b>0.62</b>	0.65	0.68	0.77

Table A7 cont.

Transcript ID	Gene Symbol	Control	PD	Jl8	SB	H <sub>2</sub> O <sub>2</sub>	PD+H <sub>2</sub> O <sub>2</sub>	Jl8+H <sub>2</sub> O <sub>2</sub>	SB+H <sub>2</sub> O <sub>2</sub>
		(Raw values)	(Relative to controls)						
17637939	Ebf3	321	1.16	1.10	1.14	<b>0.59</b>	0.73	0.62	0.72
17776634	Fbn1	1963	1.01	0.98	0.96	<b>0.62</b>	0.77	0.75	0.76
17772756	Fign	139	1.07	1.17	1.15	<b>0.64</b>	0.70	0.70	0.75
17696327	Fignl1	167	1.07	0.94	0.93	<b>0.64</b>	0.68	0.65	0.68
17675438	Fry	645	0.98	0.99	0.90	<b>0.66</b>	0.55	0.67	0.66
17687729	G0s2	527	1.20	1.09	0.93	<b>0.49</b>	0.54	0.54	0.48
17815757	G2e3	171	1.09	1.17	1.00	<b>0.67</b>	0.68	0.79	0.75
17821495	Gpr22	156	1.04	1.09	0.75	<b>0.60</b>	0.72	0.63	0.57
17655129	Hba1	972	0.92	0.80	0.77	<b>0.28</b>	0.25	0.33	0.29
17655118	Hba-a1	221	0.98	0.80	0.80	<b>0.33</b>	0.38	0.36	0.33
17635616	Hbb-b1	315	0.95	0.82	0.77	<b>0.33</b>	0.33	0.37	0.35
17700037	Htr2a	367	1.03	1.01	0.92	<b>0.66</b>	0.60	0.64	0.59
17762176	Intron to Cacnb4	235	0.89	0.80	0.87	<b>0.60</b>	0.75	0.69	0.64
17748808	Intron to Fdps	173	0.98	1.20	0.94	<b>0.59</b>	0.55	0.62	0.56
17855024	Intron to Ppp2r3a	166	1.24	1.01	0.98	<b>0.66</b>	0.75	0.56	0.81
17837524	Intron to Tmem65	116	0.97	0.84	0.88	<b>0.66</b>	0.79	0.67	0.77
17865965	Irs1	279	0.79	0.92	0.97	<b>0.61</b>	0.65	0.59	0.64
17717602	Irx4	418	0.94	1.05	0.79	<b>0.60</b>	0.67	0.71	0.64
17764518	Kcna4	96	0.69	0.95	0.85	<b>0.64</b>	0.57	0.57	0.56
17796225	Kcnj8	466	0.76	1.12	1.00	<b>0.67</b>	0.65	0.81	0.77
17809656	Kif2c	103	1.12	1.07	1.09	<b>0.67</b>	0.75	0.82	0.79

Table A7 cont.

Transcript ID	Gene Symbol	Control	PD	Jl8	SB	H <sub>2</sub> O <sub>2</sub>	PD+H <sub>2</sub> O <sub>2</sub>	Jl8+H <sub>2</sub> O <sub>2</sub>	SB+H <sub>2</sub> O <sub>2</sub>
		(Raw values)	(Relative to controls)						
17785455	Klf15	128	1.05	1.16	0.97	<b>0.56</b>	0.67	0.66	0.64
17837495	Klhl38	160	1.25	1.29	1.39	<b>0.56</b>	0.68	0.58	0.65
17813889	Kpna2	2186	0.92	1.02	0.88	<b>0.59</b>	0.61	0.74	0.65
17662569	Kpna2	1843	0.97	1.06	0.90	<b>0.63</b>	0.64	0.76	0.65
17828320	Lrrc10	260	0.76	1.04	0.82	<b>0.59</b>	0.61	0.72	0.66
17810315	Macf1	1159	1.05	1.04	1.03	<b>0.61</b>	0.64	0.68	0.74
17735024	Mef2c	392	0.83	0.96	0.92	<b>0.66</b>	0.72	0.70	0.75
17782472	Mir490	64	1.01	1.06	0.83	<b>0.63</b>	0.62	0.58	0.64
17720028	MPP7	383	1.04	1.11	0.94	<b>0.58</b>	0.52	0.64	0.61
17720030	Mpp7	858	1.20	1.22	1.09	<b>0.67</b>	0.62	0.69	0.68
17704998	Mycbp2	491	1.12	1.02	0.99	<b>0.63</b>	0.76	0.73	0.78
17808303	Nfib	1999	0.94	0.98	0.99	<b>0.62</b>	0.68	0.70	0.74
17835031	Nr1h4	128	1.24	0.96	1.02	<b>0.62</b>	0.76	0.63	0.67
17633908	Nr2f2	574	0.95	0.96	0.87	<b>0.66</b>	0.60	0.80	0.61
17635740	Olr194	58	0.93	1.03	0.78	<b>0.66</b>	0.72	0.79	0.69
17747228	Pcdh18	332	1.28	1.04	1.05	<b>0.56</b>	0.59	0.68	0.70
17694650	Pcdh7	765	1.13	1.11	1.03	<b>0.66</b>	0.60	0.75	0.68
17665547	Phldb2	1041	0.84	1.12	0.98	<b>0.66</b>	0.60	0.76	0.76
17670970	Prkdc	212	1.04	1.04	1.03	<b>0.64</b>	0.74	0.74	0.79
17687572	Prox1	247	0.98	1.11	0.97	<b>0.57</b>	0.55	0.65	0.60

Table A7 cont.

Transcript ID	Gene Symbol	Control	PD	Jl8	SB	H <sub>2</sub> O <sub>2</sub>	PD+H <sub>2</sub> O <sub>2</sub>	Jl8+H <sub>2</sub> O <sub>2</sub>	SB+H <sub>2</sub> O <sub>2</sub>
		(Raw values)	(Relative to controls)						
17766923	Rin2	354	0.85	1.00	1.07	<b>0.65</b>	0.62	0.71	0.75
17800088	Ror1	519	0.97	1.01	0.99	<b>0.64</b>	0.75	0.74	0.72
17797354	Runx1t1	347	1.43	1.17	1.22	<b>0.55</b>	0.58	0.56	0.62
17716433	Ryr2	1853	1.02	1.00	0.95	<b>0.61</b>	0.50	0.62	0.64
17789488	Samd9l	382	0.89	0.75	0.93	<b>0.54</b>	0.62	0.57	0.64
17789483	Samd9l	211	0.91	0.93	1.04	<b>0.66</b>	0.61	0.60	0.63
17807544	Svep1	360	0.96	0.99	0.97	<b>0.63</b>	0.75	0.70	0.73
17850618	Tbx20	3376	1.09	1.12	0.89	<b>0.62</b>	0.69	0.75	0.67
17688028	Tgfb3	1314	1.11	1.05	1.05	<b>0.63</b>	0.71	0.70	0.73
17827700	Tmcc3	125	0.78	1.00	0.98	<b>0.56</b>	0.54	0.55	0.63
17830802	Tnrc6b	610	1.24	1.08	1.02	<b>0.66</b>	0.74	0.74	0.81
17773418	Ttn	2498	1.03	1.02	0.90	<b>0.53</b>	0.47	0.53	0.57
17851236	Unknown	74	0.87	0.71	0.70	<b>0.62</b>	0.72	0.72	0.78
17862549	Unknown	113	0.79	0.83	0.95	<b>0.65</b>	0.69	0.74	0.80
17686829	Unknown	71	0.76	1.03	0.89	<b>0.61</b>	0.70	0.77	0.76
17676207	Unknown	94	0.94	0.95	1.04	<b>0.65</b>	0.80	0.79	0.80
17824985	Unknown	75	0.87	0.79	0.92	<b>0.66</b>	0.69	0.78	0.79
17640505	Unknown	72	0.69	0.74	0.85	<b>0.64</b>	0.73	0.60	0.71
17755940	Unknown	66	0.69	0.98	0.87	<b>0.63</b>	0.54	0.67	0.70
17667572	Unknown	249	0.81	0.89	0.95	<b>0.63</b>	0.78	0.78	0.70
17734970	Unknown	110	0.94	0.90	0.78	<b>0.65</b>	0.74	0.67	0.69

Table A7 cont.

Transcript ID	Gene Symbol	Control	PD	Jl8	SB	H <sub>2</sub> O <sub>2</sub>	PD+H <sub>2</sub> O <sub>2</sub>	Jl8+H <sub>2</sub> O <sub>2</sub>	SB+H <sub>2</sub> O <sub>2</sub>
		(Raw values)	(Relative to controls)						
17824511	Unknown	121	0.84	0.88	0.95	<b>0.66</b>	0.73	0.70	0.67
17815738	Unknown	336	0.57	0.63	0.79	<b>0.55</b>	0.46	0.55	0.56
17867308	Unknown	1570	1.11	1.32	1.17	<b>0.48</b>	0.52	0.51	0.49
17867314	Unknown	2176	1.00	1.05	1.00	<b>0.56</b>	0.68	0.59	0.57
17690416	Unknown	59	0.87	0.88	0.71	<b>0.62</b>	0.73	0.66	0.62
17878327	Unknown	233	0.93	1.08	1.03	<b>0.63</b>	0.61	0.73	0.60
17867296	Unknown	85	1.07	1.10	1.07	<b>0.63</b>	0.69	0.59	0.59
17791192	Zfp467	201	1.05	0.90	0.74	<b>0.57</b>	0.65	0.54	0.61
17829163	Zfpm2	348	1.03	0.95	0.96	<b>0.67</b>	0.70	0.66	0.75

**Table A8 Transcripts upregulated by H<sub>2</sub>O<sub>2</sub> and unaffected by PD184352**

Cardiomyocytes were unstimulated (Control) or exposed to H<sub>2</sub>O<sub>2</sub> (0.2 mM, 2 h) with or without pre-treatment (15 min) with 2 µM PD184352 or with or without pre-treatment (15 min), or were exposed to the PD184352 alone (2 h 15 min) Changes in RNA expression were determined using Affymetrix Rat Gene 2.0 ST microarrays, using GeneSpring 14.5 analysis to identify RNAs with significant increase in expression in response to H<sub>2</sub>O<sub>2</sub> (>1.5-fold change relative to control; moderated t-test with Benjamini-Hochberg FDR correction, p<0.05) with no effect of PD184352. Raw values are given for controls and results are the mean fold change relative to controls (n=3/4 independent hybridisations). PD, PD184352.

Transcript ID	Gene Symbol	Control	PD	H <sub>2</sub> O <sub>2</sub>	PD+H <sub>2</sub> O <sub>2</sub>
		(Raw values)	(Relative to controls)		
17810550	Adprhl2	153	0.97	<b>1.53</b>	1.41
17617581	Aen	113	1.01	<b>3.48</b>	3.49
17858347	Arid5a	218	1.02	<b>2.18</b>	2.26
17717253	Arl5b	261	1.03	<b>1.90</b>	1.62
17670615	Arvcf	113	1.20	<b>1.53</b>	1.59
17687609	Atf3	132	1.81	<b>7.45</b>	9.28
17673406	Atp5j2	65	1.04	<b>1.51</b>	1.00
17726777	Atp8b1	277	1.06	<b>1.53</b>	1.89
17664484	Bach1	517	0.77	<b>2.21</b>	1.78
17621224	Bag3	801	1.09	<b>1.58</b>	1.48
17653231	Baiap2	212	1.64	<b>1.75</b>	2.04
17796337	Bcat1	357	0.95	<b>1.55</b>	1.59
17766015	Bcl2l11	160	1.70	<b>1.76</b>	1.69
17636338	Btbd10	136	1.13	<b>1.65</b>	2.01
17826458	Cbarp	109	0.86	<b>1.51</b>	1.24
17664759	Cbr1	1116	1.02	<b>1.51</b>	1.19
17664780	Cbr3	105	1.17	<b>1.64</b>	1.35
17655535	Ccng1	2202	1.11	<b>1.51</b>	1.66
17774921	Cd44	663	0.80	<b>1.66</b>	1.61
17669098	Cd80	104	1.15	<b>5.00</b>	5.95
17753672	Cdkn1a	604	1.24	<b>5.59</b>	5.88
17765084	Chac1	119	1.25	<b>3.03</b>	2.44
17748939	Chrn2	70	1.14	<b>1.58</b>	1.52
17610582	Cited2	1010	1.12	<b>1.68</b>	1.76
17859270	Coq10b	187	1.19	<b>1.72</b>	2.08
17716200	Crem	139	1.25	<b>1.93</b>	2.08
17750384	Csf1	1259	1.30	<b>1.58</b>	1.92
17856536	Csrnp1	120	1.19	<b>3.28</b>	3.03
17727278	Ctdp1	247	1.14	<b>1.64</b>	1.39
17628832	Dact2	146	1.06	<b>1.85</b>	1.59
17828625	Ddit3	227	1.31	<b>2.07</b>	1.91
17833617	Dot1l	431	1.03	<b>2.12</b>	2.04
17850594	Dpy19l2	39	1.13	<b>1.55</b>	1.37
17682903	Dusp10	353	1.33	<b>1.61</b>	1.88
17877966	Eda2r	204	1.44	<b>3.65</b>	3.49
17705094	Ednrb	836	1.19	<b>1.70</b>	1.79

**Table A8 cont.**

Transcript ID	Gene Symbol	Control	PD	H <sub>2</sub> O <sub>2</sub>	PD+H <sub>2</sub> O <sub>2</sub>
		(Raw values)	(Relative to controls)		
17834736	Eid3	82	1.02	<b>3.13</b>	3.00
17734860	Eil2	198	1.19	<b>1.80</b>	2.24
17735400	Enc1	549	0.92	<b>1.50</b>	1.35
17735859	Esm1	217	1.50	<b>1.82</b>	2.00
17664927	Ets2	517	1.34	<b>1.93</b>	1.98
17815275	Fam110c	100	2.12	<b>3.24</b>	4.75
17741698	Fam212b	82	1.39	<b>2.51</b>	2.96
17806608	Fam219a	115	1.08	<b>1.52</b>	1.44
17610500	Fbxo30	329	0.86	<b>1.72</b>	1.82
17852444	Fdx1	196	0.97	<b>1.57</b>	1.32
17817508	Fos	121	0.73	<b>2.25</b>	2.13
17630236	Fosb	59	0.94	<b>6.02</b>	5.07
17623115	Fosl1	115	0.44	<b>5.16</b>	4.42
17791733	Gadd45a	695	1.06	<b>2.40</b>	1.98
17742399	Gclm	337	1.32	<b>1.69</b>	1.95
17707117	Gdf15	116	1.19	<b>15.19</b>	13.41
17654535	Gfer	173	1.15	<b>1.71</b>	1.89
17645401	Gfpt2	1557	0.91	<b>1.83</b>	2.27
17815053	Grhl1	87	1.22	<b>1.67</b>	1.42
17716626	Gtpbp4	176	1.10	<b>1.66</b>	1.63
17837405	Has2	286	0.52	<b>2.05</b>	1.83
17669934	Hes1	471	0.86	<b>1.70</b>	1.38
17715802	Hist1h4b	153	1.30	<b>1.66</b>	1.90
17610557	Hivep2	489	0.98	<b>1.71</b>	1.55
17728071	Hmox1	1149	1.12	<b>3.41</b>	3.24
17816804	Hspa2	112	1.10	<b>1.59</b>	1.89
17674382	Hspb8	908	0.97	<b>1.65</b>	1.66
17718644	Id4	107	1.22	<b>1.83</b>	1.47
17685432	Ier5	332	0.90	<b>1.90</b>	1.78
17719769	Inhba	220	0.68	<b>2.47</b>	3.48
17769167	Intron to LOC100911177	311	0.93	<b>1.53</b>	1.56
17769169	Intron to LOC100911177	73	1.17	<b>1.54</b>	1.64
17617588	Isg20	64	1.25	<b>5.97</b>	6.37
17840711	Kansl2	389	1.05	<b>1.54</b>	1.39
17654269	Kctd5	233	1.05	<b>1.55</b>	1.25
17836999	Klf10	245	0.99	<b>1.66</b>	1.70
17707169	Klhl26	148	1.19	<b>1.60</b>	1.62
17807593	LOC102550203	284	1.16	<b>1.86</b>	2.24
17637453	LOC102554302	229	1.04	<b>1.66</b>	1.60
17663983	Mafg	204	0.89	<b>1.77</b>	1.70
17708402	Mak16	229	1.02	<b>1.56</b>	1.58
17836020	Mdm2	366	1.14	<b>5.14</b>	5.35

**Table A8 cont.**

Transcript ID	Gene Symbol	Control	PD	H <sub>2</sub> O <sub>2</sub>	PD+H <sub>2</sub> O <sub>2</sub>
		(Raw values)	(Relative to controls)		
17648510	Mir22	147	1.23	<b>1.77</b>	1.95
17732589	Mir27a	55	1.15	<b>1.56</b>	1.71
17714890	Mirlet7f-1	38	1.68	<b>2.09</b>	1.92
17792604	Mthfd2	348	1.19	<b>1.54</b>	1.88
17792855	Mxd1	231	1.32	<b>1.86</b>	1.79
17796946	Mybl1	70	0.88	<b>3.00</b>	3.03
17829696	Myc	264	0.60	<b>2.41</b>	1.97
17659041	NF1	142	1.14	<b>1.86</b>	1.76
17714621	Nfil3	203	1.14	<b>1.68</b>	1.99
17733371	Nob1	441	1.11	<b>1.58</b>	1.38
17738403	Noct	206	0.75	<b>2.53</b>	2.13
17733363	Nqo1	347	1.12	<b>2.83</b>	3.29
17832476	Nr4a1	178	0.97	<b>4.78</b>	4.97
17798725	Nr4a3	63	1.06	<b>11.10</b>	11.07
17779084	Oser1	444	1.08	<b>1.62</b>	1.93
17730529	Osgin1	76	1.11	<b>3.12</b>	3.41
17634940	Pcf11	359	1.10	<b>1.50</b>	1.72
17716849	Pfkfb3	397	1.27	<b>1.50</b>	1.27
17680418	Phlda3	220	1.08	<b>2.84</b>	2.97
17614190	Plaur	252	0.84	<b>1.68</b>	1.55
17735703	Plk2	1381	0.61	<b>1.55</b>	1.62
17723942	Pmaip1	45	0.89	<b>1.86</b>	2.26
17842335	Ppan	192	0.88	<b>1.57</b>	1.53
17756153	Ppp1r10	465	1.03	<b>1.57</b>	1.66
17632926	Ppp1r15a	311	1.05	<b>1.78</b>	1.98
17793342	Prickle2	230	0.70	<b>1.76</b>	1.75
17775140	Prrg4	582	0.89	<b>1.52</b>	1.29
17771568	Psmd5	183	1.24	<b>1.56</b>	1.61
17680795	Ptgs2	712	0.47	<b>2.22</b>	2.46
17859412	Ptp4a1	1544	1.09	<b>1.72</b>	1.83
17863629	Ptp4a1	1246	1.11	<b>1.76</b>	1.87
17679974	Rab7b	122	1.51	<b>1.84</b>	2.41
17738821	Rap2b	152	1.09	<b>1.63</b>	1.90
17734548	Rbm34	180	0.95	<b>1.52</b>	1.47
17689820	Rbm47	84	0.89	<b>1.55</b>	1.34
17805250	Rdh10	153	1.02	<b>1.57</b>	1.76
17861997	RGD1562136	96	0.98	<b>1.73</b>	1.40
17834704	RGD1563365	120	0.90	<b>1.51</b>	1.21
17774787	RGD1564664	158	1.87	<b>1.84</b>	2.51
17649347	Rhot1	42	1.22	<b>1.53</b>	1.39
17721512	Riok3	590	0.93	<b>1.50</b>	1.55
17806037	Ripk2	421	1.02	<b>1.68</b>	1.36

**Table A8 cont.**

Transcript ID	Gene Symbol	Control	PD	H <sub>2</sub> O <sub>2</sub>	PD+H <sub>2</sub> O <sub>2</sub>
		(Raw values)		(Relative to controls)	
17730862	Rpl13	206	1.07	<b>1.58</b>	1.43
17766170	Rpl22l2	54	1.75	<b>1.72</b>	2.41
17614756	Rpl28	41	1.14	<b>1.53</b>	1.36
17610687	Rps13	40	1.27	<b>1.69</b>	1.45
17772976	Rps3	53	1.09	<b>1.56</b>	1.31
17639867	Sac3d1	89	1.04	<b>1.83</b>	1.90
17614694	Sertad1	176	1.06	<b>1.62</b>	1.46
17802844	Sesn2	163	1.45	<b>3.65</b>	4.20
17747564	Siah2	355	1.09	<b>1.56</b>	1.38
17681552	Slc19a2	147	1.00	<b>2.74</b>	2.78
17696492	Slc1a4	361	1.06	<b>1.86</b>	1.99
17777498	Slc23a2	197	1.05	<b>1.69</b>	1.48
17683239	Slc30a1	236	1.21	<b>2.19</b>	2.19
17836034	Slc35e3	537	1.03	<b>1.56</b>	1.37
17725180	Slc39a6	603	0.94	<b>1.62</b>	1.77
17864290	Slc40a1	246	1.72	<b>1.62</b>	1.50
17671549	Slc7a1	575	0.90	<b>1.67</b>	1.72
17747235	Slc7a11	99	1.20	<b>4.32</b>	4.37
17735293	Snora47	63	1.11	<b>1.56</b>	1.77
17793995	Snora7a	295	0.97	<b>1.61</b>	1.81
17844990	Snord16a	100	1.19	<b>1.53</b>	1.82
17709866	Snord19	121	1.13	<b>1.55</b>	1.86
17736124	Snord72	43	1.14	<b>1.52</b>	1.71
17645306	Snord95	137	1.11	<b>1.51</b>	1.41
17745308	Snx18	693	0.69	<b>1.60</b>	1.34
17663683	Socs3	503	0.89	<b>1.57</b>	1.76
17655823	Sqstm1	609	1.36	<b>1.95</b>	2.15
17819714	Srsf7	158	1.22	<b>1.57</b>	1.81
17767319	Srxn1	94	1.36	<b>8.55</b>	7.84
17712330	Star	109	0.93	<b>1.80</b>	1.58
17777978	Thbd	107	1.02	<b>1.55</b>	1.27
17654148	Tnfrsf12a	877	0.78	<b>1.87</b>	1.59
17638748	Tnfrsf22	170	0.85	<b>2.15</b>	1.91
17797247	Tp53inp1	549	1.09	<b>2.97</b>	3.54
17778298	Trib3	100	0.95	<b>1.89</b>	1.54
17738669	Tsc22d2	425	0.89	<b>1.52</b>	1.54
17652422	Ttyh2	285	0.83	<b>1.63</b>	1.50
17723990	Tubb6	1014	0.94	<b>1.74</b>	1.60
17834717	Txnrd1	630	1.00	<b>2.68</b>	2.38
17686443	Uap1	169	1.11	<b>6.08</b>	7.05
17814012	Uap1l2	64	0.93	<b>3.74</b>	4.05
17673512	Ubc	1018	1.22	<b>1.84</b>	2.16

**Table A8 cont.**

Transcript ID	Gene Symbol	Control	PD	H <sub>2</sub> O <sub>2</sub>	PD+H <sub>2</sub> O <sub>2</sub>
		(Raw values)		(Relative to controls)	
17691637	Unknown	63	1.07	<b>1.62</b>	1.39
17674327	Unknown	235	1.03	<b>1.59</b>	1.44
17808103	Unknown	119	1.01	<b>1.58</b>	1.52
17873757	Unknown	145	0.84	<b>1.79</b>	1.50
17624595	Unknown	175	1.22	<b>1.52</b>	1.53
17831177	Unknown	130	0.90	<b>1.67</b>	1.61
17844970	Unknown	130	0.90	<b>1.67</b>	1.61
17769925	Unknown	201	1.38	<b>1.55</b>	1.90
17868712	Unknown	58	1.04	<b>1.53</b>	1.53
17868967	Unknown	190	0.96	<b>1.63</b>	1.56
17857041	Unknown	195	1.10	<b>1.53</b>	1.33
17761562	Unknown	189	1.22	<b>1.69</b>	1.89
17881046	Unknown	268	0.98	<b>1.57</b>	1.69
17825181	Unknown	295	0.97	<b>1.61</b>	1.81
17612614	Unknown	40	1.33	<b>1.53</b>	1.25
17848154	Unknown	73	1.13	<b>1.75</b>	1.67
17709357	Unknown	414	1.47	<b>1.52</b>	1.66
17820466	Wdr43	598	0.84	<b>1.50</b>	1.41
17628094	Zbtb2	134	0.96	<b>1.59</b>	1.45
17852451	Zc3h12c	302	1.17	<b>1.87</b>	1.64
17672229	Zfand2a	306	1.06	<b>3.57</b>	3.85
17624514	Zfand5	1288	1.10	<b>1.66</b>	1.47
17631103	Zfp36	617	0.81	<b>2.06</b>	1.82
17614769	Zfp626	95	1.38	<b>1.55</b>	1.28
17737682	Zmat3	198	1.08	<b>1.94</b>	1.68

**Table A9 Transcripts upregulated by H<sub>2</sub>O<sub>2</sub> and inhibited by PD184352**

Cardiomyocytes were unstimulated (Control) or exposed to H<sub>2</sub>O<sub>2</sub> (0.2 mM, 2 h) with or without pre-treatment (15 min) with 2 µM PD184352, or were exposed to PD184352 alone (2 h 15 min). Changes in RNA expression were determined using Affymetrix Rat Gene 2.0 ST microarrays, using GeneSpring 14.5 analysis to identify RNAs with significant increase in expression in response to H<sub>2</sub>O<sub>2</sub> (>1.5-fold change relative to control; moderated t-test with Benjamini-Hochberg FDR correction, p<0.05). RNAs inhibited >1.25-fold in the presence of PD184352 were selected, with or without a significant effect of the inhibitor (one-way ANOVA with SNK post-test and Benjamini-Hochberg FDR correction, p<0.05). RNAs with significant changes in the presence of PD184352 are indicated with an asterisk (\*). Raw values are given for controls and results are the mean fold change relative to controls (n=3/4 independent hybridisations). PD, PD184352.

Transcript ID	Gene Symbol	Control (Raw values)	PD	H <sub>2</sub> O <sub>2</sub> (Relative to controls)	PD+H <sub>2</sub> O <sub>2</sub>	
17782314	Akr1b8	564	1.11	<b>2.33</b>	1.60	*
17693425	Areg	82	0.99	<b>1.61</b>	1.26	
17705843	Arhgef3	189	0.80	<b>2.09</b>	1.06	*
17652634	Armc7	131	0.94	<b>2.20</b>	1.51	*
17759590	Arrdc3	1034	0.90	<b>1.58</b>	1.27	
17861066	B3gnt7	67	0.95	<b>1.58</b>	1.13	
17818164	Bdkrb2	181	1.03	<b>2.83</b>	1.79	
17766552	Bmp2	193	0.89	<b>2.06</b>	1.44	
17684316	Btg2	308	0.75	<b>2.91</b>	1.78	*
17664770	Cbr1	246	0.96	<b>2.84</b>	1.36	*
17630241	Cd3eap	85	0.99	<b>1.50</b>	1.18	*
17808573	Cdkn2b	257	0.60	<b>1.56</b>	0.74	*
17847383	Cish	357	0.91	<b>2.15</b>	1.54	
17769238	Dok5	182	1.00	<b>1.64</b>	1.21	
17765931	Dusp2	145	0.91	<b>3.21</b>	1.79	*
17712103	Dusp4	267	0.27	<b>1.85</b>	1.15	
17626435	Dusp5	197	0.45	<b>2.70</b>	1.03	*
17706222	Eaf1	208	0.75	<b>1.82</b>	1.33	*
17748848	Efna1	336	0.95	<b>1.86</b>	0.97	*
17722348	Egr1	1291	0.05	<b>1.68</b>	0.13	*
17699889	Egr3	90	0.79	<b>1.69</b>	0.81	*
17803896	Epha2	112	0.52	<b>2.95</b>	1.30	*
17804459	Errfi1	1256	0.74	<b>1.94</b>	1.50	*
17739583	Etv3	287	0.92	<b>1.60</b>	1.24	*
17669931	Fam43a	306	0.89	<b>1.59</b>	1.23	
17716029	Gabpb1l	215	1.09	<b>1.57</b>	1.22	*
17718415	Gadd45g	412	0.94	<b>3.17</b>	2.50	
17846065	Gclc	634	0.91	<b>2.69</b>	2.02	*
17797288	Gem	317	1.17	<b>1.98</b>	1.28	*
17693015	Gpat3	105	1.12	<b>3.32</b>	2.52	
17730641	Gse1	202	0.99	<b>1.58</b>	1.16	*
17725668	Hbegf	363	0.61	<b>2.19</b>	1.26	*

Table A9 cont.

Transcript ID	Gene Symbol	Control	PD	H <sub>2</sub> O <sub>2</sub>	PD+H <sub>2</sub> O <sub>2</sub>	
		(Raw values)		(Relative to controls)		
17753387	Hmga1	774	0.92	<b>1.66</b>	1.14	*
17728750	Ier2	191	0.63	<b>1.98</b>	1.02	*
17756250	Ier3	782	0.72	<b>1.93</b>	1.33	*
17858730	Il1r1	430	0.93	<b>2.14</b>	1.47	
17700736	Ipo5	764	0.98	<b>1.58</b>	1.20	*
17700455	Klf5	270	1.01	<b>1.53</b>	1.05	*
17880605	Klf5	333	1.00	<b>1.72</b>	0.98	*
17856642	Klhl40	98	0.93	<b>3.05</b>	1.33	*
17691166	Lif	167	0.42	<b>3.09</b>	1.75	*
17785906	Lmcd1	441	0.72	<b>2.38</b>	1.58	
17787531	LOC689800	59	0.80	<b>1.90</b>	0.93	*
17646559	Map2k3	364	0.96	<b>1.93</b>	1.31	*
17711465	Mfap3l	169	0.80	<b>1.62</b>	1.09	*
17700626	Mir18a	37	0.86	<b>1.57</b>	1.12	*
17700628	Mir19a	39	0.89	<b>1.69</b>	1.34	
17749411	Milt11	412	0.74	<b>1.57</b>	1.11	
17869377	Nid2	146	1.03	<b>1.66</b>	1.14	*
17619333	Olr230	36	1.04	<b>1.73</b>	1.18	
17717422	Otud1	152	0.68	<b>1.69</b>	1.23	
17769225	Pard6b	74	1.12	<b>2.74</b>	1.36	*
17745324	Pelo	489	0.75	<b>1.83</b>	1.21	*
17828155	Phlda1	306	0.15	<b>2.35</b>	1.05	*
17844002	Plet1	62	1.32	<b>5.15</b>	2.72	
17712060	Pragmin	239	0.58	<b>2.18</b>	0.82	*
17719280	Prl6a1	31	0.82	<b>1.92</b>	1.11	*
17630418	PVR	516	0.84	<b>2.32</b>	1.82	
17668004	Rcan1	1895	0.79	<b>1.52</b>	1.21	
17684906	Rgs2	370	0.40	<b>3.29</b>	2.06	
17840784	Rnd1	444	0.86	<b>2.00</b>	1.59	
17857692	Runx2	160	0.57	<b>1.67</b>	0.61	*
17814680	Sdc1	560	1.14	<b>1.58</b>	1.11	*
17679473	Serpinb2	251	0.69	<b>6.69</b>	4.39	
17751449	Sgms2	152	1.05	<b>2.73</b>	1.73	*
17757468	Sik1	457	0.76	<b>1.67</b>	0.94	
17652327	Slc16a6	203	0.87	<b>2.23</b>	1.64	
17801572	Slc2a1	1520	0.80	<b>1.61</b>	1.07	*
17649532	Slfn2	280	0.90	<b>1.57</b>	1.16	*
17789522	Tfpi2	101	0.44	<b>1.78</b>	1.16	*
17758158	Tmem26	160	1.00	<b>1.53</b>	0.93	*
17646726	Trim16	182	0.88	<b>1.51</b>	1.15	
17856543	Xirp1	1051	0.56	<b>2.79</b>	0.89	*

**Table A10 Transcripts upregulated by H<sub>2</sub>O<sub>2</sub> and enhanced by PD184352**

Cardiomyocytes were unstimulated (Control) or exposed to H<sub>2</sub>O<sub>2</sub> (0.2 mM, 2 h), with or without pre-treatment (15 min) with 2 μM PD184352, or were exposed to PD184352 alone (2h 15 min). Changes in RNA expression were determined using Affymetrix Rat Gene 2.0 ST microarrays, using GeneSpring 14.5 analysis to identify RNAs with significant increase in expression in response to H<sub>2</sub>O<sub>2</sub> (>1.5-fold change relative to control; moderated t-test with Benjamini-Hochberg FDR correction, p<0.05). RNAs enhanced >1.25-fold in the presence of PD184352 were selected, with or without a significant effect of the inhibitor (one-way ANOVA with SNK post-test and Benjamini-Hochberg FDR correction, p<0.05). RNAs with significant changes in the presence of PD184352 are indicated with an asterisk (\*). Raw values are given for controls and results are the mean fold change relative to controls (n=3/4 independent hybridisations). PD, PD184352.

Transcript ID	Gene Symbol	Control	PD	H <sub>2</sub> O <sub>2</sub>	PD+H <sub>2</sub> O <sub>2</sub>	
		(Raw values)	(Relative to controls)			
17781129	Abcb1a	541	1.26	<b>3.48</b>	4.97	*
17821662	Arl4a	120	1.37	<b>1.57</b>	2.35	*
17632894	Bax	143	1.17	<b>1.76</b>	2.39	*
17753161	Brd2	722	1.34	<b>1.70</b>	2.16	*
17747788	Ccnl1	471	1.35	<b>1.52</b>	2.40	*
17868794	Cd80	54	1.22	<b>5.22</b>	6.60	
17708936	Ckap2	81	1.28	<b>1.81</b>	3.12	*
17751869	Cyr61	872	0.67	<b>1.50</b>	2.87	*
17634960	Ddias	67	0.99	<b>1.75</b>	2.37	
17693433	Ereg	68	1.42	<b>4.14</b>	6.41	*
17831416	Gtse1	101	1.14	<b>2.45</b>	3.29	*
17628982	Has1	81	1.52	<b>1.69</b>	5.35	*
17715718	Hist1h2bh	527	1.49	<b>1.65</b>	2.20	
17752874	Hspa1a/b	103	0.91	<b>2.07</b>	2.61	
17788345	Il6	108	0.37	<b>1.99</b>	3.30	*
17681323	Intron to Gas5	133	1.69	<b>1.61</b>	2.22	
17623687	Intron to Snhg1	78	1.16	<b>1.51</b>	2.00	
17710887	Jund	470	1.34	<b>1.62</b>	2.32	*
17807351	Klf4	345	1.26	<b>1.91</b>	3.95	*
17741409	Ngf	102	1.00	<b>1.68</b>	2.28	
17772385	Nr4a2	165	1.27	<b>1.70</b>	2.44	
17645338	Olr1387	40	1.05	<b>2.12</b>	3.49	
17666316	Ppp1r2	470	1.29	<b>1.74</b>	2.43	*
17821038	Rhob	597	1.60	<b>1.65</b>	4.56	*
17676856	Serpine1	764	0.72	<b>2.76</b>	4.18	*
17770731	Snhg7	1268	1.15	<b>1.70</b>	2.62	
17623689	Snord22	111	1.26	<b>1.59</b>	2.23	
17737660	Terc	118	1.33	<b>1.86</b>	2.67	
17650292	Tob1	871	1.10	<b>1.76</b>	2.20	*
17862389	Unknown	192	1.21	<b>1.83</b>	2.76	

**Table A10 cont.**

<b>Transcript ID</b>	<b>Gene Symbol</b>	<b>Control</b>	<b>PD</b>	<b>H<sub>2</sub>O<sub>2</sub></b>	<b>PD+H<sub>2</sub>O<sub>2</sub></b>	
		<b>(Raw values)</b>	<b>(Relative to controls)</b>			
17862391	Unknown	106	1.59	<b>2.62</b>	3.72	
17719481	Unknown	81	1.56	<b>1.82</b>	2.58	*
17862387	Unknown	214	1.12	<b>1.86</b>	2.60	
17692310	Zfp120	57	1.13	<b>1.84</b>	2.32	

**Table A11 Transcripts downregulated by H<sub>2</sub>O<sub>2</sub> and unaffected by PD184352**

Cardiomyocytes were unstimulated (Control) or exposed to H<sub>2</sub>O<sub>2</sub> (0.2 mM, 2 h) with or without pre-treatment (15 min) with 2 µM PD184352, or exposed to PD184352 alone (2 h 15 min). Changes in RNA expression were determined using Affymetrix Rat Gene 2.0 ST microarrays, using GeneSpring 14.5 analysis to identify RNAs with significant decrease in expression in response to H<sub>2</sub>O<sub>2</sub> (>1.5-fold change relative to control; moderated t-test with Benjamini-Hochberg FDR correction, p<0.05) with no effect of PD184352. Raw values are given for controls and results are the mean fold change relative to controls (n=3/4 independent hybridisations). PD, PD184352.

Transcript ID	Gene Symbol	Control	PD	H <sub>2</sub> O <sub>2</sub>	PD+H <sub>2</sub> O <sub>2</sub>
		(Raw values)	(Relative to controls)		
17799707	Acer2	313	0.62	<b>0.47</b>	0.44
17815851	Akap6	742	0.91	<b>0.66</b>	0.55
17789297	Akap9	477	0.91	<b>0.67</b>	0.70
17846985	Amotl2	396	0.93	<b>0.66</b>	0.73
17837080	Angpt1	232	0.88	<b>0.60</b>	0.71
17845894	Arpp19	97	1.17	<b>0.66</b>	0.59
17878335	Atrx	629	0.91	<b>0.65</b>	0.71
17673260	Auts2l	238	0.97	<b>0.64</b>	0.67
17680721	B3galt2	333	1.06	<b>0.59</b>	0.51
17880642	Ccdc141	132	0.75	<b>0.62</b>	0.63
17744890	Ccnb1	118	1.06	<b>0.58</b>	0.69
17742771	Cenpe	140	0.87	<b>0.61</b>	0.67
17687536	Cenpf	178	0.88	<b>0.58</b>	0.64
17782474	Chrm2	1605	0.93	<b>0.58</b>	0.55
17872611	Dmd	954	0.91	<b>0.58</b>	0.46
17858146	Dst	1133	0.98	<b>0.66</b>	0.64
17699765	Ebf2	122	0.88	<b>0.62</b>	0.65
17637939	Ebf3	321	1.16	<b>0.59</b>	0.73
17746602	Ect2	112	1.16	<b>0.64</b>	0.77
17865182	Erbp4	159	1.08	<b>0.66</b>	0.62
17815588	Etv1	226	0.60	<b>0.65</b>	0.69
17771237	Fam78a	231	0.92	<b>0.64</b>	0.54
17776634	Fbn1	1963	1.01	<b>0.62</b>	0.77
17772756	Fign	139	1.07	<b>0.64</b>	0.70
17696327	Fign1	167	1.07	<b>0.64</b>	0.68
17675438	Fry	645	0.98	<b>0.66</b>	0.55
17687729	G0s2	527	1.20	<b>0.49</b>	0.54
17815757	G2e3	171	1.09	<b>0.67</b>	0.68
17821495	Gpr22	156	1.04	<b>0.60</b>	0.72
17655129	Hba1	972	0.92	<b>0.28</b>	0.25
17655107	Hba1/2	155	0.77	<b>0.30</b>	0.27
17655118	Hba-a1	221	0.98	<b>0.33</b>	0.38
17635616	Hbb-b1	315	0.95	<b>0.33</b>	0.33
17700037	Htr2a	367	1.03	<b>0.66</b>	0.60
17762176	Intron to Cacnb4	235	0.89	<b>0.60</b>	0.75
17759530	Intron to Ebf3	79	1.00	<b>0.66</b>	0.71
17748808	Intron to Fdps	173	0.98	<b>0.59</b>	0.55
17855024	Intron to Ppp2r3a	166	1.24	<b>0.66</b>	0.75
17837524	Intron to Tmem65	116	0.97	<b>0.66</b>	0.79
17865965	Irs1	279	0.79	<b>0.61</b>	0.65
17717602	Irx4	418	0.94	<b>0.60</b>	0.67
17764518	Kcna4	96	0.69	<b>0.64</b>	0.57

**Table A11 cont.**

Transcript ID	Gene Symbol	Control	PD	H <sub>2</sub> O <sub>2</sub>	PD+H <sub>2</sub> O <sub>2</sub>
		(Raw values)	(Relative to controls)		
17796225	Kcnj8	466	0.76	<b>0.67</b>	0.65
17625128	Kif20b	69	0.97	<b>0.61</b>	0.73
17809656	Kif2c	103	1.12	<b>0.67</b>	0.75
17785455	Klf15	128	1.05	<b>0.56</b>	0.67
17837495	Klhl38	160	1.25	<b>0.56</b>	0.68
17813889	Kpna2	2186	0.92	<b>0.59</b>	0.61
17662569	Kpna2	1843	0.97	<b>0.63</b>	0.64
17736233	Lifr	841	0.81	<b>0.56</b>	0.61
17813883	LOC100359600	671	0.96	<b>0.59</b>	0.57
17713890	LOC102551451	615	1.21	<b>0.55</b>	0.59
17849251	LOC102553278	65	0.87	<b>0.59</b>	0.73
17728554	LOC685411	104	0.74	<b>0.66</b>	0.55
17714742	LOC689587	55	0.79	<b>0.67</b>	0.82
17836590	Lrp1	1961	1.11	<b>0.62</b>	0.74
17828320	Lrrc10	260	0.76	<b>0.59</b>	0.61
17810315	Macf1	1159	1.05	<b>0.61</b>	0.64
17735024	Mef2c	392	0.83	<b>0.66</b>	0.72
17782472	Mir490	64	1.01	<b>0.63</b>	0.62
17822197	Mis18bp1	86	1.11	<b>0.66</b>	0.76
17720028	MPP7	383	1.04	<b>0.58</b>	0.52
17720030	Mpp7	858	1.20	<b>0.67</b>	0.62
17704998	Mycbp2	491	1.12	<b>0.63</b>	0.76
17721099	Nabl	1255	0.99	<b>0.65</b>	0.65
17808303	Nfib	1999	0.94	<b>0.62</b>	0.68
17835031	Nr1h4	128	1.24	<b>0.62</b>	0.76
17633908	Nr2f2	574	0.95	<b>0.66</b>	0.60
17877478	Obp1f	68	1.09	<b>0.62</b>	0.73
17635740	Olr194	58	0.93	<b>0.66</b>	0.72
17747228	Pcdh18	332	1.28	<b>0.56</b>	0.59
17694650	Pcdh7	765	1.13	<b>0.66</b>	0.60
17711915	Pcm1	687	0.92	<b>0.65</b>	0.72
17694084	Pdgfra	2983	1.11	<b>0.58</b>	0.63
17665547	Phldb2	1041	0.84	<b>0.66</b>	0.60
17620368	Plk1	372	1.09	<b>0.45</b>	0.50
17690210	Ppargc1a	581	0.95	<b>0.55</b>	0.54
17670970	Prkdc	212	1.04	<b>0.64</b>	0.74
17687572	Prox1	247	0.98	<b>0.57</b>	0.55
17659777	Prr11	74	1.01	<b>0.58</b>	0.69
17795994	Rerg	393	0.98	<b>0.59</b>	0.68
17766923	Rin2	354	0.85	<b>0.65</b>	0.62
17800088	Ror1	519	0.97	<b>0.64</b>	0.75
17797354	Runx1t1	347	1.43	<b>0.55</b>	0.58
17716433	Ryr2	1853	1.02	<b>0.61</b>	0.50
17789488	Samd9l	382	0.89	<b>0.54</b>	0.62
17789483	Samd9l	211	0.91	<b>0.66</b>	0.61
17853413	Smad6	564	1.23	<b>0.53</b>	0.66

**Table A11 cont.**

Transcript ID	Gene Symbol	Control	PD	H <sub>2</sub> O <sub>2</sub>	PD+H <sub>2</sub> O <sub>2</sub>
		(Raw values)	(Relative to controls)		
17852869	Snx33	406	1.10	<b>0.53</b>	0.66
17636071	St5	431	1.00	<b>0.51</b>	0.58
17807544	Svep1	360	0.96	<b>0.63</b>	0.75
17850618	Tbx20	3376	1.09	<b>0.62</b>	0.69
17758246	Tet1	386	1.23	<b>0.63</b>	0.75
17688028	Tgfbr3	1314	1.11	<b>0.63</b>	0.71
17827700	Tmcc3	125	0.78	<b>0.56</b>	0.54
17865381	Tnp1	64	0.84	<b>0.66</b>	0.80
17830802	Tnrc6b	610	1.24	<b>0.66</b>	0.74
17748341	Trim2	262	1.11	<b>0.63</b>	0.69
17628672	Tll2	70	0.71	<b>0.64</b>	0.79
17773733	Ttn	283	1.43	<b>0.46</b>	0.52
17773418	Ttn	2498	1.03	<b>0.53</b>	0.47
17834493	Unknown	131	0.73	<b>0.66</b>	0.71
17870224	Unknown	89	1.01	<b>0.64</b>	0.75
17681386	Unknown	77	0.86	<b>0.65</b>	0.80
17867695	Unknown	95	1.02	<b>0.67</b>	0.71
17748455	Unknown	209	0.87	<b>0.65</b>	0.77
17725000	Unknown	227	0.68	<b>0.62</b>	0.69
17702423	Unknown	109	0.91	<b>0.66</b>	0.66
17719529	Unknown	98	0.92	<b>0.66</b>	0.77
17618570	Unknown	77	0.87	<b>0.60</b>	0.61
17735950	Unknown	67	0.62	<b>0.59</b>	0.57
17851236	Unknown	74	0.87	<b>0.62</b>	0.72
17862549	Unknown	113	0.79	<b>0.65</b>	0.69
17686829	Unknown	71	0.76	<b>0.61</b>	0.70
17676207	Unknown	94	0.94	<b>0.65</b>	0.80
17824985	Unknown	75	0.87	<b>0.66</b>	0.69
17640505	Unknown	72	0.69	<b>0.64</b>	0.73
17755940	Unknown	66	0.69	<b>0.63</b>	0.54
17667572	Unknown	249	0.81	<b>0.63</b>	0.78
17734970	Unknown	110	0.94	<b>0.65</b>	0.74
17824511	Unknown	121	0.84	<b>0.66</b>	0.73
17815738	Unknown	336	0.57	<b>0.55</b>	0.46
17867308	Unknown	1570	1.11	<b>0.48</b>	0.52
17867314	Unknown	2176	1.00	<b>0.56</b>	0.68
17690416	Unknown	59	0.87	<b>0.62</b>	0.73
17878327	Unknown	233	0.93	<b>0.63</b>	0.61
17867296	Unknown	85	1.07	<b>0.63</b>	0.69
17628732	Vom2r-ps18	80	0.84	<b>0.64</b>	0.76
17791192	Zfp467	201	1.05	<b>0.57</b>	0.65
17829163	Zfpm2	348	1.03	<b>0.67</b>	0.70

**Table A12 Transcripts downregulated by H<sub>2</sub>O<sub>2</sub> and downregulated further by PD184352**

Cardiomyocytes were unstimulated (Control) or exposed to H<sub>2</sub>O<sub>2</sub> (0.2 mM, 2 h) with or without pre-treatment (15 min) with 2 μM PD184352, or exposed to PD184352 alone (2 h 15 min). Changes in RNA expression were determined using Affymetrix Rat Gene 2.0 ST microarrays, using GeneSpring 14.5 analysis to identify RNAs with significant decrease in expression in response to H<sub>2</sub>O<sub>2</sub> (>1.5-fold change relative to control; moderated t-test with Benjamini-Hochberg FDR correction, p<0.05). RNAs further decreased >1.25-fold in the presence of PD184352 were selected, with or without a significant effect of the inhibitor (one-way ANOVA with SNK post-test and Benjamini-Hochberg FDR correction, p<0.05). RNAs with significant changes in the presence of PD184352 are indicated with an asterisk (\*). Raw values are given for controls and results are the mean fold change relative to controls (n=3/4 independent hybridisations). PD, PD184352.

Transcript ID	Gene Symbol	Control	PD	H <sub>2</sub> O <sub>2</sub>	PD+H <sub>2</sub> O <sub>2</sub>	
		(Raw values)		(Relative to controls)		
17763560	Aplnr	199	1.01	<b>0.65</b>	0.52	
17611079	Eya4	111	0.79	<b>0.63</b>	0.46	
17711829	Intron to Sorbs2	217	0.55	<b>0.60</b>	0.33	
17618664	Kcne3	453	0.33	<b>0.61</b>	0.35	*
17731247	Nrp1	1316	0.60	<b>0.65</b>	0.48	*
17699814	Stc1	1401	1.15	<b>0.49</b>	0.37	
17821133	Trib2	346	0.43	<b>0.60</b>	0.37	
17726303	Zfp608	468	0.57	<b>0.61</b>	0.44	*

**Table A13 Transcripts downregulated by H<sub>2</sub>O<sub>2</sub> and enhanced by PD184352**

Cardiomyocytes were unstimulated (Control) or exposed to H<sub>2</sub>O<sub>2</sub> (0.2 mM, 2 h) with or without pre-treatment (15 min) with 2 µM PD184352, or exposed to PD184352 alone (2 h 15 min). Changes in RNA expression were determined using Affymetrix Rat Gene 2.0 ST microarrays, using GeneSpring 14.5 analysis to identify RNAs with significant decrease in expression in response to H<sub>2</sub>O<sub>2</sub> (>1.5-fold change relative to control; moderated t-test with Benjamini-Hochberg FDR correction, p<0.05). RNAs enhanced >1.25-fold relative to H<sub>2</sub>O<sub>2</sub> alone in the presence of PD184352 were selected, with or without a significant effect of the inhibitor (one-way ANOVA with SNK post-test and Benjamini-Hochberg FDR correction, p<0.05). RNAs with significant changes in the presence of PD184352 are indicated with an asterisk (\*). Raw values are given for controls and results are the mean fold change relative to controls (n=3/4 independent hybridisations). PD, PD184352.

Transcript ID	Gene Symbol	Control (Raw values)	PD	H <sub>2</sub> O <sub>2</sub> (Relative to controls)	PD+H <sub>2</sub> O <sub>2</sub>	
17667628	Adamts5	510	0.74	<b>0.58</b>	0.96	
17719191	Agtr1a	357	1.41	<b>0.66</b>	0.91	*
17796393	Antisens to Rassf8	129	1.03	<b>0.66</b>	1.09	
17680619	Aspm	97	1.10	<b>0.57</b>	0.79	
17792236	Atoh8	268	1.18	<b>0.59</b>	0.82	*
17843642	Bcl9l	503	1.28	<b>0.57</b>	0.76	*
17764983	Casc5	125	0.88	<b>0.62</b>	0.84	
17843026	Cdon	918	1.49	<b>0.49</b>	0.68	
17854478	Cep162	112	1.07	<b>0.63</b>	0.87	
17777174	Ckap2l	90	1.17	<b>0.60</b>	0.75	
17768463	Fam83d	136	1.10	<b>0.62</b>	0.89	
17808333	Frem1	241	0.94	<b>0.62</b>	0.81	
17635606	Hbb	308	0.98	<b>0.24</b>	0.34	
17635600	Hbb-b1	97	1.47	<b>0.42</b>	0.54	
17715833	Hist1h1b	299	1.30	<b>0.59</b>	0.86	
17755547	Intron to Rev3l	59	0.98	<b>0.66</b>	0.86	
17860796	Kcne4	319	1.54	<b>0.64</b>	0.81	
17853237	Kif23	132	1.27	<b>0.65</b>	0.94	*
17748476	Kirrel	682	1.07	<b>0.66</b>	0.83	*
17686320	LOC685351	118	0.74	<b>0.39</b>	0.80	
17825088	LOC100359978	73	0.96	<b>0.46</b>	0.59	
17633383	LOC103691130	86	0.83	<b>0.57</b>	0.77	
17669287	LOC689217	70	0.93	<b>0.58</b>	0.87	
17637913	Mki67	646	1.10	<b>0.50</b>	0.66	
17618063	Olr20	63	0.91	<b>0.60</b>	0.97	
17849828	Olr1115	83	0.75	<b>0.59</b>	0.73	
17645356	Olr1397	206	0.94	<b>0.64</b>	0.81	
17840683	Olr1877	64	0.87	<b>0.53</b>	0.76	
17690991	Pik3ip1	330	1.87	<b>0.51</b>	0.80	*
17845217	Rasl12	190	1.08	<b>0.59</b>	0.77	*
17856909	Sgol1	65	1.17	<b>0.64</b>	0.80	

**Table A13 cont.**

Transcript ID	Gene Symbol	Control	PD	H <sub>2</sub> O <sub>2</sub>	PD+H <sub>2</sub> O <sub>2</sub>	
		(Raw values)		(Relative to controls)		
17859327	Sgol2	62	1.10	0.61	0.78	
17737579	Slc2a2	147	0.85	<b>0.63</b>	0.86	
17854985	Slc35g2	103	0.79	<b>0.65</b>	0.88	
17649522	Slfn5	528	0.97	<b>0.60</b>	0.77	
17738567	Smad9	208	1.33	<b>0.60</b>	0.88	*
17813989	Ston1	363	1.62	<b>0.62</b>	0.85	
17795793	Tas2r113	54	0.77	<b>0.64</b>	0.82	
17611107	Tcf21	281	1.24	<b>0.58</b>	0.80	
17798353	Tmem8b	107	0.85	<b>0.51</b>	0.81	
17660863	Top2a	326	1.18	<b>0.53</b>	0.73	
17767437	Tpx2	179	1.15	<b>0.62</b>	0.79	*
17846281	Ttk	97	1.10	<b>0.66</b>	0.91	
17784265	Unknown	291	0.96	<b>0.62</b>	1.02	
17824838	Unknown	49	1.04	<b>0.59</b>	0.89	
17688837	Unknown	97	1.03	<b>0.62</b>	0.92	
17696705	Unknown	72	0.86	<b>0.61</b>	0.90	
17869552	Unknown	72	1.01	<b>0.62</b>	0.90	
17778194	Unknown	80	1.25	<b>0.62</b>	0.90	
17673323	Unknown	555	1.00	<b>0.58</b>	0.82	
17846920	Unknown	146	0.91	<b>0.67</b>	0.93	
17739289	Unknown	212	0.79	<b>0.66</b>	0.91	
17617825	Unknown	105	0.93	<b>0.59</b>	0.81	
17669427	Unknown	276	0.99	<b>0.62</b>	0.80	
17683590	Unknown	95	0.91	<b>0.61</b>	0.77	
17612467	Vom1r19	80	0.94	<b>0.67</b>	0.87	
17709537	Zcchc24	834	1.34	<b>0.62</b>	0.78	

**Table A14 Transcripts upregulated by H<sub>2</sub>O<sub>2</sub> and unaffected by JNK-IN-8**

Cardiomyocytes were unstimulated (Control) or exposed to H<sub>2</sub>O<sub>2</sub> (0.2 mM, 2 h) with or without pre-treatment (15 min) with 1 μM JNK-IN-8, or exposed to JNK-IN-8 alone (2 h 15 min). Changes in RNA expression were determined using Affymetrix Rat Gene 2.0 ST microarrays, using GeneSpring 14.5 analysis to identify RNAs with significant increase in expression in response to H<sub>2</sub>O<sub>2</sub> (>1.5-fold change relative to control; moderated t-test with Benjamini-Hochberg FDR correction, p<0.05) with no effect of JNK-IN-8. Raw values are given for controls and results are the mean fold change relative to controls (n=3/4 independent hybridisations). JI8, JNK-IN-8.

Transcript ID	Gene Symbol	Control	JI8	H <sub>2</sub> O <sub>2</sub>	JI8+H <sub>2</sub> O <sub>2</sub>
		(Raw values)		(Relative to controls)	
17781129	Abcb1a	541	1.15	<b>3.48</b>	3.47
17810550	Adprhl2	153	1.01	<b>1.53</b>	1.37
17617581	Aen	113	1.16	<b>3.48</b>	3.34
17782314	Akr1b8	564	1.17	<b>2.33</b>	2.13
17821662	Arl4a	120	1.29	<b>1.57</b>	1.84
17717253	Arl5b	261	1.10	<b>1.90</b>	1.82
17652634	Armc7	131	1.06	<b>2.20</b>	2.67
17759590	Arrdc3	1034	1.08	<b>1.58</b>	1.74
17726777	Atp8b1	277	1.00	<b>1.53</b>	1.36
17861066	B3gnt7	67	0.81	<b>1.58</b>	1.27
17664484	Bach1	517	1.12	<b>2.21</b>	2.16
17621224	Bag3	801	0.91	<b>1.58</b>	1.44
17653231	Baiap2	212	1.28	<b>1.75</b>	1.84
17796337	Bcat1	357	1.04	<b>1.55</b>	1.52
17766015	Bcl2l11	160	1.31	<b>1.76</b>	1.93
17753161	Brd2	722	1.13	<b>1.70</b>	1.68
17636338	Btbd10	136	1.21	<b>1.65</b>	1.71
17826458	Cbarp	109	0.93	<b>1.51</b>	1.61
17664770	Cbr1	246	1.17	<b>2.84</b>	3.32
17664759	Cbr1	1116	1.06	<b>1.51</b>	1.80
17664780	Cbr3	105	1.05	<b>1.64</b>	1.76
17655535	Ccng1	2202	1.10	<b>1.51</b>	1.56
17747788	Ccnl1	471	1.24	<b>1.52</b>	1.61
17630241	Cd3eap	85	0.94	<b>1.50</b>	1.27
17774921	Cd44	663	1.07	<b>1.66</b>	1.70
17868794	Cd80	54	1.08	<b>5.22</b>	5.54
17669098	Cd80	104	1.06	<b>5.00</b>	5.09
17753672	Cdkn1a	604	0.88	<b>5.59</b>	4.96
17808573	Cdkn2b	257	1.11	<b>1.56</b>	1.63
17765084	Chac1	119	1.13	<b>3.03</b>	3.18
17748939	Chrb2	70	1.10	<b>1.58</b>	1.56
17847383	Cish	357	0.79	<b>2.15</b>	1.78
17859270	Coq10b	187	1.17	<b>1.72</b>	1.49
17716200	Crem	139	1.24	<b>1.93</b>	1.76
17750384	Csf1	1259	1.08	<b>1.58</b>	1.61
17727278	Ctdp1	247	1.14	<b>1.64</b>	1.61

**Table A14 cont.**

Transcript ID	Gene Symbol	Control	Jl8	H <sub>2</sub> O <sub>2</sub>	Jl8+H <sub>2</sub> O <sub>2</sub>
		(Raw values)	(Relative to controls)		
17828625	Ddit3	227	1.20	<b>2.07</b>	1.90
17769238	Dok5	182	1.28	<b>1.64</b>	1.71
17850594	Dpy19l2	39	1.03	<b>1.55</b>	1.70
17712103	Dusp4	267	0.88	<b>1.85</b>	1.53
17626435	Dusp5	197	0.94	<b>2.70</b>	2.41
17706222	Eaf1	208	1.04	<b>1.82</b>	1.63
17877966	Eda2r	204	1.49	<b>3.65</b>	3.68
17705094	Ednrb	836	1.24	<b>1.70</b>	1.90
17748848	Efna1	336	1.25	<b>1.86</b>	1.62
17834736	Eid3	82	1.25	<b>3.13</b>	3.13
17734860	Ell2	198	1.22	<b>1.80</b>	1.74
17735400	Enc1	549	1.05	<b>1.50</b>	1.56
17693433	Ereg	68	1.10	<b>4.14</b>	3.83
17735859	Esm1	217	1.47	<b>1.82</b>	1.89
17664927	Ets2	517	1.05	<b>1.93</b>	1.67
17739583	Etv3	287	1.08	<b>1.60</b>	1.58
17815275	Fam110c	100	1.65	<b>3.24</b>	3.10
17741698	Fam212b	82	1.12	<b>2.51</b>	2.41
17806608	Fam219a	115	1.03	<b>1.52</b>	1.32
17669931	Fam43a	306	1.19	<b>1.59</b>	1.59
17610500	Fbxo30	329	0.99	<b>1.72</b>	1.70
17852444	Fdx1	196	1.14	<b>1.57</b>	1.50
17817508	Fos	121	1.05	<b>2.25</b>	2.12
17623115	Fosl1	115	1.11	<b>5.16</b>	4.15
17716029	Gabpb1l	215	1.23	<b>1.57</b>	1.55
17791733	Gadd45a	695	1.07	<b>2.40</b>	2.27
17846065	Gclc	634	1.17	<b>2.69</b>	2.68
17742399	Gclm	337	1.38	<b>1.69</b>	1.71
17654535	Gfer	173	1.12	<b>1.71</b>	1.73
17645401	Gfpt2	1557	1.27	<b>1.83</b>	2.12
17815053	Grhl1	87	1.24	<b>1.67</b>	1.67
17716626	Gtpbp4	176	1.31	<b>1.66</b>	1.49
17628982	Has1	81	1.19	<b>1.69</b>	1.57
17837405	Has2	286	0.89	<b>2.05</b>	1.74
17669934	Hes1	471	1.17	<b>1.70</b>	1.73
17715718	Hist1h2bh	527	1.24	<b>1.65</b>	1.59
17715802	Hist1h4b	153	1.27	<b>1.66</b>	1.72
17610557	Hivep2	489	1.11	<b>1.71</b>	1.67
17753387	Hmga1	774	1.02	<b>1.66</b>	1.50
17728071	Hmox1	1149	1.19	<b>3.41</b>	3.53
17752874	Hspa1a/b	103	0.83	<b>2.07</b>	1.89
17816804	Hspa2	112	0.89	<b>1.59</b>	1.53
17718644	Id4	107	1.14	<b>1.83</b>	1.49

**Table A14 cont.**

Transcript ID	Gene Symbol	Control	Jl8	H <sub>2</sub> O <sub>2</sub>	Jl8+H <sub>2</sub> O <sub>2</sub>
		(Raw values)	(Relative to controls)		
17756250	ler3	782	0.81	<b>1.93</b>	1.74
17685432	ler5	332	0.88	<b>1.90</b>	1.58
17858730	Il1rl1	430	1.29	<b>2.14</b>	2.12
17788345	Il6	108	0.75	<b>1.99</b>	1.92
17769167	Intron to LOC100911177	311	1.08	<b>1.53</b>	1.44
17769169	Intron to LOC100911177	73	1.28	<b>1.54</b>	1.44
17623687	Intron to Snhg1	78	1.21	<b>1.51</b>	1.80
17700736	Ipo5	764	1.07	<b>1.58</b>	1.41
17617588	Isg20	64	1.48	<b>5.97</b>	6.41
17840711	Kansl2	389	1.11	<b>1.54</b>	1.28
17654269	Kctd5	233	1.08	<b>1.55</b>	1.50
17836999	Klf10	245	1.04	<b>1.66</b>	1.42
17807351	Klf4	345	0.98	<b>1.91</b>	2.02
17700455	Klf5	270	0.97	<b>1.53</b>	1.32
17707169	Klhl26	148	1.08	<b>1.60</b>	1.74
17691166	Lif	167	0.92	<b>3.09</b>	2.61
17739110	LOC100910449	80	0.99	<b>2.02</b>	1.74
17807593	LOC102550203	284	1.20	<b>1.86</b>	2.24
17692310	LOC102551714	57	1.24	<b>1.84</b>	2.19
17637453	LOC102554302	229	0.93	<b>1.66</b>	1.64
17787531	LOC689800	59	1.01	<b>1.90</b>	2.00
17663983	Mafg	204	1.13	<b>1.77</b>	1.72
17708402	Mak16	229	1.22	<b>1.56</b>	1.58
17646559	Map2k3	364	1.17	<b>1.93</b>	1.98
17836020	Mdm2	366	1.10	<b>5.14</b>	4.66
17711465	Mfap3l	169	1.20	<b>1.62</b>	1.77
17700626	Mir18a	37	1.09	<b>1.57</b>	1.82
17700628	Mir19a	39	1.11	<b>1.69</b>	1.64
17648510	Mir22	147	1.41	<b>1.77</b>	1.87
17732589	Mir27a	55	0.97	<b>1.56</b>	1.33
17792604	Mthfd2	348	1.29	<b>1.54</b>	1.81
17792855	Mxd1	231	1.13	<b>1.86</b>	1.70
17796946	Mybl1	70	1.11	<b>3.00</b>	2.83
17829696	Myc	264	0.92	<b>2.41</b>	2.14
17659041	NF1	142	1.23	<b>1.86</b>	1.79
17714621	Nfil3	203	0.81	<b>1.68</b>	1.37
17741409	Ngf	102	1.26	<b>1.68</b>	1.77
17869377	Nid2	146	1.01	<b>1.66</b>	1.69
17733371	Nob1	441	1.18	<b>1.58</b>	1.43
17733363	Nqo1	347	1.25	<b>2.83</b>	3.32
17772385	Nr4a2	165	1.46	<b>1.70</b>	1.92
17779084	Oser1	444	1.12	<b>1.62</b>	1.70
17730529	Osgin1	76	1.18	<b>3.12</b>	3.04
17745324	Pelo	489	0.97	<b>1.83</b>	1.62
17716849	Pfkfb3	397	0.91	<b>1.50</b>	1.26
17828155	Phlda1	306	0.89	<b>2.35</b>	2.10

**Table A14 cont.**

Transcript ID	Gene Symbol	Control	Jl8	H <sub>2</sub> O <sub>2</sub>	Jl8+H <sub>2</sub> O <sub>2</sub>
		(Raw values)	(Relative to controls)		
17680418	Phlda3	220	1.07	<b>2.84</b>	2.82
17844002	Plet1	62	2.17	<b>5.15</b>	5.41
17735703	Plk2	1381	0.71	<b>1.55</b>	1.29
17723942	Pmaip1	45	0.95	<b>1.86</b>	1.62
17842335	Ppan	192	1.11	<b>1.57</b>	1.66
17756153	Ppp1r10	465	0.97	<b>1.57</b>	1.59
17632926	Ppp1r15a	311	0.90	<b>1.78</b>	1.50
17666316	Ppp1r2	470	1.20	<b>1.74</b>	1.75
17712060	Pragmin	239	1.06	<b>2.18</b>	1.89
17793342	Prickle2	230	1.02	<b>1.76</b>	1.78
17719280	Prl6a1	31	1.07	<b>1.92</b>	1.57
17775140	Prrg4	582	0.85	<b>1.52</b>	1.39
17771568	Psm5	183	1.12	<b>1.56</b>	1.48
17680795	Ptgs2	712	1.05	<b>2.22</b>	2.00
17859412	Ptp4a1	1544	1.14	<b>1.72</b>	1.84
17863629	Ptp4a1	1246	1.16	<b>1.76</b>	1.85
17679974	Rab7b	122	1.26	<b>1.84</b>	1.56
17738821	Rap2b	152	1.21	<b>1.63</b>	1.67
17734548	Rbm34	180	1.21	<b>1.52</b>	1.59
17689820	Rbm47	84	1.05	<b>1.55</b>	1.42
17805250	Rdh10	153	1.17	<b>1.57</b>	1.61
17861997	RGD1562136	96	1.32	<b>1.73</b>	1.63
17834704	RGD1563365	120	1.18	<b>1.51</b>	1.53
17774787	RGD1564664	158	1.24	<b>1.84</b>	1.60
17684906	Rgs2	370	0.85	<b>3.29</b>	2.74
17649347	Rhot1	42	1.72	<b>1.53</b>	1.43
17721512	Riok3	590	1.04	<b>1.50</b>	1.56
17806037	Ripk2	421	1.07	<b>1.68</b>	1.59
17730862	Rpl13	206	0.98	<b>1.58</b>	1.54
17614756	Rpl28	41	1.05	<b>1.53</b>	1.30
17857692	Runx2	160	1.05	<b>1.67</b>	1.53
17639867	Sac3d1	89	1.04	<b>1.83</b>	1.79
17814680	Sdc1	560	1.06	<b>1.58</b>	1.37
17614694	Sertad1	176	1.04	<b>1.62</b>	1.51
17802844	Sesn2	163	1.47	<b>3.65</b>	3.62
17747564	Siah2	355	1.17	<b>1.56</b>	1.44
17681552	Slc19a2	147	1.08	<b>2.74</b>	3.13
17696492	Slc1a4	361	1.18	<b>1.86</b>	1.89
17777498	Slc23a2	197	1.19	<b>1.69</b>	1.61
17801572	Slc2a1	1520	0.87	<b>1.61</b>	1.30
17683239	Slc30a1	236	1.06	<b>2.19</b>	1.97
17836034	Slc35e3	537	0.97	<b>1.56</b>	1.40
17725180	Slc39a6	603	0.93	<b>1.62</b>	1.59
17864290	Slc40a1	246	1.29	<b>1.62</b>	1.90
17671549	Slc7a1	575	1.10	<b>1.67</b>	1.66
17649532	Slfn2	280	1.18	<b>1.57</b>	1.71
17770731	Snhg7	1268	1.13	<b>1.70</b>	1.75

**Table A14 cont.**

Transcript ID	Gene Symbol	Control	Jl8	H <sub>2</sub> O <sub>2</sub>	Jl8+H <sub>2</sub> O <sub>2</sub>
		(Raw values)	(Relative to controls)		
17735293	Snora47	63	1.24	<b>1.56</b>	1.52
17793995	Snora7a	295	1.03	<b>1.61</b>	1.60
17844990	Snord16a	100	1.27	<b>1.53</b>	1.57
17709866	Snord19	121	1.26	<b>1.55</b>	1.84
17736124	Snord72	43	1.39	<b>1.52</b>	1.51
17645306	Snord95	137	1.28	<b>1.51</b>	1.66
17745308	Snx18	693	0.93	<b>1.60</b>	1.44
17663683	Socs3	503	0.85	<b>1.57</b>	1.42
17655823	Sqstm1	609	1.20	<b>1.95</b>	2.14
17819714	Srsf7	158	1.19	<b>1.57</b>	1.57
17767319	Srxn1	94	1.31	<b>8.55</b>	7.79
17712330	Star	109	1.05	<b>1.80</b>	1.78
17737660	Terc	118	1.17	<b>1.86</b>	2.13
17777978	Thbd	107	0.91	<b>1.55</b>	1.38
17758158	Tmem26	160	0.97	<b>1.53</b>	1.38
17638748	Tnfrsf22	170	0.96	<b>2.15</b>	2.08
17650292	Tob1	871	0.97	<b>1.76</b>	1.59
17797247	Tp53inp1	549	0.98	<b>2.97</b>	2.90
17778298	Trib3	100	0.98	<b>1.89</b>	1.96
17652422	Ttyh2	285	1.21	<b>1.63</b>	2.01
17723990	Tubb6	1014	0.95	<b>1.74</b>	1.46
17834717	Txnrd1	630	1.11	<b>2.68</b>	2.70
17686443	Uap1	169	1.67	<b>6.08</b>	5.52
17814012	Uap1l2	64	1.32	<b>3.74</b>	3.60
17673512	Ubc	1018	0.99	<b>1.84</b>	1.84
17624595	Unknown	175	1.13	<b>1.52</b>	1.43
17831177	Unknown	130	0.94	<b>1.67</b>	1.62
17844970	Unknown	130	0.94	<b>1.67</b>	1.62
17719481	Unknown	81	1.34	<b>1.82</b>	1.74
17862387	Unknown	214	1.15	<b>1.86</b>	2.26
17862389	Unknown	192	1.34	<b>1.83</b>	2.29
17868712	Unknown	58	0.96	<b>1.53</b>	1.47
17868967	Unknown	190	0.86	<b>1.63</b>	1.54
17857041	Unknown	195	1.19	<b>1.53</b>	1.52
17761562	Unknown	189	1.37	<b>1.69</b>	1.70
17881046	Unknown	268	1.16	<b>1.57</b>	1.58
17825181	Unknown	295	1.03	<b>1.61</b>	1.60
17612614	Unknown	40	1.42	<b>1.53</b>	1.27
17848154	Unknown	73	1.32	<b>1.75</b>	1.66
17709357	Unknown	414	1.35	<b>1.52</b>	1.35
17820466	Wdr43	598	1.01	<b>1.50</b>	1.47
17628094	Zbtb2	134	1.07	<b>1.59</b>	1.50
17852451	Zc3h12c	302	1.20	<b>1.87</b>	2.28
17672229	Zfand2a	306	1.10	<b>3.57</b>	3.49
17624514	Zfand5	1288	1.00	<b>1.66</b>	1.61
17631103	Zfp36	617	0.87	<b>2.06</b>	1.82
17614769	Zfp626	95	1.37	<b>1.55</b>	1.74
17737682	Zmat3	198	1.01	<b>1.94</b>	1.78

**Table A15 Transcripts upregulated by H<sub>2</sub>O<sub>2</sub> and enhanced by JNK-IN-8**

Cardiomyocytes were unstimulated (Control) or exposed to H<sub>2</sub>O<sub>2</sub> (0.2 mM, 2 h) with or without pre-treatment (15 min) with 1 μM JNK-IN-8, or exposed to JNK-IN-8 alone (2 h 15 min). Changes in RNA expression were determined using Affymetrix Rat Gene 2.0 ST microarrays, using GeneSpring 14.5 analysis to identify RNAs with significant increase in expression in response to H<sub>2</sub>O<sub>2</sub> (>1.5-fold change relative to control; moderated t-test with Benjamini-Hochberg FDR correction, p<0.05). RNAs enhanced >1.25-fold relative to H<sub>2</sub>O<sub>2</sub> alone in the presence of JNK-IN-8 were selected, with or without a significant effect of the inhibitor (one-way ANOVA with SNK post-test and Benjamini-Hochberg FDR correction, p<0.05). RNAs with significant changes in the presence of JNK-IN-8 are indicated with an asterisk (\*). Raw values are given for controls and results are the mean fold change relative to controls (n=3/4 independent hybridisations). JI8, JNK-IN-8.

Transcript ID	Gene Symbol	Control	JI8	H <sub>2</sub> O <sub>2</sub>	JI8+H <sub>2</sub> O <sub>2</sub>	
		(Raw values)		(Relative to controls)		
17632894	Bax	143	1.32	<b>1.76</b>	2.24	
17708936	Ckap2	81	1.36	<b>1.81</b>	2.39	
17634960	Ddias	67	1.13	<b>1.75</b>	2.23	
17831416	Gtse1	101	1.05	<b>2.45</b>	3.06	*
17681323	Intron to Gas5	133	1.70	<b>1.61</b>	2.39	
17645338	Olr1387	40	1.41	<b>2.12</b>	2.79	
17634940	Pcf11	359	1.28	<b>1.50</b>	1.91	
17766170	Rpl22l2	54	1.71	<b>1.72</b>	2.41	
17747235	Slc7a11	99	1.21	<b>4.32</b>	5.50	
17623689	Snord22	111	1.36	<b>1.59</b>	2.07	
17769925	Unknown	201	1.41	<b>1.55</b>	1.97	
17862391	Unknown	106	1.59	<b>2.62</b>	3.29	

**Table A16 Transcripts upregulated by H<sub>2</sub>O<sub>2</sub> and inhibited by JNK-IN-8**

Cardiomyocytes were unstimulated (Control) or exposed to H<sub>2</sub>O<sub>2</sub> (0.2 mM, 2 h) with or without pre-treatment (15 min) with 1  $\mu$ M JNK-IN-8, or exposed to JNK-IN-8 alone (2 h 15 min). Changes in RNA expression were determined using Affymetrix Rat Gene 2.0 ST microarrays, using GeneSpring 14.5 analysis to identify RNAs with significant increase in expression in response to H<sub>2</sub>O<sub>2</sub> (>1.5-fold change relative to control; moderated t-test with Benjamini-Hochberg FDR correction,  $p < 0.05$ ). RNAs inhibited >1.25-fold relative to H<sub>2</sub>O<sub>2</sub> alone in the presence of JNK-IN-8 were selected, with or without a significant effect of the inhibitor (one-way ANOVA with SNK post-test and Benjamini-Hochberg FDR correction,  $p < 0.05$ ). RNAs with significant changes in the presence of JNK-IN-8 are indicated with an asterisk (\*). Raw values are given for controls and results are the mean fold change relative to controls (n=3/4 independent hybridisations). J18, JNK-IN-8.

Transcript ID	Gene Symbol	Control	J18	H <sub>2</sub> O <sub>2</sub>	J18+H <sub>2</sub> O <sub>2</sub>	
		(Raw values)	(Relative to controls)			
17693425	Areg	82	0.78	<b>1.61</b>	1.10	*
17705843	Arhgef3	189	0.94	<b>2.09</b>	1.60	*
17858347	Arid5a	218	0.73	<b>2.18</b>	1.32	*
17670615	Arvcf	113	0.97	<b>1.53</b>	1.13	*
17687609	Atf3	132	0.69	<b>7.45</b>	2.92	*
17673406	Atp5j2	65	1.08	<b>1.51</b>	1.08	
17818164	Bdkrb2	181	0.79	<b>2.83</b>	1.80	
17766552	Bmp2	193	0.81	<b>2.06</b>	1.50	
17684316	Btg2	308	0.64	<b>2.91</b>	1.52	*
17610582	Cited2	1010	0.84	<b>1.68</b>	1.30	*
17856536	Csrnp1	120	0.97	<b>3.28</b>	2.20	
17751869	Cyr61	872	0.50	<b>1.50</b>	0.80	*
17628832	Dact2	146	0.79	<b>1.85</b>	1.32	
17833617	Dot1l	431	0.96	<b>2.12</b>	1.53	
17682903	Dusp10	353	0.97	<b>1.61</b>	1.15	
17765931	Dusp2	145	0.86	<b>3.21</b>	2.36	*
17722348	Egr1	1291	0.70	<b>1.68</b>	1.18	*
17699889	Egr3	90	0.89	<b>1.69</b>	1.33	
17803896	Epha2	112	0.82	<b>2.95</b>	1.99	
17804459	Errfi1	1256	0.96	<b>1.94</b>	1.41	*
17630236	Fosb	59	1.34	<b>6.02</b>	4.73	
17718415	Gadd45g	412	0.61	<b>3.17</b>	2.15	
17707117	Gdf15	116	0.85	<b>15.19</b>	11.38	
17797288	Gem	317	0.91	<b>1.98</b>	1.43	*
17693015	Gpat3	105	1.37	<b>3.32</b>	2.63	
17730641	Gse1	202	0.85	<b>1.58</b>	1.21	*
17725668	Hbegf	363	0.47	<b>2.19</b>	1.07	*
17674382	Hspb8	908	0.91	<b>1.65</b>	1.27	
17728750	Ier2	191	0.96	<b>1.98</b>	1.51	*
17719769	Inhba	220	1.06	<b>2.47</b>	1.97	
17710887	Jund	470	0.60	<b>1.62</b>	0.97	*
17880605	Klf5	333	0.97	<b>1.72</b>	1.37	
17856642	Klhl40	98	0.92	<b>3.05</b>	1.43	*

**Table A16 cont.**

Transcript ID	Gene Symbol	Control	Jl8	H <sub>2</sub> O <sub>2</sub>	Jl8+H <sub>2</sub> O <sub>2</sub>	
		(Raw values)	(Relative to controls)			
17785906	Lmcd1	441	0.52	<b>2.38</b>	0.96	*
17714890	Mirlet7f-1	38	1.77	<b>2.09</b>	1.62	
17749411	Mllt11	412	0.63	<b>1.57</b>	1.09	
17738403	Noct	206	0.78	<b>2.53</b>	1.61	*
17832476	Nr4a1	178	0.91	<b>4.78</b>	3.72	
17798725	Nr4a3	63	1.31	<b>11.10</b>	8.72	
17619333	Olr230	36	1.26	<b>1.73</b>	1.35	
17717422	Otud1	152	0.61	<b>1.69</b>	0.77	*
17769225	Pard6b	74	0.92	<b>2.74</b>	1.43	*
17614190	Plaur	252	0.98	<b>1.68</b>	1.25	*
17630418	PVR	516	0.96	<b>2.32</b>	1.76	
17668004	Rcan1	1895	0.70	<b>1.52</b>	1.02	
17821038	Rhob	597	0.84	<b>1.65</b>	1.27	*
17840784	Rnd1	444	0.62	<b>2.00</b>	1.34	
17610687	Rps13	40	1.22	<b>1.69</b>	1.06	
17772976	Rps3	53	1.29	<b>1.56</b>	1.15	
17679473	Serpib2	251	1.59	<b>6.69</b>	5.12	
17676856	Serpine1	764	0.81	<b>2.76</b>	1.95	
17751449	Sgms2	152	1.16	<b>2.73</b>	2.01	
17757468	Sik1	457	0.87	<b>1.67</b>	1.18	*
17652327	Slc16a6	203	0.79	<b>2.23</b>	1.20	*
17789522	Tfpi2	101	0.91	<b>1.78</b>	1.39	
17654148	Tnfrsf12a	877	0.77	<b>1.87</b>	1.34	
17646726	Trim16	182	0.80	<b>1.51</b>	1.03	
17738669	Tsc22d2	425	0.87	<b>1.52</b>	1.19	
17674327	Unknown	235	0.94	<b>1.59</b>	1.25	
17808103	Unknown	119	0.92	<b>1.58</b>	1.17	
17691637	Unknown	63	0.76	<b>1.62</b>	1.13	
17873757	Unknown	145	0.91	<b>1.79</b>	1.18	
17856543	Xirp1	1051	0.91	<b>2.79</b>	1.42	*

**Table A17 Transcripts downregulated by H<sub>2</sub>O<sub>2</sub> and unaffected by JNK-IN-8**

Cardiomyocytes were unstimulated (Control) or exposed to H<sub>2</sub>O<sub>2</sub> (0.2 mM, 2 h) with or without pre-treatment (15 min) with 1  $\mu$ M JNK-IN-8, or exposed to JNK-IN-8 alone (2 h 15 min). Changes in RNA expression were determined using Affymetrix Rat Gene 2.0 ST microarrays, using GeneSpring 14.5 analysis to identify RNAs with significant decrease in expression in response to H<sub>2</sub>O<sub>2</sub> (>1.5-fold change relative to control; moderated t-test with Benjamini-Hochberg FDR correction, p<0.05) with no effect of JNK-IN-8. Raw values are given for controls and results are the mean fold change relative to controls (n=3/4 independent hybridisations). JI8, JNK-IN-8.

Transcript ID	Gene Symbol	Control	JI8	H <sub>2</sub> O <sub>2</sub>	JI8+H <sub>2</sub> O <sub>2</sub>
		(Raw values)	(Relative to controls)		
17667628	Adamts5	510	0.76	<b>0.58</b>	0.57
17815851	Akap6	742	0.98	<b>0.66</b>	0.64
17789297	Akap9	477	0.98	<b>0.67</b>	0.72
17846985	Amotl2	396	0.98	<b>0.66</b>	0.63
17837080	Angpt1	232	0.88	<b>0.60</b>	0.64
17845894	Arpp19	97	1.17	<b>0.66</b>	0.56
17792236	Atoh8	268	1.00	<b>0.59</b>	0.72
17878335	Atrx	629	1.01	<b>0.65</b>	0.74
17673260	Auts2l	238	0.97	<b>0.64</b>	0.69
17680721	B3galt2	333	1.12	<b>0.59</b>	0.62
17843642	Bcl9l	503	0.92	<b>0.57</b>	0.61
17744890	Ccnb1	118	1.15	<b>0.58</b>	0.65
17843026	Cdon	918	1.01	<b>0.49</b>	0.53
17742771	Cenpe	140	1.02	<b>0.61</b>	0.72
17687536	Cenpf	178	0.98	<b>0.58</b>	0.68
17782474	Chrm2	1605	1.06	<b>0.58</b>	0.64
17872611	Dmd	954	0.98	<b>0.58</b>	0.55
17858146	Dst	1133	1.00	<b>0.66</b>	0.69
17699765	Ebf2	122	1.04	<b>0.62</b>	0.68
17637939	Ebf3	321	1.10	<b>0.59</b>	0.62
17611079	Eya4	111	1.00	<b>0.63</b>	0.78
17768463	Fam83d	136	1.23	<b>0.62</b>	0.76
17776634	Fbn1	1963	0.98	<b>0.62</b>	0.75
17772756	Fign	139	1.17	<b>0.64</b>	0.70
17696327	Figl1	167	0.94	<b>0.64</b>	0.65
17675438	Fry	645	0.99	<b>0.66</b>	0.67
17687729	G0s2	527	1.09	<b>0.49</b>	0.54
17815757	G2e3	171	1.17	<b>0.67</b>	0.79
17821495	Gpr22	156	1.09	<b>0.60</b>	0.63
17655129	Hba1	972	0.80	<b>0.28</b>	0.33
17655107	Hba1/2	155	0.74	<b>0.30</b>	0.31
17655118	Hba-a1	221	0.80	<b>0.33</b>	0.36
17635600	Hbb-b1	97	1.32	<b>0.42</b>	0.49
17635616	Hbb-b1	315	0.82	<b>0.33</b>	0.37
17700037	Htr2a	367	1.01	<b>0.66</b>	0.64
17762176	Intron to Cacnb4	235	0.80	<b>0.60</b>	0.69
17759530	Intron to Ebf3	79	0.86	<b>0.66</b>	0.61
17748808	Intron to Fdps	173	1.20	<b>0.59</b>	0.62
17855024	Intron to Ppp2r3a	166	1.01	<b>0.66</b>	0.56
17755547	Intron to Rev3l	59	1.13	<b>0.66</b>	0.80
17837524	Intron to Tmem65	116	0.84	<b>0.66</b>	0.67

**Table A17 cont.**

Transcript ID	Gene Symbol	Control	Jl8	H <sub>2</sub> O <sub>2</sub>	Jl8+H <sub>2</sub> O <sub>2</sub>
		(Raw values)	(Relative to controls)		
17865965	Irs1	279	0.92	<b>0.61</b>	0.59
17717602	Irx4	418	1.05	<b>0.60</b>	0.71
17764518	Kcna4	96	0.95	<b>0.64</b>	0.57
17618664	Kcne3	453	1.27	<b>0.61</b>	0.69
17796225	Kcnj8	466	1.12	<b>0.67</b>	0.81
17625128	Kif20b	69	1.21	<b>0.61</b>	0.71
17809656	Kif2c	103	1.07	<b>0.67</b>	0.82
17748476	Kirrel	682	0.87	<b>0.66</b>	0.71
17785455	Klf15	128	1.16	<b>0.56</b>	0.66
17837495	Klhl38	160	1.29	<b>0.56</b>	0.58
17813889	Kpna2	2186	1.02	<b>0.59</b>	0.74
17662569	Kpna2	1843	1.06	<b>0.63</b>	0.76
17714742	LOC689587	55	0.74	<b>0.67</b>	0.72
17836590	Lrp1	1961	1.10	<b>0.62</b>	0.76
17828320	Lrrc10	260	1.04	<b>0.59</b>	0.72
17810315	Macf1	1159	1.04	<b>0.61</b>	0.68
17735024	Mef2c	392	0.96	<b>0.66</b>	0.70
17782472	Mir490	64	1.06	<b>0.63</b>	0.58
17720028	MPP7	383	1.11	<b>0.58</b>	0.64
17720030	Mpp7	858	1.22	<b>0.67</b>	0.69
17704998	Mycbp2	491	1.02	<b>0.63</b>	0.73
17721099	Nebi	1255	1.18	<b>0.65</b>	0.72
17808303	Nfib	1999	0.98	<b>0.62</b>	0.70
17835031	Nr1h4	128	0.96	<b>0.62</b>	0.63
17633908	Nr2f2	574	0.96	<b>0.66</b>	0.80
17731247	Nrp1	1316	1.09	<b>0.65</b>	0.77
17849828	Olr1115	83	0.64	<b>0.59</b>	0.71
17840683	Olr1877	64	0.83	<b>0.53</b>	0.63
17635740	Olr194	58	1.03	<b>0.66</b>	0.79
17747228	Pcdh18	332	1.04	<b>0.56</b>	0.68
17694650	Pcdh7	765	1.11	<b>0.66</b>	0.75
17711915	Pcm1	687	0.97	<b>0.65</b>	0.72
17665547	Phldb2	1041	1.12	<b>0.66</b>	0.76
17690991	Pik3ip1	330	1.11	<b>0.51</b>	0.57
17620368	Plk1	372	1.17	<b>0.45</b>	0.54
17690210	Ppargc1a	581	1.18	<b>0.55</b>	0.67
17670970	Prkdc	212	1.04	<b>0.64</b>	0.74
17687572	Prox1	247	1.11	<b>0.57</b>	0.65
17659777	Prr11	74	1.10	<b>0.58</b>	0.69
17845217	Rasl12	190	1.08	<b>0.59</b>	0.67
17795994	Rerg	393	1.22	<b>0.59</b>	0.70
17766923	Rin2	354	1.00	<b>0.65</b>	0.71
17800088	Ror1	519	1.01	<b>0.64</b>	0.74
17797354	Runx1t1	347	1.17	<b>0.55</b>	0.56
17716433	Ryr2	1853	1.00	<b>0.61</b>	0.62
17789488	Samd9l	382	0.75	<b>0.54</b>	0.57
17789483	Samd9l	211	0.93	<b>0.66</b>	0.60
17856909	Sgol1	65	1.13	<b>0.64</b>	0.79
17859327	Sgol2	62	1.27	<b>0.61</b>	0.72
17852869	Snx33	406	0.97	<b>0.53</b>	0.55

**Table A17 cont.**

Transcript ID	Gene Symbol	Control	Jl8	H <sub>2</sub> O <sub>2</sub>	Jl8+H <sub>2</sub> O <sub>2</sub>
		(Raw values)	(Relative to controls)		
17636071	St5	431	0.89	<b>0.51</b>	0.53
17699814	Stc1	1401	1.07	<b>0.49</b>	0.44
17813989	Ston1	363	0.96	<b>0.62</b>	0.66
17807544	Svep1	360	0.99	<b>0.63</b>	0.70
17795793	Tas2r113	54	0.98	<b>0.64</b>	0.68
17850618	Tbx20	3376	1.12	<b>0.62</b>	0.75
17611107	Tcf21	281	0.95	<b>0.58</b>	0.57
17758246	Tet1	386	1.02	<b>0.63</b>	0.70
17688028	Tgfbr3	1314	1.05	<b>0.63</b>	0.70
17827700	Tmcc3	125	1.00	<b>0.56</b>	0.55
17798353	Tmem8b	107	0.99	<b>0.51</b>	0.54
17865381	Tnp1	64	0.90	<b>0.66</b>	0.72
17830802	Tnrc6b	610	1.08	<b>0.66</b>	0.74
17821133	Trib2	346	0.80	<b>0.60</b>	0.50
17748341	Trim2	262	1.13	<b>0.63</b>	0.74
17773733	Ttn	283	1.16	<b>0.46</b>	0.45
17773418	Ttn	2498	1.02	<b>0.53</b>	0.53
17669427	Unknown	276	0.93	<b>0.62</b>	0.71
17673323	Unknown	555	0.90	<b>0.58</b>	0.60
17784265	Unknown	291	0.73	<b>0.62</b>	0.64
17617825	Unknown	105	0.98	<b>0.59</b>	0.69
17748455	Unknown	209	0.85	<b>0.65</b>	0.72
17725000	Unknown	227	0.89	<b>0.62</b>	0.72
17702423	Unknown	109	0.92	<b>0.66</b>	0.72
17719529	Unknown	98	1.07	<b>0.66</b>	0.83
17618570	Unknown	77	0.94	<b>0.60</b>	0.74
17735950	Unknown	67	0.70	<b>0.59</b>	0.64
17851236	Unknown	74	0.71	<b>0.62</b>	0.72
17862549	Unknown	113	0.83	<b>0.65</b>	0.74
17686829	Unknown	71	1.03	<b>0.61</b>	0.77
17676207	Unknown	94	0.95	<b>0.65</b>	0.79
17824985	Unknown	75	0.79	<b>0.66</b>	0.78
17640505	Unknown	72	0.74	<b>0.64</b>	0.60
17755940	Unknown	66	0.98	<b>0.63</b>	0.67
17667572	Unknown	249	0.89	<b>0.63</b>	0.78
17734970	Unknown	110	0.90	<b>0.65</b>	0.67
17824511	Unknown	121	0.88	<b>0.66</b>	0.70
17815738	Unknown	336	0.63	<b>0.55</b>	0.55
17867308	Unknown	1570	1.32	<b>0.48</b>	0.51
17867314	Unknown	2176	1.05	<b>0.56</b>	0.59
17690416	Unknown	59	0.88	<b>0.62</b>	0.66
17878327	Unknown	233	1.08	<b>0.63</b>	0.73
17867296	Unknown	85	1.10	<b>0.63</b>	0.59
17612467	Vom1r19	80	0.88	<b>0.67</b>	0.79
17709537	Zcchc24	834	1.13	<b>0.62</b>	0.65
17791192	Zfp467	201	0.90	<b>0.57</b>	0.54
17726303	Zfp608	468	0.90	<b>0.61</b>	0.64
17829163	Zfpm2	348	0.95	<b>0.67</b>	0.66

**Table A18 Transcripts downregulated by H<sub>2</sub>O<sub>2</sub> and affected by JNK-IN-8**

Cardiomyocytes were unstimulated (Control) or exposed to H<sub>2</sub>O<sub>2</sub> (0.2 mM, 2 h) with or without pre-treatment (15 min) with 1 μM JNK-IN-8, or exposed to JNK-IN-8 alone (2 h 15 min). Changes in RNA expression were determined using Affymetrix Rat Gene 2.0 ST microarrays, using GeneSpring 14.5 analysis to identify RNAs with significant decrease in expression in response to H<sub>2</sub>O<sub>2</sub> (>1.5-fold change relative to control; moderated t-test with Benjamini-Hochberg FDR correction, p<0.05). RNAs changed >1.25-fold relative to H<sub>2</sub>O<sub>2</sub> alone in the presence of JNK-IN-8 were selected, with or without a significant effect of the inhibitor (one-way ANOVA with SNK post-test and Benjamini-Hochberg FDR correction, p<0.05). RNAs with significant changes in the presence of JNK-IN-8 are indicated with an asterisk (\*). Raw values are given for controls and results are the mean fold change relative to controls (n=3/4 independent hybridisations). JI8, JNK-IN-8.

**RNAs downregulated by H<sub>2</sub>O<sub>2</sub> and enhanced by JNK-IN-8**

Transcript ID	Gene Symbol	Control	JI8	H <sub>2</sub> O <sub>2</sub>	JI8+H <sub>2</sub> O <sub>2</sub>	
		(Raw values)	(Relative to controls)			
17799707	Acer2	313	1.22	<b>0.47</b>	0.62	
17796393	Antisens to Rassf8	129	0.95	<b>0.66</b>	0.90	
17763560	Aplnr	199	1.47	<b>0.65</b>	0.84	
17680619	Aspm	97	1.08	<b>0.57</b>	0.71	
17764983	Casc5	125	0.94	<b>0.62</b>	0.86	
17880642	Ccdc141	132	1.33	<b>0.62</b>	0.79	
17854478	Cep162	112	1.04	<b>0.63</b>	0.81	
17777174	Ckap2l	90	1.17	<b>0.60</b>	0.77	
17746602	Ect2	112	1.30	<b>0.64</b>	0.80	
17865182	ErbB4	159	1.19	<b>0.66</b>	0.84	
17815588	Etv1	226	1.08	<b>0.65</b>	0.82	*
17771237	Fam78a	231	1.14	<b>0.64</b>	0.84	
17808333	Frem1	241	1.22	<b>0.62</b>	0.84	
17635606	Hbb	308	0.97	<b>0.24</b>	0.35	
17715833	Hist1h1b	299	1.05	<b>0.59</b>	0.75	
17860796	Kcne4	319	1.36	<b>0.64</b>	0.82	
17736233	Lifr	841	1.17	<b>0.56</b>	0.74	
17813883	LOC100359600	671	1.08	<b>0.59</b>	0.79	*
17825088	LOC100359978	73	0.69	<b>0.46</b>	0.89	
17713890	LOC102551451	615	1.07	<b>0.55</b>	0.71	
17849251	LOC102553278	65	0.98	<b>0.59</b>	0.74	
17633383	LOC103691130	86	0.76	<b>0.57</b>	0.73	
17686320	LOC685351	118	0.67	<b>0.39</b>	0.71	
17728554	LOC685411	104	0.75	<b>0.66</b>	0.85	
17669287	LOC689217	70	0.78	<b>0.58</b>	0.90	
17822197	Mis18bp1	86	1.08	<b>0.66</b>	0.86	
17637913	Mki67	646	1.13	<b>0.50</b>	0.67	
17877478	Obp1f	68	0.89	<b>0.62</b>	0.81	
17645356	Olr1397	206	0.91	<b>0.64</b>	0.80	
17618063	Olr20	63	0.77	<b>0.60</b>	0.82	
17694084	Pdgfra	2983	1.12	<b>0.58</b>	0.74	

**Table A18 cont.**

**RNAs downregulated by H<sub>2</sub>O<sub>2</sub> and enhanced by JNK-IN-8 cont.**

<b>Transcript ID</b>	<b>Gene Symbol</b>	<b>Control</b>	<b>Jl8</b>	<b>H<sub>2</sub>O<sub>2</sub></b>	<b>Jl8+H<sub>2</sub>O<sub>2</sub></b>	
		<b>(Raw values)</b>	<b>(Relative to controls)</b>			
17737579	Slc2a2	147	0.90	<b>0.63</b>	0.81	
17854985	Slc35g2	103	0.91	<b>0.65</b>	0.89	
17649522	Sfn5	528	1.00	<b>0.60</b>	0.82	
17853413	Smad6	564	1.02	<b>0.53</b>	0.68	
17738567	Smad9	208	1.31	<b>0.60</b>	0.89	*
17660863	Top2a	326	1.21	<b>0.53</b>	0.74	
17767437	Tpx2	179	1.17	<b>0.62</b>	0.84	*
17846281	Ttk	97	1.21	<b>0.66</b>	0.91	
17628672	Ttl2	70	0.84	<b>0.64</b>	0.84	
17688837	Unknown	97	0.96	<b>0.62</b>	0.95	
17834493	Unknown	131	0.72	<b>0.66</b>	0.94	
17846920	Unknown	146	1.05	<b>0.67</b>	0.94	
17870224	Unknown	89	0.81	<b>0.64</b>	0.89	
17681386	Unknown	77	0.79	<b>0.65</b>	0.90	
17683590	Unknown	95	0.93	<b>0.61</b>	0.83	
17824838	Unknown	49	1.04	<b>0.59</b>	0.80	
17869552	Unknown	72	0.81	<b>0.62</b>	0.82	
17867695	Unknown	95	0.67	<b>0.67</b>	0.87	
17696705	Unknown	72	1.09	<b>0.61</b>	0.78	
17778194	Unknown	80	1.30	<b>0.62</b>	0.80	
17739289	Unknown	212	0.90	<b>0.66</b>	0.84	
17628732	Vom2r-ps18	80	0.93	<b>0.64</b>	0.80	

**RNAs downregulated by H<sub>2</sub>O<sub>2</sub> and downregulated further by JNK-IN-8**

<b>Transcript ID</b>	<b>Gene Symbol</b>	<b>Control</b>	<b>Jl8</b>	<b>H<sub>2</sub>O<sub>2</sub></b>	<b>Jl8+H<sub>2</sub>O<sub>2</sub></b>	
		<b>(Raw values)</b>	<b>(Relative to controls)</b>			
17711829	Intron to Sorbs2	217	0.72	<b>0.60</b>	0.40	

**Table A19 Transcripts upregulated by H<sub>2</sub>O<sub>2</sub> and unaffected by SB203580**

Cardiomyocytes were unstimulated (Control) or exposed to H<sub>2</sub>O<sub>2</sub> (0.2 mM, 2 h) with or without pre-treatment (15 min) with 0.7 μM SB203580 or with or without pre-treatment (15 min), or were exposed to the SB203580 alone (2 h 15 min) Changes in RNA expression were determined using Affymetrix Rat Gene 2.0 ST microarrays, using GeneSpring 14.5 analysis to identify RNAs with significant increase in expression in response to H<sub>2</sub>O<sub>2</sub> (>1.5-fold change relative to control; moderated t-test with Benjamini-Hochberg FDR correction, p<0.05) with no effect of SB203580. Raw values are given for controls and results are the mean fold change relative to controls (n=3/4 independent hybridisations). SB, SB203580.

Transcript ID	Gene Symbol	Control	SB	H <sub>2</sub> O <sub>2</sub>	SB+H <sub>2</sub> O <sub>2</sub>
		(Raw values)	(Relative to controls)		
17781129	Abcb1a	541	1.13	<b>3.48</b>	3.41
17810550	Adprhl2	153	1.01	<b>1.53</b>	1.39
17617581	Aen	113	1.01	<b>3.48</b>	3.20
17693425	Areg	82	1.09	<b>1.61</b>	1.31
17858347	Arid5a	218	0.91	<b>2.18</b>	1.83
17821662	Arl4a	120	1.11	<b>1.57</b>	1.44
17717253	Arl5b	261	1.03	<b>1.90</b>	1.93
17652634	Armc7	131	0.98	<b>2.20</b>	1.82
17759590	Arrdc3	1034	0.94	<b>1.58</b>	1.45
17670615	Arvcf	113	1.18	<b>1.53</b>	1.49
17726777	Atp8b1	277	1.03	<b>1.53</b>	1.49
17664484	Bach1	517	1.09	<b>2.21</b>	2.03
17653231	Baiap2	212	1.23	<b>1.75</b>	1.72
17632894	Bax	143	1.30	<b>1.76</b>	2.00
17796337	Bcat1	357	0.98	<b>1.55</b>	1.56
17766015	Bcl2l1	160	1.09	<b>1.76</b>	1.49
17753161	Brd2	722	1.05	<b>1.70</b>	1.36
17636338	Btbd10	136	1.11	<b>1.65</b>	1.63
17826458	Cbap	109	0.94	<b>1.51</b>	1.54
17664759	Cbr1	1116	1.00	<b>1.51</b>	1.40
17664780	Cbr3	105	1.10	<b>1.64</b>	1.49
17655535	Ccng1	2202	1.10	<b>1.51</b>	1.59
17747788	Ccn1	471	1.22	<b>1.52</b>	1.66
17774921	Cd44	663	1.04	<b>1.66</b>	1.59
17868794	Cd80	54	1.06	<b>5.22</b>	5.67
17669098	Cd80	104	1.08	<b>5.00</b>	5.13
17808573	Cdkn2b	257	1.03	<b>1.56</b>	1.44
17765084	Chac1	119	0.91	<b>3.03</b>	2.79
17748939	Chrb2	70	1.07	<b>1.58</b>	1.70
17708936	Ckap2	81	0.97	<b>1.81</b>	2.17
17859270	Coq10b	187	1.09	<b>1.72</b>	1.40
17716200	Crem	139	1.25	<b>1.93</b>	1.78
17750384	Csf1	1259	1.25	<b>1.58</b>	1.74
17856536	Csrnp1	120	1.08	<b>3.28</b>	2.83
17727278	Ctdp1	247	1.03	<b>1.64</b>	1.35
17751869	Cyr61	872	1.07	<b>1.50</b>	1.62
17628832	Dact2	146	1.08	<b>1.85</b>	1.57
17634960	Ddias	67	1.02	<b>1.75</b>	2.05
17828625	Ddit3	227	1.25	<b>2.07</b>	2.43
17769238	Dok5	182	1.12	<b>1.64</b>	1.55
17850594	Dpy19l2	39	1.06	<b>1.55</b>	1.66
17682903	Dusp10	353	0.99	<b>1.61</b>	1.44
17877966	Eda2r	204	1.37	<b>3.65</b>	3.76

**Table A19 cont.**

Transcript ID	Gene Symbol	Control	SB	H <sub>2</sub> O <sub>2</sub>	SB+H <sub>2</sub> O <sub>2</sub>
		(Raw values)	(Relative to controls)		
17722348	Egr1	1291	1.05	<b>1.68</b>	1.94
17699889	Egr3	90	1.01	<b>1.69</b>	1.37
17834736	Eid3	82	1.18	<b>3.13</b>	2.73
17734860	Eil2	198	1.03	<b>1.80</b>	1.56
17735400	Enc1	549	0.90	<b>1.50</b>	1.40
17735859	Esm1	217	1.14	<b>1.82</b>	1.49
17739583	Etv3	287	0.99	<b>1.60</b>	1.49
17741698	Fam212b	82	1.16	<b>2.51</b>	2.42
17806608	Fam219a	115	1.10	<b>1.52</b>	1.43
17669931	Fam43a	306	1.13	<b>1.59</b>	1.33
17610500	Fbxo30	329	0.90	<b>1.72</b>	1.53
17852444	Fdx1	196	1.01	<b>1.57</b>	1.32
17817508	Fos	121	1.28	<b>2.25</b>	2.35
17623115	Fosl1	115	1.10	<b>5.16</b>	4.85
17716029	Gabpb1l	215	0.99	<b>1.57</b>	1.45
17791733	Gadd45a	695	1.43	<b>2.40</b>	2.63
17718415	Gadd45g	412	1.06	<b>3.17</b>	2.62
17742399	Gclm	337	1.30	<b>1.69</b>	1.67
17654535	Gfer	173	1.07	<b>1.71</b>	1.68
17645401	Gfpt2	1557	1.04	<b>1.83</b>	1.68
17693015	Gpat3	105	1.19	<b>3.32</b>	2.68
17815053	Grhl1	87	1.10	<b>1.67</b>	1.68
17730641	Gse1	202	1.00	<b>1.58</b>	1.33
17831416	Gtse1	101	1.06	<b>2.45</b>	2.56
17628982	Has1	81	1.04	<b>1.69</b>	1.41
17669934	Hes1	471	0.96	<b>1.70</b>	1.41
17715718	Hist1h2bh	527	1.21	<b>1.65</b>	1.78
17715802	Hist1h4b	153	1.25	<b>1.66</b>	1.52
17610557	Hivep2	489	1.04	<b>1.71</b>	1.58
17753387	Hmga1	774	1.09	<b>1.66</b>	1.59
17752874	Hspa1a/b	103	0.98	<b>2.07</b>	1.76
17816804	Hspa2	112	0.88	<b>1.59</b>	1.35
17728750	Ier2	191	1.02	<b>1.98</b>	1.95
17756250	Ier3	782	0.94	<b>1.93</b>	1.61
17858730	Il1rl1	430	1.20	<b>2.14</b>	1.96
17681323	Intron to Gas5	133	1.37	<b>1.61</b>	1.63
17623687	Intron to Snhg1	78	1.08	<b>1.51</b>	1.44
17700736	Ipo5	764	1.08	<b>1.58</b>	1.43
17617588	Isg20	64	1.66	<b>5.97</b>	6.07
17710887	Jund	470	1.04	<b>1.62</b>	1.49
17840711	Kansl2	389	1.03	<b>1.54</b>	1.24
17654269	Kctd5	233	1.04	<b>1.55</b>	1.46
17836999	Klf10	245	1.17	<b>1.66</b>	1.69
17807351	Klf4	345	0.92	<b>1.91</b>	1.80
17880605	Klf5	333	1.06	<b>1.72</b>	1.62
17700455	Klf5	270	1.08	<b>1.53</b>	1.54
17707169	Klhl26	148	0.94	<b>1.60</b>	1.58
17691166	Lif	167	0.94	<b>3.09</b>	2.97
17807593	LOC102550203	284	1.13	<b>1.86</b>	1.99
17692310	LOC102551714	57	1.18	<b>1.84</b>	1.97
17637453	LOC102554302	229	0.88	<b>1.66</b>	1.80
17787531	LOC689800	59	1.03	<b>1.90</b>	1.53
17663983	Mafg	204	1.14	<b>1.77</b>	1.77
17708402	Mak16	229	0.99	<b>1.56</b>	1.40
17646559	Map2k3	364	1.30	<b>1.93</b>	2.02
17836020	Mdm2	366	0.95	<b>5.14</b>	4.55
17711465	Mfap3l	169	1.21	<b>1.62</b>	1.43
17648510	Mir22	147	1.19	<b>1.77</b>	1.49

**Table A19 cont.**

Transcript ID	Gene Symbol	Control	SB	H <sub>2</sub> O <sub>2</sub>	SB+H <sub>2</sub> O <sub>2</sub>
		(Raw values)	(Relative to controls)		
17792604	Mthfd2	348	1.15	<b>1.54</b>	1.67
17796946	Mybl1	70	0.98	<b>3.00</b>	2.82
17659041	NF1	142	1.07	<b>1.86</b>	1.90
17714621	Nfil3	203	0.85	<b>1.68</b>	1.40
17741409	Ngf	102	1.19	<b>1.68</b>	1.70
17869377	Nid2	146	1.04	<b>1.66</b>	1.46
17733371	Nob1	441	1.13	<b>1.58</b>	1.37
17738403	Noct	206	0.90	<b>2.53</b>	2.35
17733363	Nqo1	347	0.94	<b>2.83</b>	2.50
17772385	Nr4a2	165	1.27	<b>1.70</b>	1.74
17645338	Olr1387	40	1.42	<b>2.12</b>	2.57
17779084	Oser1	444	1.05	<b>1.62</b>	1.62
17730529	Osgin1	76	1.21	<b>3.12</b>	2.91
17717422	Otud1	152	1.05	<b>1.69</b>	1.43
17769225	Pard6b	74	1.16	<b>2.74</b>	2.32
17634940	Pcf11	359	1.09	<b>1.50</b>	1.82
17745324	Pelo	489	0.95	<b>1.83</b>	1.50
17716849	Pfkfb3	397	1.00	<b>1.50</b>	1.29
17844002	Plet1	62	1.91	<b>5.15</b>	4.35
17735703	Plk2	1381	1.00	<b>1.55</b>	1.42
17723942	Pmaip1	45	0.92	<b>1.86</b>	1.63
17842335	Ppan	192	1.02	<b>1.57</b>	1.46
17756153	Ppp1r10	465	0.88	<b>1.57</b>	1.61
17632926	Ppp1r15a	311	1.12	<b>1.78</b>	1.71
17666316	Ppp1r2	470	1.18	<b>1.74</b>	1.69
17712060	Pragmin	239	1.04	<b>2.18</b>	1.92
17793342	Prickle2	230	1.01	<b>1.76</b>	1.78
17775140	Prrg4	582	0.98	<b>1.52</b>	1.49
17771568	Psmc5	183	1.15	<b>1.56</b>	1.83
17859412	Ptp4a1	1544	1.08	<b>1.72</b>	1.65
17863629	Ptp4a1	1246	1.11	<b>1.76</b>	1.66
17738821	Rap2b	152	1.17	<b>1.63</b>	1.60
17734548	Rbm34	180	1.26	<b>1.52</b>	1.61
17689820	Rbm47	84	0.91	<b>1.55</b>	1.28
17668004	Rcan1	1895	1.04	<b>1.52</b>	1.29
17805250	Rdh10	153	1.17	<b>1.57</b>	1.49
17861997	RGD1562136	96	1.36	<b>1.73</b>	1.67
17834704	RGD1563365	120	1.16	<b>1.51</b>	1.43
17774787	RGD1564664	158	1.16	<b>1.84</b>	1.67
17821038	Rhob	597	1.13	<b>1.65</b>	1.65
17721512	Riok3	590	0.96	<b>1.50</b>	1.42
17806037	Ripk2	421	1.02	<b>1.68</b>	1.52
17840784	Rnd1	444	1.02	<b>2.00</b>	1.86
17766170	Rpl22l2	54	1.51	<b>1.72</b>	1.51
17857692	Runx2	160	0.97	<b>1.67</b>	1.37
17639867	Sac3d1	89	0.94	<b>1.83</b>	1.76
17814680	Sdc1	560	1.04	<b>1.58</b>	1.29
17676856	Serpine1	764	1.00	<b>2.76</b>	2.56
17614694	Sertad1	176	0.98	<b>1.62</b>	1.68
17802844	Sesn2	163	1.24	<b>3.65</b>	3.35
17751449	Sgms2	152	1.20	<b>2.73</b>	2.18
17747564	Siah2	355	1.13	<b>1.56</b>	1.40
17681552	Slc19a2	147	1.12	<b>2.74</b>	2.96

**Table A19 cont.**

Transcript ID	Gene Symbol	Control	SB	H <sub>2</sub> O <sub>2</sub>	SB+H <sub>2</sub> O <sub>2</sub>
		(Raw values)	(Relative to controls)		
17696492	Slc1a4	361	1.31	<b>1.86</b>	1.92
17777498	Slc23a2	197	1.17	<b>1.69</b>	1.67
17683239	Slc30a1	236	1.05	<b>2.19</b>	1.99
17836034	Slc35e3	537	1.08	<b>1.56</b>	1.50
17725180	Slc39a6	603	0.86	<b>1.62</b>	1.53
17864290	Slc40a1	246	1.22	<b>1.62</b>	1.60
17671549	Slc7a1	575	1.02	<b>1.67</b>	1.51
17747235	Slc7a11	99	0.99	<b>4.32</b>	4.24
17649532	Sifn2	280	1.12	<b>1.57</b>	1.63
17770731	Snhg7	1268	1.05	<b>1.70</b>	1.76
17735293	Snora47	63	1.08	<b>1.56</b>	1.50
17793995	Snora7a	295	0.96	<b>1.61</b>	1.49
17844990	Snord16a	100	1.08	<b>1.53</b>	1.32
17709866	Snord19	121	1.19	<b>1.55</b>	1.35
17623689	Snord22	111	1.02	<b>1.59</b>	1.42
17736124	Snord72	43	1.09	<b>1.52</b>	1.29
17645306	Snord95	137	1.06	<b>1.51</b>	1.48
17745308	Snx18	693	0.97	<b>1.60</b>	1.48
17663683	Socs3	503	0.90	<b>1.57</b>	1.27
17655823	Sqstm1	609	1.09	<b>1.95</b>	1.73
17819714	Srsf7	158	1.03	<b>1.57</b>	1.34
17712330	Star	109	1.05	<b>1.80</b>	1.48
17737660	Terc	118	0.98	<b>1.86</b>	1.87
17789522	Tfpi2	101	1.01	<b>1.78</b>	1.56
17758158	Tmem26	160	1.02	<b>1.53</b>	1.56
17654148	Tnfrsf12a	877	1.07	<b>1.87</b>	1.69
17638748	Tnfrsf22	170	0.94	<b>2.15</b>	2.01
17650292	Tob1	871	0.86	<b>1.76</b>	1.49
17797247	Tp53inp1	549	1.00	<b>2.97</b>	2.69
17778298	Trib3	100	0.96	<b>1.89</b>	1.78
17646726	Trim16	182	1.10	<b>1.51</b>	1.36
17738669	Tsc22d2	425	0.98	<b>1.52</b>	1.54
17652422	Ttyh2	285	1.13	<b>1.63</b>	1.78
17723990	Tubb6	1014	1.07	<b>1.74</b>	1.62
17834717	Txnrd1	630	0.97	<b>2.68</b>	2.35
17673512	Ubc	1018	0.92	<b>1.84</b>	1.49
17862391	Unknown	106	1.36	<b>2.62</b>	3.10
17769925	Unknown	201	1.25	<b>1.55</b>	1.88
17719481	Unknown	81	1.32	<b>1.82</b>	1.94
17862387	Unknown	214	1.05	<b>1.86</b>	2.29
17862389	Unknown	192	1.08	<b>1.83</b>	2.20
17868712	Unknown	58	1.04	<b>1.53</b>	1.69
17868967	Unknown	190	1.02	<b>1.63</b>	1.70
17857041	Unknown	195	1.03	<b>1.53</b>	1.54
17761562	Unknown	189	1.36	<b>1.69</b>	1.66
17881046	Unknown	268	1.04	<b>1.57</b>	1.52
17825181	Unknown	295	0.96	<b>1.61</b>	1.49
17612614	Unknown	40	1.59	<b>1.53</b>	1.33
17848154	Unknown	73	1.01	<b>1.75</b>	1.42
17709357	Unknown	414	1.45	<b>1.52</b>	1.22
17820466	Wdr43	598	0.96	<b>1.50</b>	1.37
17628094	Zbtb2	134	1.04	<b>1.59</b>	1.59
17852451	Zc3h12c	302	1.14	<b>1.87</b>	2.02
17672229	Zfand2a	306	1.00	<b>3.57</b>	2.86
17624514	Zfand5	1288	0.98	<b>1.66</b>	1.56
17614769	Zfp626	95	1.19	<b>1.55</b>	1.58
17737682	Zmat3	198	0.99	<b>1.94</b>	1.75

**Table A20 Transcripts upregulated by H<sub>2</sub>O<sub>2</sub> and affected by SB203580**

Cardiomyocytes were unstimulated (Control) or exposed to H<sub>2</sub>O<sub>2</sub> (0.2 mM, 2 h) with or without pre-treatment (15 min) with 0.7 μM SB203580, or exposed to SB203580 alone (2 h 15 min). Changes in RNA expression were determined using Affymetrix Rat Gene 2.0 ST microarrays, using GeneSpring 14.5 analysis to identify RNAs with significant increase in expression in response to H<sub>2</sub>O<sub>2</sub> (>1.5-fold change relative to control; moderated t-test with Benjamini-Hochberg FDR correction, p<0.05). RNAs changed >1.25-fold relative to H<sub>2</sub>O<sub>2</sub> alone in the presence of SB203580 were selected, with or without a significant effect of the inhibitor (one-way ANOVA with SNK post-test and Benjamini-Hochberg FDR correction, p<0.05). RNAs with significant changes in the presence of SB203580 are indicated with an asterisk (\*). Raw values are given for controls and results are the mean fold change relative to controls (n=3/4 independent hybridisations). SB, SB203580.

**RNAs upregulated by H<sub>2</sub>O<sub>2</sub> and inhibited by SB203580**

Transcript ID	Gene Symbol	Control	SB	H <sub>2</sub> O <sub>2</sub>	SB+H <sub>2</sub> O <sub>2</sub>	
		(Raw values)	(Relative to controls)			
17782314	Akr1b8	564	1.13	<b>2.33</b>	1.69	
17705843	Arhgef3	189	1.07	<b>2.09</b>	1.59	*
17687609	Atf3	132	1.12	<b>7.45</b>	5.23	
17673406	Atp5j2	65	1.15	<b>1.51</b>	1.03	
17861066	B3gnt7	67	0.73	<b>1.58</b>	0.95	*
17621224	Bag3	801	0.92	<b>1.58</b>	1.25	*
17818164	Bdkrb2	181	0.98	<b>2.83</b>	1.96	
17766552	Bmp2	193	0.79	<b>2.06</b>	1.44	
17684316	Btg2	308	0.87	<b>2.91</b>	2.18	
17664770	Cbr1	246	0.94	<b>2.84</b>	1.60	*
17630241	Cd3eap	85	1.11	<b>1.50</b>	1.12	*
17753672	Cdkn1a	604	0.85	<b>5.59</b>	4.12	
17847383	Cish	357	0.67	<b>2.15</b>	1.35	
17610582	Cited2	1010	0.94	<b>1.68</b>	1.22	
17833617	Dot1l	431	0.89	<b>2.12</b>	1.61	
17765931	Dusp2	145	0.80	<b>3.21</b>	1.84	
17712103	Dusp4	267	1.06	<b>1.85</b>	1.37	
17626435	Dusp5	197	0.85	<b>2.70</b>	2.06	
17706222	Eaf1	208	0.97	<b>1.82</b>	1.44	*
17705094	Ednrb	836	0.97	<b>1.70</b>	1.25	*
17748848	Efna1	336	1.06	<b>1.86</b>	1.45	*
17803896	Epha2	112	1.00	<b>2.95</b>	2.34	
17693433	Ereg	68	1.02	<b>4.14</b>	3.06	
17804459	Errfi1	1256	0.87	<b>1.94</b>	1.36	
17664927	Ets2	517	0.93	<b>1.93</b>	1.43	*
17815275	Fam110c	100	1.59	<b>3.24</b>	2.43	
17630236	Fosb	59	1.25	<b>6.02</b>	4.55	
17846065	Gclc	634	0.98	<b>2.69</b>	1.98	*
17707117	Gdf15	116	0.99	<b>15.19</b>	10.75	
17797288	Gem	317	0.97	<b>1.98</b>	1.54	*
17716626	Gtpbp4	176	1.16	<b>1.66</b>	1.27	
17837405	Has2	286	0.73	<b>2.05</b>	1.42	
17725668	Hbegf	363	0.89	<b>2.19</b>	1.50	
17728071	Hmox1	1149	0.94	<b>3.41</b>	2.67	
17674382	Hspb8	908	0.94	<b>1.65</b>	1.29	*
17718644	Id4	107	1.07	<b>1.83</b>	1.40	
17685432	Ier5	332	0.89	<b>1.90</b>	1.44	*

Table A20 cont.

Transcript ID	Gene Symbol	Control	SB	H <sub>2</sub> O <sub>2</sub>	SB+H <sub>2</sub> O <sub>2</sub>	
		(Raw values)	(Relative to controls)			
17788345	Il6	108	0.70	<b>1.99</b>	1.28	
17719769	Inhba	220	1.04	<b>2.47</b>	1.74	
17769169	Intron to LOC100911177	73	1.10	<b>1.54</b>	1.20	
17769167	Intron to LOC100911177	311	0.92	<b>1.53</b>	1.10	*
17856642	Klhl40	98	1.04	<b>3.05</b>	1.80	*
17785906	Lmcd1	441	0.98	<b>2.38</b>	1.57	
17739110	LOC100910449	80	1.52	<b>2.02</b>	1.52	
17700626	Mir18a	37	0.98	<b>1.57</b>	1.13	*
17700628	Mir19a	39	1.09	<b>1.69</b>	1.26	
17732589	Mir27a	55	1.10	<b>1.56</b>	1.24	
17714890	Mirlet7f-1	38	1.38	<b>2.09</b>	1.46	
17749411	Mllt11	412	0.67	<b>1.57</b>	1.03	
17792855	Mxd1	231	0.98	<b>1.86</b>	1.44	
17829696	Myc	264	0.90	<b>2.41</b>	1.86	
17832476	Nr4a1	178	0.95	<b>4.78</b>	3.06	*
17798725	Nr4a3	63	1.07	<b>11.10</b>	6.09	
17619333	Olr230	36	0.92	<b>1.73</b>	1.12	
17828155	Phlda1	306	0.96	<b>2.35</b>	1.80	
17680418	Phlda3	220	1.05	<b>2.84</b>	2.26	
17614190	Plaur	252	1.04	<b>1.68</b>	1.33	
17719280	Prl6a1	31	0.97	<b>1.92</b>	1.33	*
17680795	Ptgs2	712	0.84	<b>2.22</b>	1.64	
17630418	PVR	516	1.00	<b>2.32</b>	1.82	*
17684906	Rgs2	370	0.83	<b>3.29</b>	2.21	
17649347	Rhot1	42	1.48	<b>1.53</b>	0.99	
17730862	Rpl13	206	1.05	<b>1.58</b>	1.15	
17614756	Rpl28	41	1.06	<b>1.53</b>	1.13	
17610687	Rps13	40	1.15	<b>1.69</b>	1.18	
17772976	Rps3	53	1.20	<b>1.56</b>	0.98	
17679473	Serpinb2	251	1.51	<b>6.69</b>	5.24	
17757468	Sik1	457	0.91	<b>1.67</b>	1.23	*
17652327	Slc16a6	203	0.99	<b>2.23</b>	1.71	
17801572	Slc2a1	1520	0.80	<b>1.61</b>	1.23	*
17767319	Srxn1	94	1.17	<b>8.55</b>	6.33	*
17777978	Thbd	107	0.90	<b>1.55</b>	1.08	
17686443	Uap1	169	1.26	<b>6.08</b>	4.41	
17814012	Uap1l2	64	0.98	<b>3.74</b>	2.30	
17624595	Unknown	175	1.26	<b>1.52</b>	1.17	
17831177	Unknown	130	0.92	<b>1.67</b>	1.26	
17844970	Unknown	130	0.92	<b>1.67</b>	1.26	
17691637	Unknown	63	0.94	<b>1.62</b>	1.19	
17674327	Unknown	235	1.03	<b>1.59</b>	1.16	
17808103	Unknown	119	1.06	<b>1.58</b>	1.14	
17873757	Unknown	145	0.94	<b>1.79</b>	1.09	
17856543	Xirp1	1051	0.86	<b>2.79</b>	1.49	*
17631103	Zfp36	617	0.78	<b>2.06</b>	1.33	*

**Table A20 cont.**

**RNAs upregulated by H<sub>2</sub>O<sub>2</sub> and inhibited by SB203580**

<b>Transcript ID</b>	<b>Gene Symbol</b>	<b>Control</b>	<b>SB</b>	<b>H<sub>2</sub>O<sub>2</sub></b>	<b>SB+H<sub>2</sub>O<sub>2</sub></b>	
		<b>(Raw values)</b>	<b>(Relative to controls)</b>			
17679974	Rab7b	122	1.56	<b>1.84</b>	2.33	

**Table A21 Transcripts downregulated by H<sub>2</sub>O<sub>2</sub> and unaffected by SB203580**

Cardiomyocytes were unstimulated (Control) or exposed to H<sub>2</sub>O<sub>2</sub> (0.2 mM, 2 h) with or without pre-treatment (15 min) with 0.7 µM SB203580, or exposed to SB203580 alone (2 h 15 min). Changes in RNA expression were determined using Affymetrix Rat Gene 2.0 ST microarrays, using GeneSpring 14.5 analysis to identify RNAs with significant decrease in expression in response to H<sub>2</sub>O<sub>2</sub> (>1.5-fold change relative to control; moderated t-test with Benjamini-Hochberg FDR correction, p<0.05) with no effect of SB203580. Raw values are given for controls and results are the mean fold change relative to controls (n=3/4 independent hybridisations). SB, SB203580.

Transcript ID	Gene Symbol	Control	SB	H <sub>2</sub> O <sub>2</sub>	SB+H <sub>2</sub> O <sub>2</sub>
		(Raw values)	(Relative to controls)		
17667628	Adamts5	510	0.69	<b>0.58</b>	0.58
17719191	Agtr1a	357	1.00	<b>0.66</b>	0.76
17815851	Akap6	742	0.99	<b>0.66</b>	0.72
17789297	Akap9	477	0.96	<b>0.67</b>	0.78
17846985	Amotl2	396	0.93	<b>0.66</b>	0.74
17837080	Angpt1	232	1.01	<b>0.60</b>	0.70
17763560	Aplnr	199	1.19	<b>0.65</b>	0.61
17845894	Arpp19	97	0.95	<b>0.66</b>	0.70
17792236	Atoh8	268	1.01	<b>0.59</b>	0.72
17878335	Atrx	629	0.99	<b>0.65</b>	0.80
17673260	Auts2l	238	0.96	<b>0.64</b>	0.72
17680721	B3galt2	333	1.06	<b>0.59</b>	0.61
17843642	Bcl9l	503	0.91	<b>0.57</b>	0.65
17744890	Ccnb1	118	1.03	<b>0.58</b>	0.66
17742771	Cenpe	140	0.92	<b>0.61</b>	0.72
17687536	Cenpf	178	0.98	<b>0.58</b>	0.69
17782474	Chrm2	1605	0.93	<b>0.58</b>	0.64
17777174	Ckap2l	90	1.00	<b>0.60</b>	0.74
17872611	Dmd	954	0.97	<b>0.58</b>	0.63
17858146	Dst	1133	1.00	<b>0.66</b>	0.74
17699765	Ebf2	122	1.00	<b>0.62</b>	0.77
17637939	Ebf3	321	1.14	<b>0.59</b>	0.72
17865182	ErbB4	159	1.11	<b>0.66</b>	0.81
17611079	Eya4	111	0.88	<b>0.63</b>	0.72
17771237	Fam78a	231	1.05	<b>0.64</b>	0.77
17776634	Fbn1	1963	0.96	<b>0.62</b>	0.76
17772756	Fign	139	1.15	<b>0.64</b>	0.75
17696327	Fignl1	167	0.93	<b>0.64</b>	0.68
17675438	Fry	645	0.90	<b>0.66</b>	0.66
17687729	G0s2	527	0.93	<b>0.49</b>	0.48
17815757	G2e3	171	1.00	<b>0.67</b>	0.75
17821495	Gpr22	156	0.75	<b>0.60</b>	0.57
17655129	Hba1	972	0.77	<b>0.28</b>	0.29
17655118	Hba-a1	221	0.80	<b>0.33</b>	0.33
17635600	Hbb-b1	97	1.11	<b>0.42</b>	0.43
17635616	Hbb-b1	315	0.77	<b>0.33</b>	0.35
17700037	Htr2a	367	0.92	<b>0.66</b>	0.59
17762176	Intron to Cacnb4	235	0.87	<b>0.60</b>	0.64

**Table A21 cont.**

Transcript ID	Gene Symbol	Control	SB	H <sub>2</sub> O <sub>2</sub>	SB+H <sub>2</sub> O <sub>2</sub>
		(Raw values)	(Relative to controls)		
17748808	Intron to Fdps	173	0.94	<b>0.59</b>	0.56
17855024	Intron to Ppp2r3a	166	0.98	<b>0.66</b>	0.81
17711829	Intron to Sorbs2	217	0.82	<b>0.60</b>	0.55
17837524	Intron to Tmem65	116	0.88	<b>0.66</b>	0.77
17865965	Irs1	279	0.97	<b>0.61</b>	0.64
17717602	Irx4	418	0.79	<b>0.60</b>	0.64
17764518	Kcna4	96	0.85	<b>0.64</b>	0.56
17618664	Kcne3	453	1.26	<b>0.61</b>	0.67
17796225	Kcnj8	466	1.00	<b>0.67</b>	0.77
17809656	Kif2c	103	1.09	<b>0.67</b>	0.79
17748476	Kirrel	682	1.01	<b>0.66</b>	0.77
17785455	Klf15	128	0.97	<b>0.56</b>	0.64
17837495	Klhl38	160	1.39	<b>0.56</b>	0.65
17813889	Kpna2	2186	0.88	<b>0.59</b>	0.65
17662569	Kpna2	1843	0.90	<b>0.63</b>	0.65
17813883	LOC100359600	671	0.88	<b>0.59</b>	0.57
17633383	LOC103691130	86	0.74	<b>0.57</b>	0.67
17728554	LOC685411	104	0.94	<b>0.66</b>	0.80
17828320	Lrrc10	260	0.82	<b>0.59</b>	0.66
17810315	Macf1	1159	1.03	<b>0.61</b>	0.74
17735024	Mef2c	392	0.92	<b>0.66</b>	0.75
17782472	Mir490	64	0.83	<b>0.63</b>	0.64
17822197	Mis18bp1	86	1.13	<b>0.66</b>	0.73
17720028	MPP7	383	0.94	<b>0.58</b>	0.61
17720030	Mpp7	858	1.09	<b>0.67</b>	0.68
17704998	Mycbp2	491	0.99	<b>0.63</b>	0.78
17808303	Nfib	1999	0.99	<b>0.62</b>	0.74
17835031	Nr1h4	128	1.02	<b>0.62</b>	0.67
17633908	Nr2f2	574	0.87	<b>0.66</b>	0.61
17731247	Nrp1	1316	1.00	<b>0.65</b>	0.68
17849828	Olr1115	83	0.78	<b>0.59</b>	0.57
17645356	Olr1397	206	1.16	<b>0.64</b>	0.76
17635740	Olr194	58	0.78	<b>0.66</b>	0.69
17747228	Pcdh18	332	1.05	<b>0.56</b>	0.70
17694650	Pcdh7	765	1.03	<b>0.66</b>	0.68
17665547	Phldb2	1041	0.98	<b>0.66</b>	0.76
17670970	Prkdc	212	1.03	<b>0.64</b>	0.79
17687572	Prox1	247	0.97	<b>0.57</b>	0.60
17845217	Rasl12	190	1.08	<b>0.59</b>	0.70
17766923	Rin2	354	1.07	<b>0.65</b>	0.75
17800088	Ror1	519	0.99	<b>0.64</b>	0.72
17797354	Runx1t1	347	1.22	<b>0.55</b>	0.62
17716433	Ryr2	1853	0.95	<b>0.61</b>	0.64
17789488	Samd9l	382	0.93	<b>0.54</b>	0.64
17789483	Samd9l	211	1.04	<b>0.66</b>	0.63
17856909	Sgol1	65	0.97	<b>0.64</b>	0.75
17859327	Sgol2	62	1.05	<b>0.61</b>	0.74
17854985	Slc35g2	103	0.87	<b>0.65</b>	0.80
17853413	Smad6	564	1.05	<b>0.53</b>	0.63

**Table A21 cont.**

Transcript ID	Gene Symbol	Control	SB	H <sub>2</sub> O <sub>2</sub>	SB+H <sub>2</sub> O <sub>2</sub>
		(Raw values)	(Relative to controls)		
17807544	Svep1	360	0.97	<b>0.63</b>	0.73
17795793	Tas2r113	54	0.96	<b>0.64</b>	0.78
17850618	Tbx20	3376	0.89	<b>0.62</b>	0.67
17611107	Tcf21	281	0.86	<b>0.58</b>	0.57
17688028	Tgfbr3	1314	1.05	<b>0.63</b>	0.73
17827700	Tmcc3	125	0.98	<b>0.56</b>	0.63
17798353	Tmem8b	107	0.90	<b>0.51</b>	0.56
17830802	Tnrc6b	610	1.02	<b>0.66</b>	0.81
17767437	Tpx2	179	1.03	<b>0.62</b>	0.76
17821133	Trib2	346	0.87	<b>0.60</b>	0.69
17773418	Ttn	2498	0.90	<b>0.53</b>	0.57
17696705	Unknown	72	1.05	<b>0.61</b>	0.69
17739289	Unknown	212	0.96	<b>0.66</b>	0.74
17669427	Unknown	276	1.12	<b>0.62</b>	0.74
17673323	Unknown	555	0.93	<b>0.58</b>	0.65
17784265	Unknown	291	0.94	<b>0.62</b>	0.69
17617825	Unknown	105	1.03	<b>0.59</b>	0.66
17867695	Unknown	95	0.88	<b>0.67</b>	0.82
17851236	Unknown	74	0.70	<b>0.62</b>	0.78
17862549	Unknown	113	0.95	<b>0.65</b>	0.80
17686829	Unknown	71	0.89	<b>0.61</b>	0.76
17676207	Unknown	94	1.04	<b>0.65</b>	0.80
17824985	Unknown	75	0.92	<b>0.66</b>	0.79
17640505	Unknown	72	0.85	<b>0.64</b>	0.71
17755940	Unknown	66	0.87	<b>0.63</b>	0.70
17667572	Unknown	249	0.95	<b>0.63</b>	0.70
17734970	Unknown	110	0.78	<b>0.65</b>	0.69
17824511	Unknown	121	0.95	<b>0.66</b>	0.67
17815738	Unknown	336	0.79	<b>0.55</b>	0.56
17867308	Unknown	1570	1.17	<b>0.48</b>	0.49
17867314	Unknown	2176	1.00	<b>0.56</b>	0.57
17690416	Unknown	59	0.71	<b>0.62</b>	0.62
17878327	Unknown	233	1.03	<b>0.63</b>	0.60
17867296	Unknown	85	1.07	<b>0.63</b>	0.59
17709537	Zcchc24	834	1.13	<b>0.62</b>	0.77
17791192	Zfp467	201	0.74	<b>0.57</b>	0.61
17726303	Zfp608	468	0.91	<b>0.61</b>	0.60
17829163	Zfpm2	348	0.96	<b>0.67</b>	0.75

**Table A22 Transcripts downregulated by H<sub>2</sub>O<sub>2</sub> and affected by SB203580**

Cardiomyocytes were unstimulated (Control) or exposed to H<sub>2</sub>O<sub>2</sub> (0.2 mM, 2 h) with or without pre-treatment (15 min) with 0.7 μM SB203580, or exposed to SB203580 alone (2 h 15 min). Changes in RNA expression were determined using Affymetrix Rat Gene 2.0 ST microarrays, using GeneSpring 14.5 analysis to identify RNAs with significant decrease in expression in response to H<sub>2</sub>O<sub>2</sub> (>1.5-fold change relative to control; moderated t-test with Benjamini-Hochberg FDR correction, p<0.05). RNAs changed >1.25-fold relative to H<sub>2</sub>O<sub>2</sub> alone in the presence of SB203580 were selected, with or without a significant effect of the inhibitor (one-way ANOVA with SNK post-test and Benjamini-Hochberg FDR correction, p<0.05). RNAs with significant changes in the presence of SB203580 are indicated with an asterisk (\*). Raw values are given for controls and results are the mean fold change relative to controls (n=3/4 independent hybridisations). SB, SB203580.

**RNAs downregulated by H<sub>2</sub>O<sub>2</sub> and enhanced by SB203580**

Transcript ID	Gene Symbol	Control	SB	H <sub>2</sub> O <sub>2</sub>	SB+H <sub>2</sub> O <sub>2</sub>	
		(Raw values)	(Relative to controls)			
17799707	Acer2	313	1.43	<b>0.47</b>	0.66	
17796393	Antisens to Rassf8	129	0.97	<b>0.66</b>	0.92	
17680619	Aspm	97	0.97	<b>0.57</b>	0.80	
17764983	Casc5	125	0.91	<b>0.62</b>	0.85	
17880642	Ccdc141	132	1.19	<b>0.62</b>	0.78	
17843026	Cdon	918	0.97	<b>0.49</b>	0.62	
17854478	Cep162	112	0.95	<b>0.63</b>	0.85	
17746602	Ect2	112	1.22	<b>0.64</b>	0.85	
17815588	Etv1	226	1.19	<b>0.65</b>	0.89	*
17768463	Fam83d	136	1.06	<b>0.62</b>	0.81	
17808333	Frem1	241	1.24	<b>0.62</b>	0.89	
17655107	Hba1/2	155	0.58	<b>0.30</b>	0.50	
17635606	Hbb	308	0.78	<b>0.24</b>	0.34	
17715833	Hist1h1b	299	1.12	<b>0.59</b>	0.79	
17759530	Intron to Ebf3	79	1.03	<b>0.66</b>	0.88	
17755547	Intron to Rev3l	59	0.95	<b>0.66</b>	0.91	
17860796	Kcne4	319	1.18	<b>0.64</b>	0.81	
17625128	Kif20b	69	0.90	<b>0.61</b>	0.84	
17736233	Lifr	841	1.16	<b>0.56</b>	0.78	
17825088	LOC100359978	73	0.83	<b>0.46</b>	0.67	
17713890	LOC102551451	615	0.85	<b>0.55</b>	0.72	
17849251	LOC102553278	65	1.05	<b>0.59</b>	0.84	
17686320	LOC685351	118	0.66	<b>0.39</b>	0.67	
17669287	LOC689217	70	0.97	<b>0.58</b>	0.94	
17714742	LOC689587	55	0.97	<b>0.67</b>	0.84	
17836590	Lrp1	1961	1.09	<b>0.62</b>	0.78	*
17637913	Mki67	646	1.09	<b>0.50</b>	0.64	
17721099	Nebi	1255	1.05	<b>0.65</b>	0.83	
17877478	Obp1f	68	1.03	<b>0.62</b>	0.90	
17840683	Olr1877	64	1.00	<b>0.53</b>	0.68	
17618063	Olr20	63	1.11	<b>0.60</b>	1.00	
17711915	Pcm1	687	0.94	<b>0.65</b>	0.83	

**Table A22 cont.**

**RNAs downregulated by H<sub>2</sub>O<sub>2</sub> and enhanced by SB203580 cont.**

Transcript ID	Gene Symbol	Control	SB	H <sub>2</sub> O <sub>2</sub>	SB+H <sub>2</sub> O <sub>2</sub>	
		(Raw values)	(Relative to controls)			
17694084	Pdgfra	2983	1.07	<b>0.58</b>	0.77	
17690991	Pik3ip1	330	1.08	<b>0.51</b>	0.71	*
17620368	Plk1	372	1.08	<b>0.45</b>	0.56	
17690210	Ppargc1a	581	1.02	<b>0.55</b>	0.69	
17659777	Prr11	74	1.02	<b>0.58</b>	0.74	
17795994	Rerg	393	1.27	<b>0.59</b>	0.84	
17737579	Slc2a2	147	0.87	<b>0.63</b>	0.85	
17649522	Slfn5	528	1.07	<b>0.60</b>	0.92	
17738567	Smad9	208	1.23	<b>0.60</b>	0.99	*
17852869	Snx33	406	0.95	<b>0.53</b>	0.68	
17636071	St5	431	1.00	<b>0.51</b>	0.66	
17813989	Ston1	363	1.08	<b>0.62</b>	0.81	
17758246	Tet1	386	1.14	<b>0.63</b>	0.88	*
17865381	Tnp1	64	0.92	<b>0.66</b>	0.86	
17660863	Top2a	326	1.05	<b>0.53</b>	0.71	
17748341	Trim2	262	1.10	<b>0.63</b>	0.83	
17846281	Ttk	97	1.13	<b>0.66</b>	1.00	
17628672	Ttll2	70	0.81	<b>0.64</b>	0.81	
17773733	Ttn	283	0.96	<b>0.46</b>	0.61	
17824838	Unknown	49	1.27	<b>0.59</b>	1.15	*
17834493	Unknown	131	0.74	<b>0.66</b>	1.01	
17869552	Unknown	72	0.81	<b>0.62</b>	0.94	
17846920	Unknown	146	1.10	<b>0.67</b>	0.99	
17870224	Unknown	89	0.93	<b>0.64</b>	0.94	
17748455	Unknown	209	0.97	<b>0.65</b>	0.94	
17725000	Unknown	227	0.89	<b>0.62</b>	0.89	
17683590	Unknown	95	0.94	<b>0.61</b>	0.83	
17702423	Unknown	109	1.09	<b>0.66</b>	0.90	
17719529	Unknown	98	0.97	<b>0.66</b>	0.90	
17618570	Unknown	77	1.03	<b>0.60</b>	0.80	
17778194	Unknown	80	1.05	<b>0.62</b>	0.82	
17735950	Unknown	67	0.75	<b>0.59</b>	0.78	
17688837	Unknown	97	1.00	<b>0.62</b>	0.78	
17681386	Unknown	77	0.85	<b>0.65</b>	0.81	
17612467	Vom1r19	80	0.94	<b>0.67</b>	0.85	
17628732	Vom2r-ps18	80	1.13	<b>0.64</b>	0.82	

**RNAs downregulated by H<sub>2</sub>O<sub>2</sub> and downregulated further by SB203580.**

Transcript ID	Gene Symbol	Control	SB	H <sub>2</sub> O <sub>2</sub>	SB+H <sub>2</sub> O <sub>2</sub>
		(Raw values)	(Relative to controls)		
17699814	Stc1	1401	0.83	<b>0.49</b>	0.33

### APPENDIX III: Mouse RIPK1 DNA sequence and mutations

1 ATGCAACCAG ACATGTCCTT GGACAATATT AAGATGGCAT CCAGTGACCT  
 51 GCTGGAGAAG ACAGACCTAG ACAGCGGAGG CTTCGGGAAG GTGTCCTTGT  
 101 GTTACCACAG AAGCCATGGA TTTGTCATCC TGAAAAAAGT ATACACAGGG  
 151 CCCAACCGCG CTGAGTACAA TGAGGTTCTC TTGGAAGAGG GGAAGATGAT  
 201 GCACAGACTG AGACACAGTC GAGTGGTGAA GCTACTGGGC ATCATCATAG  
 251 AAGAAGGGAA CTATTCGCTG GTGATGGAGT ACATGGAGAA GGGCAACCTG  
 301 ATGCACGTGC TAAAGACCCA GATAGATGTC CCACTTTCAT TGAAAGGAAG  
 351 GATAATCGTG GAGGCCATAG AAGGCATGTG CTACTTACAT GACAAAGGTG  
 401 TGATACACAA GGACCTGAAG CCTGAGAATA TCCTCGTTGA TCGTGACTTT  
 451 CACATTAAGA TAGCCGATCT TGGTGTGGCT **TCC**TTTAAGA CATGG**AGC**AA  
 501 ACTGACTAAG GAGAAAGACA ACAAGCAGAA AGAAGTGAGC AGCAC**ACTA**  
 551 AGAAGAACAA TGGT**GGTACC** CTTTACTACA TGGCACCCGA ACACCTGAAT  
 601 GACATCAATG CAAAGCCAC GGAGAAGTCG GACGTGTACA GCTTTGGCAT  
 651 TGTCCTTTGG GCAATATTTG CAAAAAAGGA GCCCTATGAG AATGTCATCT  
 701 GTACTGAGCA GTTCGTGATC TGCATAAAAT CTGGGAACAG GCCAAATGTA  
 751 GAGGAAATCC TTGAGTACTG TCCAAGGGAG ATCATCAGCC TCATGGAGCG  
 801 GTGCTGGCAG GCGATCCCAG AAGACAGGCC AACATTTCTT GGCATTTGAAG  
 851 AAGAATTTAG GCCTTTTTAC TTAAGTCATT TTGAAGAATA TGTAGAAGAG  
 901 GATGTGGCAA GTTTAAAGAA AGAGTATCCA GATCAAAGCC CAGTGCTGCA  
 951 GAGAATGTTT TCACTGCAGC ATGACTGTGT ACCCTTACCT CCGAGCAGGT  
 1001 CAAATTCAGA ACAACCTGGA TCGCTGCACA GTTCCCAGGG GCTCCAGATG  
 1051 GGTCCGTGGG AGGAGTCCTG GTTTTCTTCC TCCCAGAGT ACCCACAGGA  
 1101 CGAGAATGAT CGCAGTGTGC AGGCT**AAG**CT GCAAGAGGAA GCCAGCTATC  
 1151 ATGCTTTTGG AATATTTGCA GAGAAACAGA CAAAACCGCA GCCAAGGCAG  
 1201 AATGAGGCTT ACAACAGAGA GGAGGAAAGG AAACGAAGGG TCTCTCATGA  
 1251 CCCCTTTGCA CAGCAGAGAG CTCGTGAGAA TATTAAGAGT GCAGGAGCAA  
 1301 GAGGTCATTC TGATCCCAGC ACAACGAGTC GTGGAATTGC AGTGCAACAG  
 1351 CTGTCATGGC CAGCCACCCA AACAGTTTGG AACAATGGAT TGTATAATCA  
 1401 GCATGGATTT GGAACTACAG GTACAGGAGT TTGGTATCCG CCAAATCTAA  
 1451 GCCAAATGTA TAGTACTTAT AAAACTCCAG TGCCAGAGAC CAACATACCG  
 1501 GGAAGCACAC CCACCATGCC ATACTTCTCT GGGCCAGTAG CAGATGACCT  
 1551 CATAAAATAT ACTATATTCA ATAGTTCTGG TATTCAGATT GGAAACCACA  
 1601 ATTATATGGA TGTTGGACTG AATTCACAAC CACCAAACAA TACTTGCAA  
 1651 GAAGAGTCGA CTTCCAGACA CCAAGCCATC TTTGATAACA CCACTAGTCT  
 1701 GACTGATGAA CACCTGAACC CTATCAGGGA AAACCTGGGA AGGCAGTGGA  
 1751 AAAACTGTGC CCGCAAGCTG GGCTTCACTG AGTCTCAGAT CGATGAAATC  
 1801 GACCATGACT ATGAAAGAGA TGGACTGAAA GAGAAAGTTT ACCAAATGCT  
 1851 TCAGAAGTGG CTGATGCGGG AAGGCACCAA AGGGGCCACA GTGGGAAAGT  
 1901 TGGCCAGGC ACTTCACCAA TGTTGCAGGA TAGACCTGCT GAACCACTTG  
 1951 ATTCTGTGCC GCCAGAGCTA G

Mouse RIPK1 DNA sequence (accession no. NM\_009068.3) indicating codons targeted for mutation. Codons targeted are underlined and emboldened and the specific bases mutated are indicated in red text. For FLAG-RIPK1 (KpnI site mutation): **GGTACC**→**GGAAACC** (positions 555 – 560). For FLAG-S161A **TCC**→**GCC** (positions 481 – 483). For FLAG-S166A: **AGC**→**GCC** (positions 496 – 498). For FLAG-T183A: **ACT**→**GCT** (positions 547 – 549). For FLAG-K376R **AAG**→**AGG** (positions 1126 – 1128).

## APPENDIX IV: Mouse RIPK1 protein sequence and mutations

```
1 MQPDMSLDNI KMASSDLLEK TDLDSGGFGK VSLCYHRSHG FVILKKVYTG
51 PNRAEYNEVL LEEGKMMHRL RHSRVVKLLG IIIIEEGNYSL VMEYMEKGNL
101 MHVLKTQIDV PLSLKGRIIV EAIEGMCYLH DKGVIHKDLK PENILVDRDF
151 HIKIADLGVA SFKTWSKLTK EKDNKQKEVS STTKKNNGGT LYYPEPEHLN
201 DINAKPTEKS DVYSFGIVLW AIFAKKEPYE NVICTEQFVI CIKSGNRPNV
251 EEILEYCPRE IISLMERCWQ AIPEDRPTFL GIEEEFRPFY LSHFEEYVEE
301 DVASLKKEYP DQSPVLQRMF SLQHDCVPLP PSRSNSEQPG SLHSSQGLQM
351 GPVEESWFSS SPEYPQDEND RSVQAKLQEE ASYHAFGIFA EKQTKPQPRQ
401 NEAYNREEER KRRVSHDPFA QQRARENIS AGARGHSDPS TTSRGIQVQQ
451 LSWPATQTVW NNGLYNQHGF GTTGTGVWYP PNLSQMYSTY KTPVPETNIP
501 GSTPTMPYFS GPVADDLIK Y TIFNSSGIQI GNHNYMDVGL NSQPPNNTCK
551 EESTSRHQAI FDNTTSLTDE HLNPIRENLG RQWKNCARKL GFTESQIDEI
601 DHDYERDGLK EKVYQMLQKW LMREGTKGAT VGKLAQALHQ CCRIDLLNHL
651 IRASQS
```

Mouse RIPK1 protein sequence indicating positions of amino acid residues targeted for mutation. Mutated residues are underlined, emboldened and indicated in red text: **S**161 was mutated to Ala, **S**166 was mutated to Ala, **T**183 was mutated to Ala, **K**376 was mutated to Arg.